

*Investigation of Optical Receivers  
For Use in an Underwater Environment*

**MINT 709 Capstone Project**

**Prepared by:** James R. Murtagh

**Prepared for:** Dr. M. H. MacGregor

**Submitted:** September 30, 2007

## Table of Contents

<b>Chapter 1: Introduction</b> .....	<b>4</b>
<b>Chapter 2: Overview of available photodetectors</b> .....	<b>9</b>
2.1 External photoelectric effect: .....	9
2.2 Internal photoelectric effect: .....	11
2.2.1 PN photodiodes .....	11
2.2.2 PIN Photodiodes .....	16
2.2.3 Schottky Photodiodes: .....	18
2.2.4 Avalanche Photodiodes.....	19
2.2.5 Phototransistors and Photodarlington.....	23
<b>Chapter 3: Underwater optical communication research literature review</b> .....	<b>24</b>
3.1 Attenuation of optical signals in water .....	24
3.2 Review of underwater optical communication using LED(s) for light source. ....	27
3.2.1 Clancy’s master’s thesis.....	27
3.2.2 Woods Hole Oceanographic Institution (WHOI) low power, low cost, underwater optical transceiver .....	28
3.2.3 Australian National University - underwater optical transceiver using IRDA Integrated Circuits (ICs) .....	29
<b>Chapter 4: Optical receiver design for using photodiodes</b> .....	<b>31</b>
4.1 Overview of receiver components .....	31
4.1.1 Optics .....	31
4.1.2 Photodetector .....	32
4.1.3 Preamplifier block.....	32
4.1.4 Post Amplifier and filter .....	41
4.1.5 Signal conditioning .....	41
4.1.6 Decision and clock recovery .....	43
4.2 Receiver circuits used for this project:.....	43
<b>Chapter 5: Experimental Results</b> .....	<b>50</b>
5.1 LED/ Fresnel lens evaluation:.....	50
5.2 Receiver and PIN Photodiode testing .....	58
5.2.1 Ambient light responsivity measurements: .....	61
5.2.2 Comparison of TIA output response using different PIN photodiodes, for a given input optical signal at a fixed distance from the source.....	62
5.2.3 Second stage – wideband amplifier and/or differentiator .....	67
5.2.4 Signal discriminator using differentiated signal and Schmitt trigger .....	70
5.2.5 The GIC circuit results.....	72
5.2.6 Frequency response.....	73
5.2.7 Reception of optical signal at 30 meters from source.....	74
<b>Conclusions – and future Research</b> .....	<b>77</b>
6.1 Conclusion .....	77
6.2 Recommendations for future research .....	79
<b>References</b> .....	<b>81</b>
<b>Appendix</b> .....	<b>85</b>
Appendix A: Data sheets for LEDs .....	86
Appendix B: Tables of measured data for LEDs .....	87
Appendix D – Equation Derivations for receiver circuits .....	100

*Investigation of Optical Receivers For Use in an Underwater Environment*

Appendix E: Receiver evaluation board: Schematic diagrams and PCB board  
component layout.....108

Appendix F: Receiver waveforms captured for various testing scenarios and  
photodiodes.....111

*(Use Ctrl+Click to jump to that section in soft copy)*

## Chapter 1: Introduction

To monitor/evaluate our changing environment a tool being deployed is sensor networks. Autonomous nodes, often referred to as motes, that are deployed in a terrestrial sensor networks typically consist of four functional blocks;

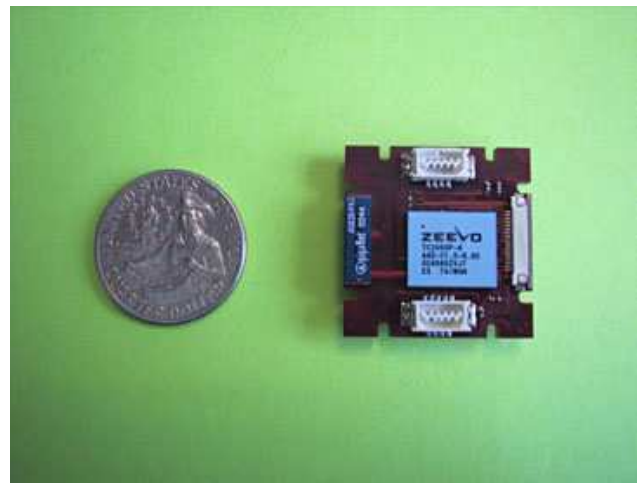
1. **a sensor section**, with one or more sensors (i.e. seismic, infrared, thermal, acoustic, motion)
2. **a processing unit** (typically an embedded controller) that draws very low power,
3. **a power system** consisting of a supply (batteries and/or solar cells) and power monitoring system to conserve power when it can
4. **RF transceiver**

When deployed, the motes communicate with those that are within range of it to form a fully distributed multi-hop wireless network.

Figure 1.1 shows two examples of motes. The larger unit developed at the Free University of Berlin (FU-BERLIN) is made available to researchers through [www.scatterweb.com](http://www.scatterweb.com). The smaller unit is a prototype currently being developed at Intel. The FU-BERLIN unit uses an off-the-shelf TR1001 radio transceiver at 868.35Mz that can transmit either on-off keyed (OOK) or amplitude-shift keyed (ASK) modulation up to a 115.2k bits/second. [3] The Intel mote takes advantage of Bluetooth technology. [2]



a) Free University of Berlin Embedded System Board Mote (FU-BERLIN-ESB).



b) Intel Mote prototype (3x3 cm)

**Figure 1.1: Examples of terrestrial motes.** [1, 2]

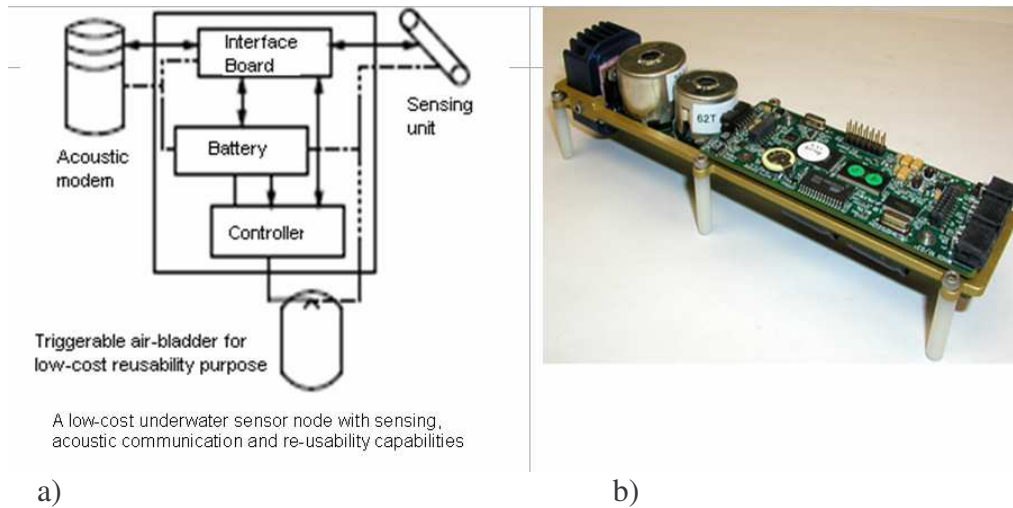
The advances made in integrated circuit design, battery technology and RF communications hardware facilitates motes being manufactured for relatively low cost, draw low power with power management extending battery life, and are physically small packages. Depending on RF power levels, motes can be spaced a few meters apart upwards to hundreds of meters and as they form into a multi-hop ad-hoc network allows

monitoring of large areas. For example, the FU-BELIN can, depending on conditions, communicate up to 1km distance with its RF transmitter at 1mW broadcast power. As an interesting side note, because of its transmission frequency at 868.35Mz, a dipole antenna at  $\frac{1}{4}$  wavelength of 8.64 cm length is required and must be correctly positioned when deploying the mote. To easily deploy motes, perhaps as simply as dropping them from a plane into a geographic region the transceiver section of motes needs to function at much higher frequencies so that antenna size is small, and can then be self contained in the package in much the way that some current cell phones do.

To achieve the power savings and therefore long battery life, motes typically do not do continuous active sensing, receiving data, and/or transmitting data; they need to cycle into a very low-power mode that keeps only the processor timing alive. For example, the full featured FU-BERLIN-ESB draws 12mA current when it is running with all sensors active; consumes an additional 8 – 12 mA when transmitting, and an additional 4.5mA for receiving. When it transitions into its “deep sleep” mode it draws only 8 $\mu$ A. The promotional literature claims that for a 1% duty cycle for transmission and sensing this mote should realize a lifespan of up to 5 years with 3 AA batteries. If however, this device was required to transmit a 250 byte message once per second at a low data rate of 19200 bits per second its life span reduces to about 32 days. Lifespan of the batteries reduced to only about 5 days if the mote is required to stay active in its listening mode rather than cycling down into sleep mode. [1, 4]

As can be surmised, a major challenge for mote design affecting its deployment and longevity is the capability of its transceiver section. Designers of terrestrial motes have been able to take advantage of the wealth of knowledge that has been developed over the last century and particularly the last two decades in wireless communications. One can only imagine the added amount of work that would have been required in the design of the FU-BERLIN mote if the transceiver section hardware had to be discretely designed rather than being available as an off-the-shelf completely self-contained miniaturized packaged component.

Unfortunately, the success that terrestrial motes have achieved is not yet achievable in underwater scenarios. Besides packaging for a very inhospitable environment, communications via RF cannot be done under water. In addition, an underwater mote package should have a recovery solution built into it, particularly for deployment in deep sea environments; this is represented in figure 1.2-a.



**Figure 1.2: Acoustic mote.** a) Underwater acoustic mote [5], b) WHOI Micro-modem - acoustic modem (1.5" x 4.5") [6]

Currently there are three approaches for un-tethered communications underwater: use of acoustic modems; use of long wave radio; and the use of optics. Figure 1.2-b shows a Woods Hole Oceanographic Institute designed acoustic modem that is marketed as “Micro-modem”. [6] It interfaces with an underwater speaker and hydrophone. In experiments conducted in March-April 2007 in Bussards Bay MA, a four node sensor network using these modems, demonstrated communications range up to 900 meters but, data rates are relatively slow. Achievable raw data rates at a distance between modems of 300 meters averaged 157 bits/sec. In addition, substantial overhead is added to each data payload to protect against corruption and each packet sent requires an acknowledgement. Adding overhead and allowing for propagation speed of sound in water for the delivery and acknowledgement of each packet resulted in an effective data rate of just under 34 bits/sec. [7]

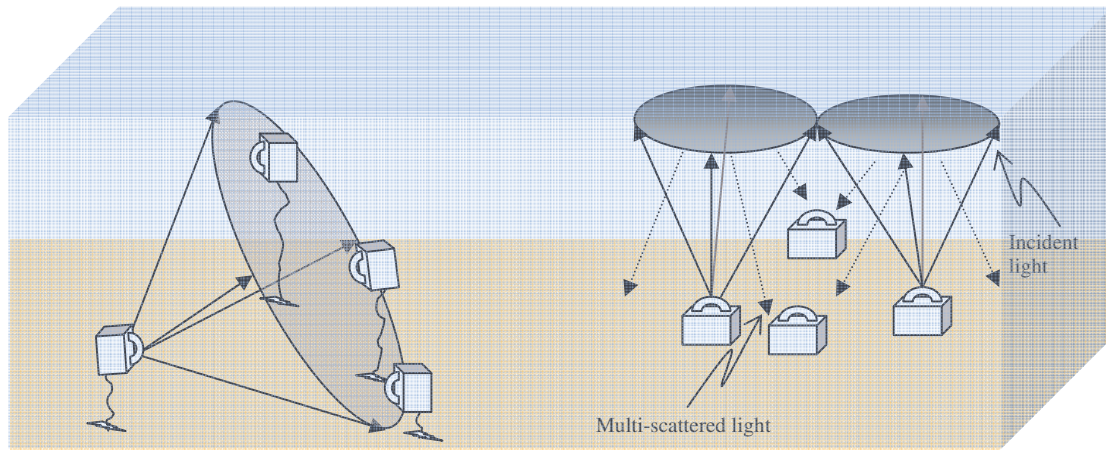
Longwave radio uses frequencies in the range of 8k Hz – 123kHz. At these low frequencies, unlike RF, attenuation in underwater environments is within workable levels for data communications to transverse the media. However, because of the low frequency carriers, available bandwidth to carry data is also limited. A group of researchers at the Australian National University have designed and tested a longwave radio system capable of 8192 bits/sec at 122.88 kHz carrier. In experiments in Pacific coastal waters using 100mW power, this team was able to attain a bit rate of 1024 bit/sec to a range of 3.9 meters and at higher power 8kbits/sec is achievable to 10 meters. [8, 9]

Although both acoustic modem motes and longwave radio can facilitate creating a sensor network underwater, their achievable bit-rates are substantially lower than achieved in terrestrial motes. As noted earlier, the transmission section of a mote while active consumes a relatively large amount of power with respect to the other mote functions. Slow data rates, requiring that the transmitter remain active for longer periods of time, worsens the power usage problem. Additionally, both approaches are typically more costly to build than terrestrial motes and the end products are physically larger in size

(though in underwater scenarios larger size may not be much of a concern). Optical communications offers the possibility of solving the low data-rate problem, hence power consumption and should result in a lower cost package.

Although optical communications provides for much higher data rates than acoustic links and longwave radio, current achieved transmission distances in water are relatively short and most accomplished through line-of-sight (LOS). For sensor network application, short distances can be overcome by adding more motes into an area; though it increases cost and the number of hops which increases networking protocol complexity. More challenging for optical mote deployment in water is LOS solutions - aligning the transmitters to receivers made more difficult due to changing currents in water that subject motes to motion.

Laser sources offer high power transmission capability as well as high switching speeds and are used extensively in fibre optics communications. Lasers are not well suited to our application due to their high cost, power consumption, and more importantly their highly focused beam, requiring exact alignment on the receiver side. Non-coherent light sources are most likely best suited in sensor network applications. Two deployment scenarios for data transmission using non-coherent light sources are possible and illustrated in figure 1.3.



LOS: Motes placed within transmitting mote's diffused beam area

Non-LOS (indirect): Motes placed within multi-scattered area of the transmitting mote's diffused beam area

**Figure 1.3: Two scenarios for placement of optical communicating motes in underwater deployment**

In both deployment scenarios, the receiver circuits need to be as sensitive as possible and capable of handling high data rates to allow for practical deployment distances between motes.

The purpose of this project is to investigate the physical layer, primarily receiver side, of the optical communications link. As part of this investigation, several detectors were

*Investigation of Optical Receivers For Use in an Underwater Environment*

evaluated and receiver circuit design investigated. Although it was originally intended to do both air and underwater measurements, the machinist that I had lined up to assist me in building the housings for underwater testing was not available so only air measurements were conducted.



## Chapter 2: Overview of available photodetectors

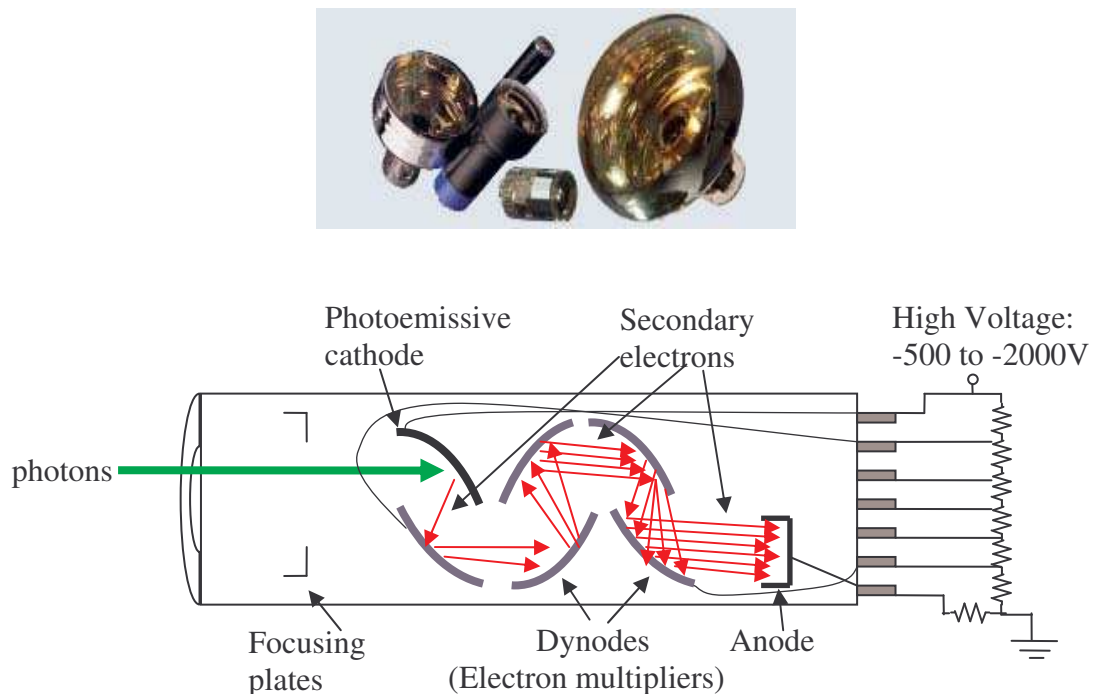
Photodetectors can be classified to one of three general categories;

1. external photoelectric effect
2. internal photoelectric effect
3. thermal effect

These types of optical detectors cover a sensitivity range from the conversion of a single photon into a measurable voltage value through to the absorption of kilowatts of optical power translated to thermocouple voltage. [10, 11] For data communications purposes, only photodetectors that belong to the external photoelectric and internal photoelectric effect categories are of interest and reviewed.

### 2.1 External photoelectric effect:

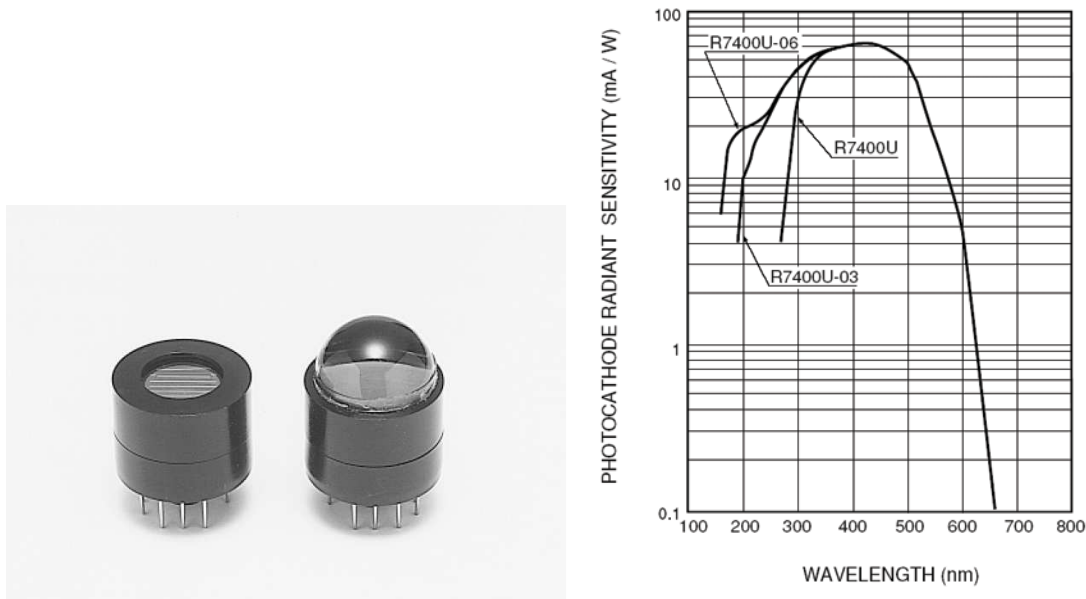
Detectors that belong to the external photoelectric effect category have a photon sensing surface, a metal plate (photoemissive cathode) or semiconductor, housed within a vacuum. When photons hit the sensing surface they are absorbed and secondary electrons emitted. Photomultiplier tubes (PMT) are built to take advantage of this effect. An example of PMTs and schematic representing their construction are shown in figure 2.1.



**Figure 2.1: Photo multiplier tubes** – commercially available detectors from [www.photonics.com](http://www.photonics.com) [12] and internal schematic representation [13, 14]

As can be seen in figure 2.1, besides containing a photoemissive cathode within the vacuum housing, two additional electrode plate types are part of the structure. At the opposite end of the vacuum environment is the Anode. The Anode is set to a much higher voltage potential than the cathode; it attracts the emitted electrons within the vacuum resulting in electron current. Between the cathode and anode are dynode plates at progressively higher voltage potentials. As the secondary electron moves from the cathode to the anode striking the dynodes, additional electrons are released giving a multiplying effect. PMTs can have a multiplication factor of  $10^5$  to  $10^7$ . The physical size can vary from the “world’s smallest 3/8-inch tubes” to the “world’s largest 20-inch hemispherical tubes” as claimed by Hamamatsu Photonics. [13]

PMTs spectral response is typically in the range of UV – near infrared light (190 – 900nm wavelength), though some special purpose tubes are designed to 1100nm wavelength. Figure 2.2 shows spectral response for an 8mm active area (16mm diameter in size) photomultiplier model R7400 from Hamamatsu.



**Figure 2.2: Hamamatsu PMT model R7400U series and spectral response. [10]**

Visible light at blue/green wavelengths (450 to 530 nm) suffers the least amount of attenuation in oceanic waters (to be discussed later in this report). Based on the spectral response of the R7400U PMT, it would appear to be an attractive option for optical communications underwater particularly as its high sensitivity peak response is in the wavelength region we are interested in. This product also has a very fast response time of 0.74nS. Unfortunately PMTs have the following 3 major disadvantages which tend to eliminate their use for underwater motes;

1. Requirement for a very stable high voltage source.
2. Mechanically very fragile.

3. Relatively expensive.

A search of literature shows that PMTs are not being used for most data communications applications with the exception of some deep space research activities.

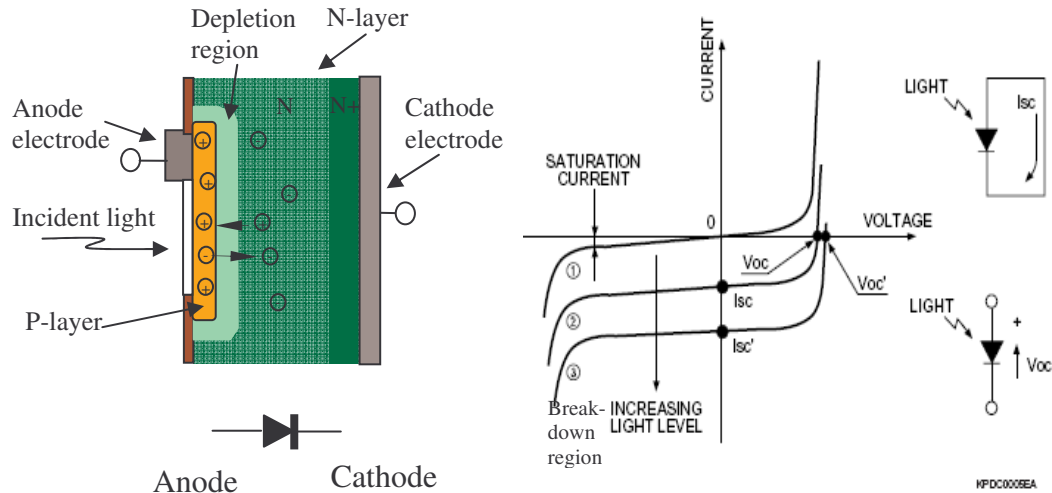
## **2.2 Internal photoelectric effect:**

Photo detectors that fall within this category are semiconductor devices that when exposed to light generate a current or voltage potential. Detectors that fit within this category include solar cells, PN photodiodes, PIN (Positive-Intrinsic-Negative) photodiodes, Schottky type photodiodes, Avalanche Photodiodes (APD), and phototransistors and photodarlington. In addition, photodiodes can be further subdivided into two subcategories, photovoltaic and photoconductive. For data communications, PN photodiodes, PIN photodiodes, and APDs are used most often. Although solar cells are included in this grouping they are not applicable to a data communications application and will not be discussed.

Photodiodes (PN and PIN) advantages include a wide spectral range from UV to IR, have excellent linearity, have relatively low noise level, relatively low cost, are very rugged, small, and have a long life.

### **2.2.1 PN photodiodes**

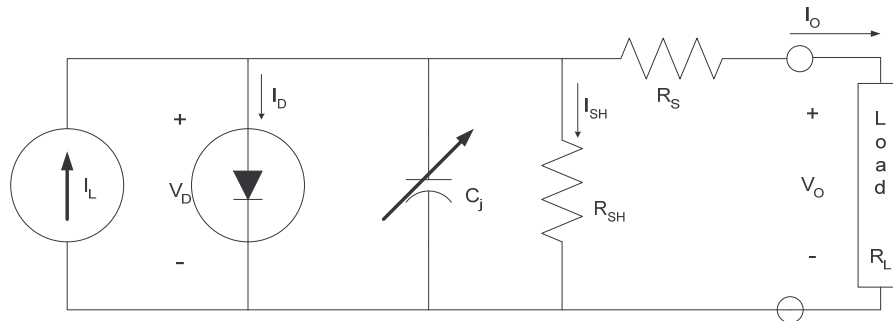
PN photodiodes share a similar physical structure to standard diodes with the exception that the package surrounding the PN junction allows light to reach the semiconductor material and the semiconductor area is typically larger. By controlling both the thickness of the layers and doping concentration, the spectral response and frequency response is set. Figure 2.3 depicts the cross section of the PN photodiode and its typical VI characteristic curves. When incident light strikes the semiconductor, electrons get stimulated. With sufficient incident light energy, the electrons will have enough energy to escape their valence band, rupturing their covalent bond, leaving a hole in the crystal structure. This results in a net positive charge (a positive ion). This positive charge attracts an electron from the valence-band of a nearby atom, leaving a hole behind, etc. Eventually the electrons are pulled from the N-semiconductor creating a depletion region at the PN junction. Because of the hole left in the n-material, it attracts an electron, building a negative charge. This movement of electrons and resulting holes create a flow of positive charge just as the electron movement creates a negative charge. The depth within the semiconductor where carriers are released is proportional to the photon wavelength. Only the carriers released near to or in the depletion region create the photodiode's current. [15] The P-semiconductor builds up a positive charge and the N-semiconductor builds a negative charge. Once a conduction path (circuit) is established from Anode to Cathode, a current proportional to the incident light level flows. [16]



**Figure 2.3 Photodiode cross section and characteristic VI curves [16]**

The photodiode may be biased in one of two ways, either with zero voltage applied across it or reversed biased (anode more negative than cathode and less than the breakdown voltage). When configured with zero volts across the diode, its operation is referred to as the “photovoltaic mode”. When reversed biased (between zero volts and the breakdown voltage) it operates in the “photoconductive mode”. Each operation has its advantage. In photovoltaic mode, there is less noise and very low dark current. In photoconductive mode, linearity is improved and more importantly improved frequency response but at a cost of higher noise and dark current.

To characterize the relationship of current and light, an equivalent circuit for the photodiode is used and shown in figure 2.4.



**Figure 2.4 Equivalent circuit model of a photodiode [16]**

As seen in Figure 2.4, the photodiode is represented by five circuit elements:

1. Current source  $I_L$  which represents the current generated by incident light
2. Ideal diode with diode current  $I_D$  and voltage drop  $V_D$

3. Junction capacitance  $C_j$ , which varies in value based on reverse DC bias – as reverse bias increases the junction capacitance decreases
4. Shunt resistance  $R_{SH}$ , a large ohmic value (in the range of  $10^7$  to  $10^{11}$  ohms) with noise current  $I_{SH}$
5. Series resistance  $R_S$ , a small ohmic value (a few ohms).

Based on the equivalent circuit mode of figure 2.4 the output current  $I_O$  is expressed as:

$$I_O = I_L - I_D - I_{SH}$$

Substituting in the expression for  $I_D$  (current through a PN junction) the final expression for current delivered by the photodiode is:

$$I_O = I_L - I_{sat} (e^{\frac{qV_D}{kT}} - 1) - I_{SH} \quad \text{Equation 2-1}$$

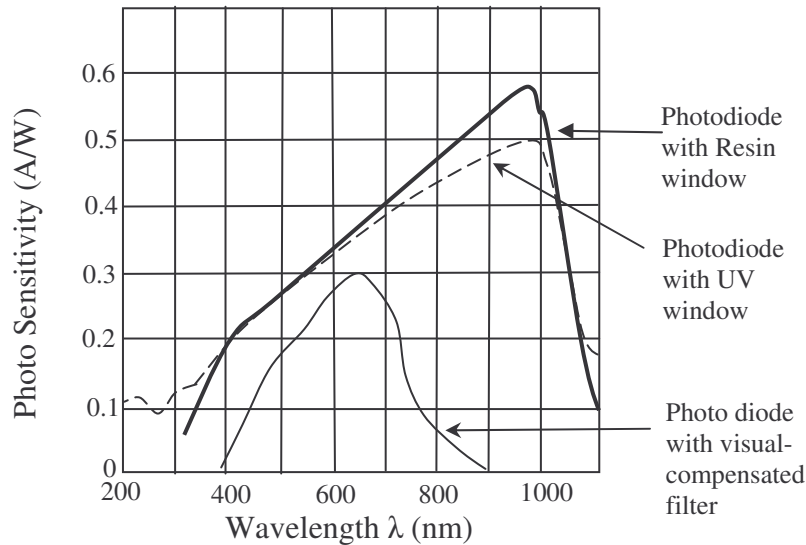
where:

- q - electron charge -  $1.6 \times 10^{-19} C$
- k - Boltzmann's constant -  $1.4 \times 10^{-23} J / K^\circ$
- T - Absolute temperature of photodiode ( $K^\circ$ )
- $I_{sat}$  - Diode reverse saturation current

Figure 2.3 shows the resulting current vs. voltage (VI) characteristics. Referring to equation 2-1, when  $V_O = 0V$ , a short circuit condition, the current  $I_D$  goes to 0. In addition, as  $R_{SH}$  is very large,  $I_{SH}$  will be very small giving  $I_{SC} \approx I_L$ . Within the region between reverse voltage breakdown and forward bias, the light to current relationship is linear. Variations in linearity, is a result of the  $I_{sat}$  and  $I_{SH}$  terms. As both these are all but eliminated when operating in photovoltaic mode, the light to current relationship is at its most linear over a wide dynamic range, to a maximum  $I_{sc}$  value that the physical structure allows (specified in manufactures data sheets).

Four parameters are of particular importance when choosing a photodiode; spectral response (wave length and light to current conversion relationship), surface area of the detector, the value of its junction capacitance (dependent on both surface area and reverse bias voltage), and the photodiode's noise characteristic.

The spectral response of the photodiode is determined by two factors, the physical structure of the diode (semiconductor size and amount of doping) and the transmittance of the window's material. Figure 2.5 shows three representative photodiodes spectral response curves. Generally Si PN photodiodes have peak response at around 950nm wavelength (infrared region), unless optically filtered, and is a magnitude of two to three times more sensitive than at the blue/green optical wavelengths. In comparing photodiodes sensitivity to PMTs, photodiodes are slightly more sensitive than PMTs and reach into the infrared range. However, PN photodiodes do not have gain, and therefore much less suitable to very low light level applications. On the plus side, a photodiode will tolerate high light levels where as a PMT, if operational, could be destroyed.



**Figure 2.5: Spectral responses of three representative PN photodiodes available from Hamamatsu [16]**

The active area of the photodiode affects its ability to collect light – the larger the area the greater amount of light collected (almost proportional) resulting in more current. But, several penalties apply when increasing the surface area and include: higher cost, potentially less robust packaging as the window material is larger, increase in noise level, higher junction capacitance which results in lower useable frequency bandwidth, and higher dark current. For example, a Hamamatsu S1337 series photodiode with an active area having a diameter of  $100\text{mm}^2$  has junction capacitance specified as  $1100\text{pF}$  where as for an active area of  $5.9\text{mm}^2$  the capacitance is  $65\text{pF}$ . In comparing their ability to collect and convert light to current, for an applied light level of 100 lux, the short circuit current  $I_{SC}$  for the  $100\text{mm}^2$  is  $95\mu\text{A}$  compared with the smaller device providing only  $5.3\mu\text{A}$ . Dark current for this series ranges from  $200\text{pA}$  for the larger active area photodiode down to  $50\text{pA}$  for the smaller package.

For low level light applications, noise defines the minimum optical power levels that can be dealt with. Noise is characterized by three relationships – Signal to noise ratio (S/N or SNR), noise equivalent power (NEP), and a figure of merit value called “specific detectivity” ( $D^*$ ). Current noise in semiconductor photodetectors results from three sources, thermal noise (often referred to as Johnson noise), shot noise (or dark current noise) which occurs when reverse bias voltage is applied, and ambient light current. [16, 17, 18, 19] The rms value of these three contributors defines the total noise current and is expressed through equations 2-2 to 2-5:

Johnson noise (thermal noise of a resistor - approximating effect of the shunt resistor):

$$i_f = \sqrt{\frac{4kTB}{Rsh}} \quad \text{A/ Hz}^{1/2} \quad \text{Equation 2-2}$$

where:

- k - Boltzmann's constant
- T - Absolute temperature
- B - Noise bandwidth
- Rsh - Photodiode shunt resistor

Shot noise (when a reverse bias voltage is applied) originates from the dark current:

$$i_{sD} = \sqrt{2qI_D B} \quad \text{A/ Hz}^{1/2} \quad \text{Equation 2-3}$$

where:

- q - Electron charge
- I<sub>D</sub> - Dark current
- B - Noise bandwidth

Incident light (ambient light) noise:

$$i_{sL} = \sqrt{2qI_L B} \quad \text{A/Hz}^{1/2} \quad \text{Equation 2-4}$$

Total current noise:

$$i_n = \sqrt{i_f^2 + i_{sD}^2 + i_{sL}^2} \quad \text{A/ Hz}^{1/2} \quad \text{Equation 2-5}$$

As evident by equations 2-2 to 2-5, current noise is directly proportional to bandwidth and ambient light and inversely proportional to shunt resistance. When the photodiode is operated in photovoltaic mode, total noise is reduced as shot noise from dark current drops to zero.

NEP in watts (W) per square root Hertz is a factor that relates noise current to the photodiode's sensitivity value at a given wavelength and is expressed in equation 2-6:

$$NEP = \frac{i_n}{S} \quad \text{W/Hz}^{1/2} \quad \text{Equation 2-6}$$

where:

- $i_n$  - total noise current (A/Hz<sup>1/2</sup>)
- S - Photo sensitivity (A/W)

NEP relates the quantity of optical input power that is applied to a photodiode that results in a SNR = 1. The incident optical power must be greater than power level expressed by NEP to distinguish signal from noise.

$D^*$ , a figure of merit that photodiode manufactures may specify, is defined as the inverse of  $NEP$  normalized to the square root of the detector' area and the bandwidth.[19]  $D^*$  may make for easier comparison of one detector with another and is expressed in equation (2-7) as follows:

$$D^* = \frac{\sqrt{AB}}{NEP} \qquad \text{Equation 2-7}$$

where:

- $A$  - is the detector area in  $\text{cm}^2$
- $B$  - bandwidth in Hertz
- $NEP$  - noise equivalent power in  $\text{W/Hz}^{1/2}$

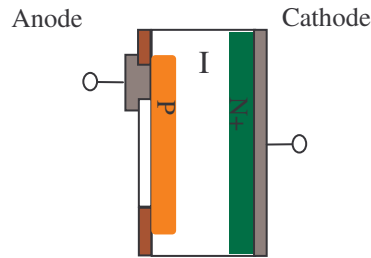
In addition to operating in photovoltaic mode the photodiode's noise level can be lowered by reducing bandwidth, reducing ambient noise, reducing temperature of the diode, and increasing the time to observe the light signal of interest (in the case an incoming pulse waveform, lower the pulse frequency rate and increase duty cycle). These methods to reduce noise are in conflict with the goal of high data rates achieved at low signal strength; compromise is required.

In addition to the above considerations, designers may also need to consider step response time and acceptance angle / field of view / directivity. Manufactures offer a large assortment of photodiode packages. The packaging variations facilitate different sizes of active areas, physical encasement and window material/lenses, and placement orientation on a circuit board and/or into an instrument/consumer product. The manufactures assist the designer by identifying typical applications for which the product may be best suited.

### **2.2.2 PIN Photodiodes**

PIN photodiodes have been developed out of the need to reduce dark current that results from reverse biasing PN photodiodes and to further increase response times. The first modification to the PN photodiode, creation of the Planar Diffusion photo diode was the addition of a  $\text{SiO}_2$  coating applied to PN junction surface, which resulted in lower dark currents. The next step in development was the low-capacitance planar diffusion photodiode. To reduce capacitance, the depletion layer needs to be enlarged (why we reverse bias the PN photodiode). Structurally this was accomplished by making a highly pure, high-resistance N-type material. The PIN diode improves on the low-capacitance planar diffusion device by placing between the P and N junction an extra high-resistance intrinsic layer (I) and additionally designing it to sustain a much greater reverse bias voltage before breakdown. Refer to figure 2.6 for a cross sectional view of the PIN diode.

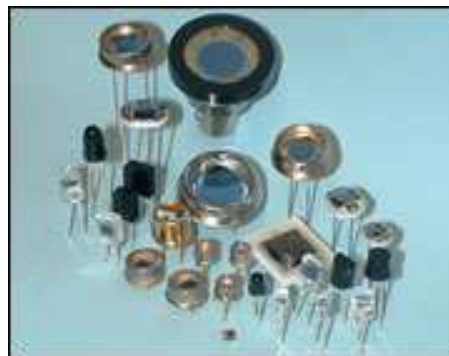




**Figure 2.6: Simplified cross-section view of PIN Photodiode [16]**

The PIN diode can function both in the photovoltaic mode and in the photoconductive mode. As was the case for the PN photodiode, the photovoltaic mode of operation will exhibit the lowest noise levels, but will have its highest capacitance value. In reverse bias, noise does increase but not as severe as with PN photodiodes. In addition, because the PIN diode tolerates more reverse bias, the junction capacitance can be reduced much greater resulting in being able to use it for much higher frequency response applications. For these reasons PIN photodiodes are preferred over PN photodiodes for data communications particularly higher data rates.

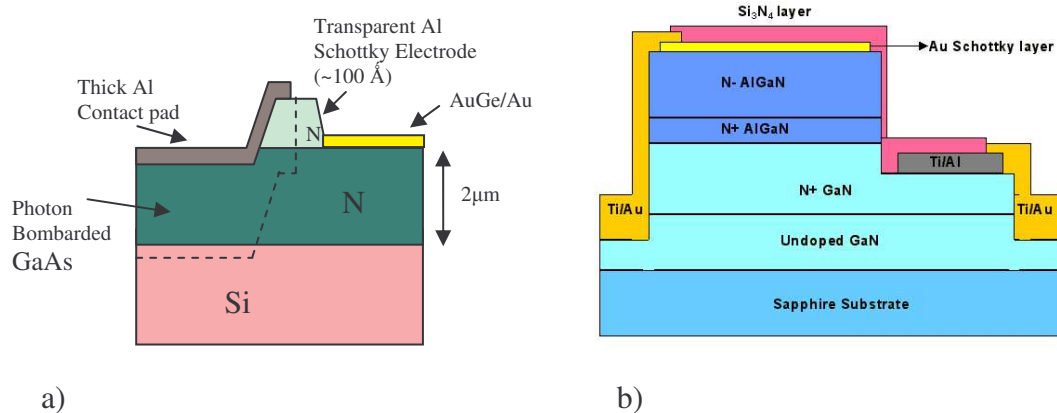
The equations developed for the PN photodiode also apply to the PIN photodiode. To determine the amount of reverse bias voltage to apply to the PIN photodiode one typically refers to manufacturers data sheets that show either capacitance vs. reverse voltage or frequency cut-off vs. reverse voltage. As is the case for PN photodiodes, PIN photodiodes come in a large assortment of active area sizes and physical packages. Refer to figure 2.7 for a sampling of PIN photodiodes available from Advanced Photonix Inc (API). The photodiodes used for this project are from API. API offers, in its PIN photodiode portfolio, red enhanced, blue enhanced, UV enhanced, and daylight filtered photodiodes.



**Figure 2.7: Available PIN photodiode products offered by Advanced Photonix Inc. [20]**

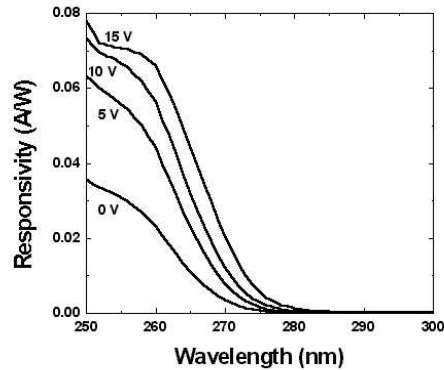
### 2.2.3 Schottky Photodiodes:

Schottky photodiodes, simpler in structure than that of PIN photodiodes, require very tight manufacturing controls for thickness of materials and doping. Figure 2.8 shows a cross sectional views for two of several variants of Schottky photodiodes.



**Figure 2.8: Cross sectional views of Schottky photodiodes** a) GaAs type b) AlGaN type [19, 21]

One of the major structural differences between Schottky photodiodes and PN/PIN types is the very thin metal layer deposited on top of the n-semiconductor material forming a Schottky effect P-N Junction. This gives Schottky photodiodes two significant advantages over PN/PIN photodiodes: not having to address the issue of facilitating low resistance electrode contact with p-doped semiconductor material, a challenge for PIN diode manufacturing; and a strong electrical field develops near the metal-semiconductor interface, which can be made stronger with reverse bias, creating a large depletion region, which increases responsiveness. Frequency bandwidths greater than 100GHz are capable using Schottky photodiodes. [19] The thin metal coating layer allows ultraviolet waves to pass but virtually no visible light or IR – they are considered solar blind. Figure 2.9 shows the spectral response of the AlGaN Schottky diode.

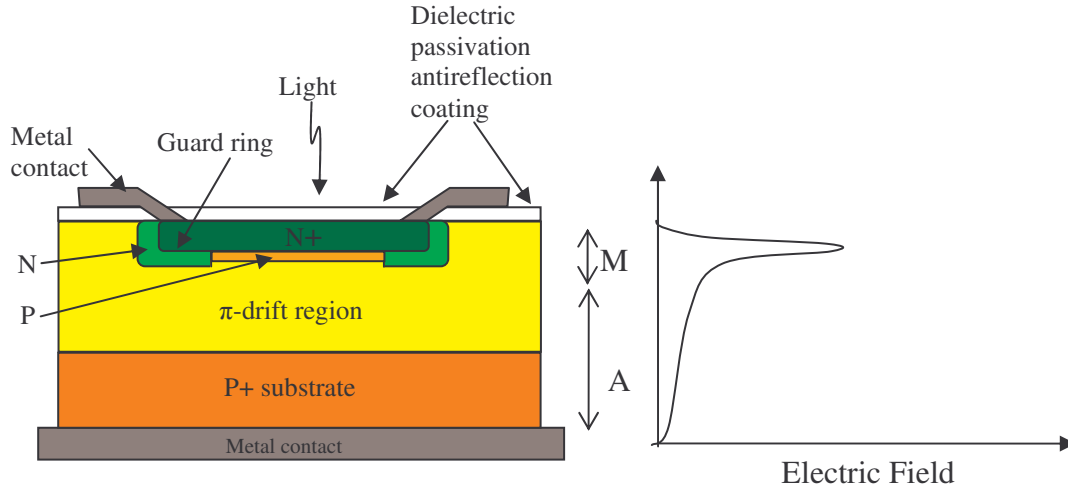


**Figure 2.9: Spectral response for AlGaIn Schottky diode [21]**

Schottky photodiodes, because of their high responsivity and spectral response to UV, are attractive for applications such as missile threat warning, space communications, and flame detection. [22] Unfortunately, Schottky photodiode advantages cannot be easily manufactured so as to extend to longer wavelengths. Additional manufacturing issues, such as defects in AlGaIn epilayers and thermal expansion between the sapphire substrate layer and GaN semiconductor layer plague the AlGaIn Schottky photodiode; research continues. [19, 22] Because current Schottky photodiodes do not respond to the blue/green visible wavelengths their use for free space underwater optical communications is not considered.

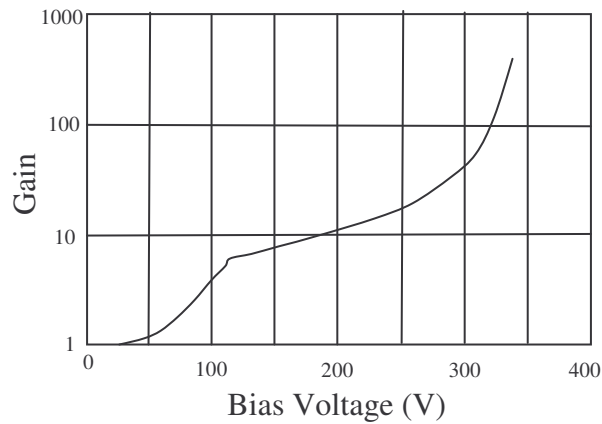
### 2.2.4 Avalanche Photodiodes

Avalanche photodiodes have a distinct advantage over PN and PIN photodiodes; they have internal gain. This is accomplished through an effect known as “impact ionization”. Figure 2.10 show a cross section of a classic silicon avalanche photodiode. For functionality, the avalanche photodiode requires reverse bias voltage which is typical at a much higher potential than used for photoconductive operation of PIN photodiodes. The high reverse bias voltage potential is required for the avalanche (multiplication) effect to occur. Carriers that are generated by photoabsorption and released into strong electric field gain energy and collide with atoms in the field, resulting in additional electrons being freed (impact ionization) from their valence band to the conduction band. The multiplication regions “M” occurs between the P and N+ junction. The electric field that is present across the absorption area “A” separates the photo generated holes and electrons and allows one carrier type to be swept towards the multiplication region. [19, 23]



**Figure 2.10** Cross sectional view of classic Si APD and electric field distribution [19, 23]

Gain in APDs increases with the bias voltage, but the relationship is not linear. In addition gain is temperature dependent. Figure 2.11 shows gain as a function of bias voltage for standard structure APDs manufactured by Perkin Elmer.



**Figure 2.11:** Gain as a function of bias voltage for standard APDs manufactured by Perkin Elmer [23]

In addition to gain being nonlinear and temperature sensitive, the gain amplification enjoyed for light conversion to electrical energy also contributes to increased noise in the form of Shot noise. Shot noise, a result of random statistical Poisson fluctuations of dark noise, is the summation of surface leakage current and gain applied to the bulk leakage current. In addition to shot noise, current fluctuations occur in the avalanche process. This fluctuation is expressed as excess noise factor (F). Equation 2-8 shows the relationship of noise current in an APD under dark conditions and equation 2-9 shows the inclusion of the incident light optical power. [23]

$$i_n = \left[ 2 \times q \times (I_{DS} + I_{DB} \times M^2 \times F) \times B \right]^{1/2} \quad \text{Equation 2-8}$$

where:

- $q$  - electron charge
- $I_{DS}$  - surface leakage current
- $I_{DB}$  - bulk leakage current
- $M$  - gain of APD for a given bias voltage
- $F$  - Excess noise Factor
- $B$  - Bandwidth

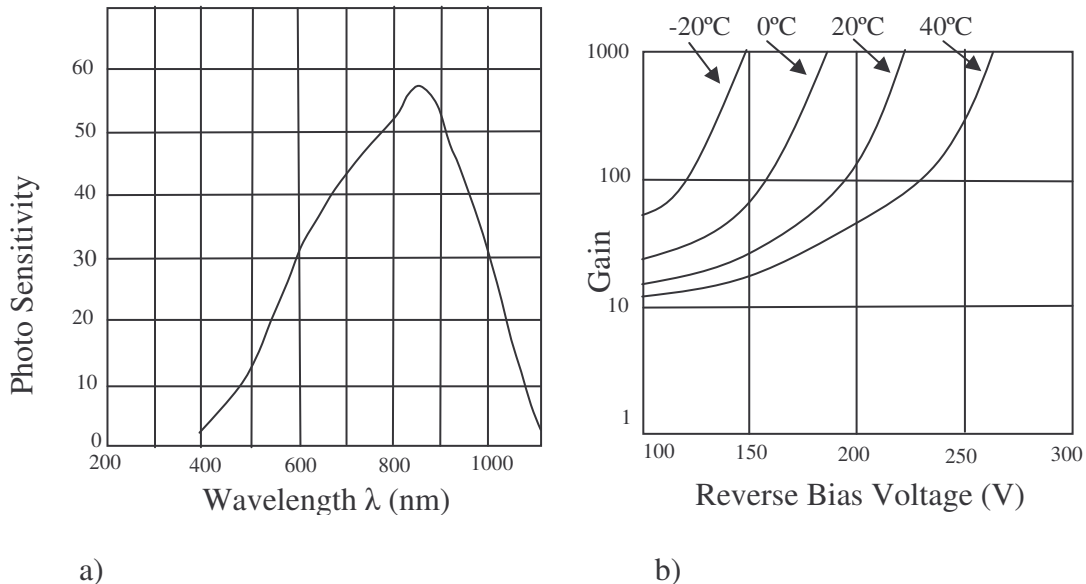
When light is added, the total current becomes:

$$i_n = \left[ 2 \times q \times (I_{DS} + (I_{DB} \times M^2 + R_o(\lambda) \times M^2 \times P_s) \times F) \times B \right]^{1/2} \quad \text{Equation 2-9}$$

Where:

- $M$  - gain of the APD
- $R_o(\lambda)$  - intrinsic responsivity of the APD at a gain  $M=1$
- $P_s$  - is the incident optical power

The spectral response for APDs range from near UV through to IR. Silicon APDs are responsive from 300-1100nm, germanium APDs are appropriate for IR wavelengths of 800-1600nm, and InGaAs APDs which exhibit lower noise than germaniums and are also more expensive, have a spectral range of 900-1700nm.[23] Figure 2.12 a) shows the spectral response for Hamamatsu series S9251 Si APD. The spectral response shapes is similar to PN and PIN diodes, but note the values of the photosensitivity scale. Figure 2.12 b) shows the relationship of gain and reverse voltage as affected by temperature.



**Figure 2.12: Hamamatsu series S9251 Si APD graphs;** a) Spectral response; b) Temperature effects on gain. [24]

In addition to having gain, APDs typically can support high bandwidth operation. For example, the S9251 series APD have a cutoff frequency of 350 to 400MHz, with terminal capacitance in the range of 0.4 to 3.6pF.

As attractive as ADPs appear for use in free space underwater optical communications, there are three reasons why they were not evaluated for this project:

First, APDs require large reverse biasing voltage. This can be implemented by using products available through companies such as MAXIM which makes a step-up inverter IC (plus external passive components) that will take an input of 3 to 3.5V and provide an output voltage of 40-90V. Special care is required in protecting components when this type of voltage is present.

Second, APD gain varies with bias voltage and temperature – additional circuitry is required to keep gain stable by controlling the voltage. There are available, packaged solutions to manage the supply/temperature problem. Some packaging includes thermoelectric cooling to allow for greater gain at lower reverse bias voltages. Thermoelectric coolers consume a relatively high amount of current.

Third, APDs are significantly higher in cost compared to PIN photodiodes. Discrete APDs, without high voltage supply and temperature control, are in the high \$10s to low \$100s in cost. APDs packaged with the additional supporting hardware, temperature/gain control and addition of thermoelectric coolers add significantly more cost. As an example, Hamamatsu's S5345 large active area (19.6 mm<sup>2</sup>) Si APD was quoted (e-mail March 9, 2007) at \$530.80 single unit price. Within the same quote, Hamamatsu recommended a complete APD module, part number C5331-13, that contains the S5345 APD and adds temperature controlled high-power supply that functions from a 5V supply. It was quoted at \$1150.08.

No discussion would be complete on APDs without mentioning their use in photon counting (Geiger) mode. Like all semiconductor photodetectors, when reversed biased, there is a point at which too much voltage causes a high amount of current to flow called breakdown as shown in figure 2.3 and is generally a catastrophic event; the voltage current combo results in high power thus extreme heat destroying the semiconductor, or the sudden current flow can arch through the semiconductor and destroys its integrity.

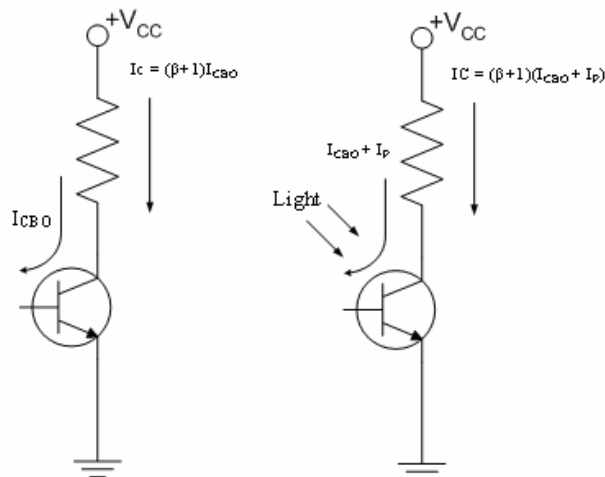
If an APD is biased at just past its breakdown region, and current is limited to less than the APD's "latching" current, there is a strong statistical probability that the current will fluctuate to zero in the multiplication region, and the APD will then remain in the "off" state until an avalanche pulse is triggered by either a bulk or photo-generated carrier. If the number of bulk carrier generated pulses is low, the APD can be used to count individual current pulses from incident photons. [25]

Some APDs are designed specifically for this purpose and can be very costly – an investigation currently being conducted at the University of Calgary is using an APD priced at around \$20,000. In addition, very low temperature cooling is usually required to minimize noise and increase sensitivity.

## 2.2.5 Phototransistors and Photodarlington

A phototransistor is a bipolar transistor that has a reverse biased collector-base junction windowed to allow exposure to light. Referring to figure 2.13, when there is no light, (analogous to zero base current) a very small reverse leakage current  $I_{CBO}$  flows from collector to base, a result of thermal induced minority carriers. When light energy reaches the exposed junction, additional current  $I_P$  due to released minority carriers by the light energy, flows. This added light energy current, results in magnified collector to emitter current (as per transistor behavior with minority carriers/majority carriers and base current). The result is light to electrical current with current gain  $\beta$ . As  $\beta$  is  $\gg 1$  and  $I_{CBO}$  is very small,  $I_C \approx \beta I_P$  which is a very desirable result. Current gain can range from 100 to over a thousand. Photodarlington, like Darlington transistors, adds a second transistor stage, which effectively result in  $\beta^2$  current gain. A phototransistor's spectral response is much like PN photodiodes, between 400nm and 1100nm.

Though phototransistors are attractive due to their internal gain, phototransistors and photodarlington rise and fall times are several magnitudes slower than photodiodes due to large capacitance. The large capacitance seen at the transistor's base is a result of the collector-emitter capacitance reflected back to the base, increased by the value of  $\beta$  (Miller effect). As the current gain increases the input capacitance also increases; photodarlington are several times slower than phototransistors. A second drawback in using phototransistors is that  $\beta$  is not linear and is dependent on the collector to emitter voltage, base drive, and temperature. The value  $\beta$  is also variable from device to device. One additional drawback to using them is that there are a limited number of packaging styles available. [26, 27]



**Figure 2-13: Phototransistor current flow without light (left) and with light (right).** [26]

## Chapter 3: Underwater optical communication research literature review

### 3.1 Attenuation of optical signals in water

The greatest challenge in designing a free space underwater optical communications system is the high attenuation imposed on the optical signal by the water medium. Two components of attenuation in water are; beam attenuation and diffuse light attenuation. [28] Factors such as the salinity of the water, water depth, time of day, turbulence, amount of organic and inorganic materials, and surface reflections all impact the amount of attenuation limiting light's propagation capability. [29, 30] To the extent that these factors attenuate light is wavelength dependent.

Beam attenuation occurs by way of two contributors, absorption and scattering as illustrated in figure 3.1. Beam loss is mathematically expressed by equation 3-1. A coefficient value “c” is used to characterize the beam loss due to absorption and scattering,

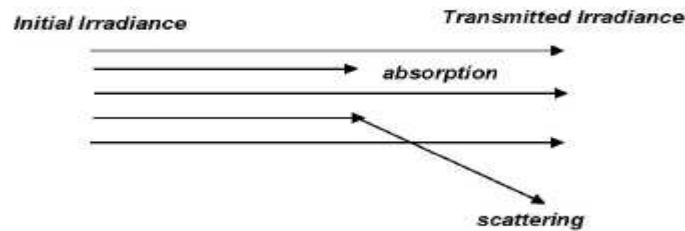


Figure 3.1: Beam attenuation [28]

$$I_t = I_0 e^{-cz}$$

Equation 3-

1

Where:

- $I_t$  - transmitted irradiance
- $I_0$  - original light irradiance (watts/m<sup>2</sup>)
- $z$  - path length
- $c$  - beam attenuation coefficient (dependent of water condition and wavelength – units of m<sup>-1</sup> or per meter)

The second component of light attenuation in water, diffuse attenuation, is a result of back scattering and absorption. It too is dependent on the light wavelength and how it interacts with the water characteristics. Diffusion attenuation is mathematically expressed by equation 3-2. The coefficient value “K” is used to characterize the beam loss due to absorption and scattering and takes into account wavelength and water type. The value of  $c$  is approximately three times the value of  $K$ .



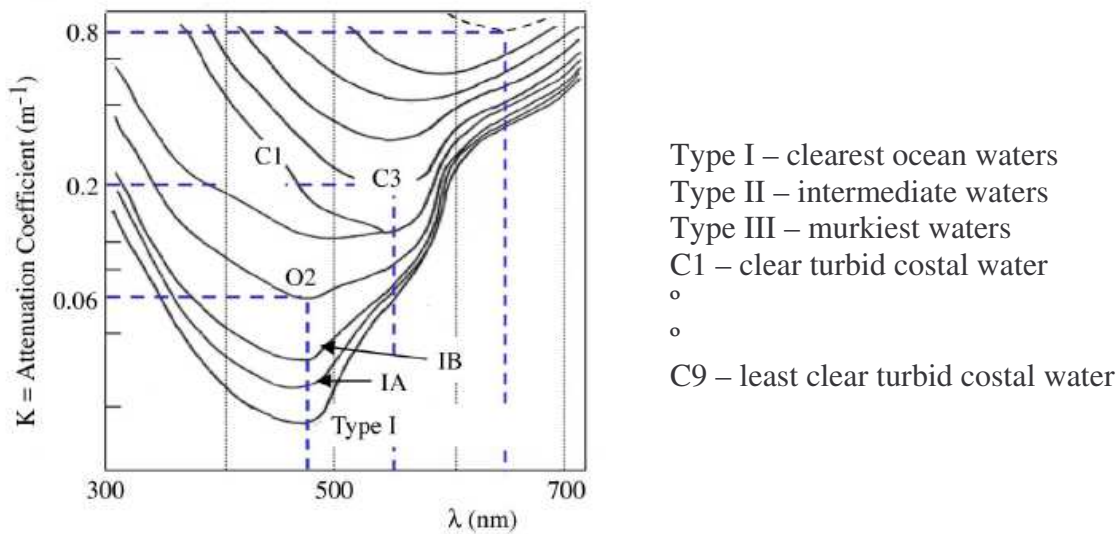
$$I_t = I_o e^{-Kz} \tag{Equation 3-2}$$

2

Where:

- $I_t$  - transmitted irradiance
- $I_o$  - original light irradiance (watts/m<sup>2</sup>)
- $z$  - path length
- $K$  - diffusion attenuation coefficient (dependent of water condition and wavelength – units m<sup>-1</sup>)

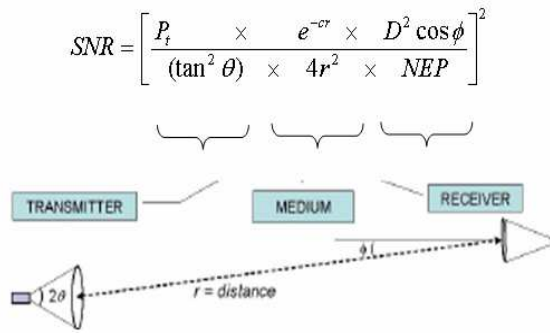
The oceanographic community has classified ocean waters based on their water clarity and colour, which is affected by the concentrations of materials (effluents, dissolved organic matter, sediments, and biologic species) in it. A classification system, referred to as Jerlov water types, developed in the 1950s, is used. Sets of curves have been developed that correlate diffuse light attenuation coefficient  $K$  to wavelength and water type. Figure 3-2 shows the Jerlov Ocean  $K$  spectra. [28, 29, 30]



**Figure 3.2: Jerlov Ocean K Spectra.** [30]

As can be seen in figure 3.2, Jerlov clear ocean water Types 1, 1A, and 1B offer the least amount of attenuation to visible light at wavelengths near 475nm (blue). For coastal waters, least amount of attenuation occurs for wavelengths near 530nm (green).

Giles and Bankman [28] have modeled LOS underwater communications and relate SNR to the value of the attenuation coefficient as is shown in figure 3.3 and expressed in equation 3-3.



### Equation 3-3

$P_t$  = transmit power  
 $c = 3K$  – attenuation coefficient  
 $D$  = receiver aperture diameter  
 $\phi$  = angle between the optical axis of the receiver and the line-of sight between transmitter and receiver  
 $\theta$  = half angle transmitter beam width  
 $r$  = communications range  
 $NEP$  = noise equivalent power

**Figure 3.3: Underwater communications model [28]**

As can be seen by equation 3-3, to achieve a good SNR and therefore ability to communicate at higher bit rates, as per Shannon’s capacity (equation 3-4), the transmitter’s power must be high, the attenuation coefficient  $K$  small, receiver aperture diameter large, and direct LOS between the transmitter and receiver. In addition, the distance  $r$  needs to be short, and NEP needs to be small.

$$BR = BW \log_2(1 + SNR)$$

### Equation 3-4

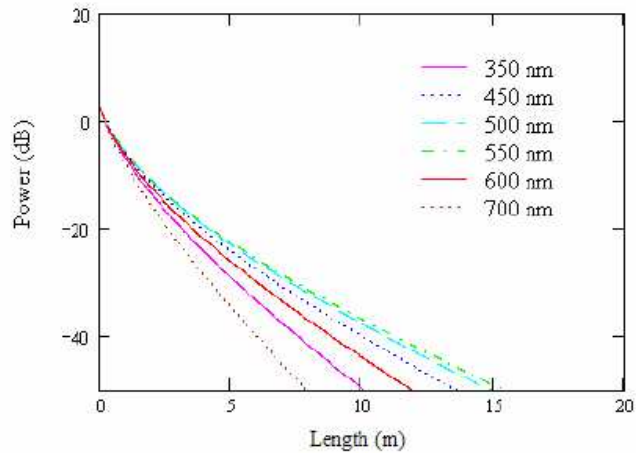
4

Where:

$BR$  – bit rate (bits/sec)

$BW$  – Bandwidth (Hz)

Clancy, in his thesis work [29] – has expanded the simplified attenuation coefficient expression of 3-1, to a more detailed mathematical model that specifies absorption by pure seawater, absorption by Chlorophyll, absorption by colour dissolved organic matter, scattering by pure seawater, scattering by small and large particles, and beam spread effects. From this detailed mathematical analysis, he has generated a graph of power loss over distance in Type II water, based on varying wavelengths of a 1W LED source. This is presented in figure 3.4.



**Figure 3.4 Predicted power loss in Type II water with particulate, CDOM, chlorophyll, and scattering using 1W LED source [29]**

From the graphs of figure 3.4, a loss of 40dB could be expected for blue light at an approximate distance of 10 meters. In clearer type I waters the distance will be further. Clancy does not identify the LED's beam angle value used in generating the graph. For comparison purposes, he also predicted losses for a 1W laser source; for a loss of 40dB, he predicts a distance of about 55 meters. The underwater experiments that were reviewed for this project, including Clancy's own work, concur with the predictions of high loss over a relatively short distance when using non-coherent light sources underwater.

### **3.2 Review of underwater optical communication using LED(s) for light source.**

Of the several underwater optical communications experiments reviewed, three will be discussed. The three were picked based on how they adapted current technology to the solution, their methodology for measuring the performance, and final outcome.

#### **3.2.1 Clancy's master's thesis [29] – adaptation of RONJA (reasonable optical near joint access) design for underwater use.**

Developed in the Czech Republic, RONJA is a free space optical data communications system designed to provide LOS communications at 10 M b/s in air. The transceivers would typically be mounted on buildings. They use high intensity LEDs, and optical lenses to collimate the beam at the transmit side and to capture light at the receive end. Their design is reported to achieve up to 1.4 km distance.

As part of the experimental phase of his thesis work, Clancy used the circuit designs of the RONJA for the transmitter, receiver, and computer interface. These were adapted and placed into an underwater casing. The primary modification made to the transmitter was to replace the high intensity red LED used for air communications with a cyan LED

(505nm). In addition, the circuit was placed in a waterproof container (4" diameter ABS tubing) with single-sided convex 4" lens. The receiver uses Vishay's BPW43 high speed PIN photodiode, with surface area  $0.78\text{mm}^2$  to a discrete MOSFET input amplifier. The receiver packaging also included a convex 4" lens.

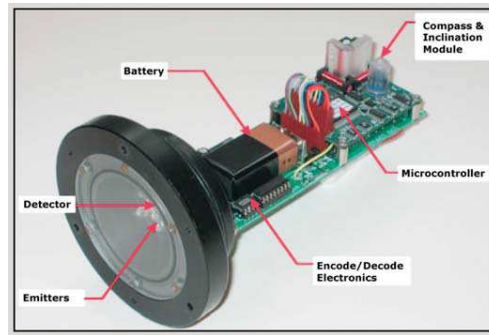
The water testing consisted of placing the transmitter and receiver into 20 gallon aquarium tanks separated apart by air. Clancy was successful in communicating up to 40 feet of distance, but he did encounter difficulty with lining up the transmitter to the receiver so as to capture the very tight collimated beam. However, the photographs show that the transmitter and receiver were placed close to the glass wall of their tanks, such that the light travel distance in water was quite short – most of the travel was in air.

### **3.2.2 Woods Hole Oceanographic Institution (WHOI) low power, low cost, underwater optical transceiver**

Tivey, Fucile, and Sichel, [31] in 2004 published the results of their work to build a low power, low cost, underwater optical communication system. The transceiver design is shown in figure 3.5. In their design approach, rather than using a single high brightness LED, they used an array of 22 standard LEDs. The receiver optical detector is a PIN photodetector with an active area of  $42\text{mm}^2$ , with a "small" Fresnel lens in front to capture light. For the data signal, they used IrDA protocol and asynchronous serial communication, at a rate of 14.4kb/s.

The underwater testing was performed in seawater. However, both the transmitter and receiver were mounted to a metal rail to ensure they were optically aligned. The whole system was submerged into the water to a depth not reported, (the photographs suggest close to the surface). As part of their testing, they used Red LEDs and Blue LEDs. The results achieved are very interesting.

100% communication was achieved at a distance of 2.7 meters with red LEDs, but only 1.5 meters for blue LEDs. The limit of communication distance was 3.7 meters for red and 3 meters for blue. In the discussion of results it is suggested that at close range, because of the PIN photodiodes spectral response peaks at the red wavelength, the loss encountered by the red signal in water for the relatively short distance was made up for by the higher sensitivity of the detector at the red wavelength. Although the blue wavelength is attenuated less, the sensitivity of the detector at this wavelength is quite low. The authors did conclude that as distance increases, the blue wavelength would perform better than red.



**Figure 3.5 Optical communications transceiver developed at WHOI [31]**

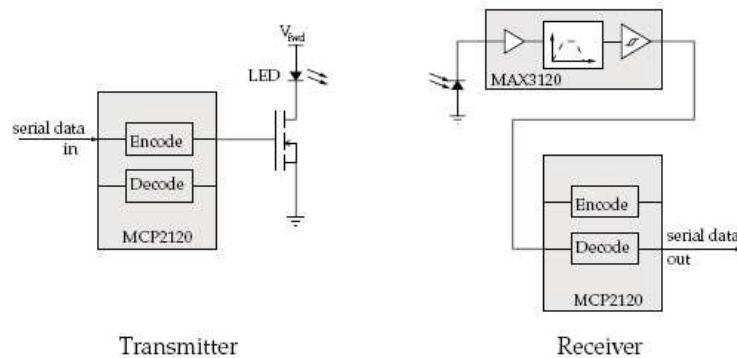
To achieve greater distance, requires more light intensity. The designers of this transceiver, predicted, that they could populate 320 standard LEDs onto the surface area of a circle with 5” diameter. With this number of LEDs they estimated a communication distance of 5 meters.

### **3.2.3 Australian National University - underwater optical transceiver using IRDA Integrated Circuits (ICs)**

Schill, Zimmer, and Trumpf [32] set as a goal, to design an optical transceiver for use in small autonomous submersibles, for “inter-swarm” communication. The design criteria included high data rate, which they identified as a minimum 57kb/s, distance or more than one meter, omnidirectional coverage (using several transceivers), small size, and low cost, and simplicity in design. To achieve their goals the designers made the following decisions:

1. Used Luxeon III LEDs – they tested blue (460nm), cyan (490nm), and green (520nm)
2. Used IrDA physical layer protocol and standard IrDA encoder/decoder ICs manufactured by Microchip
3. Selected Infrared Rejection Filter Planar photodiode SLD-70 BG2A, with active area size  $9.8\text{mm}^2$

Figure 3.6 shows the simple circuit design as a result of using the encoder/decoder ICs.



**Figure 3.6 Block/circuit diagram of IrDA transceiver [32]**

In packaging this unit, no additional lenses were added. The LED package/lens made direct contact with water. The photodiode has a clear epoxy dome lens which was placed perpendicular to the transparent perspex box's floor.

The measurement phase included two sets of tests, in air, and submerged in clear fresh water (round pool). In air, the cyan led source produced the best result and a distance of 2 meter was achieved within a cone of 120 degrees at the source LED. In water, they achieved a distance of 1.7 meters, limited by the pools size with slightly better results from the cyan LED. The designers, in assessing why the water results appeared as good as the air results, make the following observations:

1. Clear water attenuation in fresh water is very low
2. Light from the LED was reflected off the white pool sides, increasing the light intensity received
3. As the experiment was conducted outdoor, less electrical interference/noise, and the water also helps to insulate the transmitter/receiver from electrical interference

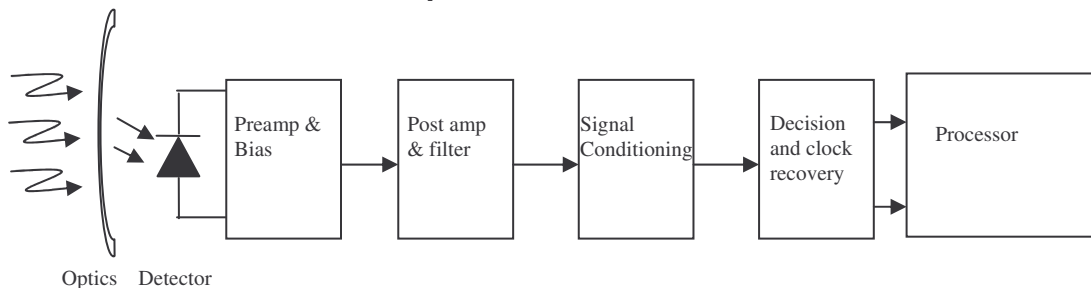
Although this approach did not achieve significant distance for underwater communications, its adaptation of the IrDA ICs, resulting in a very simple circuit solution and consuming low power, is admired.

## Chapter 4: Optical receiver design for using photodiodes

Designers of optical free-space communications must consider a number of issues such as the best wavelength to use; how divergent the transmitted optical beam pattern needs to be, what minimum power can be received to recover the transmitted signal above inherent receiver noise, the required and/or maximum signal rate of change needs or that can be achieved, what the best encoding technique at the transmit side should be used and how to recover the data from the signal at the receiver side, what the safe operating limits are, and how to package it. For this project, the front end of the receiver is investigated keeping in mind its use in an underwater mote application.

The criteria used for the optical receiver design for this project is based on achieving higher data rates over reasonable distances underwater, compared with the capability of underwater acoustic motes and comparable to that of terrestrial motes. Only on-off-keying (OOK) was used as the transmission source for this project so as to keep the optical transmitter circuit simple. Based primarily on the limitations of the transmitter, a maximum frequency limit of 100-150 kHz for the OOK pulses was established; most measurements were conducted at 40kHz. Although the frequency is lower than first envisioned for this project, the rate exceeds acoustic and longwave mote abilities, and is on par with the terrestrial motes discussed in the introduction. It also anticipated that this rate should be sufficient to carry the data generated by a mote as it samples its sensors. In addition, because the frequency is lower, larger PIN photodiode capacitance is acceptable which allows for larger active area photodiodes to be used and they can be operated in their photovoltaic mode to keep noise at a minimum. An added benefit to keeping to photovoltaic mode is that it provides the added benefit of not having to address the complexity of high voltage reverse biasing.

### 4.1 Overview of receiver components



**Figure 4.1: Block diagram of an optical receiver.** [33, 34, 35]

#### 4.1.1 Optics

The block diagram of figure 4.1 identifies typical sections of an optical receiver. The first component is the receiving optics or light collector. To achieve any significant distance from the transmitter, a receiver lens is critical. It captures and focuses the received light onto the active area of the detector and can result in significant gains in the received signal level, overcoming signal noise, for no cost in power consumption. It is also possible for the optics to be constructed wavelength selective as done often with infrared receivers which are visible light filtered. However, optical filtering will reduce the amount of transmitted signal to the detector besides blocking of the undesired wavelengths. Many photodiodes are manufactured with a lens as part of the package and defines the detectors' acceptance angle (or field of view). For short range communications, the addition of a lens beyond the photodiode's own lens is not required.

For long distance communications, Fresnel lenses may be chosen, based on their light collection ability rather than image clarity. Fresnel lenses offer large lens area and short focal lengths, and can be constructed with light weight materials (i.e. acrylic); they are also low cost compared with traditional lenses. In setting a record distance of 173.33 km for through air optical communications using a red LED source and PIN photodetector, a Fresnel lens having dimensions of 250mm x 318 mm with focal distance 318mm and a second lens with dimensions 404mm x 430mm with focal length of 229mm were used.[36]

The penalty for using large lenses is small acceptance angles. Johnson suggests as a rule-of-thumb, that a lens diameter "should not be more than 100 times larger than diameter of the active area of the PIN detector." [33] He further cautions about exposing a PIN detector with lens to bright light as it might damage the detector. The Fresnel lens used in this project had an area size greater than the rule-of-thumb and small acceptance angle was observed (value not recorded).

#### **4.1.2 Photodetector**

For optical communication in the visible to infrared wavelengths and for high data rates, the practical choices are PIN photodiodes and APDs. Although APDs offer gain, they require high reverse bias voltage, need cooling to reduce noise current, and cost substantially more than PIN Photodiodes. For high data rates, the PIN photodiode is operated in photoconductive mode; its reverse bias voltage is dependent on the maximum junction capacitance that can be allowed for the required data rate and within its operational maximum value. In photoconductive mode, PIN photodiodes are noisier; this noise can be reduced by cooling. For low data rates applications, where larger junction capacitance is not a concern, but detection of low light level is paramount, photovoltaic mode of operation presents the best solution. In addition, the larger the active area the more sensitive the detector is to light, but capacitance also increases.

#### **4.1.3 Preamplifier block**



The preamplifier section defines the receiver's ability to recover low light signal. In general, the following are required of the first stage [35]:

- Keep noise that it contributes to a minimum
- Frequency response wide enough to minimize distortion of the received signal's shape
- Able to handle a large variation in received optical power and still recover the signal
- PIN photodiodes and APDs, because they are current devices, are high impedance sources, which requires that the first stage amplifier should also have a high impedance input

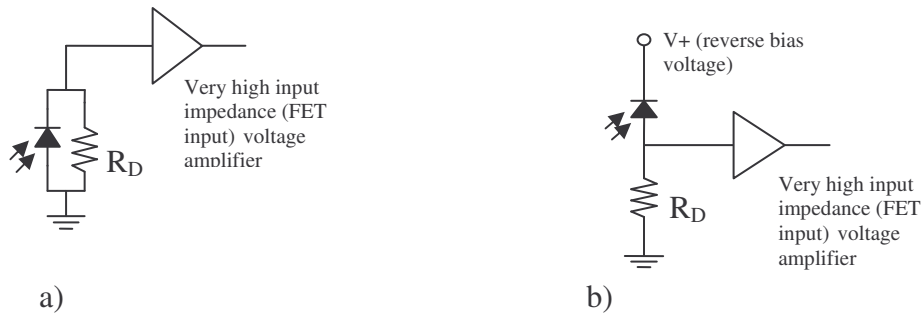
Two basic methods of converting the photodetector's current to a voltage level so that the signal can be further processed are high-impedance or integrating front end and transimpedance amplifier (TIA) front end.

The high-impedance front end approach converts the photodiode current directly to voltage by means of a high resistance load. The voltage developed across the load resistor is then amplified by a voltage amplifier. To minimize loading effect on the high resistance load, the voltage amplifier used must also have very high input impedance; typically discrete FET or "FET input" op amps are used. Two circuit scenarios, photovoltaic and photoconductive, of this arrangement are shown in figure 4.2.

This approach suffers two major weaknesses. First, frequency response is reduced due to the high-impedance /junction capacitance combination. The photodiode's junction capacitance and shunt resistance and the parallel load resistance form a low-pass RC filter. The upper cutoff frequency (if not limited by the voltage amplifier), is determined

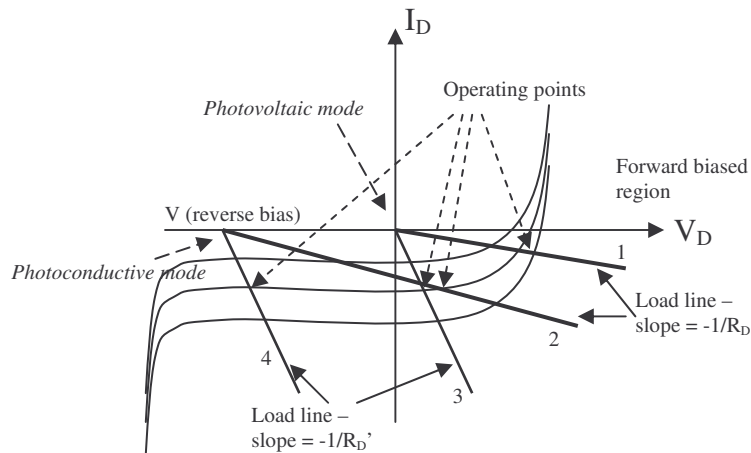
by  $f_c = \frac{1}{2\pi RC}$  therefore, the larger the resistance, the lower the cutoff frequency.

Lowering  $C$  extends the corner frequency. If the signal we are trying to recover is that of a pulse or rectangular waveform, and we are required to reproduce it in its original form we should recover as many harmonics as possible; allowing for ten or more harmonics will provide a good result. Depending on how the recovered wave is dealt with in the next block of the receiver, lower bandwidth may be acceptable (i.e. allowing for three harmonics). If the frequencies we are recovering are in the roll-off portion of the filter's response, the signal will be integrated due to the capacitor's  $IV$  characteristic. For this reason, the high-impedance approach is sometimes referred to as an integrating front end. [35]



**Figure 4.2: Using voltage gain amplifier scenario** – light converted to current develops voltage across  $R_D$  which is then amplified a) Photovoltaic mode; b) Photoconductive mode.

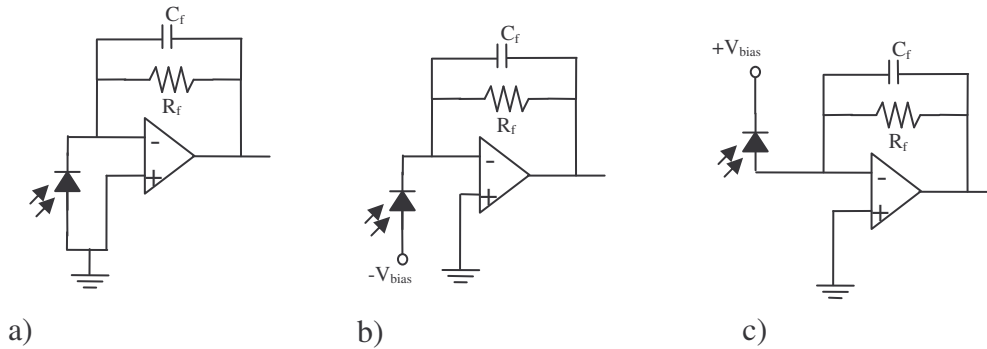
The second major concern, using high-impedance front end, is that the voltage drop developed across the resistance used to recover the signal. Current that results from ambient light, creates a DC voltage across the resistor which is also across the photodiode. The voltage drop may be sufficiently high enough to forward bias the diode as demonstrated in figure 4.3. The operating points are a result of ambient light level. For load line 1, representative of a higher  $R_D$  resistance, a change in current  $I_D$  due to incoming optical signal results in non-linear change in the diode voltage and a smaller range of operation.  $R_D'$ , its value less than  $R_D$  demonstrates less gain, but more linear response and greater range of  $I_D$  current can occur, particularly if the diode is reversed biased.



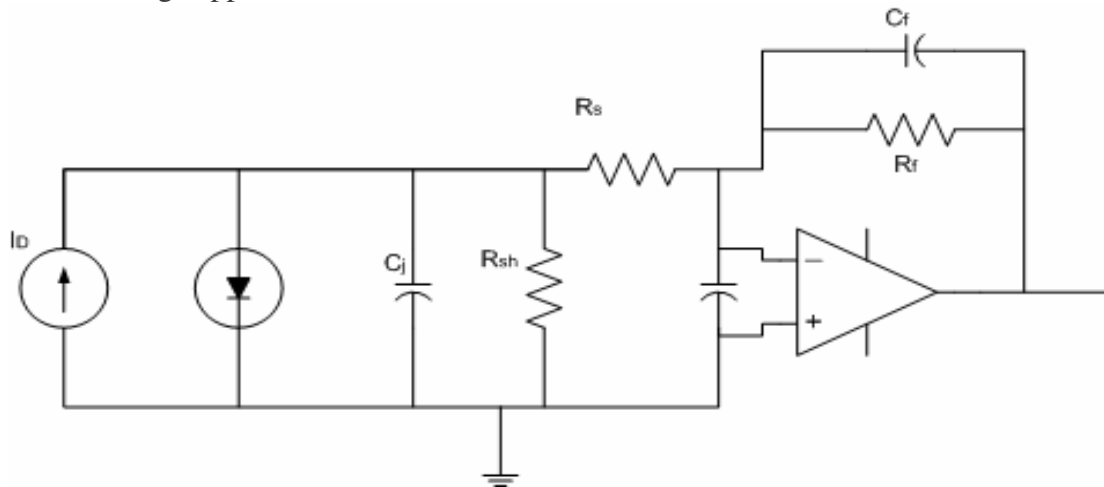
**Figure 4.3: High impedance current to voltage operating points for two values of  $R_D$  where  $R_D' < R_D$ .** [15]

The second preamp stage approach to convert a photodiode's current into a usable voltage and is the most often used approach in optical communications receivers, is the TIA. Figure 4.4 shows three connection scenarios, photovoltaic mode, and two photoconductive mode setups. The major advantage of the TIA is the op-amps characteristic, because of its very high open loop gain, that results in virtually zero volts

between the positive and negative input terminals. To the photodiode, this connectivity looks essentially as a short, so that the load line slope is infinite.



**Figure 4.4: Transimpedance amplifier configurations** a) photovoltaic mode b) photoconductive mode with negative voltage applied c) photoconductive mode with positive voltage applied



**Figure 4.5: Equivalent circuit of photodiode connected to transimpedance amp**

Figure 4.5 shows the equivalent photodiode circuit from which equations that are used in implementing this approach are derived. The feedback resistor  $R_f$  defines the TIA gain as shown in equation 4-1. The equation is derived assuming the op-amp is ideal and frequencies are low enough that capacitor reactance is not in play.

$$TIA \text{ gain} = \frac{V_{out}}{I_D} = R_f \quad \text{Equation 4-1}$$

In addition, equation 4-1 holds true if  $R_f$  is much lower than  $R_{sh}$ . If  $R_f$  is greater than  $R_{sh}$ , then the amplifier's input noise voltage and offset voltage will be amplified by

$$\left(1 + \frac{R_f}{R_{sh}}\right) \text{ and will be added to the output voltage of } I_D R_f.$$

Practical amplifiers do not have unlimited bandwidth. Their op amp's bandwidth limit plus the effects of the components associated with it, diode junction capacitance  $C_j$ ,

feedback capacitance  $C_f$ , and input capacitance of the op-amp, limit high frequency operation.

As with all op amp circuits, the larger the closed-loop gain the lower operational bandwidth; as  $R_f$  increases, bandwidth decreases. If large gain is required, but the resulting operating bandwidth due to  $R_f$  is insufficient, the designer has two choices: reduce the value of  $R_f$  to extend the bandwidth and then use a second stage amplifier for additional gain and/or obtain an amplifier with a greater Gain Bandwidth product (GBW). Equation 4-2 is used to determine the operational bandwidth for the TIA.

$$C_T = C_j + C_{cm} + C_{dm}$$

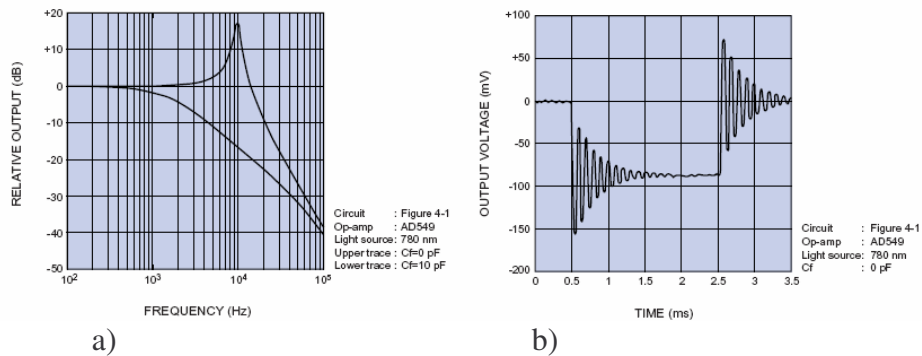
$$f_{hc} = \sqrt{\frac{GBW}{2\pi R_f C_T}} \text{ Hz}$$

**Equation 4-2**

Where:

- GBW - TIA's gain bandwidth product
- $C_{cm}$  - Common-mode input capacitance of the op-amp
- $C_{dm}$  - Differential-mode input capacitance
- $f_{hc}$  - -3dB high frequency corner

The feedback capacitance  $C_f$  is generally used to compensate for a phenomena referred to as gain peaking as shown in figure 4.6. Gain peaking occurs when the resulting impedance of the input with larger capacitance interplays with the impedance of the feedback network with smaller capacitance at high frequency, creating gain. In addition, phase shifts of the input and feedback RC networks may create more than 180 degree phase shift, resulting in positive feedback. This can result in oscillation (ringing) and an increase in noise.



**Figure 4.6: Gain peaking phenomena** a) frequency response showing gain peaking b) effect of gain peaking on transitions of a rectangular waveform. [16]

Having smaller input capacitance (photodiode with reverse bias and/or small active area), and/or using an amplifier with greater GBW, will lessen gain peaking. To fully control gain peaking the designer can add small capacitance  $C_f$  to the feedback network which combines with the amplifiers roll-off rate to creates a 2<sup>nd</sup> order roll-off response. Equation 4-3 is used to calculate  $C_f$ . This equation places the  $C_f R_f$  corner frequency such

that it combines with the amplifiers corner frequency to achieve a maximally flat 2<sup>nd</sup>-order Butterworth frequency response. [16, 38] The actual value used for  $C_f$ , may require tweaking, due to parasitic capacitance from the printed circuit board layout and type of resistor(s) used (typically 0.2pF for a surface-mount resistor). Parasitic capacitance attributed to the feedback resistor can be reduced by using two or more resistors in series to make up the value of  $R_f$ . The designer may wish to increase the value of  $C_f$  so as to purposely set the frequency corner lower than that of the amplifier's corner frequency, reducing bandwidth to reduces noise.

$$\frac{1}{2\pi R_f (C_f + C_{stray})} = \sqrt{\frac{GBW}{4\pi R_f C_T}} \quad \text{Equation 4-3}$$

( $C_T$  – see equation 4-2)

Current noise is a combination of shot noise, thermal noise, and ambient light noise, plus thermal noise from the feedback resistor  $R_f$ . There is also additional noise added by the op-amp circuit, both current and voltage. As simple as the TIA solution looks, performing noise analysis on the circuit is challenging. Figure 4.7 shows the noise analysis model for photodiode TIA

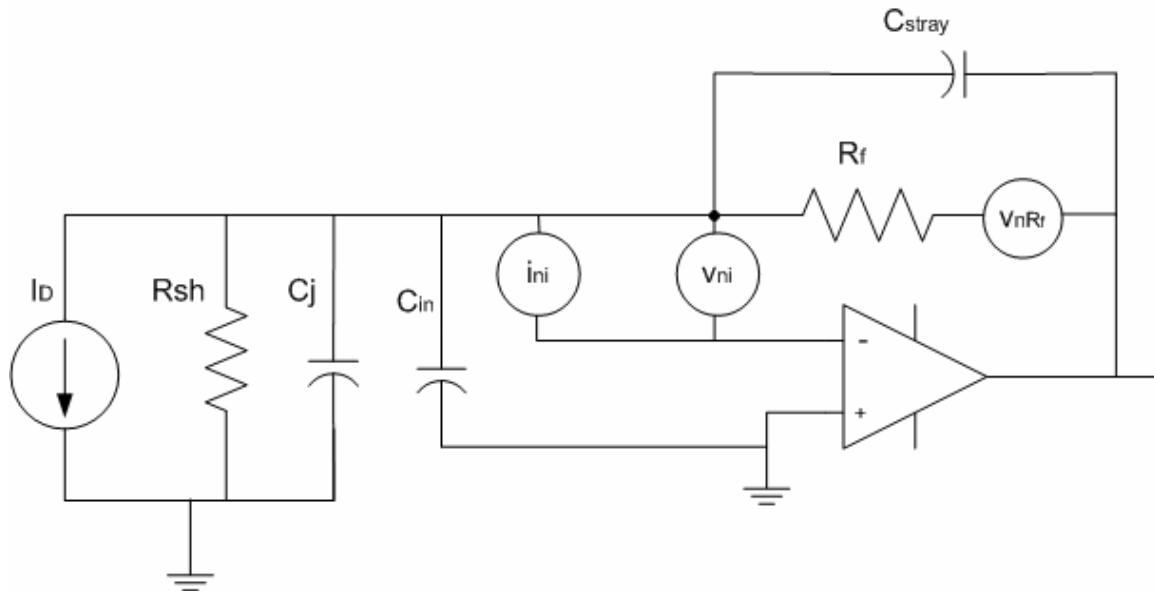


Figure 4.7: Noise analysis model of the basic photodiode TIA combination. [15]

With reference to figure 4.7 the following is derived:

The output voltage for the amplifier is:

$$V_{out} = I_D R_f + v_{no} \quad \text{Equation 4-4}$$

Where

$v_{no}$  - voltage noise spectral density – a function of frequency

$$v_{no} = \sqrt{(v_{noRf})^2 + (v_{noi})^2 + (v_{nov})^2} \quad \text{Equation 4-5}$$

Where

$v_{noRf}$  - output voltage noise spectral density equals the spectral noise density contributed by  $R_f$

$$v_{noRf} = \sqrt{4kTR_f} = v_{noRf}$$

(k – Boltzman’s constant, T – degrees Kelvin)

$v_{noi}$  - shot noise contributed by amp’s input current  $I_{B-}$  with spectral density of  $i_{ni} = \sqrt{2qI_{B-}}$  (q – electron charge) converted to voltage spectral density is:  $v_{noi} = R_f \sqrt{2qI_{B-}}$

$v_{nov}$  - this component of the output noise is the op-amps voltage noise spectral density affected by the capacitance and frequency (expression shown is the s-domain expression)

$$v_{nov} = \frac{(1 + R_f (C_D + C_{in})s)}{(1 + R_f C_{stray}s)} v_{ni}$$

Once  $v_{no}$  is determined and as this value is a function of frequency, further rms analysis is required to determine total output noise. [15] As noise was not evaluated in the experimental phase of this project the additional rms analysis is not presented.

JFET amplifiers have low current noise and bipolar amplifiers have lower voltage noise. Reducing both parameters within the same package is difficult. [37] Manufactures are creating new designs to create low noise op-amps specifically for TIA applications. It is also essential, that the amplifier used has very small input bias current as this current will be increased by a factor of  $R_f$  at the output. A larger input bias current could cause the output of the amplifier to saturate to the amplifier’s biasing voltage.

The following is an example for calculating the values  $R_f$  and  $C_f$  using Burr Brown’s TIA OPA380, and API’s PIN photodiode SD 100-12-22-021. The design requirement is to obtain a maximum TIA gain for an input rectangular pulse signal at 40kHz.

Frequency bandwidth should be  $\approx 10 \cdot 40k = 400kHz$

Specs for PIN photodiode:

$$C_j = 87pF \text{ at } V_R = 0V \text{ (photovoltaic mode)}$$

Specs for OPA380:

$$GBW = 90MHz$$

$$C_{cm} = 3pF$$

$$C_{dm} = 1.1pF$$

Using equation 4-2:

$$C_T = C_j + C_{cm} + C_{dm} = 91.1 pF$$

$$R_f = \frac{GBW}{2\pi f_{hc}^2 C_T} = \frac{90 \times 10^6}{2\pi (400 \times 10^3)^2 \cdot 91.1 \times 10^{-12}} = 983 k\Omega \therefore 1 M\Omega$$

Using equation 4-3:

$$C_f = \frac{1}{2\pi R_f \sqrt{\frac{GBW}{4\pi R_f C_T}}} - C_{stray}$$

$$= \frac{1}{2\pi \cdot 1 \times 10^6 \sqrt{\frac{90 \times 10^6}{4\pi \cdot 1 \times 10^6 \cdot 91.1 \times 10^{-12}}}} - 0.2 \times 10^{-12}$$

$$= 0.37 pF$$

As can be seen by the example calculations, the value of  $C_f$  is typically quite small and generally no more than a few picofarads unless one is deliberately reducing the high corner cutoff frequency.

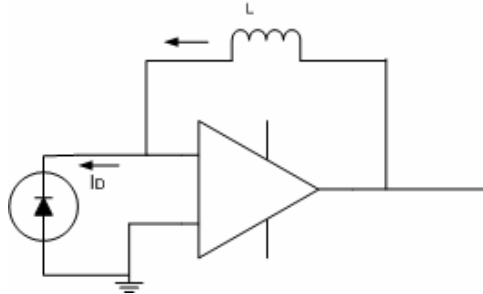
The previous discussion is based on the assumption that the designer wants a wideband linear preamp solution. Other alternatives include:

- Using a logarithmic amplifier rather than linear amp – provides high gain for low signals and its gain reduces as signal strength increases
- Using inductance in the feedback path of the TIA.

The use of a logarithmic amplifier provides for a large dynamic range of incoming optical power, but amplification is non linear. If the user is interested in only recovering signal transitions and not accurately reproducing the incoming waveform, then this approach may be attractive. However, manufactures of newer TIA amps have reduced the need for logarithmic amplifiers. Burr-Brown's OPA350 TIA, used in the previous sample calculations states in its data sheet:

As a result of the high precision and low-noise characteristics of the OPA380, a dynamic range of 4 to 5 decades can be achieved. For example, this capability allows the measurement of the signal currents on the order of 1nA, and up to 100uA in a single I/V conversion stage. In contrast to logarithmic amplifiers, the OPA380 provides very wide bandwidth throughout the full dynamic range. [38]

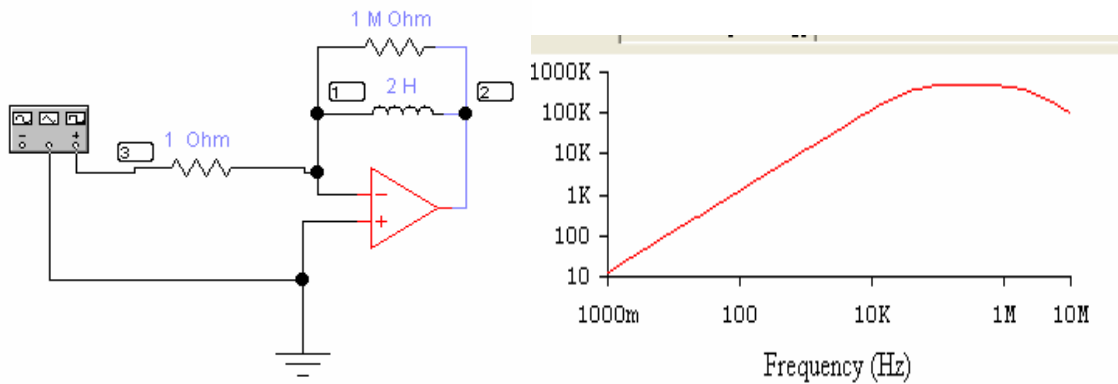
Using an inductor in the feedback path of the TIA, can eliminate DC offset caused by ambient light. Figure 4.8 shows this scenario.



**Figure 4.8: TIA amp with inductive feedback [33]**

If the input optical signal is an intensity modulated sinusoidal waveform, then the inductor will have a reactance  $X_L = 2\pi fL$ . As frequency increases the value of reactance will also increase. The output sinusoidal voltage magnitude will be  $I_D X_L$ . This provides us with a desirable result that at high input frequencies, we get high gain. For DC ambient current, the reactance is  $0\Omega$  thus eliminating the DC component. However, for other than sinusoidal waveforms, the output waveform appearance will be modified as the inductor differentiates the incoming current as it converts it to voltage due to the  $VI$  characteristics of inductors where  $V_L = L \frac{di}{dt}$ .

To mitigate the differentiation, one can place in parallel a large resistor value  $R_f$  to form a high pass filter in the feedback network. Figure 4.9 shows an example configuration and its frequency response. The amplifier model used for the frequency response is an ideal amp. The low corner frequency is calculated as  $f_l = \frac{R_f}{2\pi L} = \frac{1M}{2\pi \cdot 2} = 79.6kHz$ . The maximum impedance gain is  $R_f || (jXL)$ , which will, as frequency gets very high equal  $R_f$ .

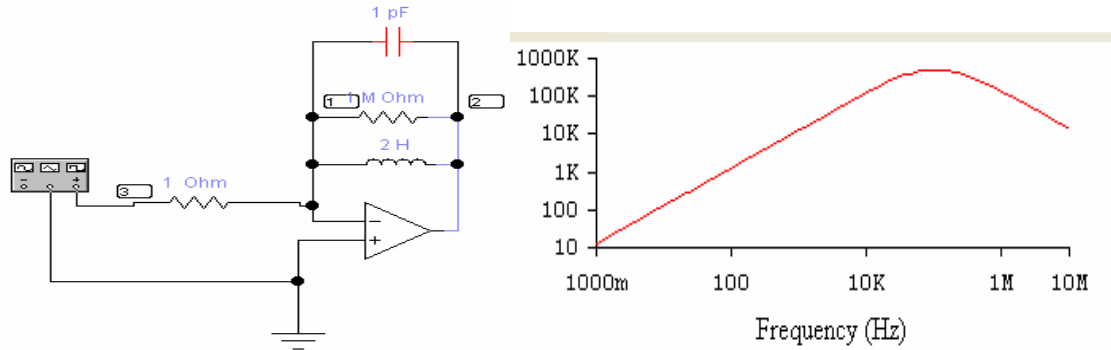


**Figure 4.9: Amplifier with inductance and resistor feedback and its frequency response (using EWB 5.2)**

Although this circuit removes the ambient light current effect at the output of the amplifier, there are two problems with this approach, the size of the inductor value and stray capacitance. An inductor that is 2 Henries (or larger) is physically quite large. To address the large inductance physical properties, a general impedance converter (GIC)



circuit comprising of two op-amps, four resistors and a capacitor can be used to create a 2 H inductance. This was experimented with in this project but with limited success (reported in chapter 5). Stray capacitance that forms in parallel with the RL feedback network creates an LC resonant circuit. Stray capacitance can dramatically change the circuit's behavior, as shown in figure 4.10.



**Figure 4.10: Effect of stray capacitance (1pF) on inductor feedback amp**

#### 4.1.4 Post Amplifier and filter

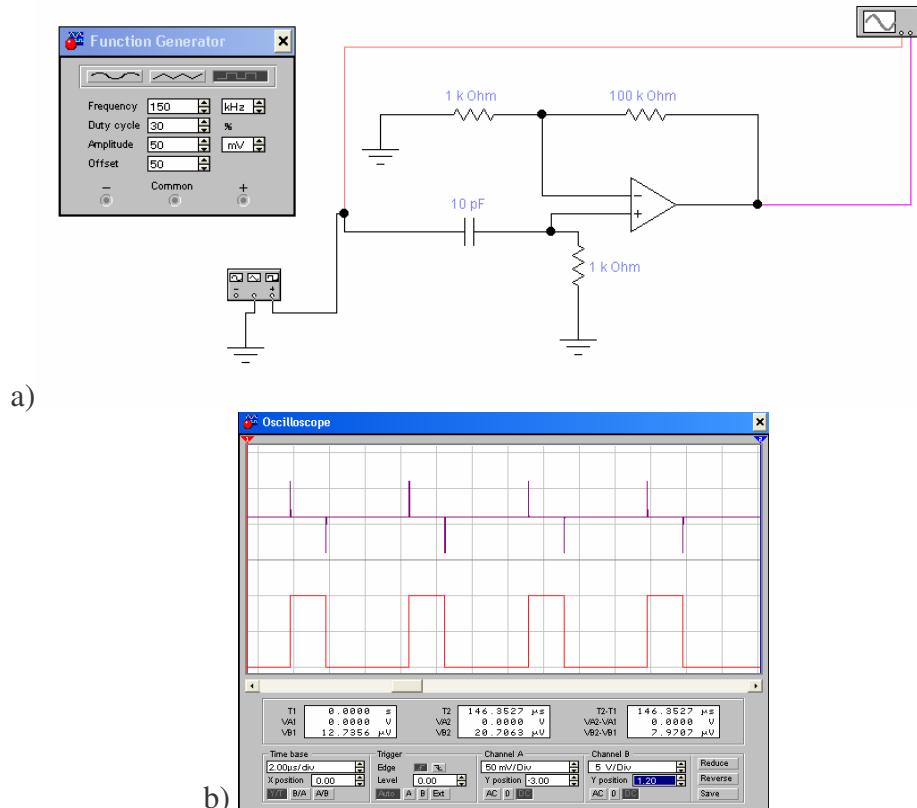
The pre-amp stage may not be able to convert the small photocurrent to a useable voltage level on its own. As discussed earlier, the wider the frequency response required the smaller the pre-amp gain can be. In addition, the preamp may be able to address to some degree the ambient DC current, but in order to further amplify the signal the DC current typically needs to be removed. The post-amp stage can perform both additional gain and low-pass filtering, using as simple a circuit as a single inverting or non-inverting op-amp circuit ac coupled. In addition to filtering low frequencies, the designer may also limit the upper frequency range, to reduce bandwidth so as to keep noise to a minimum. The second stage may also provide a solution to coping with a large dynamic range of optical signal power translated to a wide voltage range. One typical approach is to build an automatic gain control circuit (AGC) as is done by Vishay with their integrated IR receiver modules. [34] An alternative approach to an AGC circuit is to use a limiting amplifier [35] as done for this project; if the input signal (rectangular pulses) is larger than the linear range of the 2<sup>nd</sup> stage amplifier, the amplifier simply saturates at its voltage rails. The penalty for this approach is the time required to come out of saturation, as it switches. However at relatively low frequencies, and by using a very fast slew rate amplifier, this concern is lessened.

#### 4.1.5 Signal conditioning

Depending on the requirements for the recovered signal, additional signal conditioning may be required. Signal conditioning is generally done for wave shaping, for example

sharpening up rise and fall transitions in the case of received pulses, and to lessen/remove noise. One approach that shapes a wave and can reduce noise is integration. Integration of noise over time will average to zero. However, analog integration will also soften pulse transitions (rounding off the corners), and if the input wave being integrated has a long period of average DC value without crossing 0Volts, integration may result in the saturating out the voltage bias rails of an integration amplifier.

Differentiation may be used to provide high gain for both positive going and negative transitions of a pulse waveform as shown in figure 4.11. The output from the differentiator can then be applied to a comparator circuit with hysteresis to generate a very clean pulse output. Differentiation is also very risky. The higher the noise frequency, the more rapid the transitions, which when differentiated are amplified. Therefore, differentiation increases noise. However, if the pulse transitions of interest, after being differentiated, results in higher magnitude pulses than the average differentiated noise, then the comparator can be set to trigger at a level higher than the average noise, resulting in clean noise free pulse at its output.



**Figure 4.11: Differentiation of an incoming pulse train** a) Differentiating circuit b) Input (red – 50mV/div.) and output (violet 5V/div.) waveforms – notice the gain achieved.

#### **4.1.6 Decision and clock recovery**

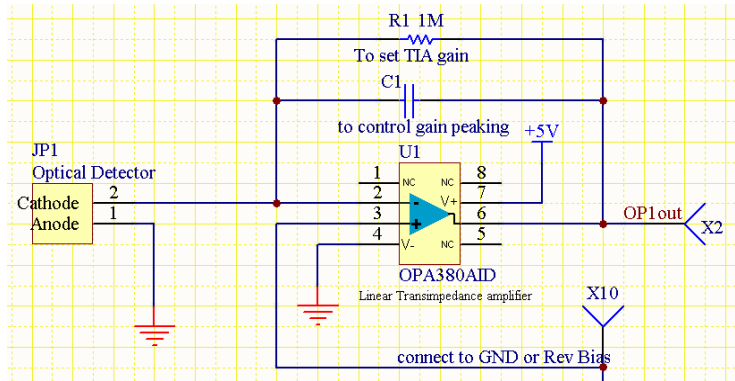
This last stage before forwarding the signal to processing is often the recovery of the clock signal required for the decision circuitry to determine if the received signal is valid data. Recovering clock may be as simple as using a phase locked loop or more complex, involving surface acoustic wave (SAW) filters or dielectric resonators. [35] If the incoming protocol is simple, as used in asynchronous protocol EIA232, then the receiver side may have its own free running clock which synchronizes to a start bit.

#### **4.2 Receiver circuits used for this project:**

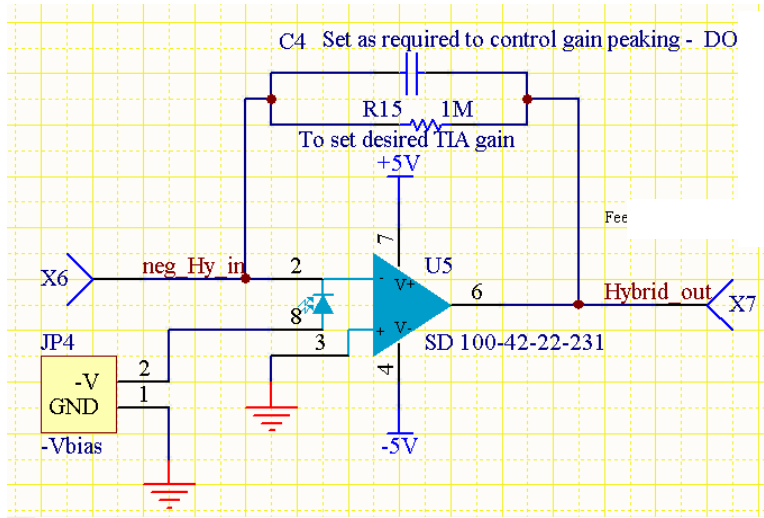
The first phase of the project was to acquire a sampling of PIN photodiodes to test. The diodes were acquired through Digikey and are manufactured by Advanced Photonix, Inc. Although Hamamatsu is a major manufacturer, and has been referenced significantly in this report, it was more difficult to acquire their product. The PIN photodiodes were chosen to provide a range of active surface area and package styles and were, with the exception of one, blue enhanced, providing slightly more sensitivity in the blue/green wavelengths. In addition, one hybrid package was purchased consisting of a TIA (without feedback resistor) and photodiode in one package. Six PIN photodiodes were obtained and ranged in cost from \$3.90 to \$106.63. The most expensive unit is the hybrid package. Chapter 5 contains a table listing their specs for comparison. The datasheets for the photodiodes are available in Appendix C.

Two TIA amplifier designs were constructed, resistor feedback and parallel resistance/inductance feedback. After reviewing several op-amp products, the Burr Brown's OPA380 was chosen because it is specifically engineered for this application with very attractive specs that include wide bandwidth, low noise, very low input current, and has fast slew-rate. The hybrid's own TIA amp has wide bandwidth and high slew rate though less than the OPA380. The third amplifier chosen is Burr Brown's OPA 2613. The OPA 2613 is a dual amplifier package and is general purpose. It has very high bandwidth and fast slew rate but input current is relatively high.

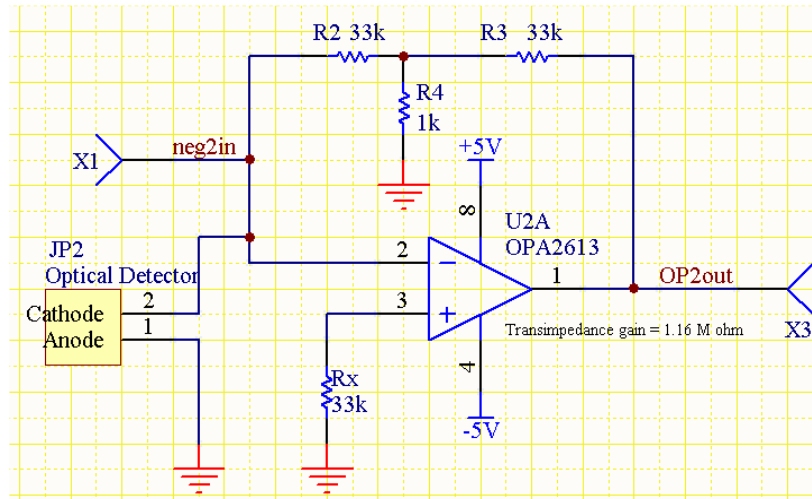
Figure 4.12 shows the TIA circuit designs; circuits a) and b) were designed as per the example calculations presented earlier in this chapter. The circuit of 4.12 c) uses the 2613 and has slightly higher gain using smaller resistance values. The design calculations are shown in Appendix D.



a)



b)



c)

Figure 4.12: Three TIA amplifiers used in evaluations

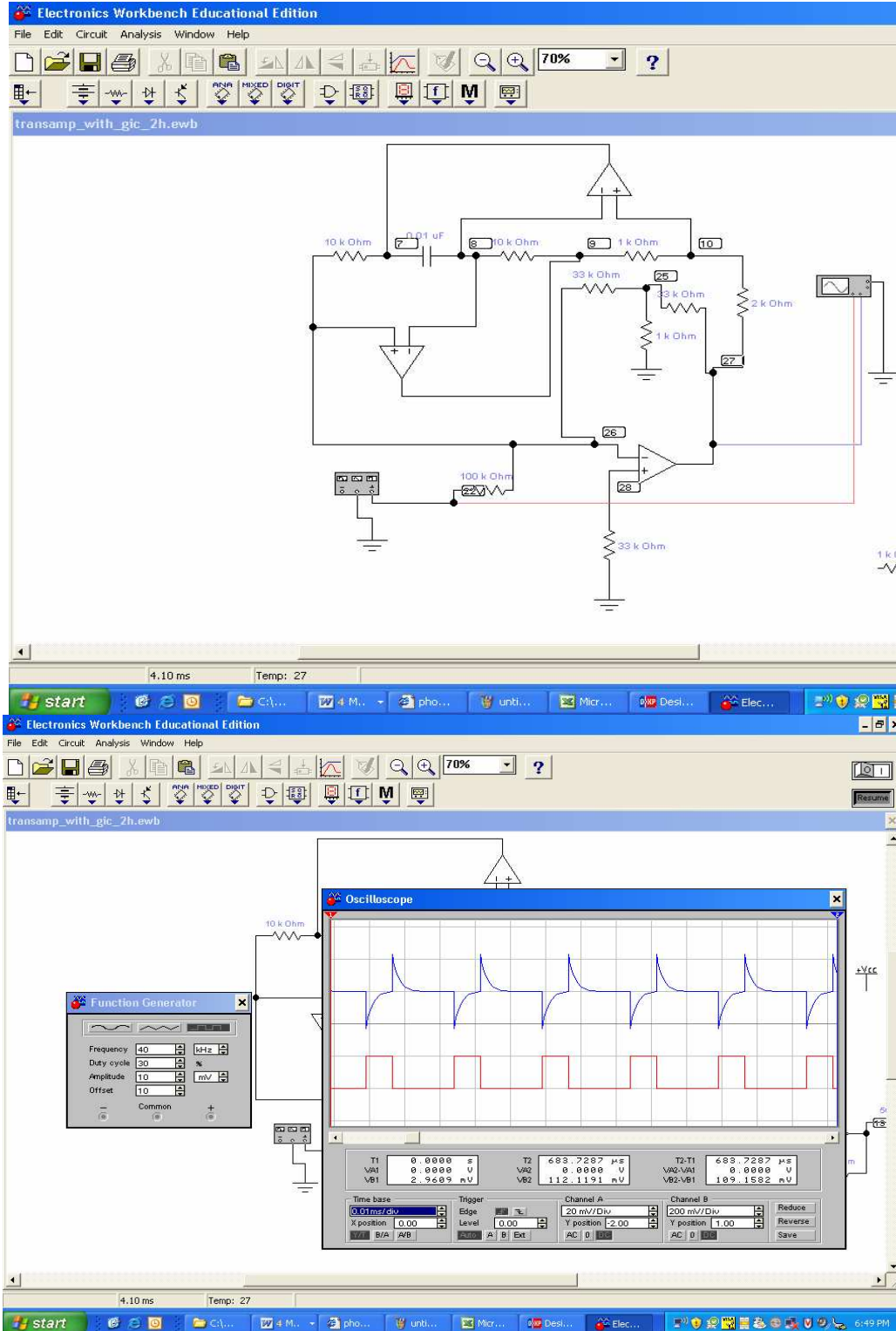
To test the inductor feedback method, a GIC circuit was designed to provide 2 Henries of inductance. Using 2 Henries, in conjunction with  $1M\Omega$ , sets the corner frequency near 80kHz. As a result of this, an incoming rectangular waveform at 40 kHz will be differentiated. This circuit achieves conversion of current to voltage with gain and differentiates at the same time resulting in removal of the ambient light DC level. Figure 4.13 shows the circuit and simulation results obtained using Electronics Workbench 5.2 software (runs over a SPICE engine). The simulation used an ideal model for the op-amp and does not address noise. The test board built allowed the GIC to be applied to the OPA2613 TIA circuit and to the Hybrid's TIA. Because the OPA380 is a single supply (+5V) amplifier, the GIC circuit was not used on it.

The post-amp stage is a simple non-inverting op-amp circuit with variable gain. The input capacitor filters low frequencies and removes the DC level from the input signal. It also allows for a large dynamic range of operation by saturating to its bias voltage rails for larger input signals. The circuit is shown in figure 4.14 and design calculations are shown in Appendix D.

Signal conditioning is facilitated by using a differentiator circuit feeding into a comparator with hysteresis. The output of the comparator circuit swings from the +5V rail to the -5V rail. The negative going portion of the waveform is clamped by a switching diode, and then fed to a Schmitt trigger buffer, to ensure a clean recovered pulse. Figure 4.15 shows the circuit and simulation done with EWB 5.2.

The amplifiers chosen draw more current than desirable. The OPA380 has a quiescent current draw of 6.5mA. Each op-amp in the OPA2613 package draws approximately 6mA. Although not extensively searched, in general the low-power op-amps were slower and had less bandwidth than the devices used in this project.

The complete circuit diagram and component layout is found in Appendix E. All components used, with the exception of the photodiodes, are surface mount. The circuit built includes switches so as to connect/disconnect the GIC circuit, the non-inverting amplifier, and the simple differentiator. In addition, as it was originally intended to do experiments in water, a 9V to 5V regulator using a LM317 was added. A 5V to -5V charge pump was also intended for the design, but was unable to supply the current drawn by the op-amp circuits and was removed from the board. Figure 4.16 shows a picture of the test circuit built.



**Figure 4.13: GIC circuit** – designed to replicate an inductance of 2H, applied to feedback of TIA amplifier; simulation result - Red waveform is the input, Blue the output.

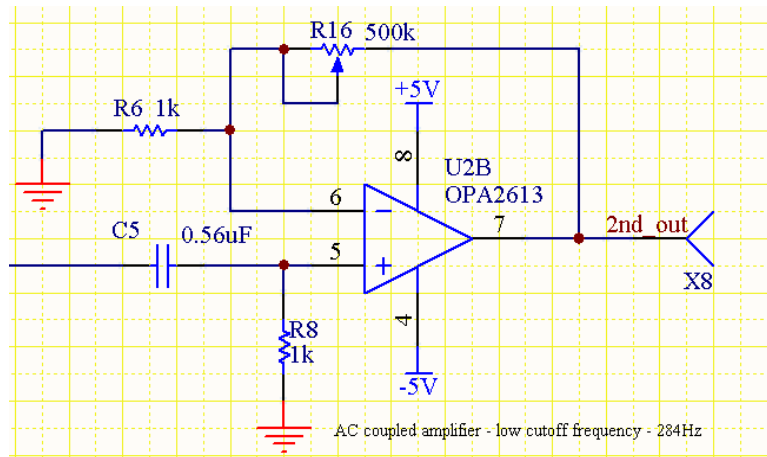


Figure 4.14: Post-amp – high-pass filter non-inverting amplifier

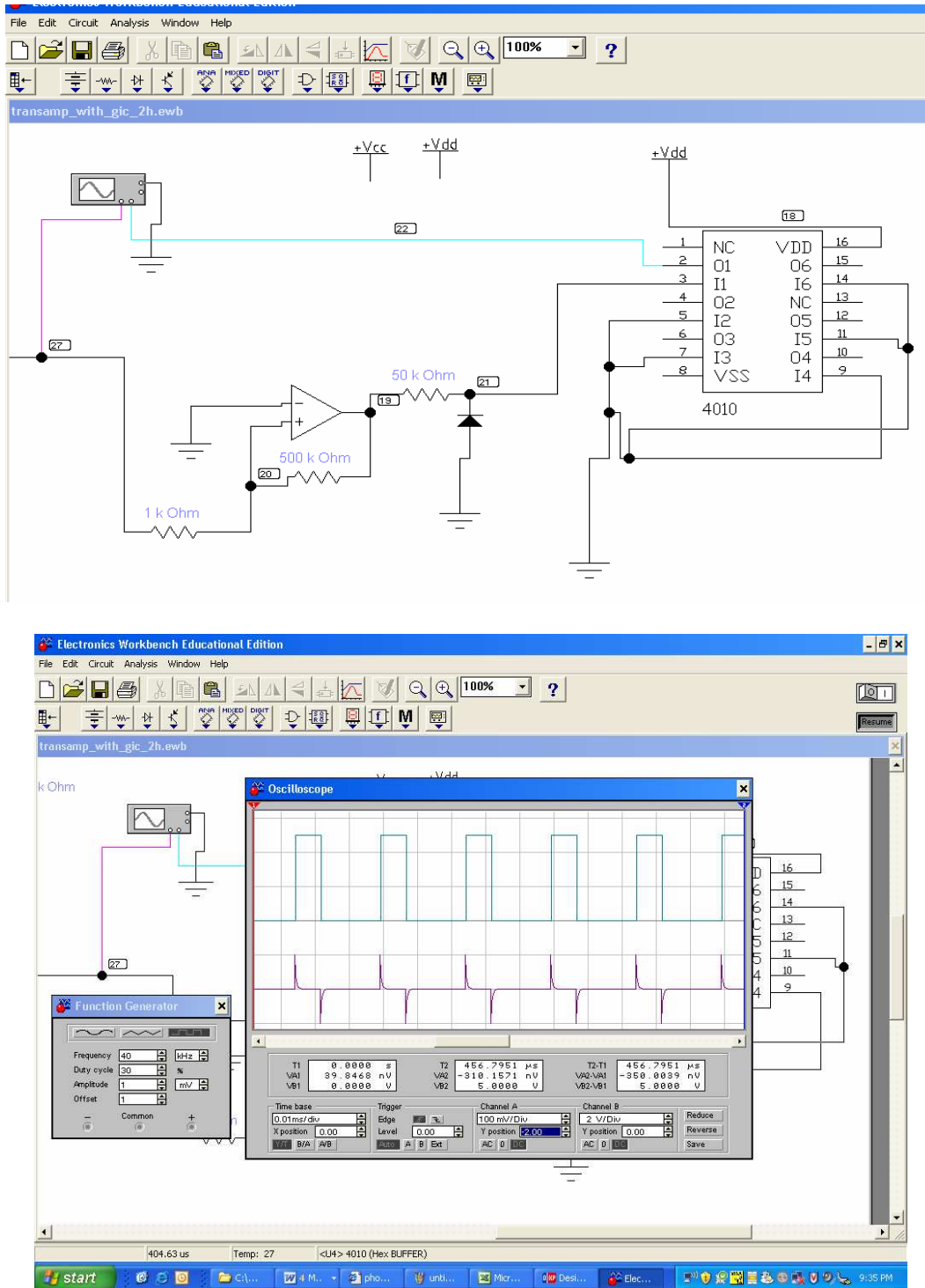
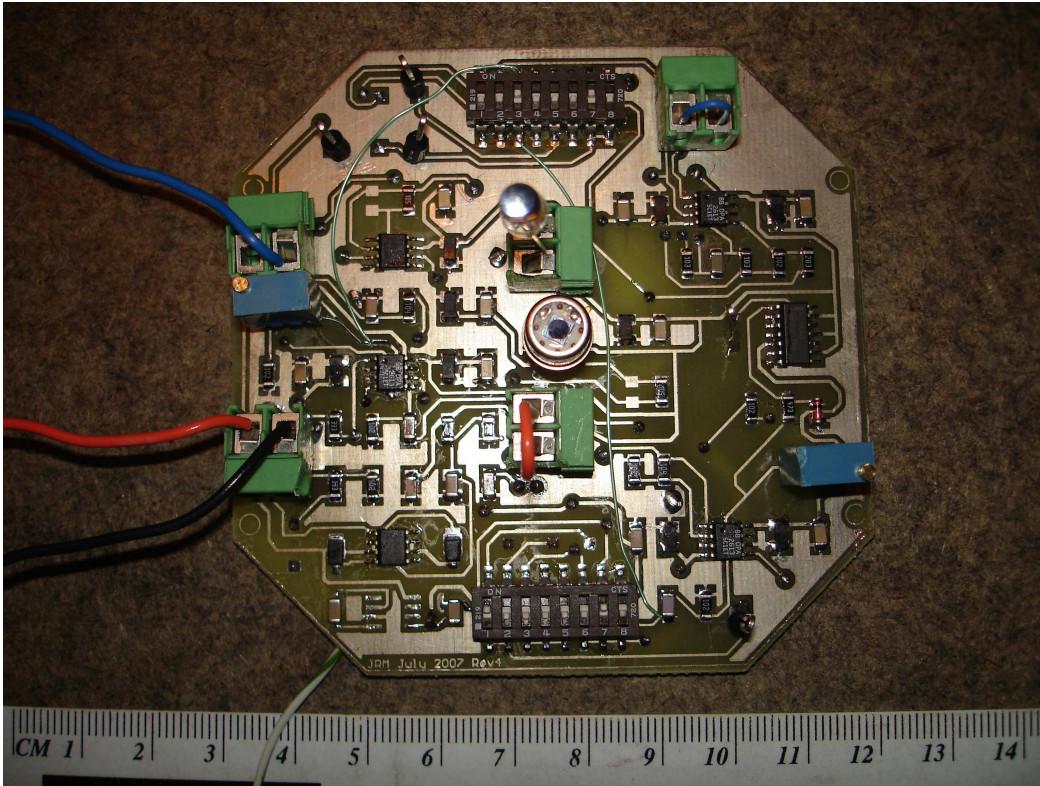


Figure 4.15: Comparator with hysteresis, output clamped and connected to Schmitt buffer a) circuit diagram; b) simulation results – violet line is differentiator output, blue line is output from Schmitt buffer.





**Figure 4.16: Circuit board for PIN photodiode/receiver testing.**

## **Chapter 5: Experimental Results**

When this project was first proposed, measurements in air and underwater was planned. Unfortunately, the underwater experiments were not conducted. As mentioned earlier in this report, the machinist that originally offered to provide assistance with construction of the waterproof containers became unavailable. The underwater housings were too complex to build without professional help.

For this project two experimental evaluations were conducted. The first set of measurement obtained, provide some reference data for the LEDs used to evaluate the receiver and to determine the advantage that adding Fresnel lenses offers. The evaluation of the LEDs and lenses was not extensive (more extensive measurements have been conducted on LEDs in an earlier MINT 709 project and only one lens type was used). The second set of evaluations looked at the receivers' ability to detect a transmitted rectangular pulse optical signal, representative of On-Off-Keying (OOK), over distance in air. PIN photodiodes manufactured by Advanced Photonix Inc., were purchased through Digikey. APDs were not evaluated due to their high cost and added complexity in using them.

### **5.1 LED/ Fresnel lens evaluation:**

Over the past few years, manufactures have developed high brightness 1W LEDs that are readily available, relatively low cost, and in several packaging options. In addition LEDs up to 4.6W (Luxeion III) are now available. But, two problems arise in using these high wattage LEDs for underwater motes, current drain and thermal management needs for both LED and the driving circuitry. One approach, which helps to address the thermal issue but not current, is to use multiple smaller powered LEDs and driving circuits. It is also possible, to drive the LED with very short high-current pulses, but the pulsing circuit is tricky to implement, requires high voltage, and may lead to wavelength shifting. For this project, only a single LED solution is used and pulsing techniques were not attempted.

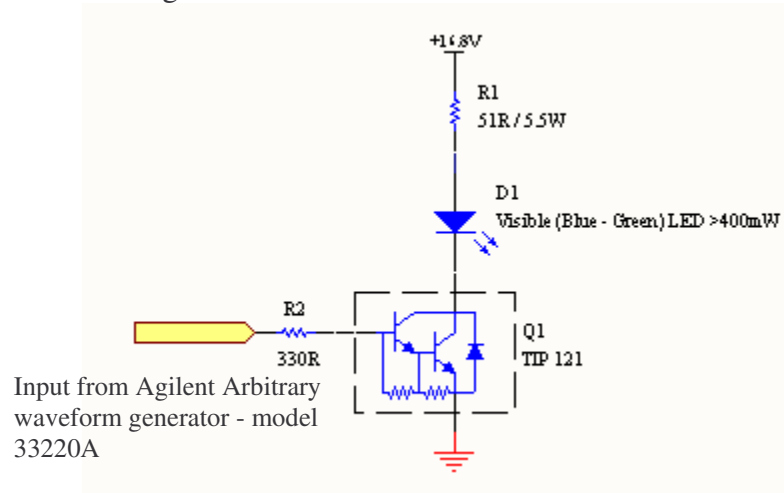
Five high brightness LEDs were evaluated for their ability to transmit optical power over distance in air; more specifically within a low-light hallway environment. Only direct LOS measurements were conducted. This evaluation had three goals: 1. to compare the LOS optical power that each LED radiated so as to choose which to work with for receiver testing; 2. to determine the qualitative gain advantage using Fresnel lenses; and 3. to confirm the relationship of optical power loss over distance in air so as to allow for a prediction of maximum distance that may be achieved. In addition to power loss over distance, additional measurement was made to determine the maximum frequency that the LED/driver circuit would function at.

The five LED sources evaluated are summarized in table 5.1. Three of the LEDs, model numbers Lv W5SG-GXHX-35Z, SSP-LX6144A2UC, and SSP-LX6144A7UC were used

in an earlier MINT709 project. The remaining two LED modules listed were sourced from Lasermate Group Inc., for their attractive optical power and packaging which has a diffusion lens and heat sink. The Lasermate LED modules are priced at \$19.00 US each. Complete datasheets for the LEDs can be found in appendix A.




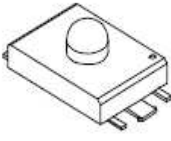
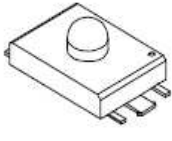
For comparison of light intensity, manufacturers use units of lumens (lm) and millicandelas (mcd), making comparison confusing. Luminous flux, in units of lumens, represents total optical power emitted by the source within the visible spectrum. Luminous intensity is “the flux per unit solid angle directed toward the observer, along the axis of the LED in candela’s” [39] and measured at the source. In addition, the measurements are based on a given set of conditions as chosen by the manufacturer. Therefore the numbers should only be considered as qualitative rather than quantitative.

To test the LEDs and in using them to generate a signal for testing the receiver circuit, a simple transistor switch circuit, shown in figure 5.1, was used. The TIP121 power-Darlington transistor was chosen based on three criteria: first, it is able to switch the high current values used in the tests; second, its high current gain (1000) keeps base current low so as not to harm the waveform generator that provides the input pulse waveform, and third, it was available in SAIT Polytechnic electronics store. The TIP121 is not a fast switching transistor; however, it proved to be adequate for the frequencies that were of interest (see receiver measurement discussion for further clarification). The collector resistor’s value was chosen simply because it was on hand and has a power rating of 5.5W ensuring adequate protection from burning out. The base resistor ensured current limit protection for the generator.



**Figure 5.1 Switching circuit used to drive LEDs.**

**Table 5.1: Comparison of LEDs specifications.**

Comparison of five LEDs tested				
<b>LED source:</b> Lasermate Group, INC.	<b>LED source:</b> Lasermate Group, INC.	<b>LED source:</b> OSRAM (by way of Digikey)	<b>LED source:</b> Sunbrite (by way of Digikey)	<b>LED source:</b> Sunbrite (by way of Digikey)
<b>Model:</b> LED-G-1W-N - 1W green LED module	<b>Model:</b> LED-B-1W-D - 1W blue LED module	<b>Model:</b> Lv W5SG-GXHX-35-Z (475-1199-1 ND) VERDE Clear No lens SMD	<b>Model:</b> SSP-LX6144A2UC (441-1089-ND) <b>420mW</b> green Water clear lens	<b>Model:</b> SSP-LX6144A7UC (441-1092-ND) <b>420mW</b> blue Water clear lens
<b>Peak Wavelength:</b> 520nm	<b>Peak Wavelength:</b> 470nm	<b>Peak Wavelength:</b> 501nm	<b>Peak Wavelength:</b> 525nm	<b>Peak Wavelength:</b> 470nm
<b>Brightness:</b> 100,000 mcd	<b>Brightness:</b> 5 Lm	<b>Brightness:</b> <b>Lumen flux</b> up to 35 lm	<b>Brightness:</b> Total flux 2.5 Lm - Axial intensity 16cd	<b>Brightness:</b> Total flux 2.0 LM - Axial intensity 12cd
Beam profile: square	Beam profile: circular	Beam profile: circular	Beam profile: circular	Beam profile: circular
Luminous angle: 20 +/- 5 degree	Luminous angle: 40 +/- 4 degree	Luminous angle:120 degree	Luminous angle:10 degree	Luminous angle:10 degree
Votage drop: 4.5V	Votage drop: 4.5V	Votage drop: 3.0 to 4.1V (3.8V typ)	Votage drop: 3.4 to 4V	Votage drop: 3.4 to 4V
Forward current: 350mA	Forward current 350mA	Peak forward current: For pulse width $\leq 10\mu\text{s}$ and 50% duty cycle 850mA up to 1.5A for duty cycle at 0.5%	Peak forward current: 250mA at $t < 10\mu\text{s}$	Peak forward current: 250mA at $t < 10\mu\text{s}$
				

The following conditions were established for making distance optical power loss measurements.

- Two of the LEDs tested have a maximum peak current of 250mA with a pulse time < 10µS. Based on this, the minimum frequency for a pulse waveform with 30% duty cycle is 33kHz. For testing purposes, a 40kHz at 30% duty cycle pulse waveform was used resulting in a pulse width of 7.5µS. The input pulse voltage magnitude was set from 0V to 1.5V (determined by observation) ensuring good switching behavior by not under or over driving the transistor.
- The forward voltage drop ( $V_F$ ) of the LEDs, measured 4V +/- 0.2V. To establish a peak current of 250mA the collector voltage was calculated as follows:

$$V_{DC} = V_F + V_{CE(sat)} + I_C R1 = 3.8 + 0.3 + 0.25 * 51 = 16.85V$$

$$\text{Resistor peak power: } P = I^2 R = 0.25^2 * 51 = 3.19W$$

$$\text{Resistor average power: } 30\% * 3.19W = 1.17W$$

Equipment used:

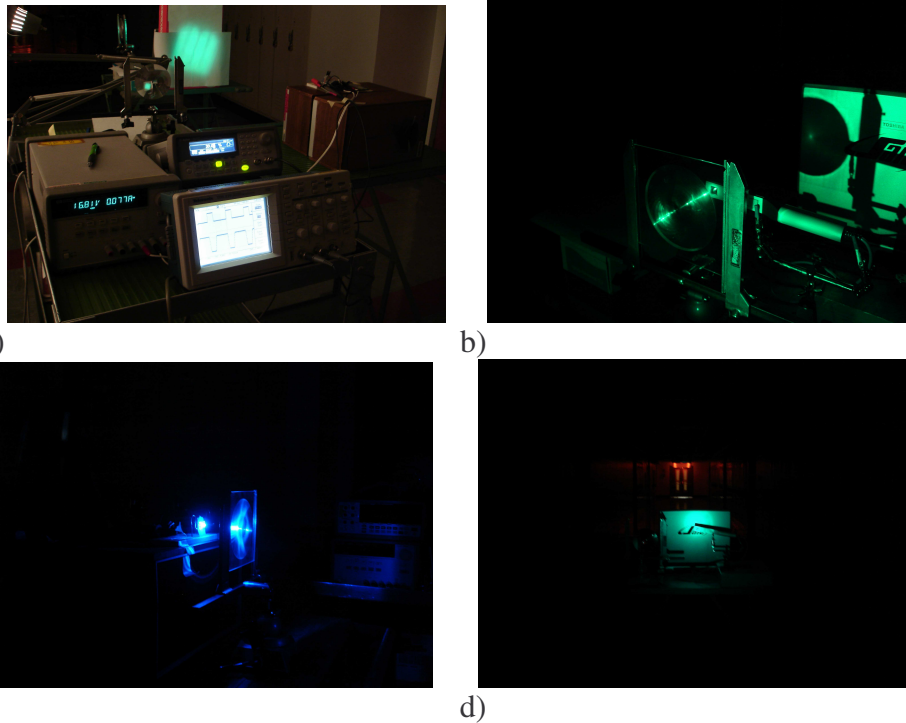
- Optical meter: Newport Optical meter Model 841-P-USB Virtual Optical Power Meter with 818-ST-UV wand detector and wavelength selection set at 514.5nm.
- Power supply: HP triple DC power supply 6V, +/- 25V@ 1Amp model E3631A.
- Generator: Agilent Arbitrary Waveform Generator model 33220A.
- Oscilloscope: Tektronix 60MHz 1Gs dual channel model TDS210 c/w RS232 serial interface. Waveforms are captured from this scope using WaveStar version 2.8.1 software.

Fresnel lenses offer three advantages over standard convex/concave lenses: they can be manufactured with large effective aperture size and short focal distance; they can be manufactured out of thin plastics making them light weight and relatively low cost. The Fresnel lenses for this project were purchased (\$19.25 ea. US) from Rolyn Optics Company in California stock number 16.720. The particular model of lens chosen was based on the following:

1. Material must have low attenuation of visible light; acrylic lens offers 92% transmission throughput.
2. Low groove count, for capture of light rather than image quality.
3. Closest size available that would fit within a 4" diameter tube, for the purpose of doing underwater experiments.

This acrylic lens, is 125mm square with the Fresnel lens aperture centered, having a diameter of 101mm. Its focal length is 70mm and has 4 grooves per mm.

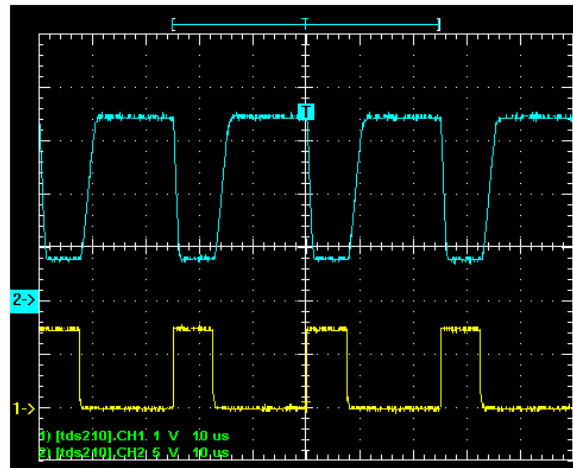
Testing was conducted in the northwest hallway, 2<sup>nd</sup> floor of the John Ware building located on SAIT's main campus. This location was chosen as it provided just over 30 meters of length, the lab doors, located along the hallway sides have no windows, and at end of the hallway are exit doors with small windows. The majority of fluorescent lights in the hallway are connected to a single accessible switch. However, fluorescent fixtures at both ends of the hallway are permanently on, but easily disabled by removal of the tubes. The end hallway door windows were covered with light brown paper that significantly reduces the amount of light entering the hallway. Some low amount of ambient light is able to enter the hallway from underneath the lab doors. At each end of the hallway is an emergency exit sign, but only one was functional throughout the several days of testing. Additional sources of ambient light includes light from the laptop screen used for recording data and for Newport's optical power meter system and low level light emitted from the oscilloscope, power supply, and generator displays. Two metal carts were used to provide platforms for equipment, light source, and optical meter/laptop, allowing easy movement of the optical meter from the LED light source. Figure 5.2 contains photographs showing testing of the LEDs, with and without Fresnel lenses.



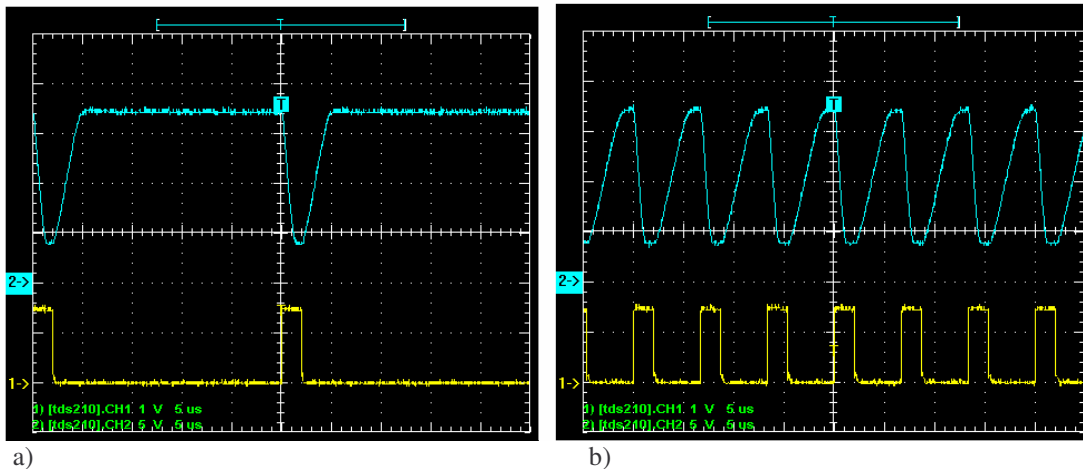
**Figure 5.2: Photographs - testing for optical power loss over distance:**

- a) Test setup and light emission using Lasermate green LED module
- b) Capturing light through Fresnel lens, focused onto the optical meter's wand photo detector
- c) Using blue LED # SSP-LX6144A7UC (441-1092-ND) with Fresnel transmit side
- d) Reception of light from LED #Lv W5SG-GXHX-35-Z (475-1199-1 ND), Fresnel lens at transmit side. Notice the variation of light intensity from outer edge to center. Exit sign at the end of the hallway is visible, behind detector.

Figure 5.3 shows oscilloscope captured waveforms from the driver circuit used for the majority of measurements conducted (both LED and receiver testing). Waveforms in figure 5.4 show the frequency limits of the LED driver circuit operation primarily caused by the Darlington's switching characteristics. The drive circuit works well from 1kHz through to 100kHz though caution is required not to exceed the pulse width of 10 $\mu$ s at 250mA peak current for two of the LEDs (as discussed earlier).



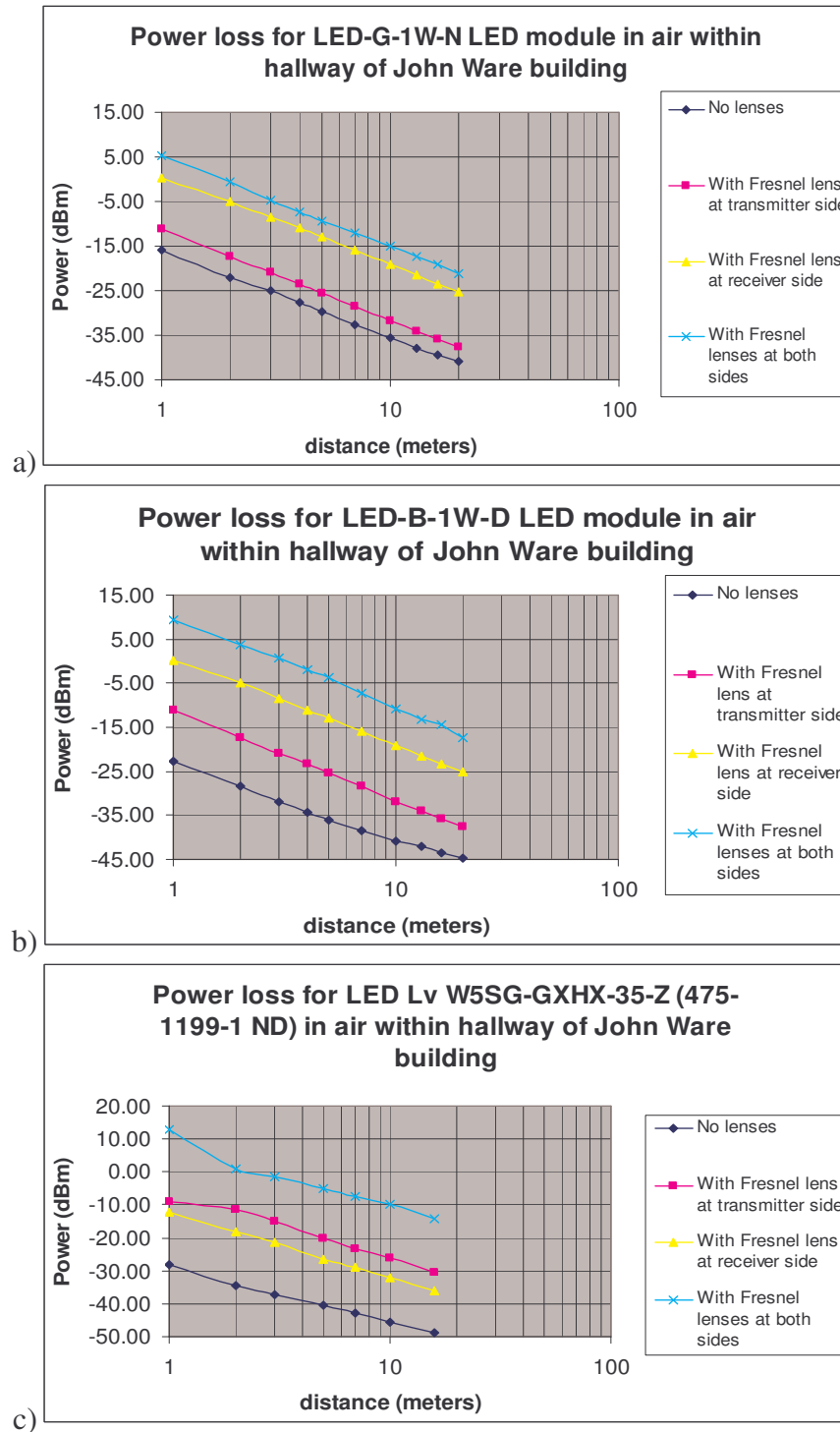
**Figure 5.3: Waveforms for transmission source.** Ch 1 (yellow trace) - input waveform from the generator set at 0- 1.5V peak, 30% duty cycle, frequency 40kHz. Ch 2 (blue trace) shows the Anode of LED with respect to ground. Signal levels are 4V (LED on) to 16.8V (LED off).



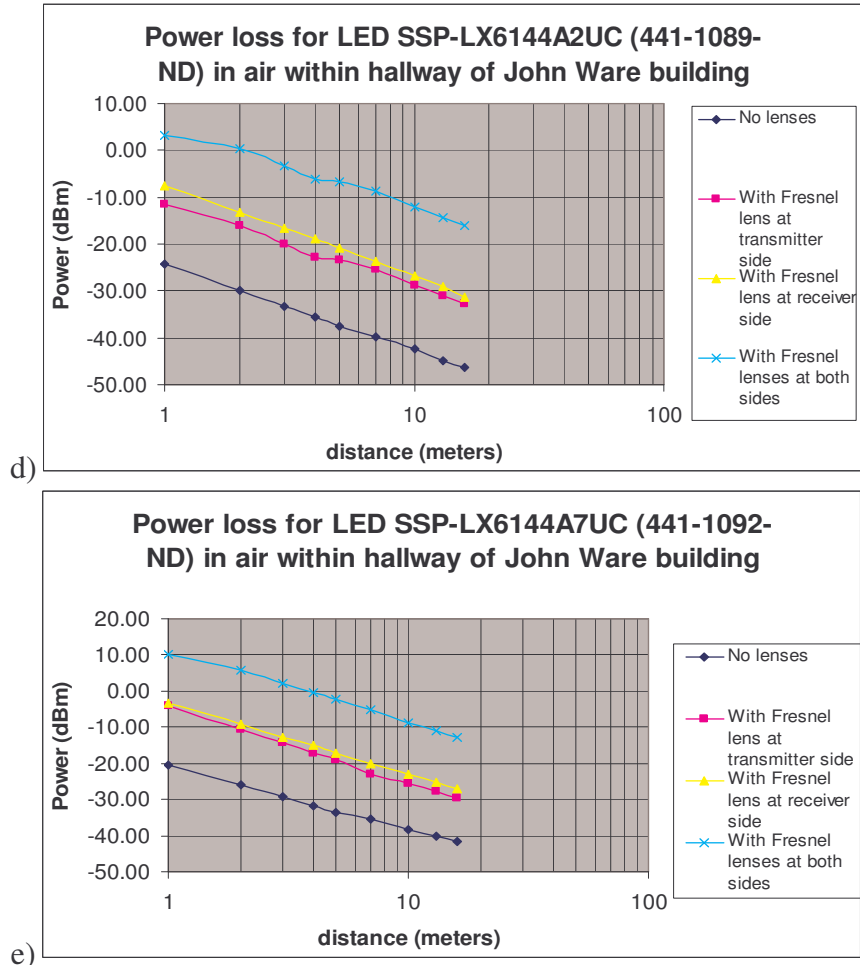
**Figure 5.4: Limits of operation for LED driver circuit:** Ch1- input, Ch2- output measured from anode to ground a) Frequency at 40kHz, duty cycle 8% giving input pulse width of 2 $\mu$ s, resulting output pulse width of 4 $\mu$ s, b) circuit operating at 150 kHz 30% duty cycle

Optical power loss, recorded by the optical meter using incident light orthogonal to the source was conducted for each of the five LEDs with and without the Fresnel lenses. The recorded data is found in Appendix B. The optical power strength of the received light

wave is determined by subtracting the received ambient light power from the combined ambient light and signal power measurement. The results of this test are plotted and presented in figure 5.5.







**Figure 5.5: Optical power loss over distance** for 5 LEDs measured within the second floor north-west hallway of the John Ware building at SAIT. The LEDs are forward biased by a rectangular waveform of 40 kHz 30% duty cycle (0 to 250mA).

The graphs of figure 5.5 show the following:

- Optical power loss over distance – in air – approximates 20dB over a decade of distance in meters, or approximately 6dB of loss for each doubling of distance in meters. It is important to note that as distance increases within the hallway, and as the source beam diverges, reflections from the floor, ceiling, and walls may be in play. The loss of power, within the first few meters, is some cases did not completely hold to the rate of loss as distance further increases. It is suspected that the variance may be due to shadowing and reflections by the lenses when close to the source, and not having a consistent intensity pattern over the beam area (as seen in figure 5.2a and 5.2d).
- The addition of Fresnel lens at the transmitter side increases the optical signal strength from 3.2 to 23.1 dB - dependent on the LED's own packaging.
- The addition of a Fresnel lens at the receiver side, increase the optical power level by 12.9 to 17.4 dB.

- With a Fresnel lens at both transmitter and receiver sides the gain advantage is from a low of 19.6 to a high of 36.1 dB.

A majority of the receiver's testing was conducted using LED model SSP-LX6144A2UC with  $\lambda= 525\text{nm}$  (green) and SSP-LX6144A7U6 with  $\lambda= 470\text{ nm}$  (blue). These two LEDs are the lowest power of the five and their packaging/plastic lens allows for only  $10^\circ$  luminous angle. However, in combination with the Fresnel lens they gave comparable power level results over distance and had a well collimated beam pattern in the shorter distances of 1 to 3 meters out to the longer distances. The LED modules from Lasermate also performed well, but the Fresnel lens interaction with the module's own lens tended to show more intensity variation over the beams projected area at the measuring distance. The Lv-W5SG-GXHX-35-Z is the highest power LED, but with a very wide luminous angle of  $120^\circ$  it lost power rapidly at short distance compared with the others.

## **5.2 Receiver and PIN Photodiode testing**

The op amp components used in this project were available only in surface mount packages. To do any prototyping/testing using these devices requires building of a printed circuit board. However, this also creates a substantial challenge when one wishes to test several circuit designs, make modifications, and change component values. In addition, because of the desire to work with low power signals and high frequencies, the PCB designer needs to employ strategies to minimize stray capacitance and protect against external noise sources, for example, judicious use of ground planes, perhaps inclusion of metal enclosures, and use of guard rings at the input of the TIA. The PCB built for this project (third version) is not optimized.

To allow for testing of individual sections of the receiver circuit and provide some variability in how the circuit sections are placed, for instance being able to interchange the voltage gain amplifier the differentiator circuit which follows the TIA, and/or the use of the GIC circuit in the TIAs feedback path, two 8 position single-pole single-throw switch banks were used and test-points distributed on the board to allow for easier scoping. In addition, junction blocks were used to allow for easily changing photodetectors. Also added were junction blocks to allow the photodiodes to be put into photoconductive mode; this feature was not used – all evaluations were done with the photodiodes in photovoltaic mode. Also of note, the hybrid photodiode/TIA device was required to be soldered to the board. Its leads were purposely left long to allow for its reuse in future projects.

Appendix E contains the evaluation board's schematics and PCB component layout. Due to the changes made to the PCB (some traces removed and jumper wires added) the top and bottom layers have not been included. Appendix D contains the circuit equation derivations and calculations.

All optical power measurement levels made for the receiver investigation were obtained by using the Newport's optical meter with 818-ST-UV wand detector and wavelength

selection set at 514.5nm. The values obtained should only be used for qualitative not quantitative interpretations. Table 5.2 summarizes the features and specifications of the photodiodes that were evaluated. The manufacture’s data sheets are in Appendix C.

**Table 5.2**

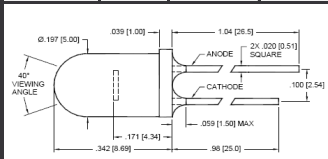
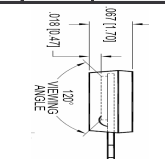
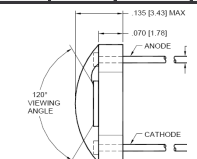
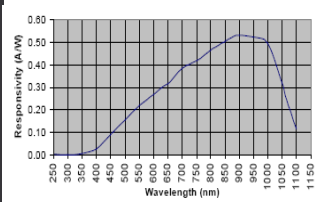
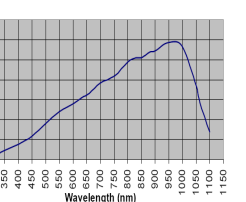
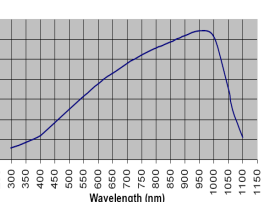
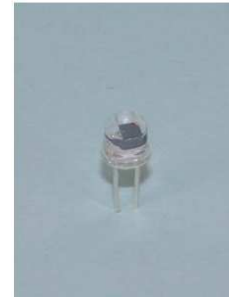


Comparison of PIN photodiodes used in evaluations												
	PDB-C142				PDB - C169				PDB-C107			
Active Area size	2.03mm square Area= 4.12 mm <sup>2</sup>				2.87mm square Area=8.24 mm <sup>2</sup>				5.69mm x 3.15mm rectangle Area = 17.92 mm <sup>2</sup>			
	Test conditions	min	typ	max	Test conditions	min	typ	max	Test conditions	min	typ	max
Reverse Voltage (VBR)				100V				200V				75V
Short Circuit current (Isc)	H=100fc, 2850K	100uA	150uA		H=100fc, 2850K	90uA	102uA		H=100fc, 2850K	170uA		
Dark Current (Id)	VR = 10V		5nA	30nA	VR = 10V		5nA	30nA	VR = 10V		150nA	300nA
Junction Capacitance (Cj)	VR =10V, f =1MHz		18pF	25pF	VR =10V, f =1MHz		25pF		VR =10V, f =1MHz		100pF	
Shunt Resistance (Rsh)	VR=10mV	100MΩ	500MΩ		VR=10mV	125MΩ	140MΩ		VR=10mV	200MΩ	1000MΩ	
Resonse Time (tr)	RL = 1k, VR=10V		50nS		RL= 1k, VR=10V		50nS		RL = 50Ω, VR=0V		190nS	
Noise Equivalent Power (NEP)	VR=10V @ λ=Peak		2x10 <sup>-14</sup> W/√Hz		VR=10V @ λ=Peak		9.0x10 <sup>-14</sup> W/√Hz		VR=10V @ λ=Peak		3.0x10 <sup>-13</sup> W/√Hz	
Viewing Angle												
Digikey Price	\$3.90				\$10.66				\$14.73			
Spectral Response												
Picture												

Table 5.2 (continued)

Comparison of PIN Photodiodes used in evaluations												
	SD100-12-22-021				SD200-12-22-041				SD100-42-22-231			
Active Area size	Circle - diameter = 2.54mm = 5.07 mm <sup>2</sup>			Area	Circle - diameter =5.08mm 20.27 mm <sup>2</sup>			Area =	Hybrid - contains PIN Diode and Transimpedance op-amp Circle - diameter = 2.54mm = 5.07 mm <sup>2</sup>			
	Test conditions	min	typ	max	Test conditions	min	typ	max	Test conditions	min	typ	max
Reverse Voltage (VBR)				75V				75V				-----
Short Circuit current (Isc)			----				----				----	
Dark Current (I <sub>d</sub> )	VR = 5V		1.6nA	6.4nA	VR = 10V		6.5nA	26nA	VR=10V			10nA
Junction Capacitance (C <sub>j</sub> )	VR =0V, f =1MHz		87pF		VR =0V, f =1MHz		345pF		VR =0V, f =1MHz		87pF	
	VR =5V, f =1MHz		26pF		VR =5V, f =1MHz		102pF		VR =10V, f =1MHz		18pF	
Shunt Resistance (R <sub>SH</sub> )	VR=10mV	300MΩ			VR=10mV	70MΩ			VR=0V	300MΩ		
Resonse Time (tr)	RL= 50Ω, VR=0V		190nS		RL= 50Ω, VR=0V		190nS				----	
Noise Equivalent Power (NEP)	VR=10V @ λ=Peak		4.2x10 <sup>-14</sup> W/√Hz		VR=10V @ λ=Peak		8.9x10 <sup>-14</sup> W/√Hz				----	
Viewing Angle												
Digikey Price	\$26.87				\$48.57				\$106.63			
Spectral Response												
Picture												

### 5.2.1 Ambient light responsivity measurements:

The purpose of this evaluation is to provide one of several qualitative comparisons between the photodiodes listed in table 5.2 and to identify the limits of allowable ambient light level that the circuits would function within. In this evaluation, the first stage TIA amplifiers, as described in chapter 4 (circuits are shown in figures 4.12 a) and b)), have their output DC voltage level measured for different levels of ambient light. The ambient light source used is sunlight through glass windows. The light level is controlled by the window shades and by moving the detector closer/further away from the light source. This technique did not have very tight measurement control, but does clearly show the light collection ability of larger area photodiodes compared to smaller area devices. PIN photodiodes have very linear response to change in optical power level, particularly in photovoltaic mode. The non-linearity that appears in this evaluation is due to poor control over the ambient light levels that the surface area of the detectors is exposed to. Figure 5.6 shows the test environment. Measured results are graphed in figure 5.7. The raw data is provided in appendix F.



Figure 5.6: Ambient light to voltage output measurement environment – light level controlled by blinds and detector distance from window.

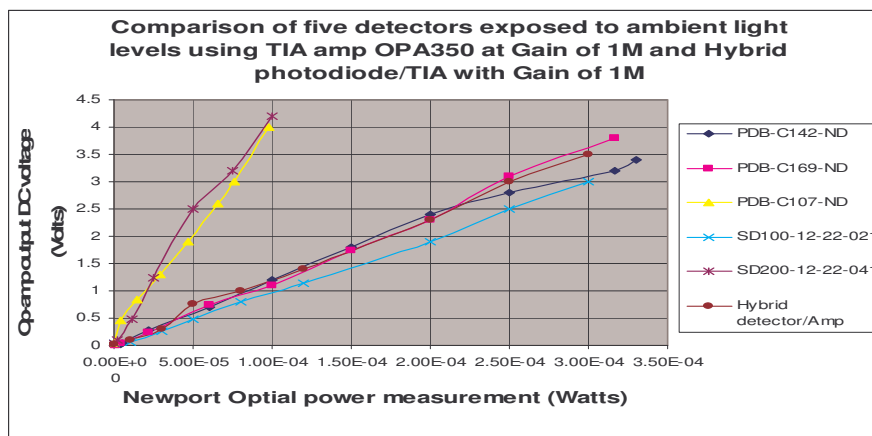


Figure 5.7: TIA output responsivity to ambient sunlight for various PIN photodiodes

The graph of figure 5.7 shows that the larger area photodiodes have a much smaller operational range of ambient light. The slopes of the plotted lines demonstrates that the larger area diodes collect approximately four times more light than the smaller area devices consistent with their area size differences. Comparing the area of the SD-200 with that of the SD-100, the SD-200 area is four times larger than the SD-100.

### **5.2.2 Comparison of TIA output response using different PIN photodiodes, for a given input optical signal at a fixed distance from the source**

For all receiver measurement, unless otherwise indicate, the LED driver circuit of figure 5.1 using the blue LED SSP-LX6144A7UC ( $\lambda=470\text{nm}$ ) with the generator input at 40kHz, 30% duty cycle, driving to 250mA peak as per figure 5.3 is used. Because the photodiodes responsivity are lower at blue rather than green wavelengths, the blue LED was used for most measurements as this yields the “worst case” condition for free-space communication in air.

As discussed in chapter 4, the TIA circuits used are those of figure 4.12. The output of the TIA was left unconnected to the next stage for this series of measurements. In addition, the feedback capacitance  $C_f$  was not installed on the board, as its value is dependent on the photodiode used and the stray capacitance in the feedback network as discussed in chapter 4 and equations 4-2 and 4-3. Table 5.3 shows the predicted values of bandwidth and values for  $C_f$  for each photodiode.

### **Table 5.3**

Predictions of upper corner cut-off frequency and value of Cf for controlling gain peaking for TIA amplifiers with gain of 1M ohms

Diode	Cj (F)	CT (F)	Predicted upper corner cut-off frequency f <sub>hc</sub> (Hz)	Predicted capacitance to minimize gain peaking Cf (F)
<b>PDB-C142</b> + *	7.20E-11	7.60E-11	434134.72	3.18E-13
<b>PDB - C169</b> +*	1.00E-10	1.04E-10	371120.25	4.06E-13
<b>PDB-C107</b> + *	4.00E-10	4.04E-10	188295.80	9.95E-13
<b>SD100-12-22-021</b> +	8.70E-11	9.10E-11	396744.23	3.67E-13
<b>SD200-12-22-041</b> +	3.45E-10	3.49E-10	202590.28	9.11E-13
<b>SD100-42-22-231</b> !	8.70E-11	9.10E-11	177429.42	1.07E-12

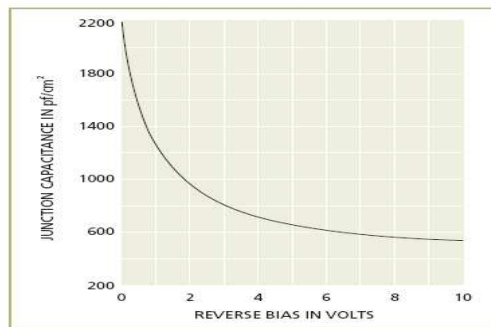
**Notes:**

+ OPA380 op-amp: GBW = 90MHz, C<sub>cm</sub>= 3pF, C<sub>dm</sub>=1pF, Feedback resistance 1M ohms

! Hybrid op-amp:GBW=18MHz, input capacitance not give assume 4pF

Junction capacitance C<sub>j</sub> is at 0V if spec given; \* if spec given at 10V, a multiplication factor of 4 is used to predict the capacitance value at 0V.

As noted in table 5.3, for three of the photodiodes the manufacturers specifications provided a value of junction capacitance at a reverse bias voltage of 10V only. To estimate the capacitance value at 0 V, a multiplication factor of 4 was used. This value was obtained from the graph shown in figure 5.8.



**Figure 5.8: Typical relationship of a silicon photodiode’s junction capacitance and applied bias. [40]**

As the hybrid package SD-100-42-22-231 was exposed to the same incident light wave that the other five photodiodes were exposed to, its output waveform was also captured for comparison purpose.

Light level: The optical power measured (combined ambient and pulse) is recorded by Newport optical meter with  $\lambda$  setting of 514.5nm.

*Investigation of Optical Receivers For Use in an Underwater Environment*

Ambient level:  $2.2\mu\text{W}$

Combined ambient light and signal power at detector:  $10.75\mu\text{W}$

Therefore, blue light signal power:  $8.55\mu\text{W}$  or  $-20.7\text{dBm}$

The measurements were conducted within a RF screen room, to minimize external noise. However, it should be noted that the instruments themselves and in particular the laptop computer contribute to noise. In addition, the digital oscilloscope used to capture the waveforms, provides a misleading representation of noise level in the waveforms. The signals appear quite noisy but a majority of the noise is internal to the scope, resulting from its 8-bit resolution. Therefore no noise measurements were conducted. Figure 5.9 shows the experimental setup and figure 5.10 shows the captured waveforms.



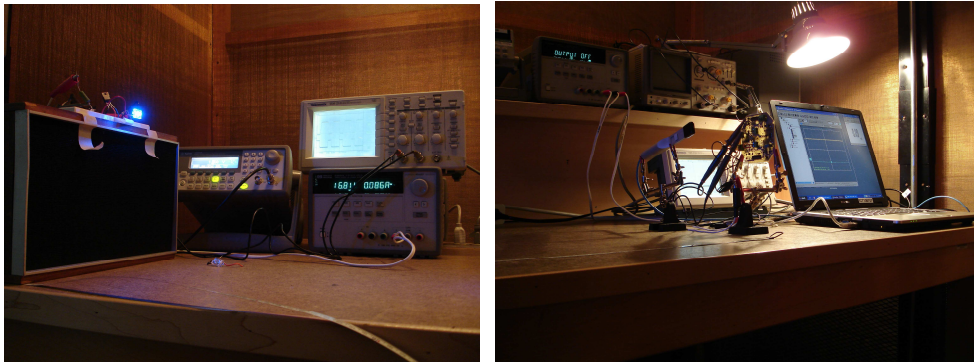
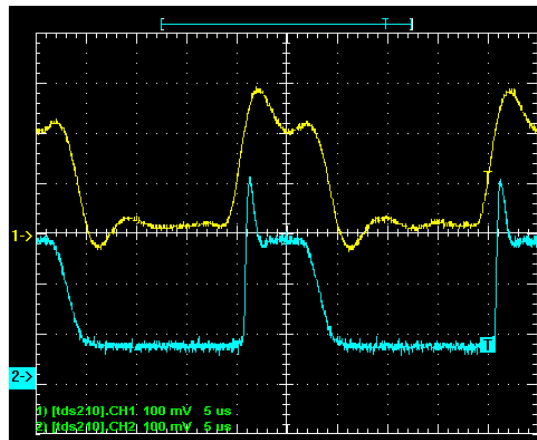
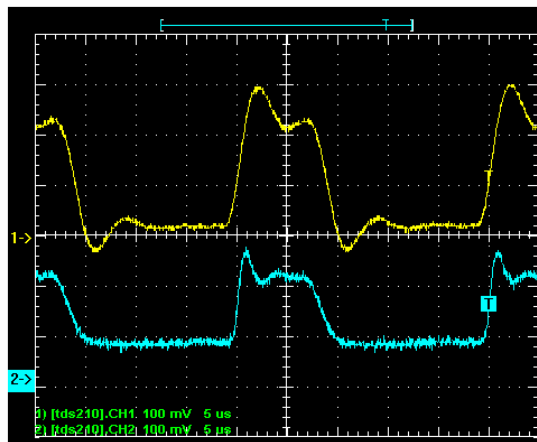


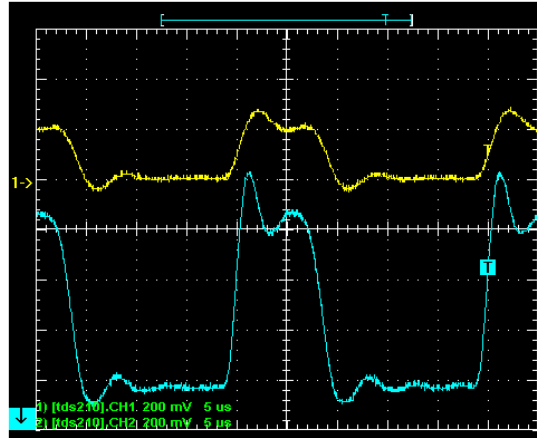
Figure 5.9: Experimental setup for testing receiver within a RF screen room (the lamp is turned off during measurements).



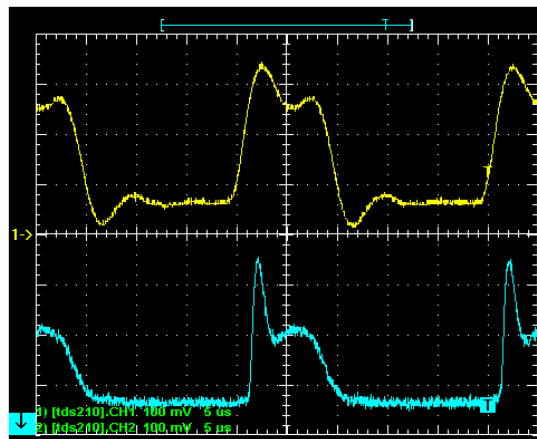
a) Ch1(yellow) - hybrid output; Ch2 (blue) - OPA350 output with detector PDB-C142



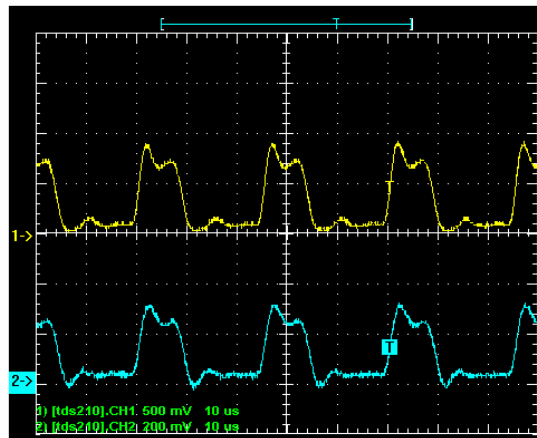
b) Ch1 (yellow) - Hybrid output; Ch2 (blue) - OPA350 with detector PDB-169 Sidelook



c) Ch1 (yellow) - Hybrid output; Ch2 (blue) - OPA 355 with **Detector PDB-C107**  
Notice the change of scale – The PDB-C107 detector's output level is approximately three times larger than the Hybrid's.



d) Ch1 (yellow) - Hybrid output; Ch2 (blue) - OPA 355 with **Detector SD100-12-22-021**  
Note: The surface areas of both detectors are the same size.



e) Ch2 (blue) - Hybrid output; Ch1(yellow) - OPA 350 with **Detector SD200-12-22-041**. Notice the scales. The SD200-12-22-041 detectors output is just over three times larger than the Hybrid's

**Figure 5.10 Waveforms observed at output of TIA amps with different photodetectors.**

With reference to figure 5.10 a) to e), four observations are made:

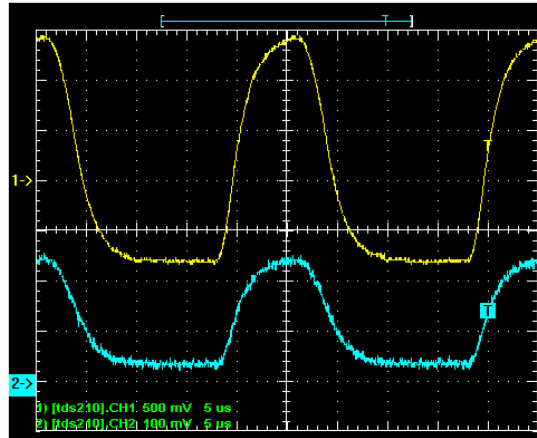
1. The Hybrid amplifier output had less DC offset bias – it's suspected that the very small acceptance angle and packaging shields it from some of the ambient light level in the room.
2. Gain peaking occurs for all the detectors.
3. The detectors with larger surface areas had higher gain, though not quite the same ratio as observed with the ambient light experiment. It is suspected that wavelength sensitivity may be in play.
4. The Hybrid amplifier's waveforms did appear to be less noisy compared to the waveforms for the discrete photodiodes in combination with the OPA380 TIA

The TIA constructed using the OPA2613, as per the circuit of figure 4.12 c), encountered a major hurdle due to the 2613's relatively high input bias current of  $-6\mu\text{A}$  typ. @  $25^\circ\text{C}$ , compared with only  $3\text{pA}$  for the OPA380 and  $15\text{pA}$  for the Hybrid's amplifier. Despite trying to compensate for the high input bias current by inclusion of a resistor added from the non-inverting input to ground, zeroing of the output for no input diode current was not achieved. The output voltage level of the OPA2613 was near its negative voltage limit of  $-4\text{V}$ . This result was not all bad, as this bias condition provided for an output voltage swing of close to  $8\text{V}$  with supply voltage of  $\pm 5\text{V}$ . The OPA380's (single supply biased at  $+5\text{V}$ ) and the Hybrid's (dual supply biased at  $\pm 5\text{V}$ ) voltage swing is from  $0\text{V}$  to approximately  $+4\text{V}$ . Although the Hybrid is dual supply biased, its low input bias current kept its output voltage swing to only the positive range as ideally expected. The circuit with OPA2613 appeared to be slightly noisier than the other two scenarios and gain just slightly higher. As the OPA2613 configured as a TIA was built primarily to test the functionality of the GIC circuit, a full set of measurements were not recorded for it as per the other two scenarios. It should be noted that the OPA2613 performed very well in its use for the other post TIA circuit applications.

### **5.2.3 Second stage – wideband amplifier and/or differentiator**

The next phase of measurements taken was to add in the wideband non-inverting amplifier circuit and/or the differentiator circuit to the output of the TIA. The wideband non-inverting amplifier, as described in chapter 4 and shown in figure 4.14 is used for two purposes, gain and to act as a high frequency filter. This amplifier stage has its low corner cut-off frequency set at  $284\text{ Hz}$  so as to remove the DC component from the TIA signal and any possible  $60\text{ Hz}$  signals picked up by the photodetector from electrical light sources. The OPA 2613 is used because of its large bandwidth and performed well for

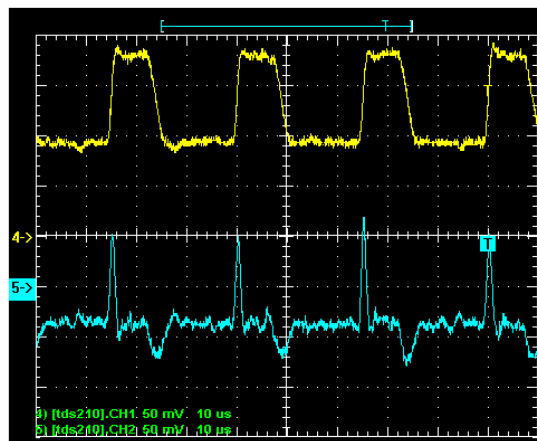
this application. It was found that setting the amplifier to a gain of about 10 worked well with the TIA and subsequent circuits. Figure 5.11 shows a sample waveform using the wideband amplifier connected to the hybrid's TIA output.



**Figure 5.11 Output of non-inverting wideband amplifier with input signal from Hybrid TIA (SD100-42-22-231).** Ch1 (yellow) – amplifier's output signal; Ch2 (blue) – input signal to the amplifier (the output of TIA).

Referring to figure 5.11, an interesting and pleasant side effect of adding the second stage amplifier was that it eliminated gain peaking from the Hybrid's TIA. Similar results were obtained by adding the amplifier to the output of the OPA380.

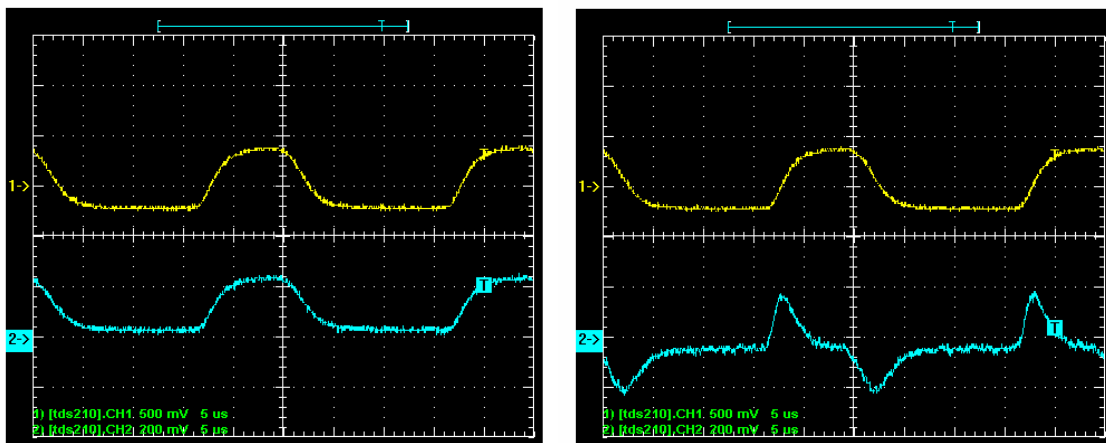
The differentiator circuit, as described in chapter 4 and shown in figure 4.11, had two placement scenarios experimented with. The first evaluation was with the differentiator placed directly following the TIA output, the second approach was to use the differentiator following the wideband amplifier connected to the TIA output. Figure 5.12 shows captured waveforms for the first scenario with differentiator following the TIA.



**Figure 5.12: Output of OPA380 TIA amplifier taken directly to differentiator circuit** – Ch1 (yellow) - output of OPA380; Ch2 (blue) - output of differentiator circuit.

Several observations are made from the results of figure 5.12. The differentiator circuit works, but because the signal transition is slower than simulations, the output level of the differentiator is not very large. It should be noted that the output from the TIA amp is also small. In addition, and as was expected, it can be seen that noise has increased on the differentiated waveform. Both transitions (positive and negative) on the TIAs output (input to the differentiator) are sufficiently fast enough to produce differentiated levels higher (on average) than the noise level. The positive going edge on the TIAs waveform is faster than the negative transition and results in the asymmetric differentiated waveform. The asymmetric waveform's average DC level is less than 0V, which makes using a comparator with hysteresis having  $UTL = -LTL$  challenging to get the trigger points not confused by noise. Lastly, like the effect the amplifier had on gain peaking on the TIA stage, the differentiator also has affected (reduced) gain peaking.

Figure 5.13 shows the second scenario, TIA to wideband amplifier and then to the differentiator circuit. For the waveform capture displayed, the Hybrid amplifier was used. The optical signal power was at a higher level than used for figure 5.12. In addition, the combination of the second stage amplifier to the output of the Hybrid TIA, results in higher amplitude signal and provides a more symmetrical rise and fall time. This is very beneficial to the differentiator circuit, as it produces a more symmetrical result which can be more easily managed by the following stage (comparator with hysteresis).

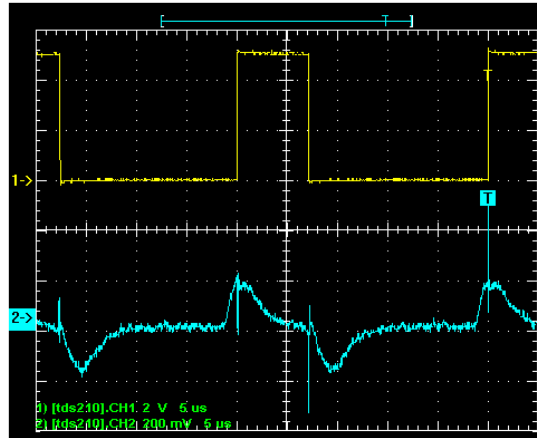


a) b)  
**Figure 5.13 – Waveforms for output of Hybrid TIA, to second stage wideband amplifier, then to differentiator.** a) Ch2 (blue) output of TIA; Ch1 (yellow) output of wideband amp. b) Ch1(yellow) wideband amplifier output; Ch2(blue) differentiator output.

As can be seen in figure 5.13, the output of the wideband amplifier has relatively slow transitions; as a result, the differentiated signal's output level is less – a drop in gain. However, the differentiated peaks are still very usable.

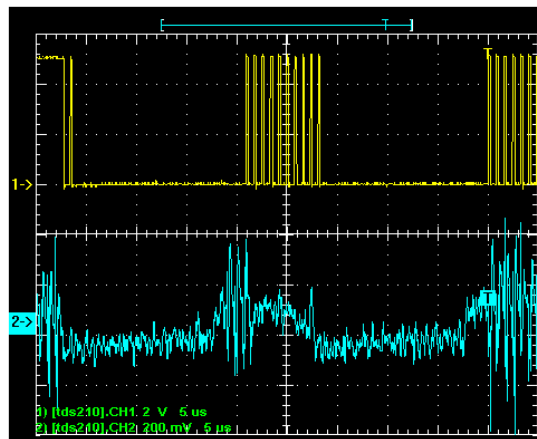
### 5.2.4 Signal discriminator using differentiated signal and Schmitt trigger

The output differentiated signal becomes the input to a comparator circuit with hysteresis which is described in chapter 4 and depicted in figure 4.15. The comparator's output negative going signal is clipped by a switching diode connected from output to ground. The comparator's output is connected to an inverting Schmitt trigger buffer, which is inverted a second time so as to shape the final output waveform as a very desirable rectangular waveform with fast edge rise/fall times and low noise replicating the transmitted waveform. Figure 5.14 shows the resultant waveform.



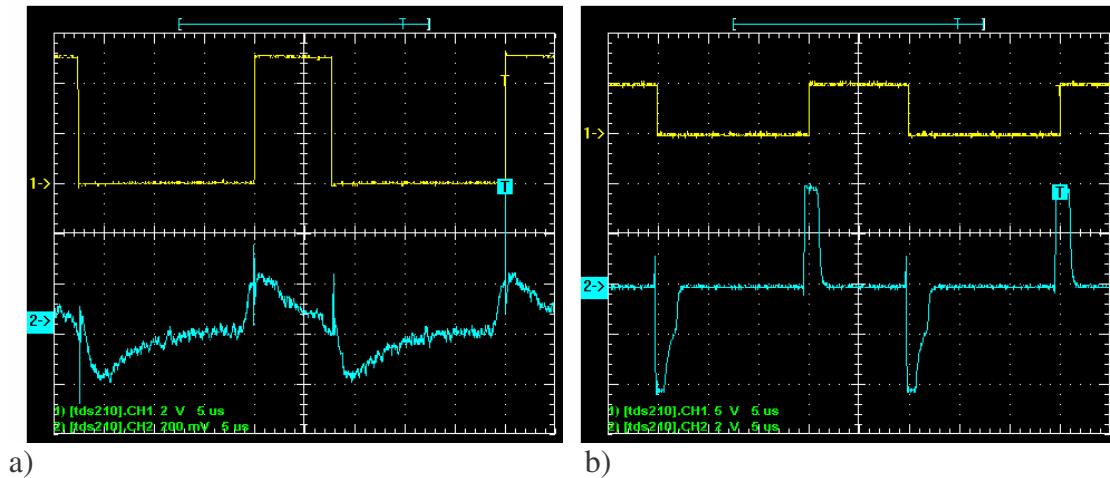
**Figure 5.14: Differentiator's output to input of comparator – Ch2(blue) Differentiated waveform; Ch1(yellow) output of the comparator circuit.**

With reference to figure 5.14, the comparator trigger points had to be carefully adjusted in order for the output to achieve the desired result. An unfortunate side effect of the fast switching relatively large output voltage of the Schmitt trigger inverters is that the output transitions appears into the differentiated waveform. It is suspected that this occurs through the power supply inputs of the op-amps used. As optical power was increased (through the addition of lens at the transmitter side) the higher level signal, created increased noise by the differentiator, caused the comparator circuit to over trigger creating a very undesirable results. This is shown in figure 5.15



**Figure 5.15: Increased input optical power creating unstable output due to higher noise levels falsely triggering the comparator circuit.** Ch2 (blue) - output of differentiator; Ch1 (yellow) - output of Schmitt trigger inverter.

Fortunately, the problem demonstrated in figure 5.15 was correctable by a careful adjustment to the comparator's UTL LTL trigger point. The figures shown in figure 5.16 show the circuit's operation over a wide range of input optical signal strength. The receiver worked with the input optical power ranging from  $9.62\mu\text{W}$  through to  $156\mu\text{W}$  (-20.2dBm to -9dBm) a range of 12.2dB. This range is possible by allowing the second stage amplifier to saturate with higher signal input; the differentiated signal could also move into saturation. The penalty for allowing saturation is an increase in the pulse time at the Schmitt trigger output.



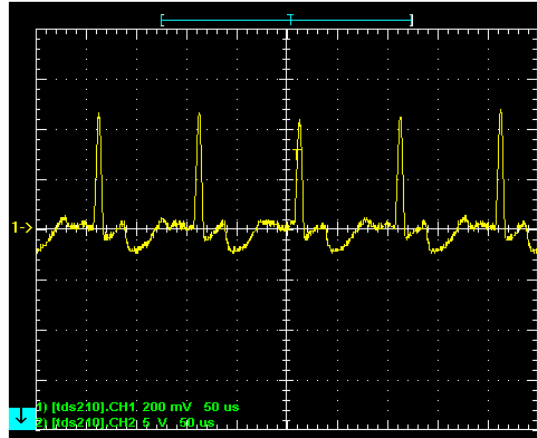
**Figure 5:16: Receiver circuit output with a wide input signal range in power** – a) Input optical power at  $9.62\mu\text{W}$  b) Input optical power at  $156\mu\text{W}$  -- Ch2 (blue) – differentiator output; Ch1 (yellow) – Schmitt trigger output

### 5.2.5 The GIC circuit results.

The GIC circuit designed so as to represent a lossless inductor having a value of 2 Henries, described in chapter 4 and depicted in figure 4.13, presents the possibility of being able to differentiate the incoming signal from the photodiode within the TIA first stage. If successful, this would eliminate the DC offset voltage resulting from ambient light and reduce one circuit element. The results obtained did not meet expectations.

The GIC circuit, when placed into the feedback loop of the Hybrid's TIA circuit, caused oscillation. The GIC, when applied to the feedback of the TIA built using the OPA2613, was stable and did differentiate. However, as mentioned earlier, the OPA2613 has relatively high input bias current that resulted in the output voltage DC base line riding close to the negative voltage rail. Although differentiation should remove the DC component, it was observed that this did not happen. It is suspected that as the GIC was built using the same op amps, it too most likely suffered from the high bias currents. With the TIA's output DC voltage being close to the negative bias voltage, when the circuit tried to differentiate the incoming signal, positive transitions acted as expected, but negative transitions were clipped as they reached the supply rail. The waveforms observed in this test are shown in figure 5.17. The input optical signal used was modified as follows: The received signal's optical power recorded at the detector is  $44\mu\text{W}$ , with the frequency reduced to 10kHz (pulse width exceeding LED source specs); the pulse duty cycle remained at 30%. The waveform recorded was with the scope AC coupled, removing the DC component, to allow for an increase in the sensitivity of the scope for better viewing of the resulting waveform. The DC level was recorded at -4V. As can be seen in the waveform, the negative going pulses are very short (clipped) compared to the positive transitions.

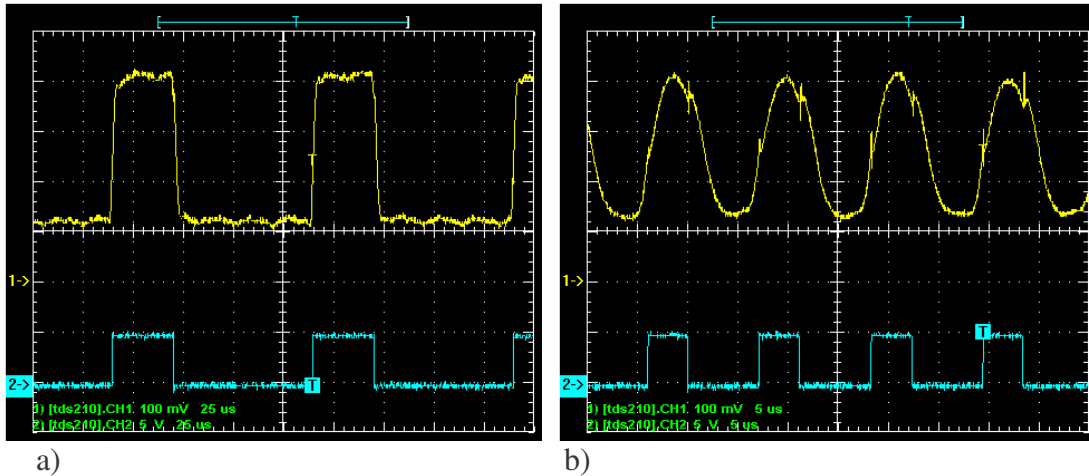




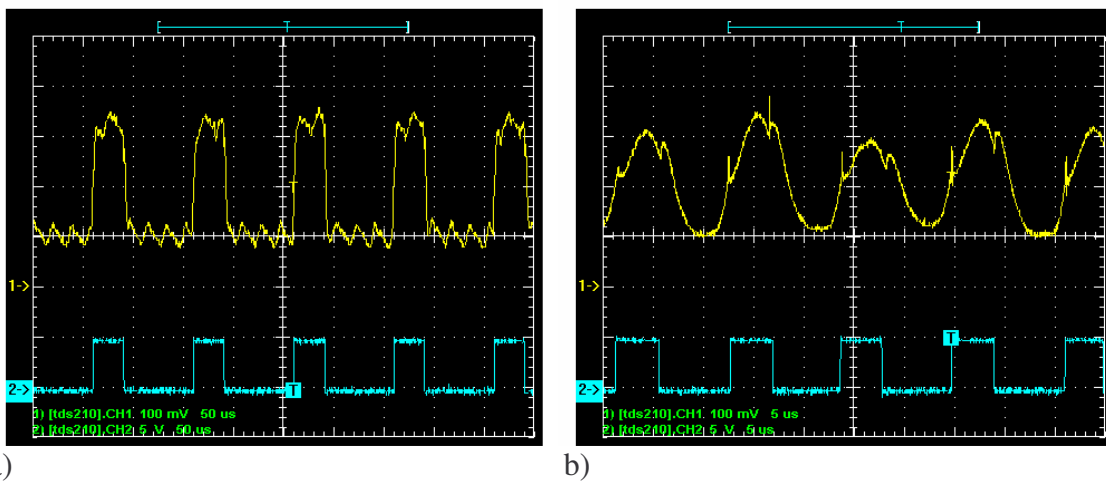
**Figure 5.17: Output waveform of TIA built with OPA2613 and using GIC circuit in feedback path.** Note: Scope AC coupled – DC level = -4V.

### 5.2.6 Frequency response

A brief evaluation of frequency response was conducted, but not done rigorously. As discussed earlier, the optical source's bandwidth is limited to approximately 125 kHz. With reference to table 5.3, three of the detector/TIA combinations have a predicted bandwidth < 300kHz but still greater than the maximum frequency of the source: the PDB-C107, the SD200-12-22-041, both of which are larger in surface area, and the SD100-42-22-231 hybrid with TIA GBW of 18MHz resulting in its lower bandwidth. For all six devices, the source frequency was increased and output level observed. Two photodiodes, the PDB-C107 and SD200-12-22-041 appeared to be limiting bandwidth rather than bandwidth limit caused by the source. Figure 5.18 shows the comparison of waveforms at 10kHz and at a higher frequency for the PDB-C107 photodiode mated to the OPA380 and figure 5.19 shows results for the SD200-12-22-041 with OPA380.



**Figure 5.18: Frequency response evaluation for PDB – C107.** a) Optical input signal 10kHz 30% duty cycle; b) 90kHz 30% duty cycle optical signal input. Ch1 (yellow) - output of TIA; Ch2 (blue) – output of Schmitt trigger.



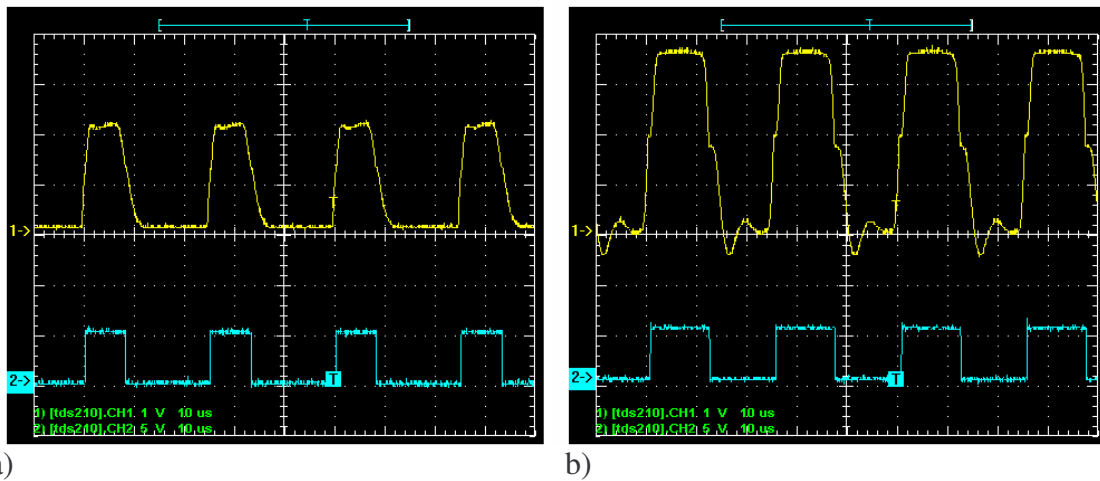
**Figure 5.19: Frequency response evaluation for SD-200-12-22-041.** a) Optical input signal 10kHz 30% duty cycle; b) 90kHz 30% duty cycle optical signal input. Ch1 (yellow) - output of TIA; Ch2 (blue) – output of Schmitt trigger.

### 5.2.7 Reception of optical signal at 30 meters from source

The final evaluation conducted for this project is a distance measurement. The same environment used for testing the power loss over distance for the LEDs was used in this evaluation. The test was conducted in the north-west hallway of the John Ware building at SAIT. The distance available is just over 30 meters. Figure 5.20 shows photographs of the test setup. The transmitter used the blue LED SSP-LX6144A7UC ( $\lambda=470\text{nm}$ ) with the generator input at 40kHz, 30% duty cycle, driving to 250mA peak. Fresnel lenses were placed at both the transmit side and the receiver side. The receiver was more than capable of recovering the signal, once the optics had been lined up. As discussed in chapter 4, because the Fresnel lens aperture is large in comparison to the surface area of

the PIN photodiode, the angle of acceptance is very small. The hallway was darkened, so as to keep ambient light to a minimum.

Only two detectors were used for this test, the lowest cost PDB-C142 and highest cost SD-100-42-22-231. In lining up the optical signal through the Fresnel lenses, at the receiver side it was easier to do using the PDB-C142 photodiode due to its plastic lens which, when the blue light was focused onto it, appears to glow. Focusing the received signal onto the active area of the hybrid was more challenging. Figure 5.20 shows the receivers' waveforms for both detectors at 30 meters.



**Figure 5.20: Resultant waveforms from received optical signal 30 meters from source.** a) PDB-C142 PIN photodetector combined with OPA380 TIA. b) SD-100-42-22-231 Hybrid. Ch1 (yellow) - signal at output of TIA; Ch2 (blue) signal at output of Schmitt trigger inverter.

The PDB-C142 received signal strength was lower than the hybrid, but a more accurate recovered signal resulted as the op amps in the receiver circuit did not get saturated. The hybrid package received signal, because it was so strong, resulted in widening the received pulse width, giving the appearance of a 48% duty cycle.

In the process of photographing this last evaluation, an interesting result occurred. In order to take the pictures shown in figure 5.21 the hallway lights were turned on. Despite what appeared to be an extremely high ambient light level, the receiver circuit continued to recover the transmitted light signal with waveforms almost identical to those observed in darkened conditions. In a closer examination, the reason for unimpeded circuit operation was that the ambient light from the ceiling fluorescents was being collected by the Fresnel lens and focused to a point below the detector.



**Figure 5.21 Distance measurement** – receiver at 30 meters from light source.

A test that should have been conducted, but a facility was not available to do it in, was to record the diameter of the area covered by the diverging source's beam at the distance for which the receiver could recover the waveform. From observations viewed from the source side towards the distant receiver, it appeared as though the beam's area had spread out far enough to reach the ceiling/wall/floor somewhere between 20 to 30 meters. Reflections from these surfaces may be aiding the recovery of the waveform by increasing the intensity of light collected.

## **Conclusions – and future Research**

### **6.1 Conclusion**

Autonomous motes, whose sensors gather data, eventually need to transmit that data and to be able to receive data from other motes or commands from a base station. The challenge for underwater sensor networks is how to transmit and receive data without physically being connected. Optical communications offers the possibility of high data rates at relatively low power and cost, unlike solutions that use acoustic or longwave radio communications.

This project focused primarily on the receiver side of the optical communication challenge, more specifically conversion of the optical signal into a useable voltage waveform that can then be further processed. In a review of optical detectors, the PIN photodiode became the obvious choice to use. Five PIN photodiodes, with various surface area sizes and packaging, and one Hybrid package were evaluated. In addition, TIA was chosen as the front end of the receiver design to convert the photodiodes' current to voltage. Time and the difficulty in building additional circuits, precluded other investigations.

One of the limiting factors to how low power of an optical signal can be and still be recovered is noise, internal to the photodiode and external. Although the TIA circuit with PIN photodiode combination appears simple, noise analysis is complex. This aspect of the receiver design was not investigated because of equipment availability and the additional time needed. There are standard techniques in printed circuit board (PCB) design that can and should be taken to help minimize noise issues. However, in creating the circuit board that was used for this evaluation and to provide some flexibility of use, standard noise suppression techniques could not be fully implemented as noted in chapter 4.

The TIA design is a compromise of gain vs. data rate vs. supply current. Manufacturers of operational amplifiers continue to improve and broaden their product offerings. Two discrete Burr-Brown op amp products were chosen for evaluation, the OPA380 designed specifically for TIA and the OPA2613, a wideband high slew rate op amp. Both products were relatively inexpensive. The OPA380 performed very well, it has wide GBW, high slew rate, and very low input bias current. The OPA2613 was a poor choice for TIA due to its high input bias currents. The Hybrid package's internal op amp, specifically designed for TIA, performed very well. All three op amp products draw approximately 6mA of current per amplifier. This is higher than desired (low current to extend battery life is needed), but compromise is required between required GBW, voltage input noise, input bias current, and cost. As most op amps used for this type of implementation are surface mount, to investigate multiple op amp products requires building several circuit boards.

The PIN photodiodes evaluated did not provide any significant surprises. The larger surface area packages received more light, making them better suited to lower light power recovery. But, their larger area also increases junction capacitance which decreases bandwidth. The physical packages also determine their FOV, important if they are used without any additional lenses in front of them. But, for long distances, lenses are required and the PIN's lens is less important. The photodiodes chosen, with the exception of one, were "blue-enhanced". Their spectral response shows a slight increase in sensitivity at the blue green wavelengths, but it was unclear in this investigation if they provided much of a significant advantage over the non-enhanced type.

One interesting observation made, was the performance of the Hybrid product compared to the discrete PIN photodiodes in combination with the TIA using OPA380. The hybrid did appear to have less noise on its recovered voltage waveform, compared with the discrete approach, but only marginally so. There was very little difference between the hybrid and PIN photodiode with same active surface area size and in the same packaging; but the Hybrid cost \$106.63, the PIN photodiode costs \$26.87 and the OPA 380 is \$4.70.

The recovered voltage waveform from the TIA may not be suitable (amplitude, noise, shape) to be passed directly to the processor, signal conditioning is required. For this evaluation, a high-pass wide bandwidth non-inverting amplifier stage followed the TIA. This amplifier removed the ambient light DC level from the TIA's output signal and provided additional gain. As a pleasant side effect, when connected to the TIA it resolved gain peaking observed at the output of the TIA when unloaded. In a more rigorous PCB design, it's most likely that this would not have happened and a feedback capacitor  $C_f$  would have to be added.

To shape the recovered voltage waveform, a differentiator followed by comparator and Schmitt trigger inverters was used. The final recovered output pulse, from 0 to 5V, had very fast transitions, and very low noise. However, caution is advised in using differentiation as a technique. Differentiators increase noise. Because bandwidth was limited to less than 500kHz, the noise level increase that did occur was manageable during this investigation.

For this evaluation, a rectangular waveform, to emulate OOK, with a frequency of 40kHz and pulse duty cycle of 30% was used for most measurement. The small area PIN photodiodes were able to easily operate at over 100kHz. The choice of frequency was based on achieving high gain at the TIA and at a frequency that seemed appropriate based on values for some current mote used today in terrestrial sensor networks.

A goal for the experimental evaluation was to achieve distance between the transmitter and the receiver. Without lens, distance was limited to a few meters (exact value was not determined). With the addition of 101mm Fresnel lenses at both the receiver and transmitter side, substantial gain in optical signal power at the receiver's PIN photodiode was achieved. A distance of 30 meters was achieved (limited by hallway length) with relative ease (LOS focusing was needed). With the TIA gain set at  $1M\Omega$  and second stage gain approximately 10, the evaluation board easily recovered signal with optical

power, as recorded by Newport's optical meter, of  $8\mu\text{W}$  (equivalent to  $-21\text{dBm}$ ), regardless of which detector used. Although the larger area diodes could go to lower power they also collected ambient light causing DC offset to increase. Referring to the graph of figure 5.5 e) it is estimated that at a distance beyond 50 meters signal recovery would become a challenge. Caution is needed on this interpretation; if the signal source optical power is set higher greater distance is achievable.

For underwater applications, it's difficult to make a prediction on actual distance that may be achievable because of the undefined power level of the source. However, the experiments reviewed in chapter 3 show that without additional lenses, one can only expect to achieve around 2 to 3 meters of distance. With lenses, distance increases, but LOS also becomes critical. If one uses Clancy's data as shown in the graph of figure 3.4, and assumes the initial optical power is  $+10\text{dBm}$ , the same optical power at 1 meter measured for this project's distance measurements, then for a minimum operational power level of  $8\mu\text{W}$  ( $-21\text{dBm}$ ) a power loss of  $31\text{dB}$  can be tolerated. This translates to a distance of near 8 meters in Type II ocean waters. In clearer Type I waters, distance will increase.

## **6.2 Recommendations for future research**

To move forward with designing and building a sensor network, using optical communications, for underwater, it is recommended that this work be done as a group project rather than through individual investigations. The team should consist of an optical engineer, mechanical engineer, electrical engineer, internetworking expert, an electronics technologist, and a machinist. It was most frustrating in this project not to have the skills of an optical designer, as lenses are critical to light propagation and detection. The Fresnel lenses used clearly show their advantage in collecting light, but also disadvantage in narrowing the acceptance angle to almost zero. Air experiments are a good starting point, but cannot replicate the underwater reality. A mechanical engineer is required to design a package that can withstand the pressures of water, for the package to be recoverable, and for aligning the optics. A machinist is required to bring the design to reality. The electrical engineer, communications engineer, and electronic technologist need to work on both the transmit side and receive side simultaneously. This investigation will also require a large budget.

One piece of information that is needed, critical to the choices made in receiver and transmitter design, is the amount of data that is collected by a mote and more importantly, what data transmission rate is required to move the data forward to its final point. Not only does one need to contend with the self generated data but also the transitioning data across the mote. A traffic study should be conducted. Perhaps as part of this study, or a separate investigation, approaches to dealing with multiple optical signals arriving at the same detector needs investigating and/or what collision avoidance protocol should be established?

Another area of research needed is the investigation of backscattering of light in water. Backscattering is viewed as a negative component when trying to achieve LOS communication as it contributes to signal attenuation. But, if we want to design a mote for underwater use that emulates that of terrestrial motes, then backscattering/ multi-scattering as depicted in figure 1.3 will need to be taken advantage of. We may be using the wrong wavelengths.

Another area of research that could be done by an individual or team, in aiding the design of the receiver, is noise cancellation methods – signal averaging is a feature available on some digital oscilloscopes such as used in this project. It averages the capture image and is very effective, but slow. The challenge is applying this in real time on high frequency signals – very fast DSPs are most likely needed (and are expensive).

Throughout this project, I could not help remembering a product being sold as a fishing aid in the 1960s early 1970s, a pulsing light packaged in clear plastic. From which, the question: does the visible light for underwater optical communications affect sea life? An environmental study is required. In addition, how quickly will the mote lenses become obscured by sediment and sea life? Will battery life exceed this event?

A final observation, throughout this project, when not thinking of fishing, I kept thinking that designing an optical receiver should be easy to do. The research conducted and my own experience now tells me that this is not a simple task; if it were, it most likely would have been done.



## References

1. T. Schiller, A. Liers, & H. Ritter, *Scatter Web the Open and Flexible Sensornet Platform*, Freie Universität Berlin. (2004) Retrieved from: <http://www.fu-berlin.de/forschung/transfer/messen/04HMISchiller.pdf>
2. Intel, *Next Generation Intel Mote*, Retrieved Sept. 9/07 from: <http://www.intel.com/research/exploratory/motes.htm>
3. *RFM T1001 Hybrid transceiver data sheet*, available at <http://www.rfm.com/index.shtml>
4. T. Haenselmann, *An FDL'ed Textbook on Sensor Networks - Chapter 1 Motivation and Introduction*, GNU Free document license (FDL), pp. 1-13. (2007) Retrieved from: [http://www.informatik.uni-mannheim.de/~haensel/sn\\_book/](http://www.informatik.uni-mannheim.de/~haensel/sn_book/)
5. J. Kong, J. Cui, D. Wu, & M. Geria, *Building Underwater Ad-Hoc Networks and Sensor Networks for Large Scale Real-Time Aquatic Applications* (2005) Retrieved from: [http://www.engr.uconn.edu/~jcui/UWSN\\_papers/uwsn\\_milcom\\_2005.pdf](http://www.engr.uconn.edu/~jcui/UWSN_papers/uwsn_milcom_2005.pdf)
6. *Micro-Modem Overview*, Retrieved Sept. 2007 from: <http://acomms.who.edu/micromodem/>
7. Z. Peng, J. Cui, B. Wang, K. Ball, & L. Freitag, *An Underwater Network Test bed: Design, Implementation and Measurement*, (2007) Retrieved from: <http://www.engr.uconn.edu/~bing/Peng07-aqua-lab.pdf>
8. F. Schill and U. Zimmer, *Effective Communication in Schools of Submersibles*, (2006) Retrieved from: [http://axiom.anu.edu.au/~felix/studies/Publications/Swarm\\_Communication.pdf](http://axiom.anu.edu.au/~felix/studies/Publications/Swarm_Communication.pdf)
9. F. Schill, U. Zimmer, & J. Trumpf, *Visible Spectrum Optical Communication and Distance Sensing for Underwater Applications*; Proceedings of the Australasian Conference on Robotics and Automation, (2004) Retrieved from: <http://www.araa.asn.au/acra/acra2004/papers/schill.pdf>
10. Hamamatsu Photonics, *Photomultiplier Tubes: Basics and Applications 3<sup>rd</sup> ed.*, (2006) Retrieved from: <http://sales.hamamatsu.com/>
11. L. Godfrey, *Choosing the Detector for You're Unique Light Sensing Application*, PerkinElmer, (2003) Retrieved from: [http://optoelectronics.perkinelmer.com/content/ApplicationNotes/APP\\_Choosin\\_gTheDetector.pdf](http://optoelectronics.perkinelmer.com/content/ApplicationNotes/APP_Choosin_gTheDetector.pdf)

12. Photonics, *Photograph of current commercially available photomultiplier tubes*, (2006) Retrieved from: <http://www.photonis.com/products/photomultiplier-tubes>
13. B. Tissue, *Photomultiplier Tubes*, Department of Chemistry KIAST, (1996) Retrieved from: <http://elchem.kaist.ac.kr/vt/chem-ed/optics/optics.htm>
14. Hamamatsu, *Photomultiplier Tubes: Construction and Operating Characteristics*, (2006) Retrieved from: [http://sales.hamamatsu.com/assets/applications/ETD/PMT\\_4-15e.pdf](http://sales.hamamatsu.com/assets/applications/ETD/PMT_4-15e.pdf)
15. J. Graeme, *Photodiode Amplifiers Op Amp Solutions*, McGraw Hill. . (1995)
16. Hamamatsu, *Photodiode Technical Information*, (2007) Retrieved from: <http://sales.hamamatsu.com/assets/html/ssd/si-photodiode/index.htm>
17. K. Kaurmann, *Choosing Your Detector*, (2005) Retrieved from: <http://sales.hamamatsu.com/>
18. F. Perry, *Predicting the performance of a photodetector*, (2005) Retrieved from: <http://www.boselec.com/products/documents>
19. J.C. Whitaker (ed.), *The Electronics Handbook 2ed.*, Taylor & Francis Group. P. K. Yu. Chapter 9.4 Optical Receivers. pp. 964-980 (2005)
20. Photograph of PIN photodiodes retrieved from: <http://www.advancedphotonix.com/>
21. N. Biyikli, T. Kartaloglu, O. Aytur, I. Kimukin, & E. Ozbay, *High-Performance Solar-Blind AlGa<sub>N</sub> Schottky Photodiodes*, MRS Internet Journal. (2003) Retrieved from: <http://nsr.mij.mrs.org/8/2/article.pdf>
22. H. Jiang; T. Egawa; H. Ishikawa, *AlGa<sub>N</sub> solar-blind Schottky photodiodes fabricated on 4H-SiC*, Photonics Technology Letters, IEEE Volume 18, Issue 12, pp. 1353 – 1355(2006)
23. Perkin Elmer, *Avalanche photodiode: A user Guide*, (2006) Retrieved from [http://optoelectronics.perkinelmer.com/content/ApplicationNotes/APP\\_APDUersGuide.pdf](http://optoelectronics.perkinelmer.com/content/ApplicationNotes/APP_APDUersGuide.pdf)
24. Hamamatsu, *Si APD S9251 Series*, (2004) Retrieved from <http://sales.hamamatsu.com/>
25. J Dakin, *The Handbook of Optoelectronics*, Taylor and Francis CRC press. p. 85(2006)

26. Borgart T., *Electronic Devices and Circuits 4<sup>th</sup>*, Ed. Prentice Hall pp. 873-874. (1997)
27. EG&C Optoelectronics, *Characteristics of Phototransistors*, (1997) Retrieved from:  
[http://www.engr.udayton.edu/faculty/jloomis/ece445/topics/egginc/pt\\_char.html](http://www.engr.udayton.edu/faculty/jloomis/ece445/topics/egginc/pt_char.html)
28. J. Giles and I. Bankman, *Underwater Optical Communications Systems Part2: Basic Design Considerations*, Military Communications Conference, 2005. MILCOM 2005. IEEE. pp. 1700-1705 Vol. 3 (2005)
29. M. Chancy, *Short Range Underwater Optical Communication Links*, Master Thesis, North Carolina State University, (2005) Retrieved from:  
<http://www.lib.ncsu.edu/theses/available/etd-07252005-171301/unrestricted/etd.pdf>
30. J. Smart, *Underwater Optical Communications Systems Part 1: Variability of Water Optical Parameters*, Military Communications Conference, 2005. MILCOM 2005. IEEE pp. 1140-1146 Vol. 2 (2005).
31. M. Tivey, P. Fucile, and E. Sichel, *A Low Power, Low Cost, Underwater Optical Communication System*, Ridge 2000 Events, Volume 2 Number 1, April 2004 pp. 27-29 (2004)
32. F. Schill, U. Zimmer, and J. Trumpf, *Visible Spectrum Optical Communication and Distance Sensing for Underwater Applications*, Proceedings of the Australasian Conference on Robotics and Automation (2004)
33. D. Johnson, *Handbook of Optical Through the Air Communications*, Chapter 6: Optical Receiver Circuits, (2002) Retrieved from:  
<http://www.imagineeringezine.com/air-bk2.html>
34. Vishay Semiconductors, *Circuit Description of the IR Receiver Modules*, Document number 80069. (2003) Retrieved from: <http://www.vishay.com>
35. J. Gibson, *The Communications Handbook 2<sup>nd</sup> ed.*, Chapter 48: Optical Receivers, R. Smith and B. Kasper, CRC Press. (2002)
36. *A 107.7 mile 2-way optical contact*, (2007) Retrieved from:  
[http://ka7oei.com/optical\\_comms/optical\\_qso\\_107mile.html](http://ka7oei.com/optical_comms/optical_qso_107mile.html)
37. National Semiconductor, *Photodiode Amplifiers: Changing Light into Electricity On-Line Seminar* (slides and transcripts), (2004) Retrieved from  
<http://www.national.com/onlineseminar/>

38. Burr-Brown, *OPA380/OPA2380 Precision, High-speed Transimpedance Amplifier data sheet*, (2005) Retrieved from:  
<http://focus.ti.com/docs/prod/folders/print/opa380.html>
39. Melles Griot, *LED measurements*, (2007), Retrieved from:  
<http://www.mellesgriot.com/products/technicalliterature.asp>
40. Melles Griot, *Fundamentals of Power and Energy Measurement*, (2005)  
Retrieved from: [http://www.mellesgriot.com/pdf/X\\_43\\_4-11.pdf](http://www.mellesgriot.com/pdf/X_43_4-11.pdf)

## **Appendix**

## **Appendix A: Data sheets for LEDs**

Model: LED-G-1W-N - 1W green LED module

Available at: <http://www.lasermate.com/LEDModule.html>

Model: LED-B-1W-D - 1W blue LED module

Available at: <http://www.lasermate.com/LEDModule.html>

Model: LV W5SG-GXHX-35-Z (475-1199-1 ND) VERDE Clear No lens SMD

Available at: <http://www.osram-os.com/> or <http://parts.digikey.com/>


Model: SSP-LX6144A2UC (441-1089-ND)420mW green Water clear lens

Available at: <http://www.sunbriteleds.com/> or <http://parts.digikey.com/>

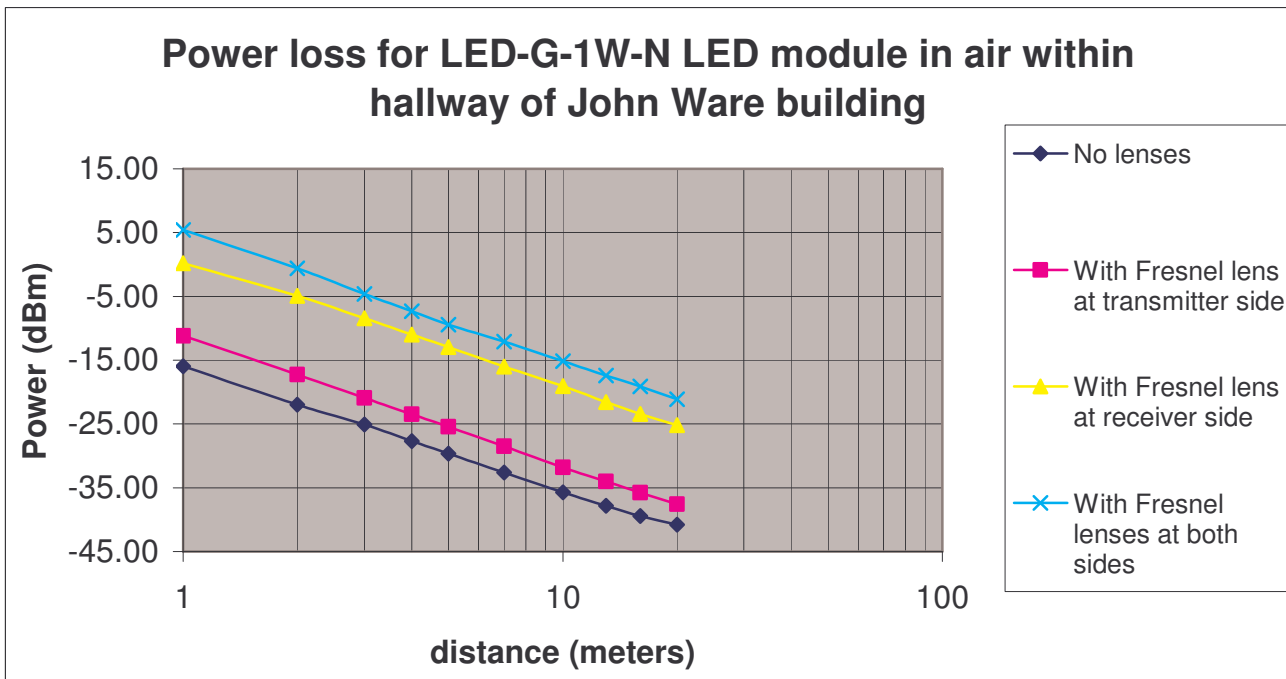
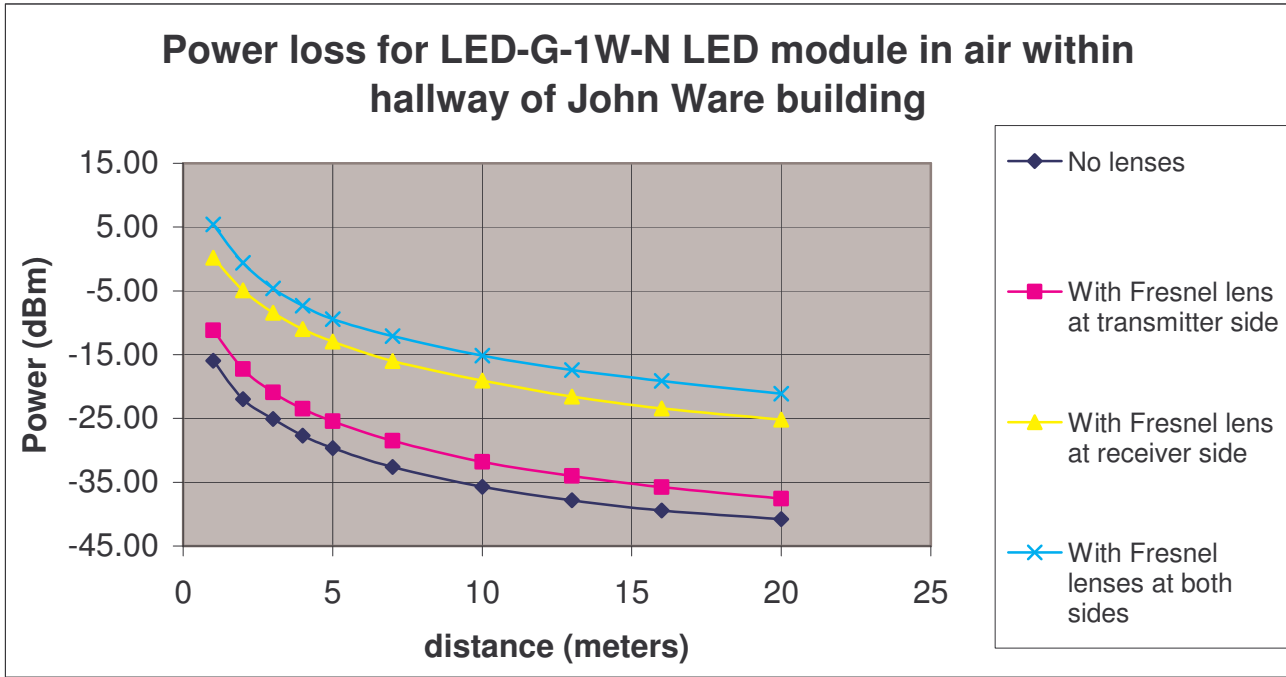
Model: SSP-LX6144A7UC (441-1092-ND)420mW blue Water clear lens

Available at: <http://www.sunbriteleds.com/> or <http://parts.digikey.com/>

**Appendix B: Tables of measured data for LEDs**


Model: LED-G-1W-N - 1W green - $\lambda=520\text{nm}$ LED module									
	Measured Light power (W): No Fresnel lenses		Measured Light power (W): With transmit Fresnel lens only		Measured Light power (W): With receiver Fresnel lens only		Measured Light power (W): With both transmit and receive Fresnel lenses		
	Distance (meters)	Light + ambient	Ambient light only	Light + ambient	Ambient light only	Light + ambient	Ambient light only	Light + ambient	Ambient light only
	1	2.55E-05	1.98E-08	7.61E-05	2.39E-08	1.05E-03	3.69E-08	3.48E-03	2.22E-08
	2	6.35E-06	1.72E-08	1.89E-05	2.25E-08	3.22E-04	3.94E-08	8.73E-04	3.29E-08
	3	3.12E-06	1.37E-08	8.13E-06	2.05E-08	1.43E-04	4.50E-08	3.44E-04	3.92E-08
	4	1.71E-06	1.15E-08	4.52E-06	1.60E-08	7.93E-05	3.55E-08	1.85E-04	4.53E-08
	5	1.10E-06	9.90E-09	2.86E-06	1.15E-08	5.06E-05	3.92E-08	1.14E-04	4.42E-08
	7	5.60E-07	8.70E-09	1.42E-06	1.02E-08	2.52E-05	3.27E-08	6.19E-05	3.87E-08
	10	2.75E-07	6.60E-09	6.70E-07	9.40E-09	1.24E-05	3.00E-08	3.07E-05	3.23E-08
	13	1.72E-07	6.15E-09	4.05E-07	9.60E-09	7.00E-06	3.60E-08	1.82E-05	2.94E-08
16	1.19E-07	5.50E-09	2.74E-07	8.90E-09	4.57E-06	4.30E-08	1.23E-05	2.76E-08	
20	9.10E-08	7.10E-09	1.85E-07	1.05E-08	3.06E-06	3.90E-08	7.71E-06	2.83E-08	
	Incident light minus ambient		Incident light minus ambient		Incident light minus ambient		Incident light minus ambient		
	power (W)	power (dBm)	power (W)	power (dBm)	power (W)	power (dBm)	power (W)	power (dBm)	
1	2.55E-05	-15.94	7.61E-05	-11.19	1.05E-03	0.21	3.48E-03	5.42	
2	6.33E-06	-21.98	1.89E-05	-17.24	3.22E-04	-4.92	8.73E-04	-0.59	
3	3.11E-06	-25.08	8.11E-06	-20.91	1.43E-04	-8.45	3.44E-04	-4.63	
4	1.70E-06	-27.70	4.50E-06	-23.46	7.93E-05	-11.01	1.85E-04	-7.33	
5	1.09E-06	-29.63	2.85E-06	-25.45	5.06E-05	-12.96	1.14E-04	-9.43	
7	5.51E-07	-32.59	1.41E-06	-28.51	2.52E-05	-15.99	6.19E-05	-12.09	
10	2.68E-07	-35.71	6.61E-07	-31.80	1.24E-05	-19.08	3.07E-05	-15.13	
13	1.66E-07	-37.80	3.95E-07	-34.03	6.96E-06	-21.57	1.82E-05	-17.41	
16	1.14E-07	-39.45	2.65E-07	-35.77	4.53E-06	-23.44	1.23E-05	-19.11	
20	8.39E-08	-40.76	1.75E-07	-37.58	3.02E-06	-25.20	7.68E-06	-21.15	

**Test conditions: Transistor part # TIP121, in classical transistor switch configuration;** Collector Bias voltage - 16.8V; Collector resistor - 51 $\Omega$  5.5W; Base resistor 330 $\Omega$  1/2W; Source connected to base resistor - Pulse 0-1.5V, at frequency of 40kHz 30% du

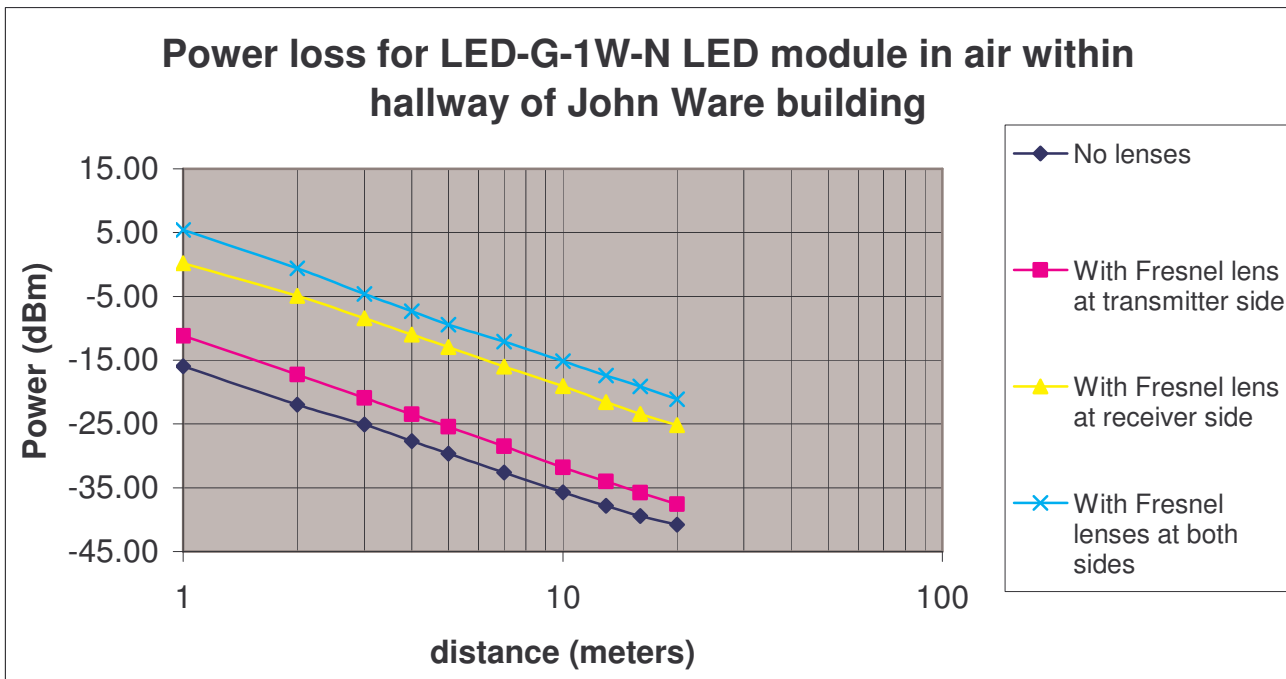
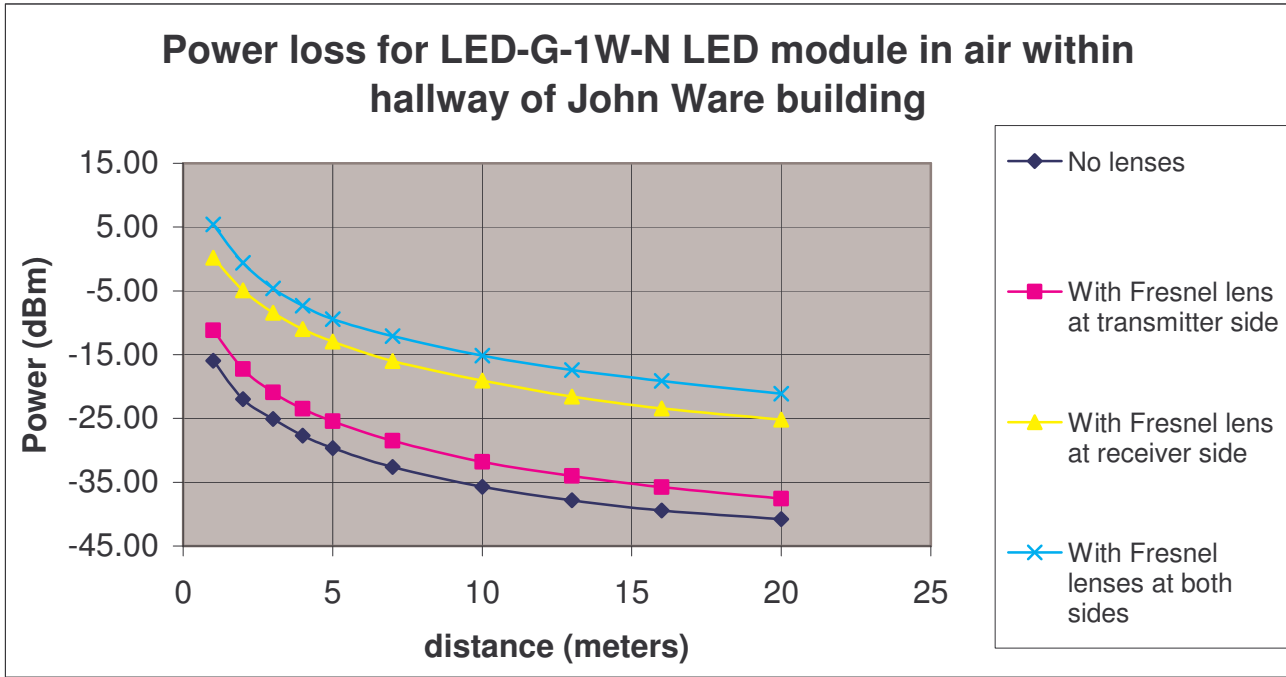





Investigation of Optical Receivers For Use in an Underwater Environment

Model: LED-G-1W-N - 1W green - $\lambda=520\text{nm}$ LED module									
	Measured Light power (W): No Fresnel lenses		Measured Light power (W): With transmit Fresnel lens only		Measured Light power (W): With receiver Fresnel lens only		Measured Light power (W): With both transmit and receive Fresnel lenses		
	Distance (meters)	Light + ambient	Ambient light only	Light + ambient	Ambient light only	Light + ambient	Ambient light only	Light + ambient	Ambient light only
	1	2.55E-05	1.98E-08	7.61E-05	2.39E-08	1.05E-03	3.69E-08	3.48E-03	2.22E-08
	2	6.35E-06	1.72E-08	1.89E-05	2.25E-08	3.22E-04	3.94E-08	8.73E-04	3.29E-08
	3	3.12E-06	1.37E-08	8.13E-06	2.05E-08	1.43E-04	4.50E-08	3.44E-04	3.92E-08
	4	1.71E-06	1.15E-08	4.52E-06	1.60E-08	7.93E-05	3.55E-08	1.85E-04	4.53E-08
	5	1.10E-06	9.90E-09	2.86E-06	1.15E-08	5.06E-05	3.92E-08	1.14E-04	4.42E-08
	7	5.60E-07	8.70E-09	1.42E-06	1.02E-08	2.52E-05	3.27E-08	6.19E-05	3.87E-08
	10	2.75E-07	6.60E-09	6.70E-07	9.40E-09	1.24E-05	3.00E-08	3.07E-05	3.23E-08
	13	1.72E-07	6.15E-09	4.05E-07	9.60E-09	7.00E-06	3.60E-08	1.82E-05	2.94E-08
16	1.19E-07	5.50E-09	2.74E-07	8.90E-09	4.57E-06	4.30E-08	1.23E-05	2.76E-08	
20	9.10E-08	7.10E-09	1.85E-07	1.05E-08	3.06E-06	3.90E-08	7.71E-06	2.83E-08	
	Incident light minus ambient		Incident light minus ambient		Incident light minus ambient		Incident light minus ambient		
	power (W)	power (dBm)	power (W)	power (dBm)	power (W)	power (dBm)	power (W)	power (dBm)	
1	2.55E-05	-15.94	7.61E-05	-11.19	1.05E-03	0.21	3.48E-03	5.42	
2	6.33E-06	-21.98	1.89E-05	-17.24	3.22E-04	-4.92	8.73E-04	-0.59	
3	3.11E-06	-25.08	8.11E-06	-20.91	1.43E-04	-8.45	3.44E-04	-4.63	
4	1.70E-06	-27.70	4.50E-06	-23.46	7.93E-05	-11.01	1.85E-04	-7.33	
5	1.09E-06	-29.63	2.85E-06	-25.45	5.06E-05	-12.96	1.14E-04	-9.43	
7	5.51E-07	-32.59	1.41E-06	-28.51	2.52E-05	-15.99	6.19E-05	-12.09	
10	2.68E-07	-35.71	6.61E-07	-31.80	1.24E-05	-19.08	3.07E-05	-15.13	
13	1.66E-07	-37.80	3.95E-07	-34.03	6.96E-06	-21.57	1.82E-05	-17.41	
16	1.14E-07	-39.45	2.65E-07	-35.77	4.53E-06	-23.44	1.23E-05	-19.11	
20	8.39E-08	-40.76	1.75E-07	-37.58	3.02E-06	-25.20	7.68E-06	-21.15	

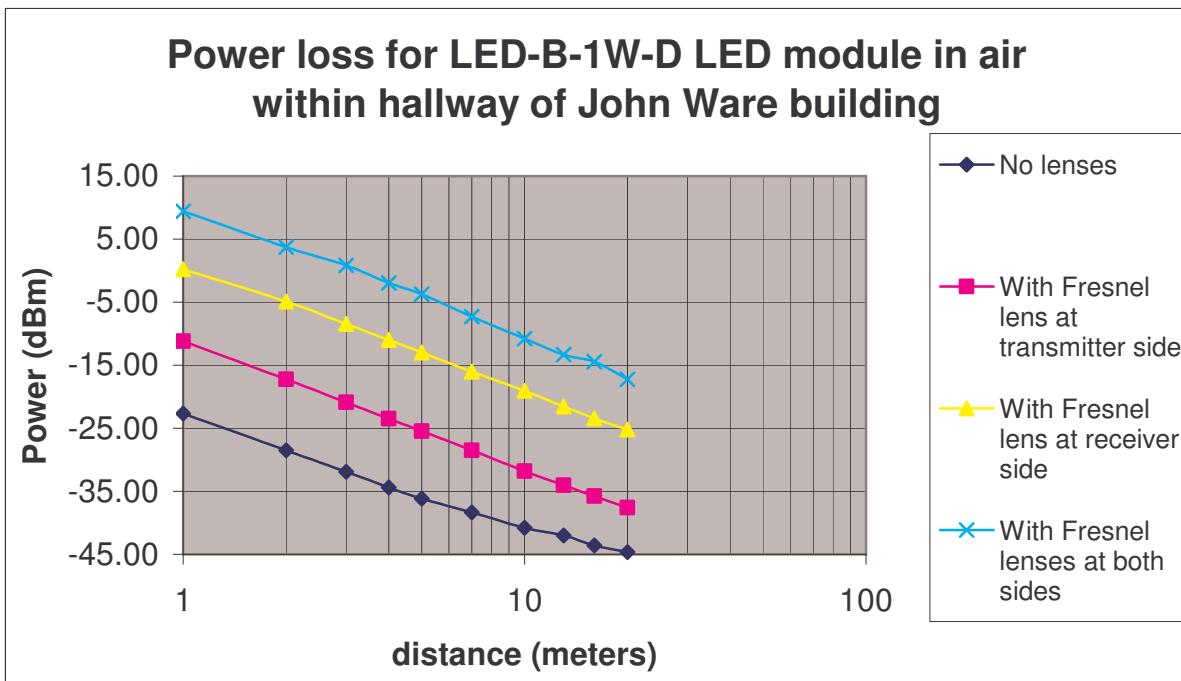
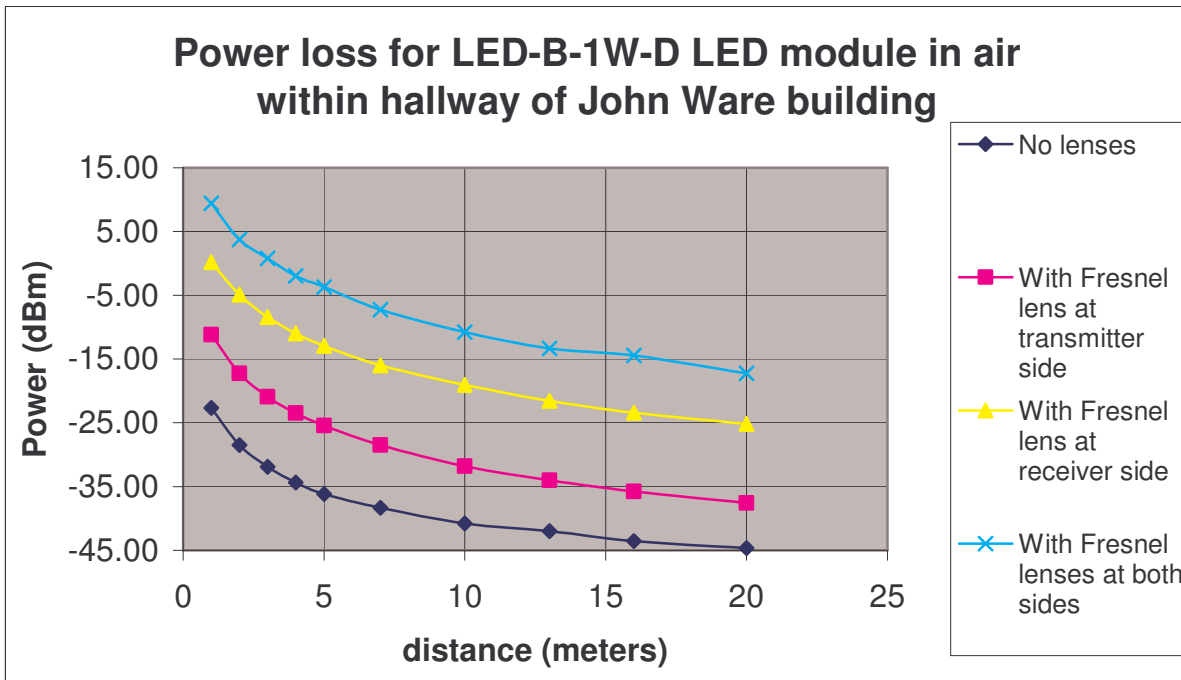
**Test conditions:** Transistor part # TIP121, in classical transistor switch configuration; Collector Bias voltage - 16.8V; Collector resistor - 51 $\Omega$  5.5W; Base resistor 330 $\Omega$  1/2W; Source connected to base resistor - Pulse 0-1.5V, at frequency of 40kHz 30% du




Investigation of Optical Receivers For Use in an Underwater Environment

Model: LED-B-1W-N - 1W Blue - $\lambda=470\text{nm}$ LED module									
	Measured Light power (W): No Fresnel lenses		Measured Light power (W): With transmit Fresnel lens only		Measured Light power (W): With receiver Fresnel lens only		Measured Light power (W): With both transmit and receive Fresnel		
	Distance (meters)	Light + ambient	Ambient light only	Light + ambient	Ambient light only	Light + ambient	Ambient light only	Light + ambient	Ambient light only
	1	5.45E-06	2.17E-08	2.92E-04	2.11E-08	3.03E-04	3.69E-08	8.78E-03	2.22E-08
	2	1.43E-06	1.87E-08	6.90E-05	1.99E-08	7.61E-05	3.33E-08	2.37E-03	3.06E-08
	3	6.63E-07	1.56E-08	2.58E-05	1.76E-08	3.38E-05	3.46E-08	1.21E-03	3.19E-08
	4	3.77E-07	1.28E-08	1.29E-05	1.56E-08	1.88E-05	4.02E-08	6.34E-04	4.21E-08
	5	2.52E-07	1.10E-08	8.59E-06	1.12E-08	1.20E-05	2.77E-08	4.25E-04	3.98E-08
	7	1.55E-07	8.80E-09	3.61E-06	8.65E-09	6.20E-06	3.71E-08	1.88E-04	3.80E-08
	10	9.15E-08	7.90E-09	2.19E-06	7.76E-09	3.03E-06	3.16E-08	1.15E-04	3.20E-08
	13	7.09E-08	7.99E-09	9.30E-07	7.40E-09	1.78E-06	3.31E-08	4.65E-05	2.89E-08
16	5.18E-08	7.83E-09	6.97E-07	7.43E-09	1.20E-06	2.93E-08	3.61E-05	2.77E-08	
20	4.35E-08	9.11E-09	3.82E-07	8.84E-09	7.80E-07	2.70E-08	1.89E-05	2.82E-08	
	Incident light minus ambient		Incident light minus ambient		Incident light minus ambient		Incident light minus ambient		
	power (W)	power (dBm)	power (W)	power (dBm)	power (W)	power (dBm)	power (W)	power (dBm)	
1	5.43E-06	-22.65	2.92E-04	-5.35	3.03E-04	-5.19	8.78E-03	9.43	
2	1.41E-06	-28.50	6.90E-05	-11.61	7.61E-05	-11.19	2.37E-03	3.75	
3	6.47E-07	-31.89	2.58E-05	-15.89	3.38E-05	-14.72	1.21E-03	0.83	
4	3.64E-07	-34.39	1.29E-05	-18.90	1.88E-05	-17.27	6.34E-04	-1.98	
5	2.41E-07	-36.18	8.58E-06	-20.67	1.20E-05	-19.22	4.25E-04	-3.72	
7	1.46E-07	-38.35	3.60E-06	-24.44	6.16E-06	-22.10	1.88E-04	-7.26	
10	8.36E-08	-40.78	2.18E-06	-26.61	3.00E-06	-25.23	8.30E-05	-10.81	
13	6.29E-08	-42.01	9.23E-07	-30.35	1.75E-06	-27.58	4.65E-05	-13.33	
16	4.40E-08	-43.57	6.90E-07	-31.61	1.17E-06	-29.32	3.61E-05	-14.43	
20	3.44E-08	-44.64	3.73E-07	-34.28	7.53E-07	-31.23	1.89E-05	-17.24	

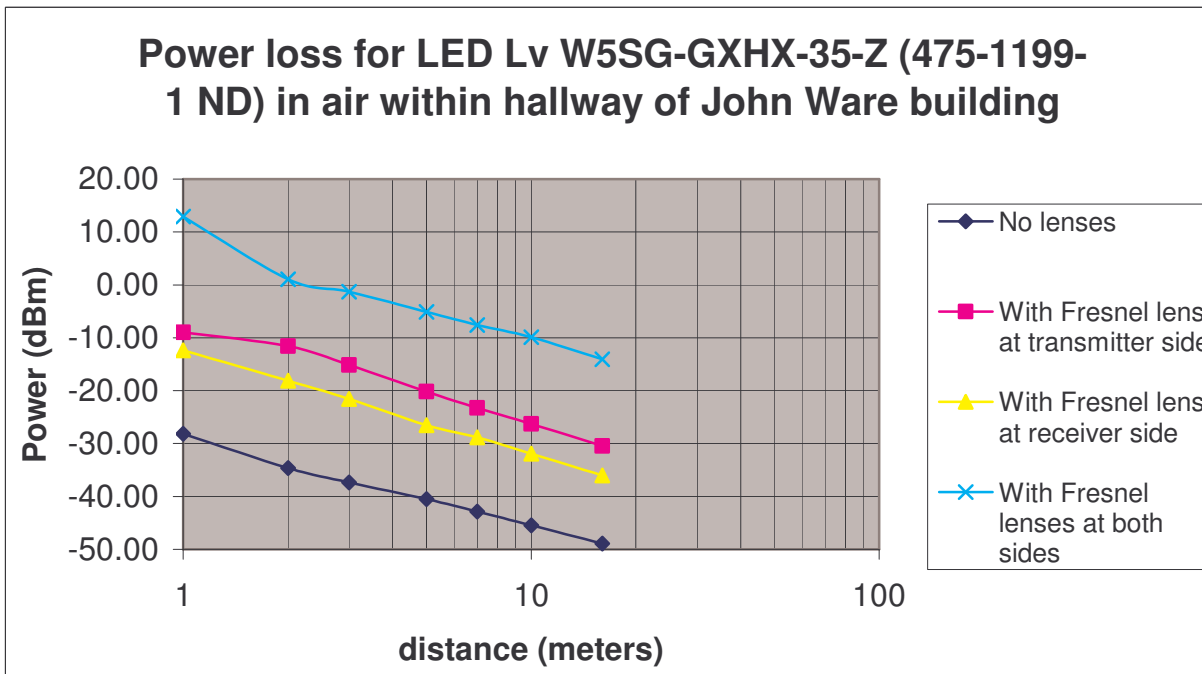
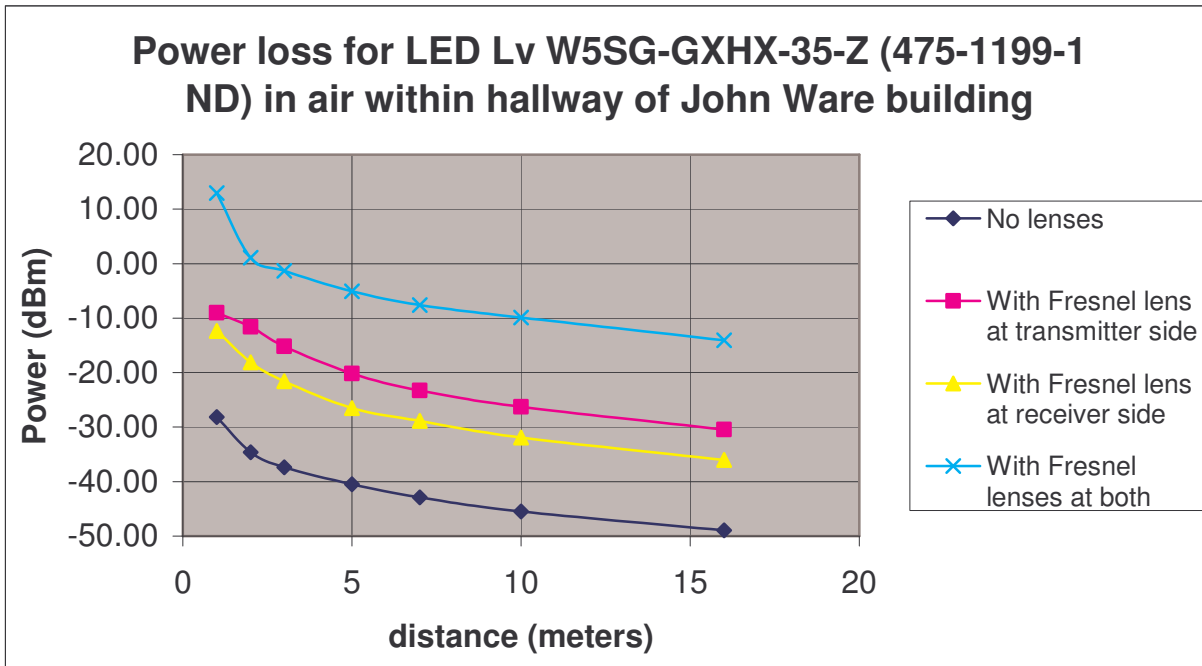
**Test conditions: Transistor part # TIP121, in classical transistor switch configuration;** Collector Bias voltage - 16.8V; Collector resistor - 51 $\Omega$  5.5W; Base resistor 330 $\Omega$  1/2W; Source connected to base resistor - Pulse 0-1.5V, at frequency of 40kHz 30% du

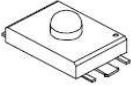


Investigation of Optical Receivers For Use in an Underwater Environment

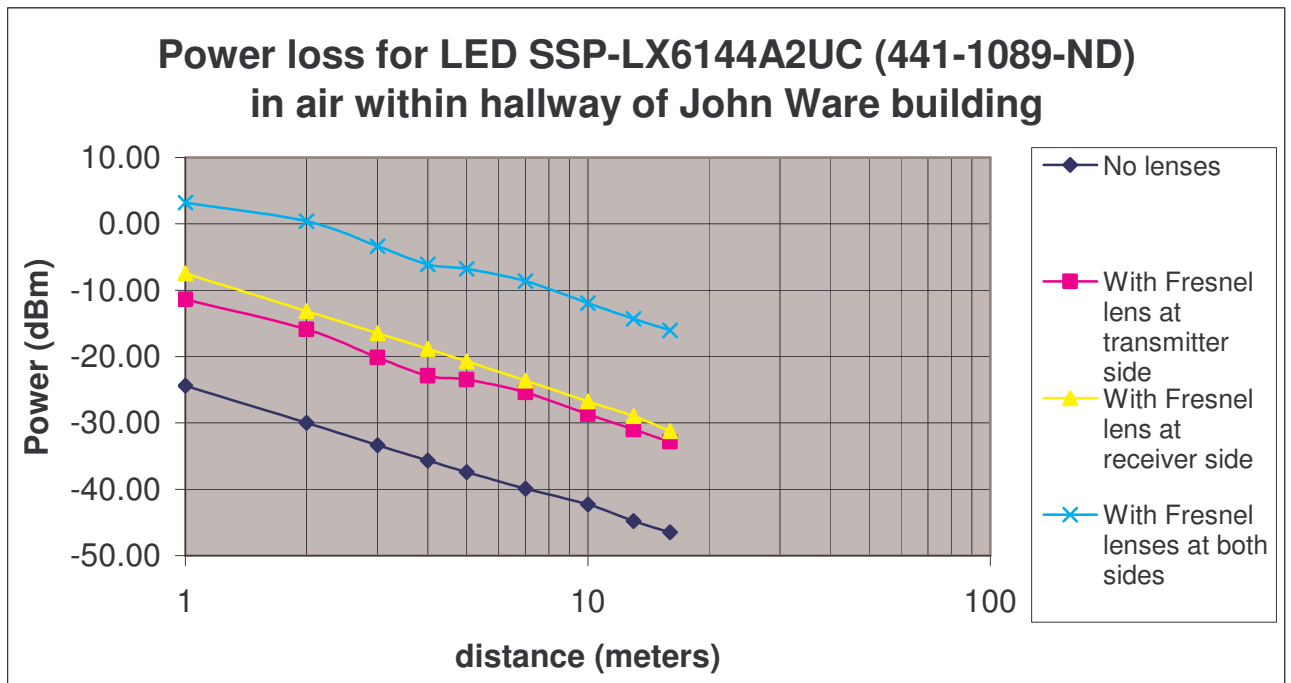
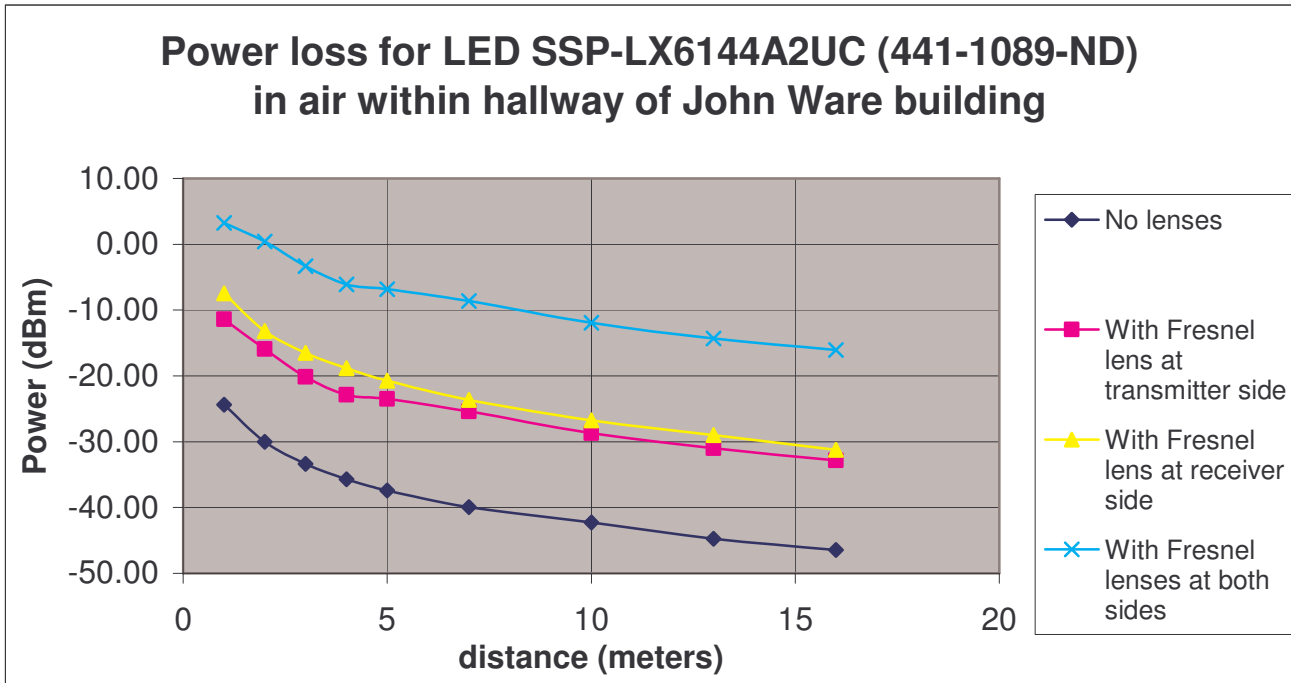
Model:Lv W5SG-GXHX-35-Z (475-1199-1 ND) VERDE - $\lambda=501\text{nm}$ Clear No lens SMD									
	Measured Light power (W): No Fresnel lenses		Measured Light power (W): With transmit Fresnel lens only		Measured Light power (W): With receiver Fresnel lens only		Measured Light power (W):With both transmit and receive Fresnel		
	Distance (meters)	Light + ambient	Ambient light only	Light + ambient	Ambient light only	Light + ambient	Ambient light only	Light + ambient	Ambient light only
	1	1.55E-06	2.76E-08	1.26E-04	2.60E-08	5.78E-05	4.18E-08	1.97E-02	3.80E-08
	2	3.66E-07	2.24E-08	6.97E-05	2.20E-08	1.55E-05	3.94E-08	1.28E-03	4.48E-08
	3	2.01E-07	1.77E-08	3.05E-05	1.79E-08	7.04E-06	4.34E-08	7.41E-04	4.82E-08
	5	1.02E-07	1.29E-08	9.64E-06	1.29E-08	2.26E-06	3.93E-08	3.10E-04	4.59E-08
	7	6.12E-08	9.63E-09	4.74E-06	9.96E-09	1.35E-06	4.35E-08	1.74E-04	4.51E-08
	10	3.65E-08	8.24E-09	2.37E-06	8.48E-09	6.80E-07	3.49E-08	1.02E-04	3.62E-08
	16	2.11E-08	8.29E-09	9.13E-07	8.42E-09	2.78E-07	2.85E-08	3.94E-05	2.93E-08
	Incident light minus ambient		Incident light minus ambient		Incident light minus ambient		Incident light minus ambient		
	power (W)	power (dBm)	power (W)	power (dBm)	power (W)	power (dBm)	power (W)	power (dBm)	
1	1.52E-06	-28.17	1.26E-04	-9.00	5.78E-05	-12.38	1.97E-02	12.94	
2	3.44E-07	-34.64	6.97E-05	-11.57	1.55E-05	-18.11	1.28E-03	1.07	
3	1.83E-07	-37.37	3.05E-05	-15.16	7.00E-06	-21.55	7.41E-04	-1.30	
5	8.91E-08	-40.50	9.63E-06	-20.17	2.22E-06	-26.54	3.10E-04	-5.09	
7	5.16E-08	-42.88	4.73E-06	-23.25	1.31E-06	-28.84	1.74E-04	-7.60	
10	2.83E-08	-45.49	2.36E-06	-26.28	6.45E-07	-31.90	1.02E-04	-9.92	
16	1.28E-08	-48.92	9.05E-07	-30.44	2.50E-07	-36.03	3.94E-05	-14.05	

**Test conditions: Transistor part # TIP121, in classical transistor switch configuration;**  
 Collector Bias voltage - 16.8V; Collector resistor - 51Ω 5.5W; Base resistor 330Ω 1/2W;  
 Source connected to base resistor - Pulse 0-1.5V, at frequency of 40kHz 30% du



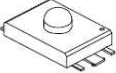
Model:SSP-LX6144A2UC (441-1089-ND)420mW green - λ=525nm Water clear lens									
	Measured Light power (W): No Fresnel lenses		Measured Light power (W): With transmit Fresnel lens only		Measured Light power (W): With receiver Fresnel lens only		Measured Light power (W):With both transmit and receive Fresnel lenses		
	Distance (meters)	Light + ambient	Ambient light only	Light + ambient	Ambient light only	Light + ambient	Ambient light only	Light + ambient	Ambient light only
	1	3.68E-06	2.54E-08	7.29E-05	2.54E-08	1.80E-04	2.52E-08	2.10E-03	2.49E-08
	2	1.02E-06	1.99E-08	2.56E-05	2.03E-08	4.82E-05	3.69E-08	1.10E-03	2.80E-08
	3	4.78E-07	1.69E-08	9.72E-06	1.68E-08	2.25E-05	2.59E-08	4.63E-04	2.49E-08
	4	2.84E-07	1.43E-08	5.16E-06	1.45E-08	1.31E-05	3.38E-08	2.45E-04	3.84E-08
	5	1.94E-07	1.24E-08	4.50E-06	1.24E-08	8.52E-06	4.06E-08	2.09E-04	4.19E-08
	7	1.11E-07	9.40E-09	2.89E-06	9.48E-09	4.38E-06	4.19E-08	1.37E-04	4.20E-08
	10	6.69E-08	7.60E-09	1.36E-06	7.49E-09	2.15E-06	3.26E-08	6.39E-05	3.40E-08
	13	4.06E-08	7.24E-09	8.05E-07	7.68E-09	1.29E-06	2.95E-08	3.70E-05	2.96E-08
16	2.98E-08	7.20E-09	5.30E-07	7.46E-09	7.80E-07	2.65E-08	2.48E-05	2.69E-08	
	Incident light minus ambient		Incident light minus ambient		Incident light minus ambient		Incident light minus ambient		
	power (W)	power (dBm)	power (W)	power (dBm)	power (W)	power (dBm)	power (W)	power (dBm)	
1	3.65E-06	-24.37	7.29E-05	-11.37	1.80E-04	-7.45	2.10E-03	3.22	
2	1.00E-06	-30.00	2.56E-05	-15.92	4.82E-05	-13.17	1.10E-03	0.41	
3	4.61E-07	-33.36	9.70E-06	-20.13	2.25E-05	-16.48	4.63E-04	-3.34	
4	2.70E-07	-35.69	5.15E-06	-22.89	1.31E-05	-18.84	2.45E-04	-6.11	
5	1.82E-07	-37.41	4.49E-06	-23.48	8.48E-06	-20.72	2.09E-04	-6.80	
7	1.02E-07	-39.93	2.88E-06	-25.41	4.34E-06	-23.63	1.37E-04	-8.63	
10	5.93E-08	-42.27	1.35E-06	-28.69	2.11E-06	-26.75	6.39E-05	-11.95	
13	3.34E-08	-44.77	7.97E-07	-30.98	1.26E-06	-28.99	3.70E-05	-14.32	
16	2.26E-08	-46.46	5.23E-07	-32.82	7.54E-07	-31.23	2.48E-05	-16.06	

**Test conditions: Transistor part # TIP121, in classical transistor switch configuration;** Collector Bias voltage - 16.8V; Collector resistor - 51Ω 5.5W; Base resistor 330Ω 1/2W; Source connected to base resistor - Pulse 0-1.5V, at frequency of 40kHz 30% du

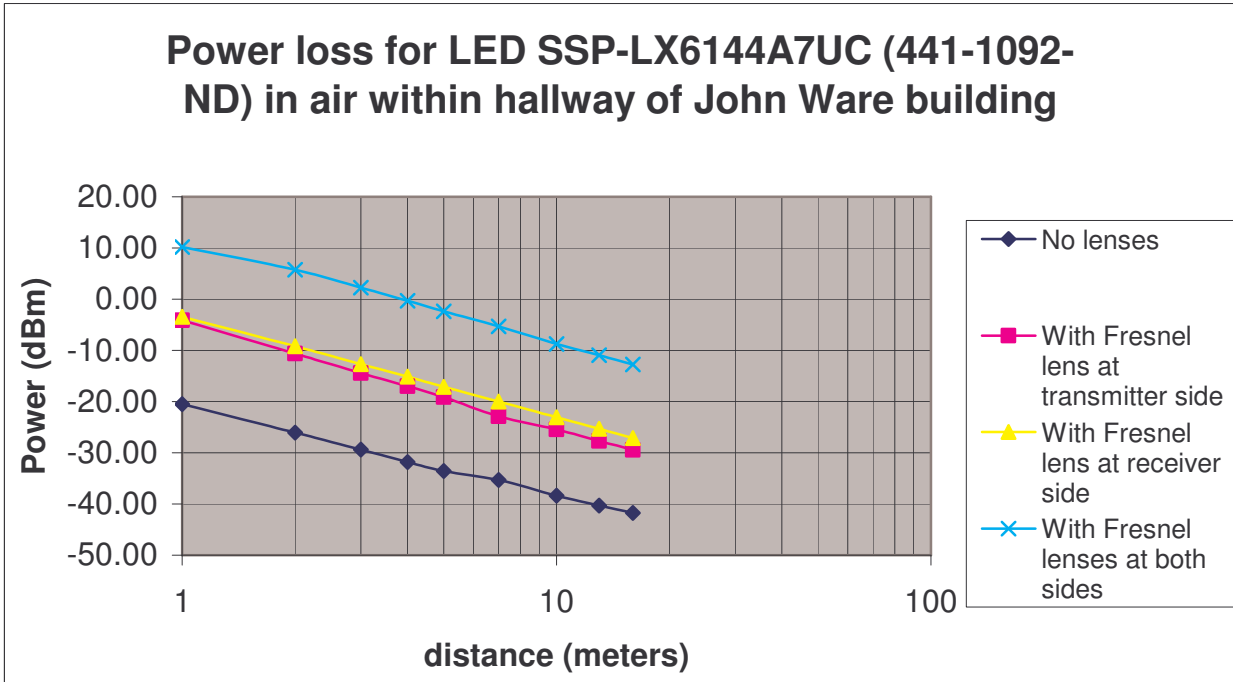
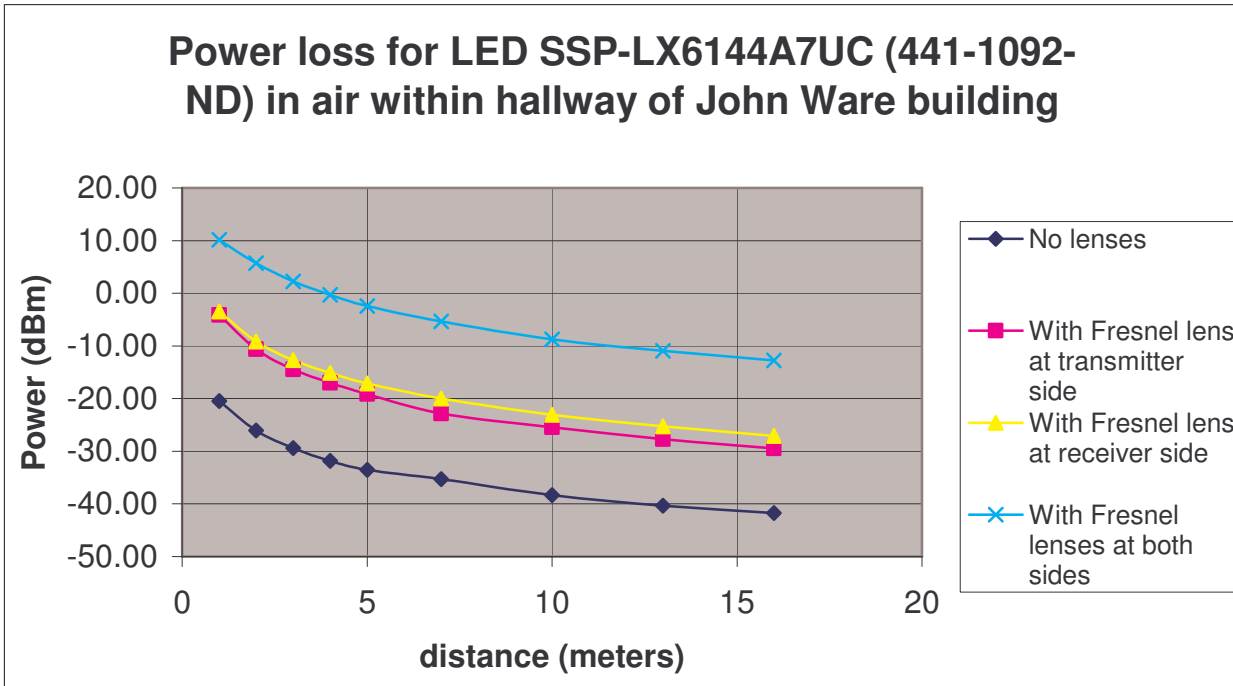




Investigation of Optical Receivers For Use in an Underwater Environment

Model:SSP-LX6144A7UC (441-1092-ND)420mW blue - λ=470nm - Water clear lens									
	Measured Light power (W): No Fresnel lenses		Measured Light power (W): With transmit Fresnel lens only		Measured Light power (W): With receiver Fresnel lens only		Measured Light power (W):With both transmit and receive Fresnel lenses		
	Distance (meters)	Light + ambient	Ambient light only	Light + ambient	Ambient light only	Light + ambient	Ambient light only	Light + ambient	Ambient light only
	1	9.00E-06	2.66E-08	3.88E-04	2.59E-08	4.54E-04	3.98E-08	1.04E-02	3.94E-08
	2	2.49E-06	2.19E-08	8.66E-05	2.49E-08	1.21E-04	4.59E-08	3.74E-03	5.02E-08
	3	1.17E-06	1.77E-08	3.61E-05	1.95E-08	5.40E-05	4.45E-08	1.69E-03	5.93E-08
	4	6.72E-07	1.47E-08	1.99E-05	1.59E-08	3.09E-05	5.30E-08	9.35E-04	5.49E-08
	5	4.55E-07	1.28E-08	1.22E-05	1.28E-08	1.95E-05	4.79E-08	5.75E-04	5.23E-08
	7	3.03E-07	9.46E-09	5.18E-06	1.01E-08	1.01E-05	4.09E-08	2.93E-04	4.08E-08
	10	1.54E-07	8.20E-09	2.87E-06	9.80E-09	4.98E-06	3.25E-08	1.34E-04	3.73E-08
	13	1.03E-07	9.85E-09	1.72E-06	1.60E-08	2.99E-06	3.13E-08	8.06E-05	3.46E-08
16	7.58E-08	8.98E-09	1.15E-06	9.94E-09	1.98E-06	2.89E-08	5.32E-05	2.74E-08	
	Incident light minus ambient		Incident light minus ambient		Incident light minus ambient		Incident light minus ambient		
	power (W)	power (dBm)	power (W)	power (dBm)	power (W)	power (dBm)	power (W)	power (dBm)	
1	8.97E-06	-20.47	3.88E-04	-4.11	4.54E-04	-3.43	1.04E-02	10.17	
2	2.47E-06	-26.08	8.66E-05	-10.63	1.21E-04	-9.17	3.74E-03	5.73	
3	1.15E-06	-29.38	3.61E-05	-14.43	5.40E-05	-12.68	1.69E-03	2.28	
4	6.57E-07	-31.82	1.99E-05	-17.01	3.08E-05	-15.11	9.35E-04	-0.29	
5	4.42E-07	-33.54	1.22E-05	-19.14	1.95E-05	-17.11	5.75E-04	-2.40	
7	2.94E-07	-35.32	5.17E-06	-22.87	1.01E-05	-19.97	2.93E-04	-5.33	
10	1.46E-07	-38.36	2.86E-06	-25.44	4.95E-06	-23.06	1.34E-04	-8.73	
13	9.32E-08	-40.31	1.70E-06	-27.69	2.96E-06	-25.29	8.06E-05	-10.94	
16	6.68E-08	-41.75	1.14E-06	-29.45	1.95E-06	-27.10	5.32E-05	-12.74	

**Test conditions: Transistor part # TIP121, in classical transistor switch configuration;** Collector Bias voltage - 16.8V; Collector resistor - 51Ω 5.5W; Base resistor 330Ω 1/2W; Source connected to base resistor - Pulse 0-1.5V, at frequency of 40kHz 30% du



Appendix C: Data sheets for PIN Photodiodes

PDB-C107 – Blue Enhanced Photoconductive Silicon Photodiode

Available at: [http://www.advancedphotonix.com/ap\\_products/pdfs/PDB-C107.pdf](http://www.advancedphotonix.com/ap_products/pdfs/PDB-C107.pdf)

PDB-C142 – Plastic Photodiode Package with Leads

Available at: [http://www.advancedphotonix.com/ap\\_products/pdfs/PDB-C142.pdf](http://www.advancedphotonix.com/ap_products/pdfs/PDB-C142.pdf)

PDB-C169 - Plastic Photodiode Package with Leads (Sidelooker package)

Available at: [http://www.advancedphotonix.com/ap\\_products/pdfs/PDB-C169.pdf](http://www.advancedphotonix.com/ap_products/pdfs/PDB-C169.pdf)

SD100-12-22-021 – Blue Enhanced Silicon Photodiode

Available at: [http://www.advancedphotonix.com/ap\\_products/pdfs/SD100-12-22-021.pdf](http://www.advancedphotonix.com/ap_products/pdfs/SD100-12-22-021.pdf)

SD200-12-22-041 – Blue Enhanced Silicon Photodiode

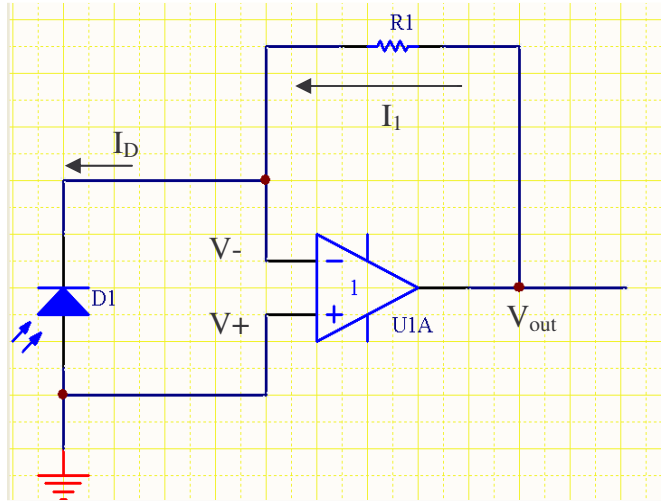
Available at: [http://www.advancedphotonix.com/ap\\_products/pdfs/SD200-12-22-041.pdf](http://www.advancedphotonix.com/ap_products/pdfs/SD200-12-22-041.pdf)

SD 100-42-22-231 – Detector/Amplifier Hybrid without feedback resistor – Blue Enhanced

Available at: [http://www.advancedphotonix.com/ap\\_products/pdfs/SD100-42-22-231.pdf](http://www.advancedphotonix.com/ap_products/pdfs/SD100-42-22-231.pdf)

### Appendix D – Equation Derivations for receiver circuits

D.1: Standard TIA:



Assumptions: Ideal op-amp therefore:

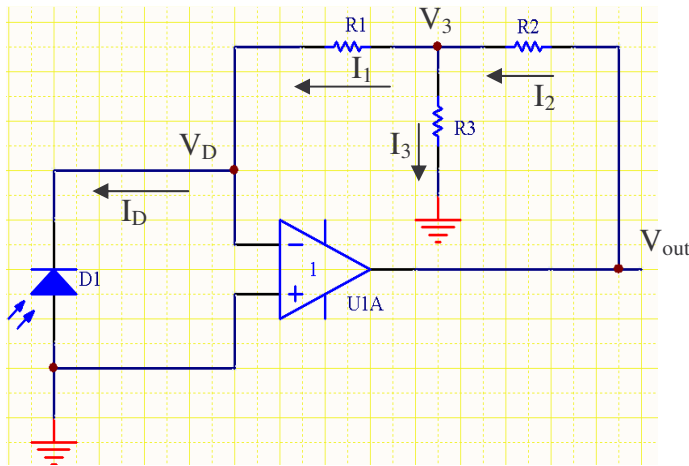
$$V_- = V_+ = 0V \text{ and input current to op-amp} = 0A$$

$$I_D = I_1$$

$$V_{out} = I_1 R_1 = I_D R_1$$

$$\text{Transimpedance gain} = \frac{V_{out}}{I_{in}} = \frac{I_D R_1}{I_D} = R_1$$

D.2 Modified TIA



Assumption: Ideal op-amp

$$V_D = 0V \quad I_1 = I_D$$

$$I_2 = I_1 + I_3 = I_D + I_3$$

$$V_3 = I_1 R_1 = I_D R_1$$

$$I_3 = \frac{V_3}{R_3} = \frac{I_1 R_1}{R_3} = \frac{I_D R_1}{R_3}$$

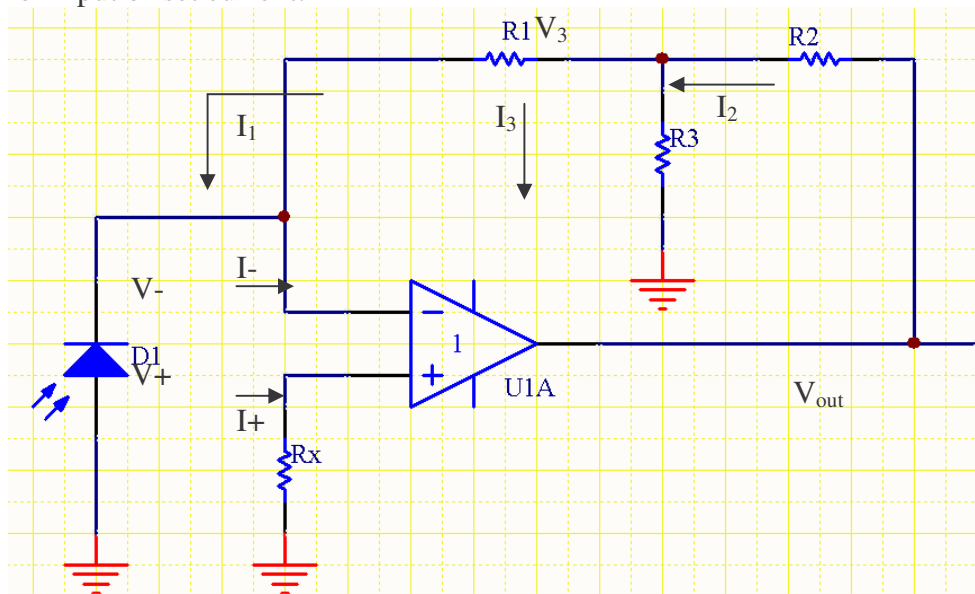
$$V_{out} = I_2 R_2 + V_3 = R_2 \left( I_D + \frac{I_D R_1}{R_3} \right) + I_D R_1 = I_D \left( R_2 + \frac{R_1 R_2}{R_3} \right) + I_D R_1$$

$$Gain = \frac{V_{out}}{I_D} = R_1 + R_2 + \frac{R_1 R_2}{R_3}$$

if  $R_1 = R_2 = 33k\Omega$  &  $R_3 = 1k\Omega$

$$\frac{V_{out}}{I_D} = 33k + 33k + \frac{33k \cdot 33k}{1k} = 1.155M\Omega$$

Compensating for input offset current:



Add R<sub>x</sub> for input offset current.

Assumptions: I<sub>D</sub> = 0A (dark), V<sub>-</sub> = V<sub>+</sub>, & I<sub>-</sub> = I<sub>+</sub>

$$I_1 = I_- = I_+$$

$$V_- = V_+ = -R_x(I_+) = -R_x I_1$$

$$V_{out} = I_2 R_2 + V_3 = I_2 R_2 + (I_1 R_1 - I_1 R_x)$$

$$I_2 = I_1 + I_3 = I_1 + \frac{V_3}{R_3} = I_1 + \frac{I_1 R_1 - I_1 R_x}{R_3} = I_1 \left( 1 + \frac{R_1 - R_x}{R_3} \right)$$

$$V_{out} = I_1 \left( 1 + \frac{R_1 - R_x}{R_3} \right) R_2 + (I_1 R_1 - I_1 R_x) = I_1 \left( R_1 - R_x + \left( 1 + \frac{R_1 - R_x}{R_3} \right) R_2 \right)$$

We want V<sub>out</sub> = 0V

continued on next page

$$0 = I_1 \left( R_1 - Rx + \left( 1 + \frac{R_1 - Rx}{R_3} \right) R_2 \right)$$

$$0 = R_1 - Rx + R_2 + \frac{R_1 R_2}{R_3} - \frac{Rx R_2}{R_3}$$

$$0 = -Rx \left( 1 + \frac{R_2}{R_3} \right) + R_1 + R_2 + \frac{R_1 R_2}{R_3}$$

$$Rx \left( 1 + \frac{R_2}{R_3} \right) = R_1 + R_2 + \frac{R_1 R_2}{R_3}$$

$$Rx = \frac{R_3}{R_2 + R_3} \left( \frac{R_1 R_3 + R_2 R_3 + R_1 R_2}{R_3} \right)$$

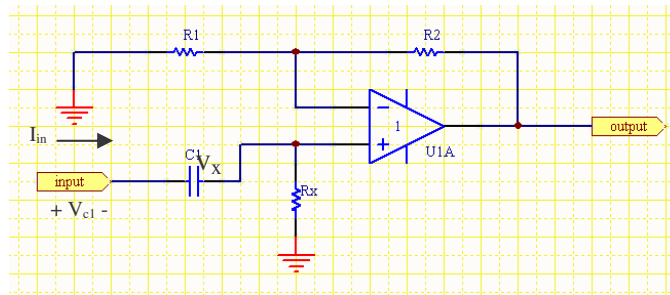
$$= \frac{R_1 R_3 + R_2 R_3 + R_1 R_2}{R_2 + R_3}$$

*if*  $R_1 = 33k\Omega$ ,  $R_2 = 33k\Omega$ , &  $R_3 = 1k\Omega$

*then*  $Rx = 33.97k\Omega$

D.3 Differentiator Design:

Standard Circuit approach:



$$V_{out} = V_x \left( 1 + \frac{R2}{R1} \right)$$

Using frequency domain - impedances (sinusoid input) to start:

$$V_{C1} = \frac{V_{in} \cdot X_c}{Z} = \frac{V_{in} X_c}{\sqrt{X_c^2 + R_x^2}} \quad \text{If } X_c \gg R_x, \text{ then: } \sqrt{X_c^2 + R_x^2} \approx X_c$$

As  $X_c = \frac{1}{2\pi f C}$ ,  $X_c$  is large when both  $C$  is very small and  $f$  is small. For example if  $R_x = 1k\Omega$ , max frequency input = 100kHz. As this is a pulse input, allow for up to 10 harmonics, so  $f_{max} = 1MHz$ . At 1MHz,  $X_c \gg R_x$ , therefore,  $X_c \gg 10k\Omega$

$$\text{Therefore } X_c = \frac{1}{2\pi f C} > 10k \quad C < \frac{1}{2\pi \cdot 10k \cdot 1M} = 159pF$$

Actual capacitance used was 10pF. Originally it was intended to run this circuit at higher frequencies. The capacitance's value was not adjusted higher when the frequency of operation was reduced.

Given that,  $C$  is small such that  $X_c \gg R_x$  for frequencies of interest, then  $V_c \approx V_{in}$ . Therefore,

$$I_{in} = C \frac{d(V_{in})}{dt} \text{ thus, } V_x = I_{in} R_x = R_x C \frac{d(V_{in})}{dt}$$

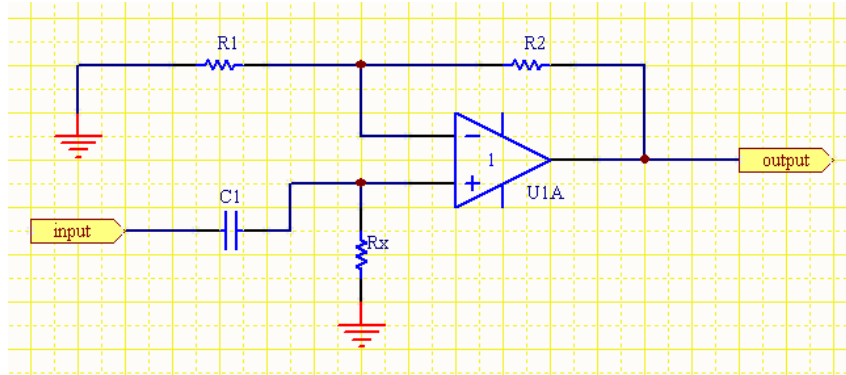
$$\text{As output voltage is } V_{out} = V_x \left( 1 + \frac{R2}{R1} \right)$$

$$\text{Then, under the stated conditions, } V_{out} = R_x C \left( 1 + \frac{R2}{R1} \right) \frac{d(V_{in})}{dt}$$

$V_{out}$  is a derivative of  $V_{in}$  with low gain except when  $V_{in}$  transitions very quickly



D.4 Non-inverting amplifier with first-order high pass filter:



Gain:

$$\frac{V_{output}}{V_{input}} = 1 + \frac{R_2}{R_1}$$

Value of Rx:

$$R_x = R_2 // R_1 = \frac{R_1 R_2}{R_1 + R_2}$$

Value of C<sub>1</sub> to set low corner frequency:

$$R_x = X_c$$

$$\text{For corner frequency } R_x = \frac{1}{2\pi f_c C_1}$$

$$C_1 = \frac{1}{2f_c R_x}$$

Circuit values:

Gain 1 to 500: Let R<sub>1</sub> = 1kΩ therefore R<sub>2</sub> = variable resistor 0-500kΩ

R<sub>x</sub>: For the resistor values of R<sub>1</sub> and R<sub>2</sub>, R<sub>x</sub> = 1k//500k ≈ 1kΩ

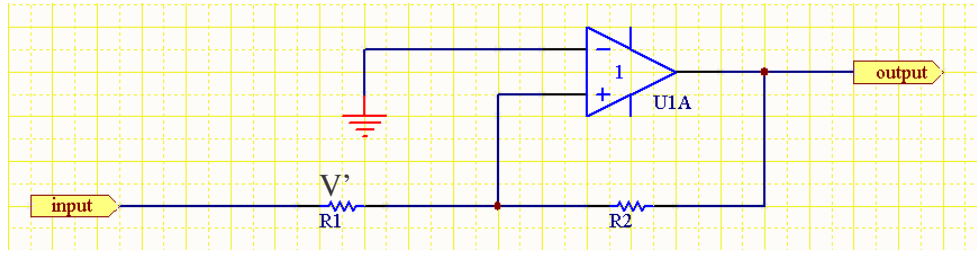
For C<sub>1</sub>: Let corner frequency << operating frequency

Therefore set f<sub>c</sub> < 40k/10 < 400Hz.

Let corner frequency = 300Hz, then C<sub>1</sub> = 0.53μF

For available off-the-shelf, C<sub>1</sub> = 0.56μF, therefore corner frequency = 284Hz

D.5 Voltage comparator with Hysteresis



When  $V' =$  positive voltage, input must be go below  $-V'$ , the Lower Trigger Level (LTL) to cause the comparator to switch states. Conversely, when  $V' =$  negative voltage, input must go higher than the magnitude of  $V'$  for state to switch, the Upper Trigger Level.

$$LTL = \frac{-R1}{R2} (Max\ Pos.\ voltage)$$

$$UTL = \frac{R1}{R2} |(Max\ Neg.\ voltage)|$$

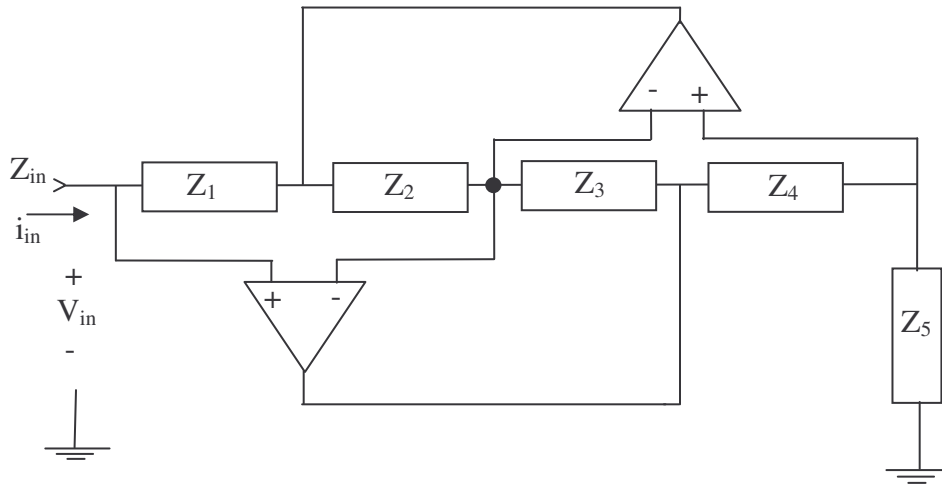
If op-amp is biased  $\pm 5V$ , then let max. swing  $\approx \pm 4.8V$

If we want  $LTL = -0.5V$  and  $UTL = +0.5V$ , and we let  $R1 = 1k\Omega$  then

$$R2 = \frac{R1}{UTL} 4.8V = \frac{-R1}{LTL} (-4.8V) = \frac{1k}{0.5} 4.8 = 9.6k\Omega$$

If we want LTL and UTL smaller in magnitude, e.g.  $10mV$ , then with  $R1=1k\Omega$ ,  $R2 = 480k\Omega$ .

D.6 Generalized Impedance Converter (GIC)



$$Z_{in} = v_{in}/i_{in}$$

It can be shown that 
$$\frac{v_{in}}{i_{in}} = \frac{Z_1 Z_3 Z_5}{Z_2 Z_4}$$

If  $Z_1 = R_1$ ,  $Z_2 = X_C$ ,  $Z_3 = R_3$ ,  $Z_4 = R_4$ , &  $Z_5 = R_5$  and desired  $Z_{in} = j\omega L = j\omega L$

$$Z_{in} = \frac{R_1 R_3 R_5}{X_C R_4} = \frac{R_1 R_3 R_5 j\omega C}{R_4} = j\omega L$$

∴

$$L = \frac{R_1 R_3 R_5 C}{R_4}$$

Therefore, if desired  $L = 2H$

assume 4 values and solve for fifth:

Let  $R_1 = R_3 = 10k\Omega$ ,  $C_1 = 0.001\mu F$ , and  $R_4 = 1k\Omega$

$$\text{Then } R_5 = \frac{1k \cdot 2}{10k \cdot 10k \cdot 0.001\mu} = 20k\Omega$$

**Appendix E: Receiver evaluation board: Schematic diagrams and PCB board component layout**

Schematic 1:

PDF writer would not replicate schematic – available by request to [jim.murtagh@sait.ca](mailto:jim.murtagh@sait.ca)

*Investigation of Optical Receivers For Use in an Underwater Environment*

Schematic 2:

PDF writer would not replicate schematic – available by request to [jim.murtagh@sait.ca](mailto:jim.murtagh@sait.ca)

*Investigation of Optical Receivers For Use in an Underwater Environment*

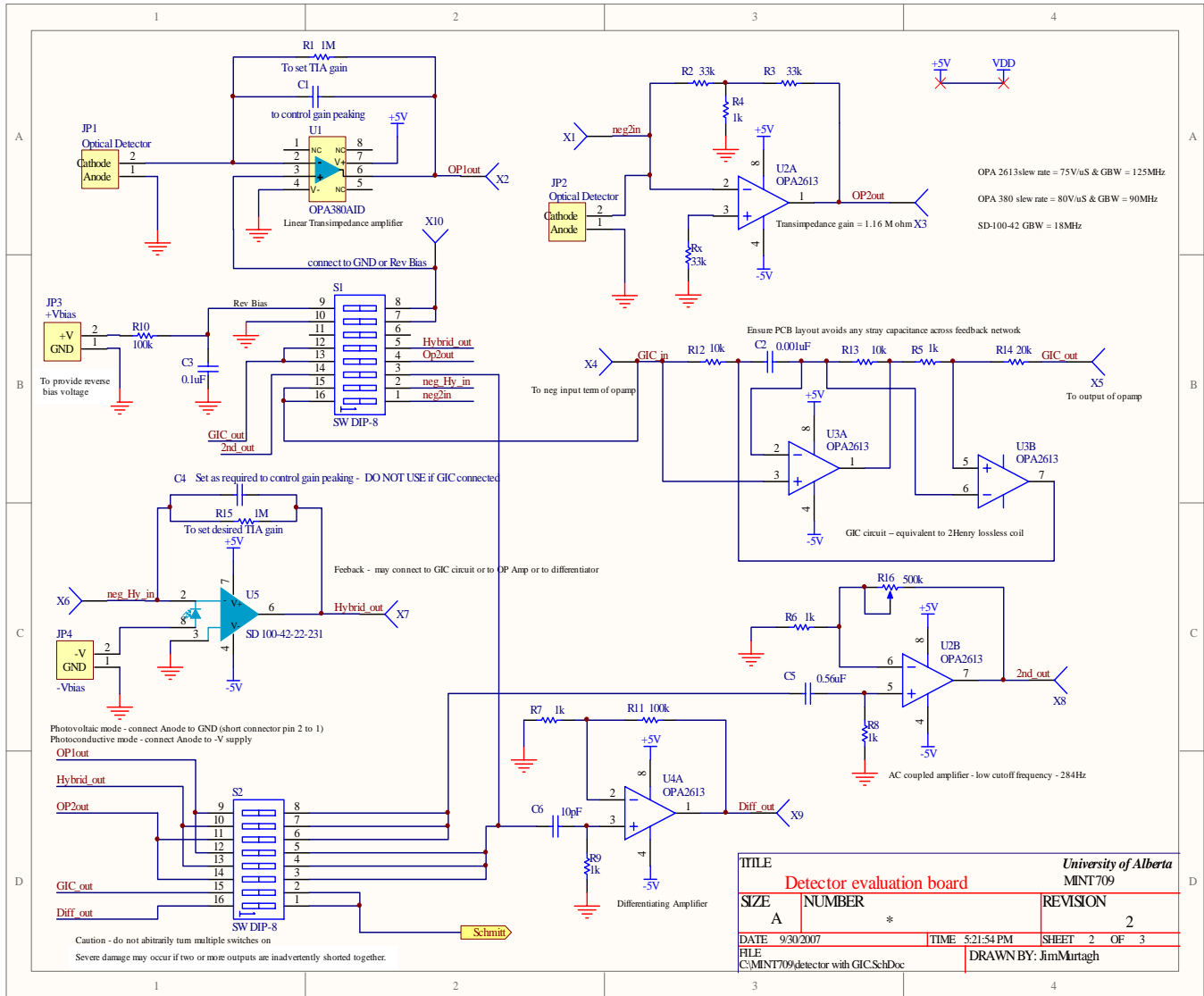
Board (component) Layout:

PDF writer would not replicate schematic – available by request to [jim.murtagh@sait.ca](mailto:jim.murtagh@sait.ca)

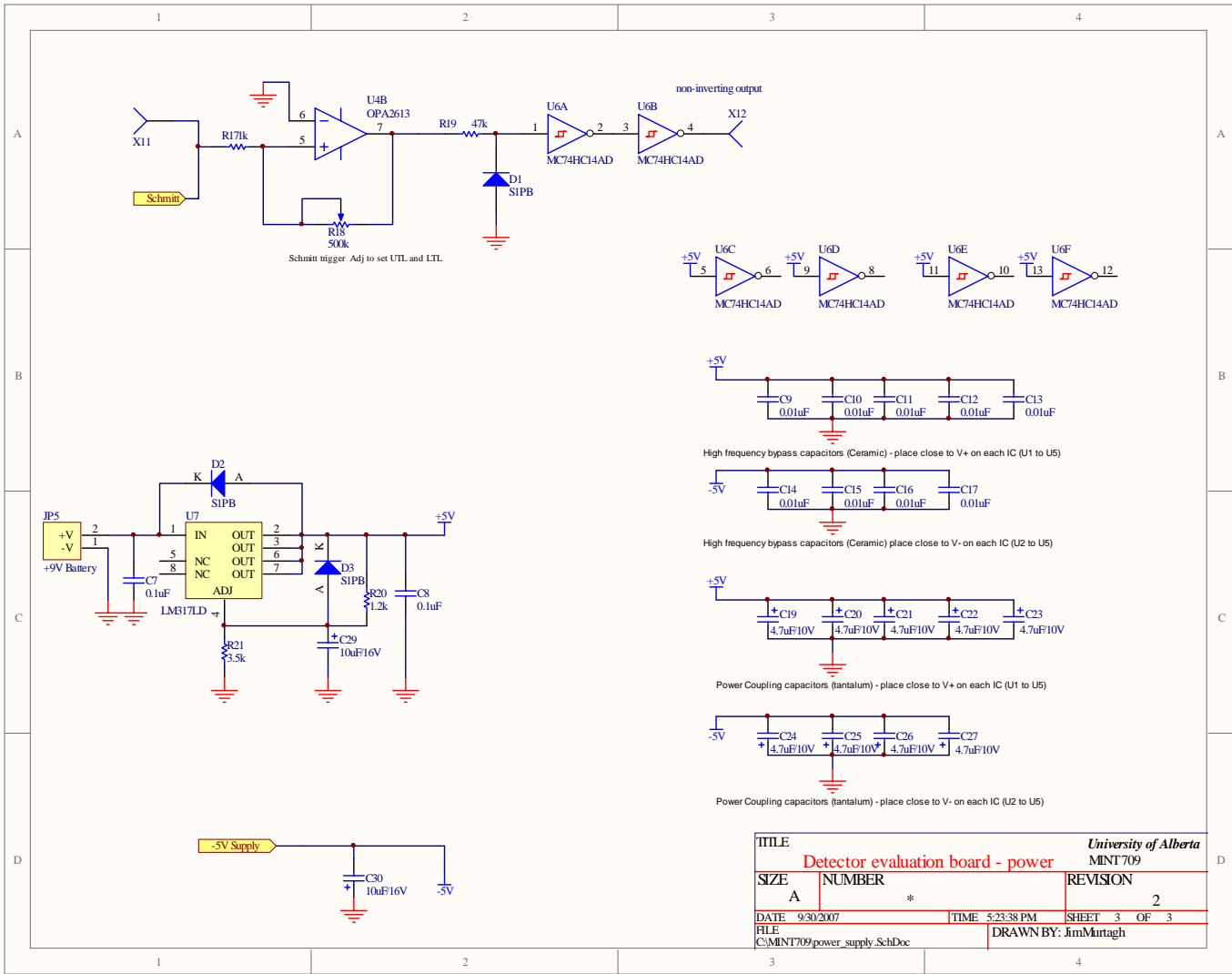
**Appendix F: Receiver waveforms captured for various testing scenarios and photodiodes**

As this file is 54 pages in length, it is available by request – e-mail [jim.murtagh@sait.ca](mailto:jim.murtagh@sait.ca)

# Appendix E: Receiver evaluation board: Schematic diagrams and PCB board component layout

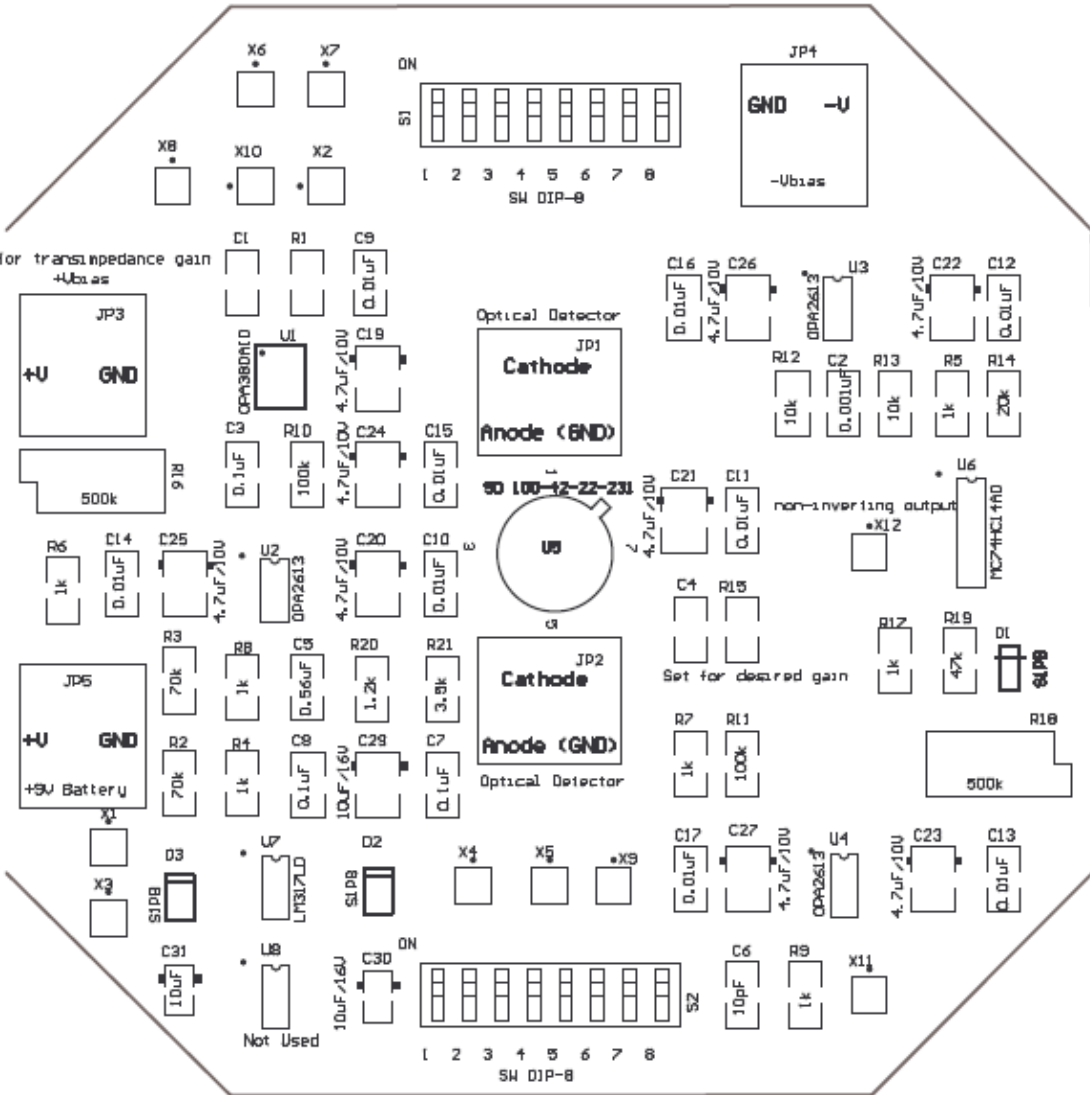






TITLE		University of Alberta
Detector evaluation board - power		MNT709
SIZE	NUMBER	REVISION
A	*	2
DATE	TIME	SHEET
9/30/2007	5:23:38 PM	3 OF 3
FILE	DRAWN BY: JimMurtagh	
C:\MINT709\power_supply_SchDoc		

set as required for transimpedance gain  
+Ubias



## Waveforms for transmitting source.

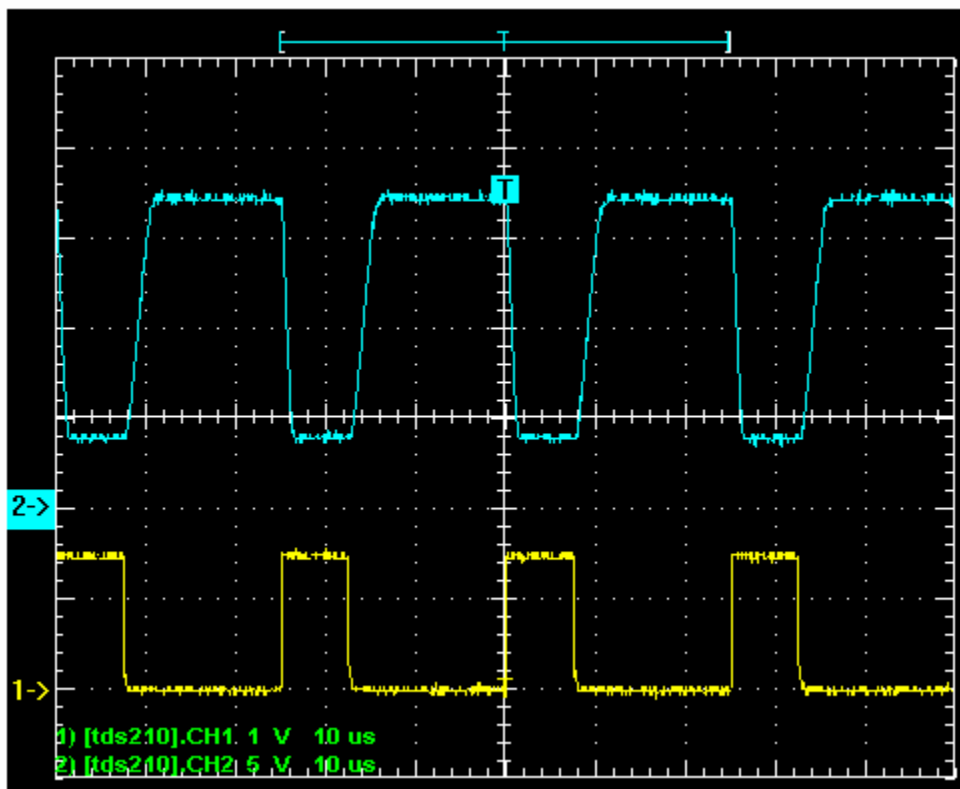
LED Digikey part # 441-1092-ND Blue – wavelength 470nm

Note: Waveforms shown on transmitter side were similar for all LED sources evaluated.

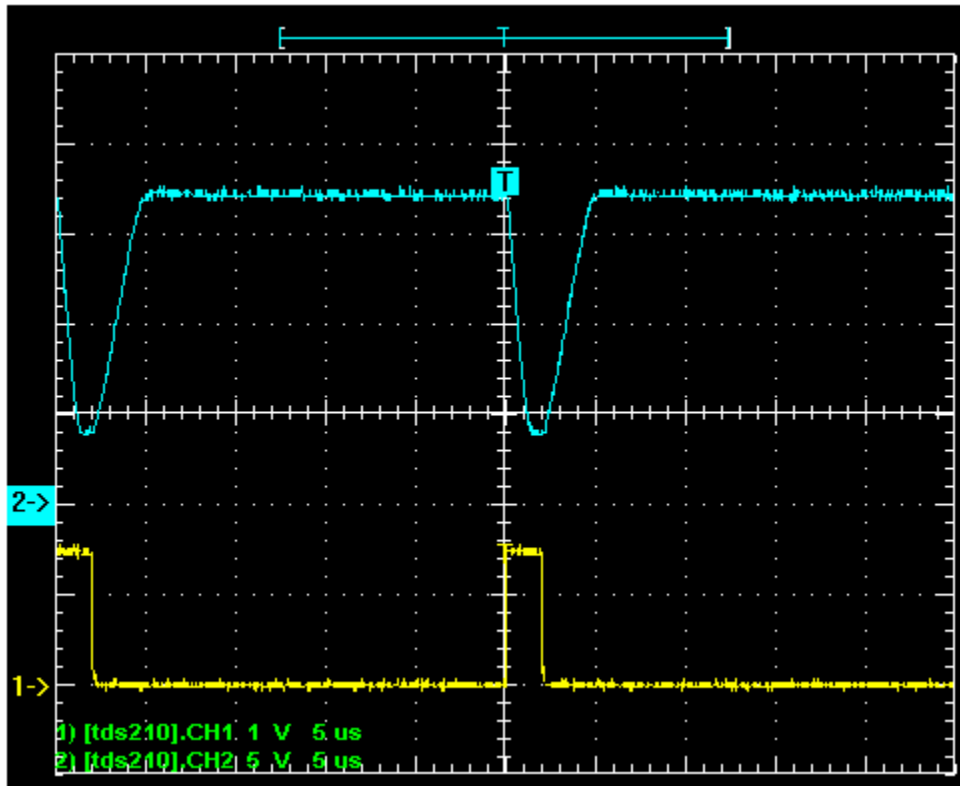
Test setup for most measurements:

$$V_{DC} = 16.8V \quad R_C = 51 \text{ ohms } 5W \quad V_{in} = 0 - 1.5V \quad f = 40kHz \text{ duty cycle} = 30\%$$

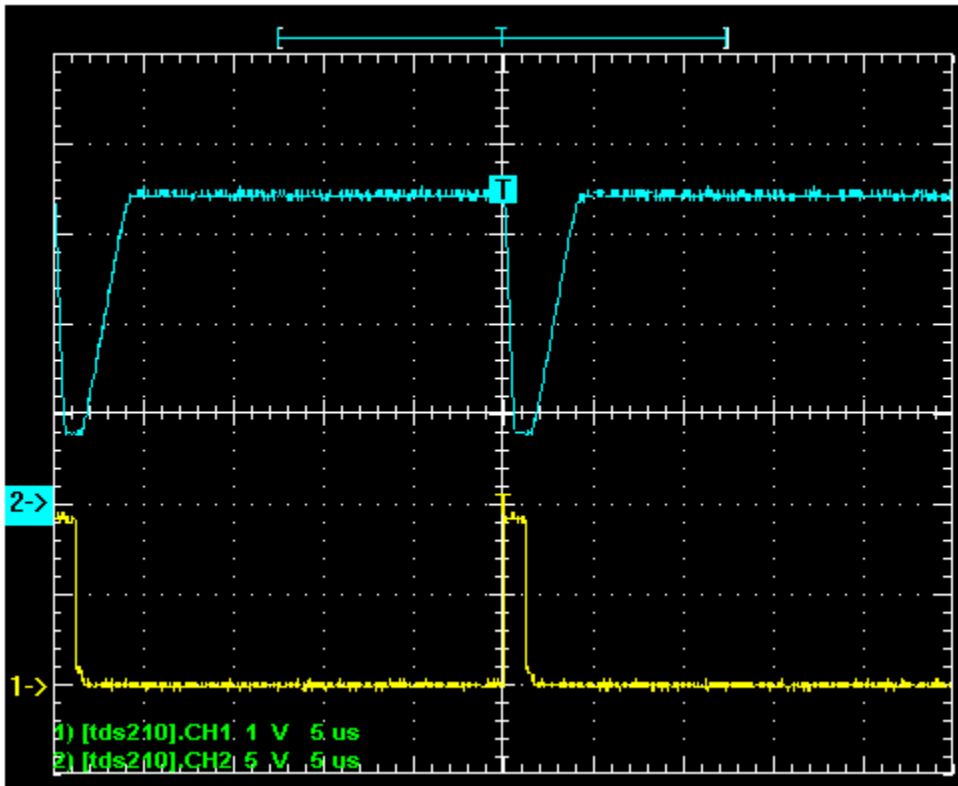
Measurements taken Ch1 – at generator input to 330 ohm and Ch2 at Anode to Gnd  
(includes voltage across Diode and Collector to emitter)



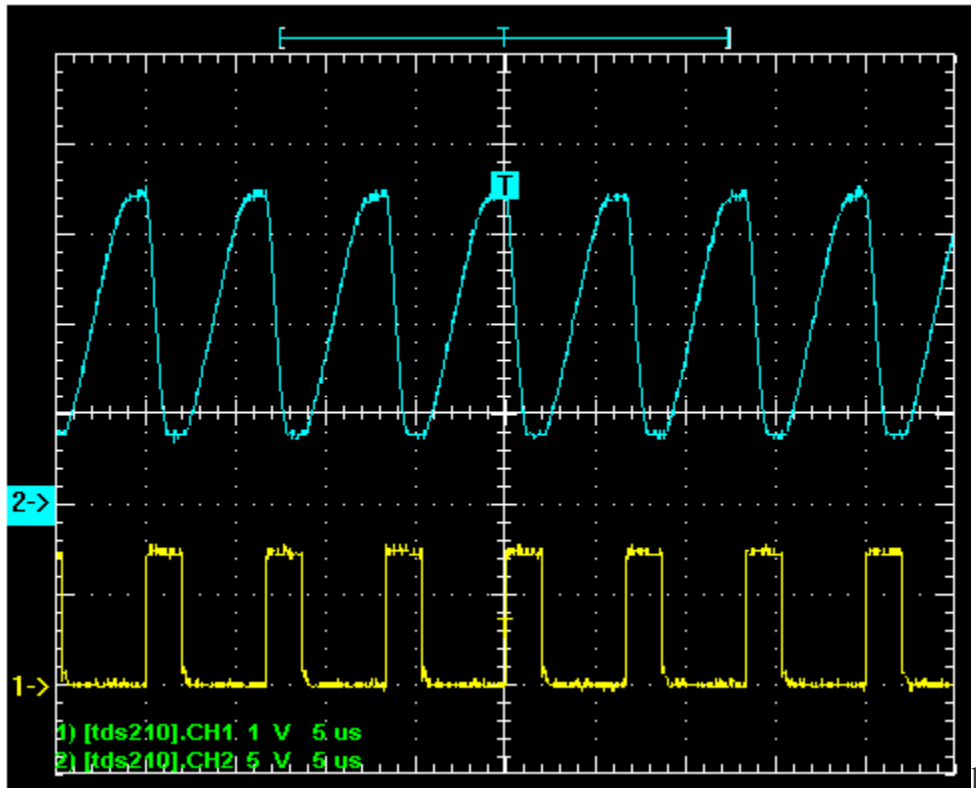
Duty cycle reduced to 8%



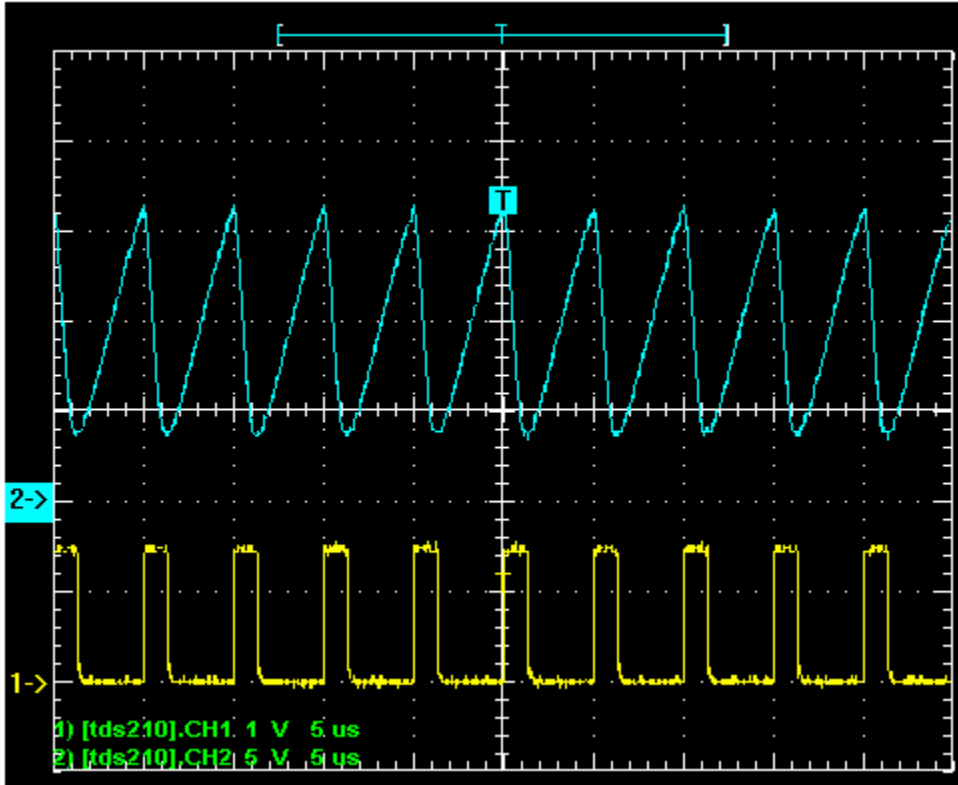
Duty cycle reduced to 5% - Base voltage increased to 1.8V



Duty cycle 30% Frequency increased to: 150kHz



Limit of frequency about 200kHz



## Receiver measurements

Oct. 31/07

Receiver waveforms – initial distance = 2 Meters – observed inside screen room.

Source LED 441-1092-ND Blue – wavelength 470nm

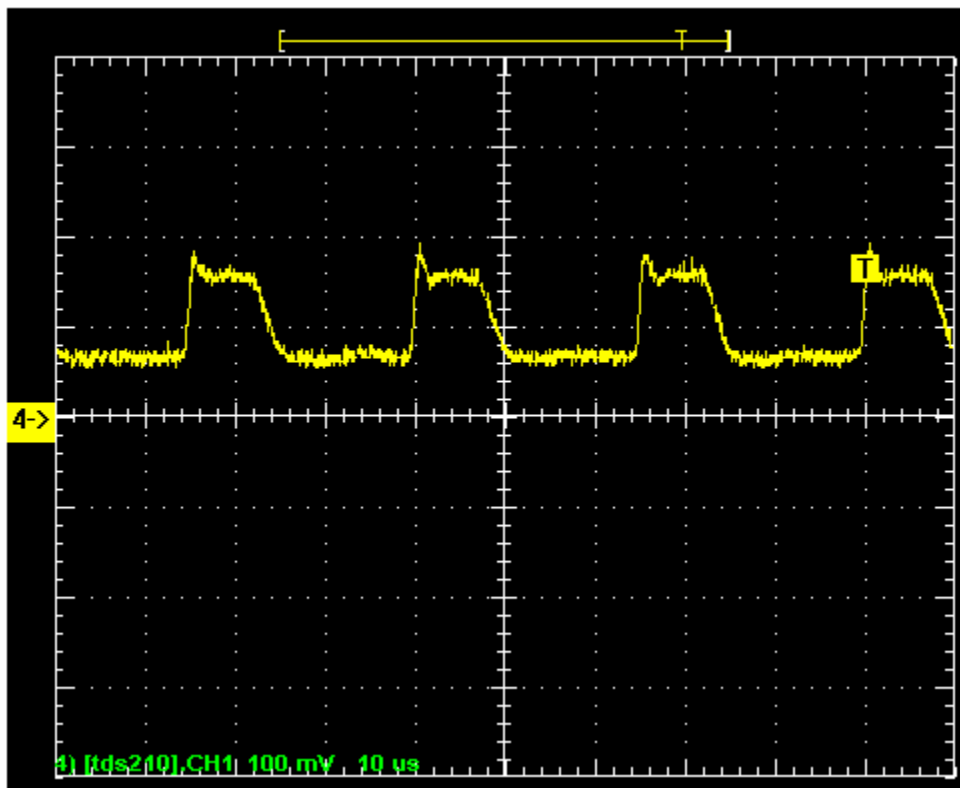
Collector supply = 16.8V

Base supply – rectangular pulse 0 to 1.5Vp, operating at frequency = 40kHz, 30% duty cycle

Ambient light - measured level on Newport optical meter (setting at 514.5) =  $3.5e-6W$

Combined measured level – ambient light + blue light pulsing at 30% duty cycle, 40kHz =  $6.78e-6W$

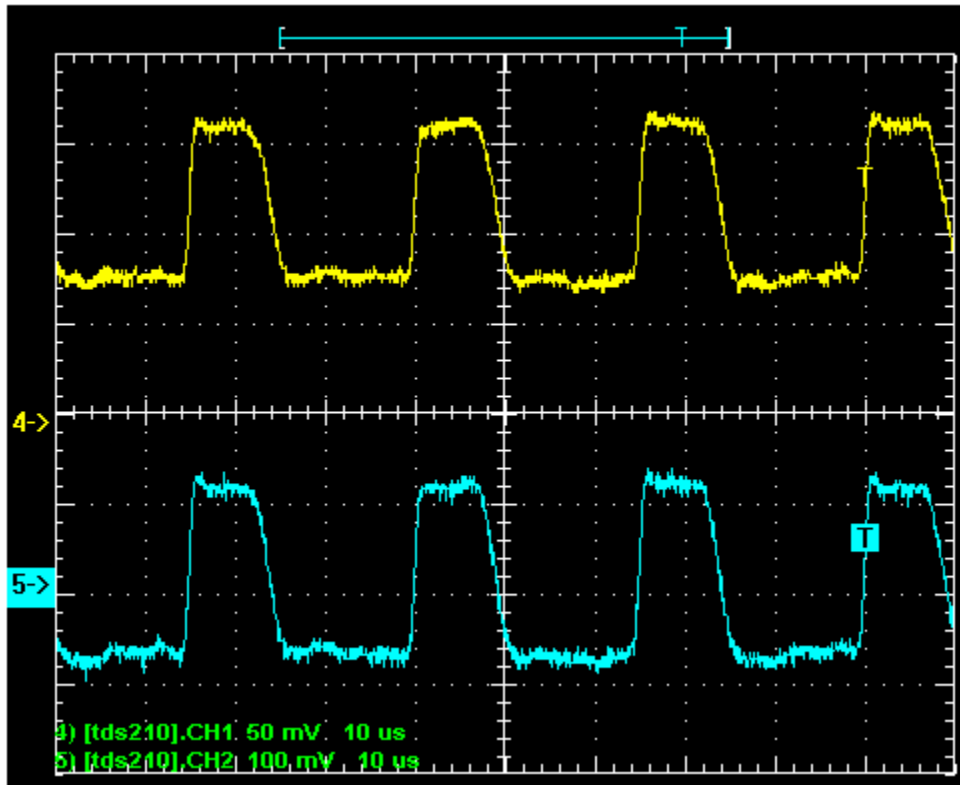
**Detector: PDB-C142** – Output from OPA350 (test point X2) – TIA gain is  $1M\Omega$



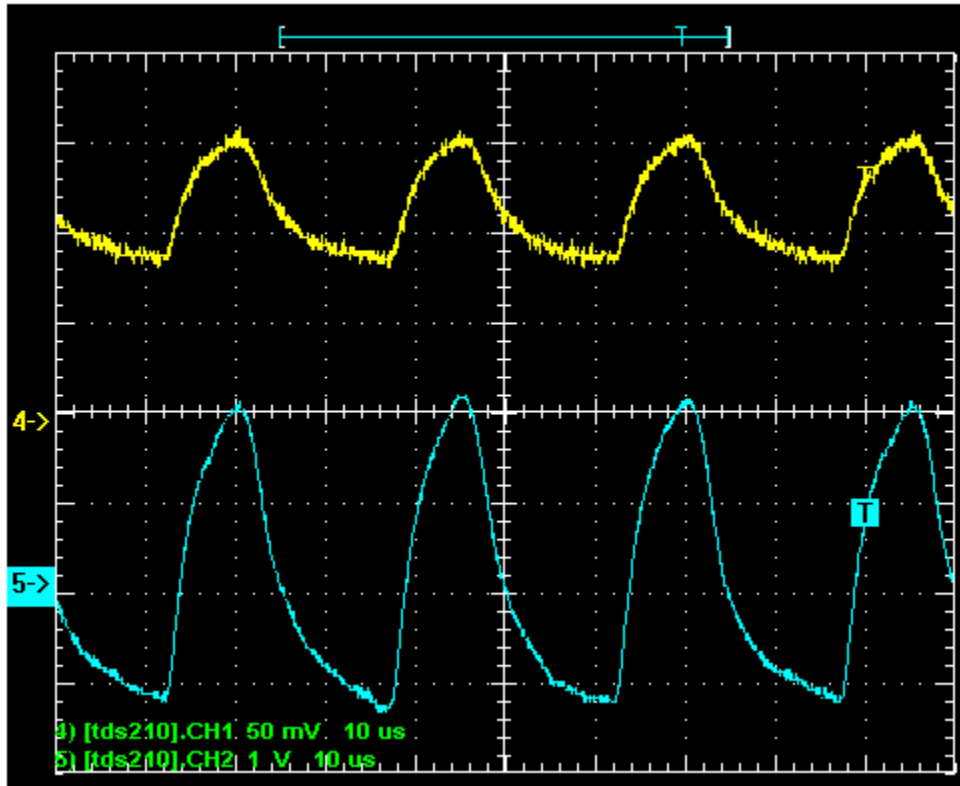


Output of OPA350 connected to second stage ac coupled op-amp. Note, it was observed that adjusting stage 2 gain does affect the waveform of stage 1 – notice that the gain peaking has reduced (see first oscilloscope capture vs. this capture)

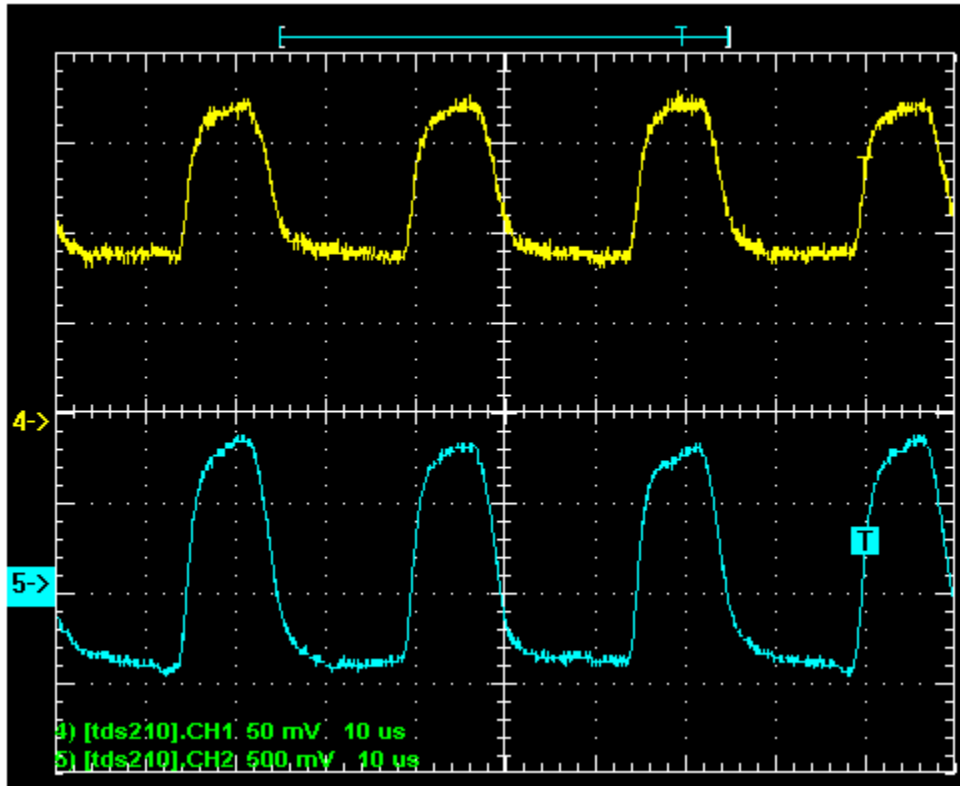
Voltage gain on second stage set to approximately 2 (Ch 1 at X2 and C2 at X8)



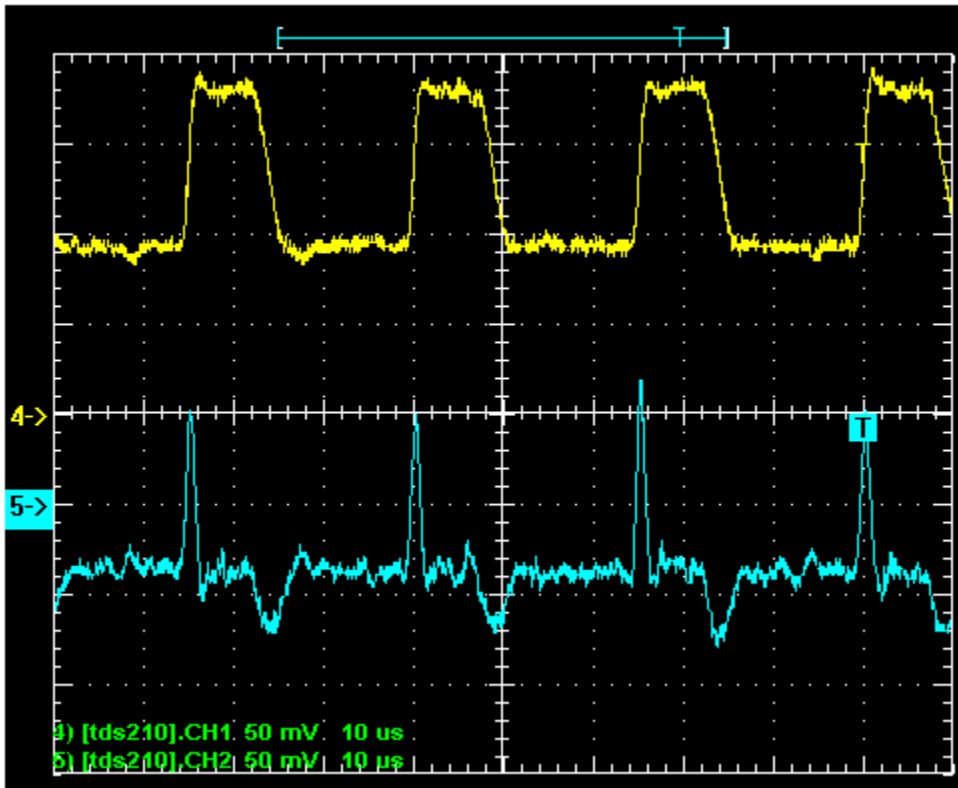
High gain on second stage (note the gain peaking is gone – and note the settings on Ch1 vs. ch2. Gain of second stage is approx.57



Second stage setting with gain around 10 seems to present best results

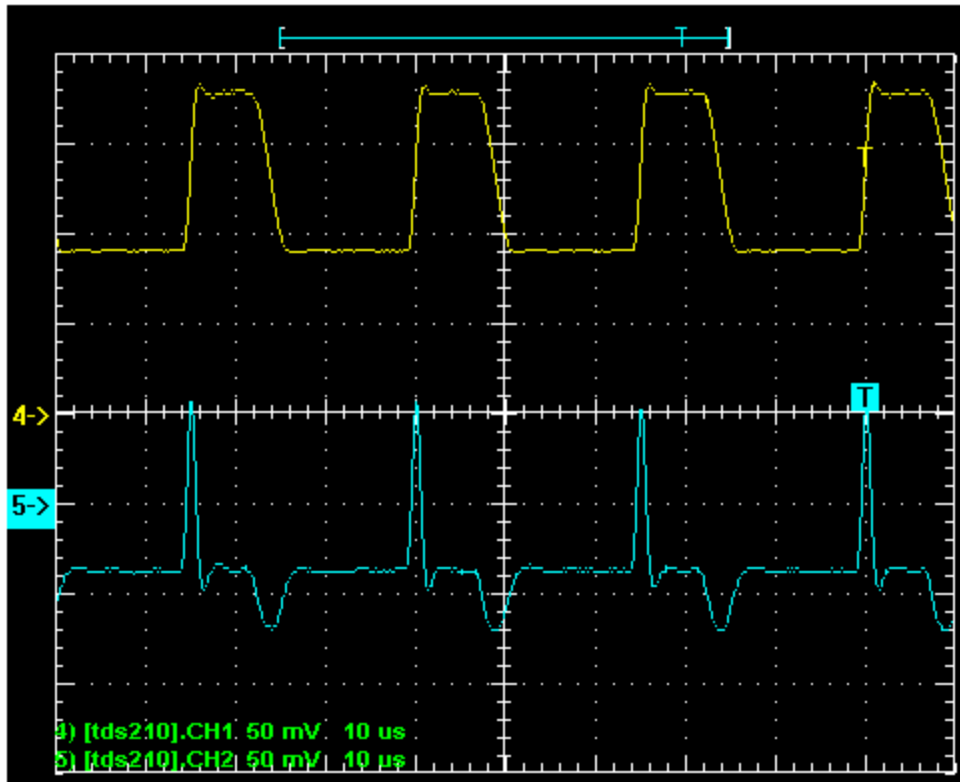


Taking Output of OPA350 directly to differentiator – no second stage gain



Notice that noise has increased because of differentiation – but positive spike, and negative spike above noise level

With signal averaging on the TDS210 turned on (set 16 samples), performed of the captured waveform – noise is averaged out.



For the waveform above – note that to recover the transmitted pulses, the comparator circuit with hysteresis will have to trigger at  $\pm 50\text{mV}$

The DC offset is a concern – as well as the smaller of the two negative going peaks. – See results from placing stage two op-amp ahead of differentiator.

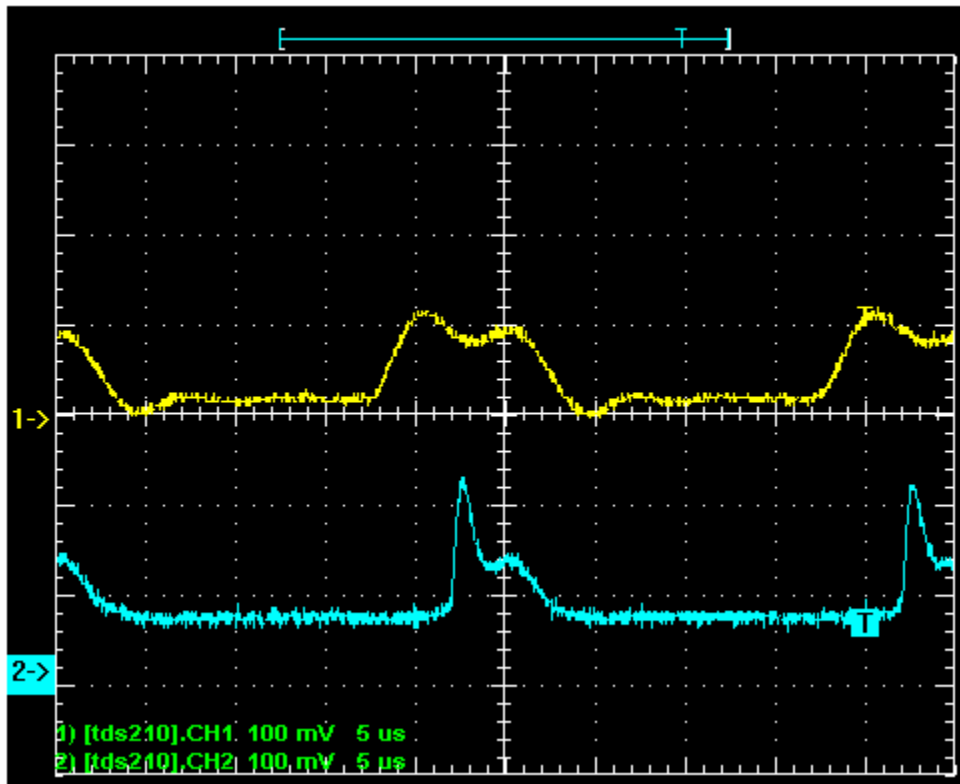
Sept. 2/07 - continuation

This waveform compares the Hybrid amp output (Ch 1 at x7 with Ch 2 output off of X2 – using PDB-C142

Light source Blue

Ambient light measured at 2.19uW with light source on, measures 5.26uW at 2 meters distance. Difference Pulse light level only = 3.07uW or -25.13dBm

It is unclear as to why Ch2 has higher gain peaking compared to previous experiments – Notice the difference in DC offsets also for both gain peaking.



Repeat using same conditions, but closer to source: Distance is 1.2 meter

No circuits connected to the TIA amps output.

Each Detector is compared with Hybrid output.

Distance is 1.2 meter

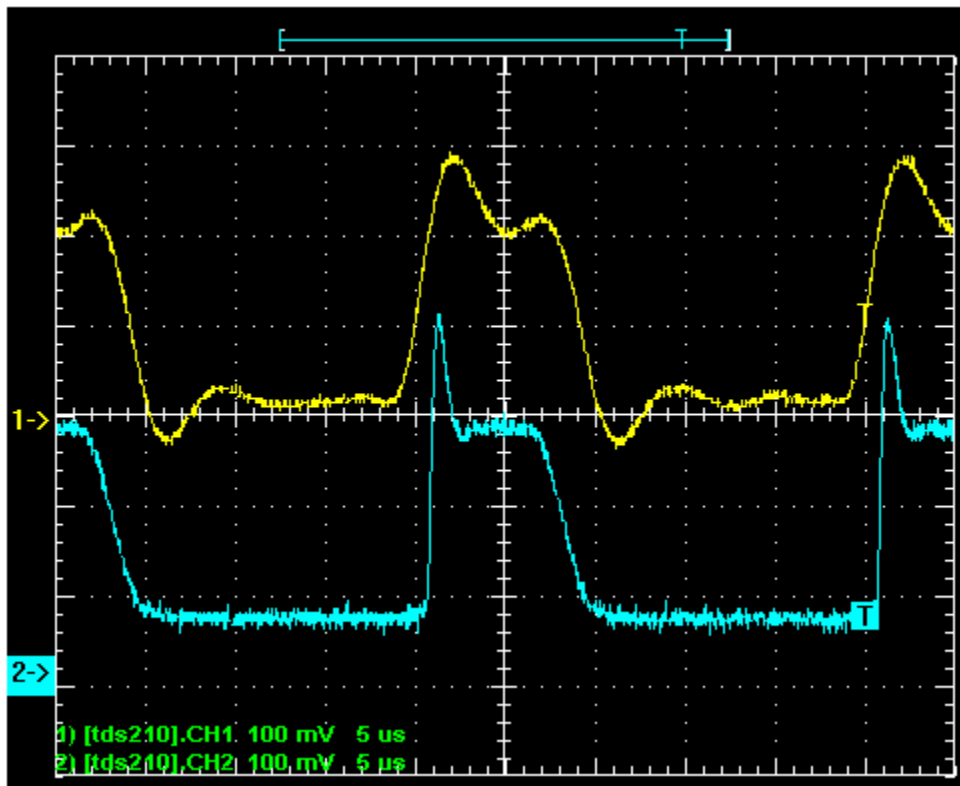
Light level: The optical power measured (combined ambient and pulse) is 10.75uW.

Ambient level: 2.2uW

Blue light pulse power: -20.7dBm

Ch1 – hybrid output

Ch2 – OPA350 output with **Detector PDB-C142**

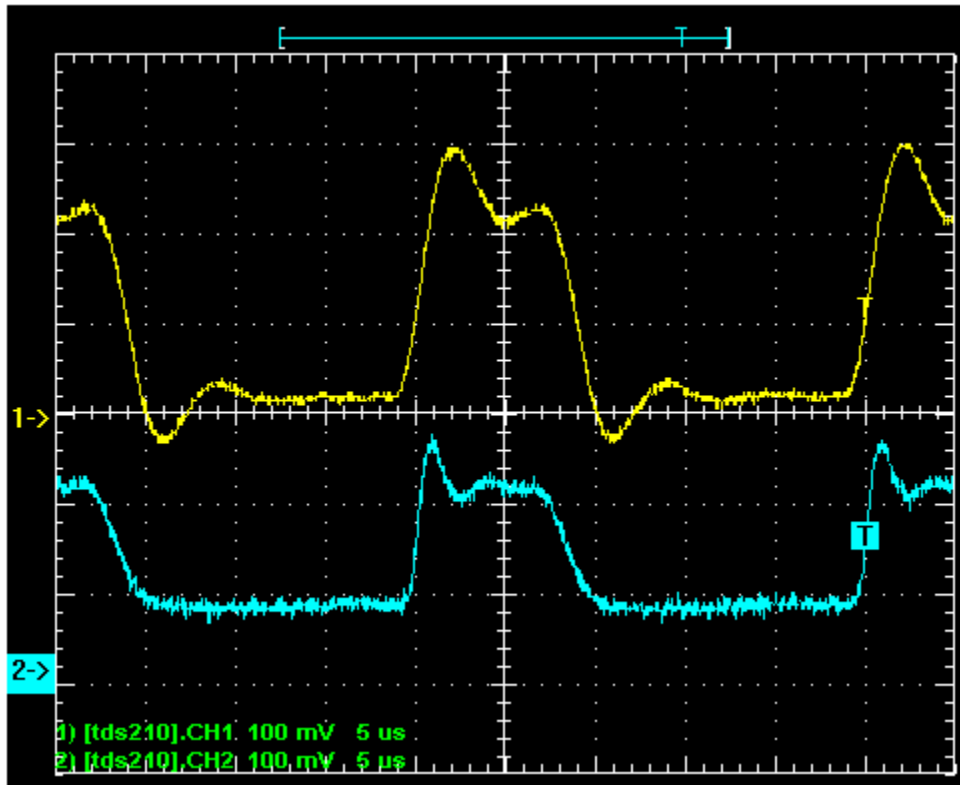


Distance 1.2 meters.

Light level: The optical power measured (combined ambient and pulse) is 10.75uW.

Hybrid output (ch1)

OPA 350 with detector PDB-169 Sidelook (ch2)





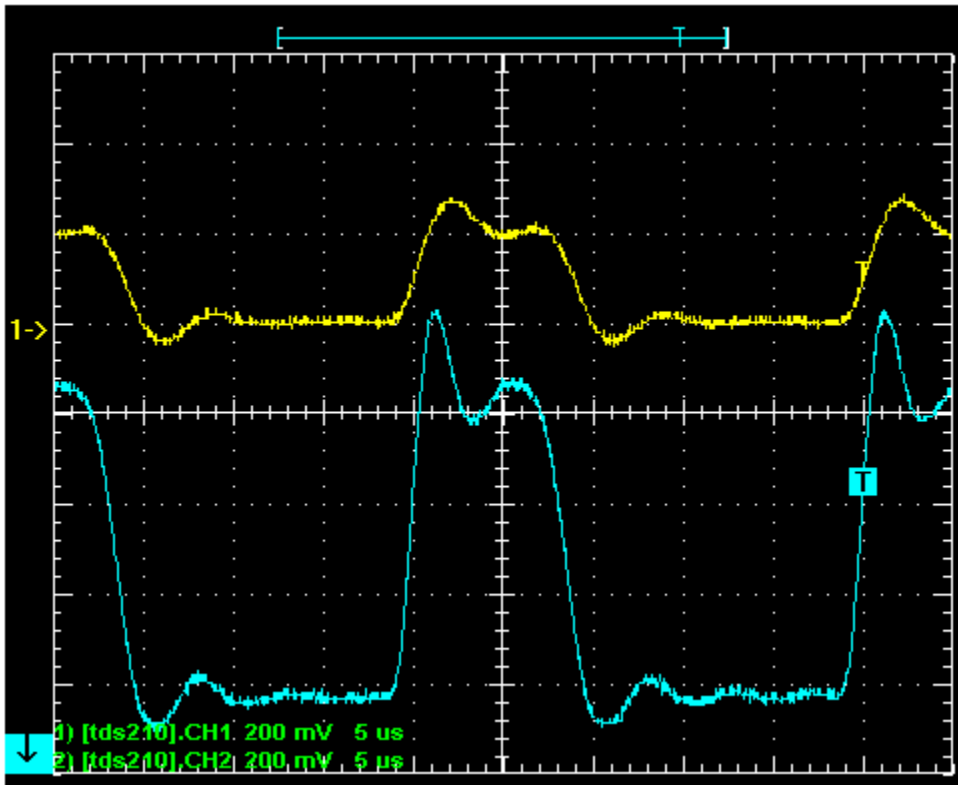
Distance 1.2 meters.

Light level: The optical power measured (combined ambient and pulse) is 10.75uW.

Hybrid output (ch1)

OPA 350 with **Detector PDB-C107** (ch2)

Notice the change of scale – this detector's output is substantially higher.

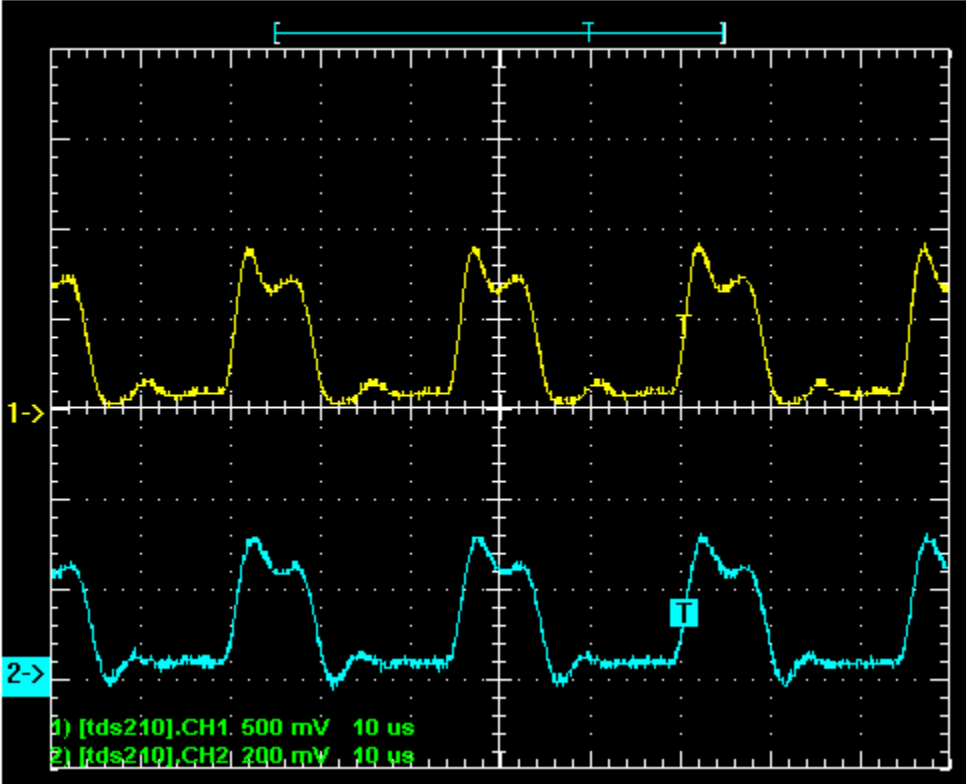


Distance 1.2 meters.

Light level: The optical power measured (combined ambient and pulse) is 10.75uW.

Hybrid output (ch2)

OPA 350 with **Detector SD200-12-22-041 ND** (ch1)



Notice the scales Ch1 discrete detector/OPA350; Ch2 output Hybrid is at x7

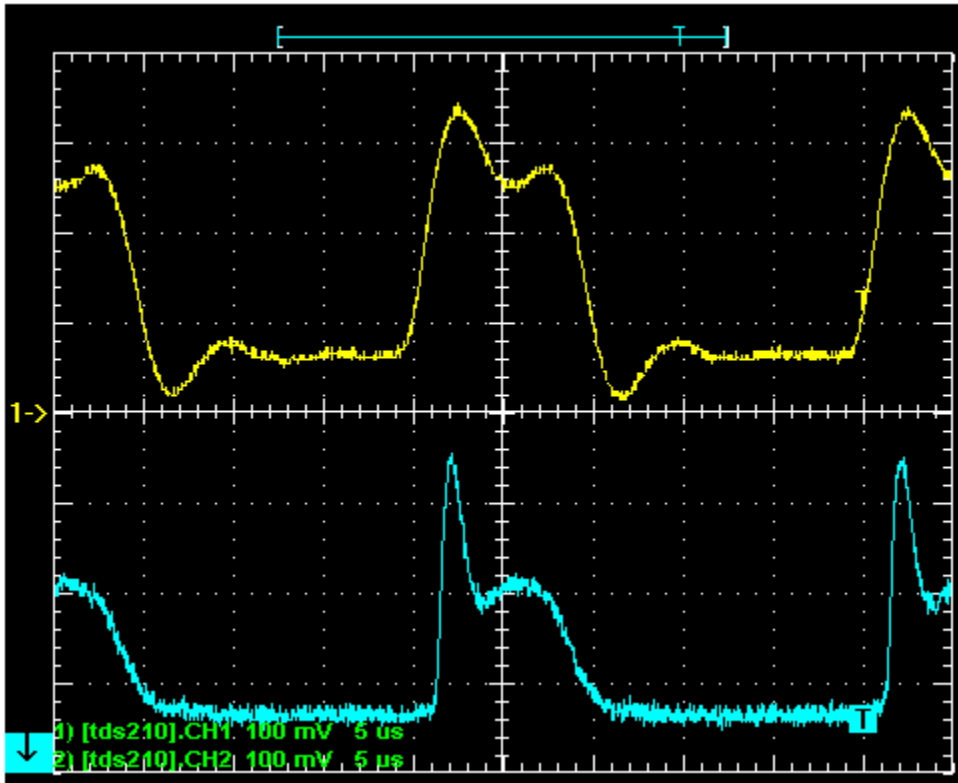
Distance 1.2 meters.

Light level: The optical power measured (combined ambient and pulse) is 10.75uW.

Hybrid output (ch1)

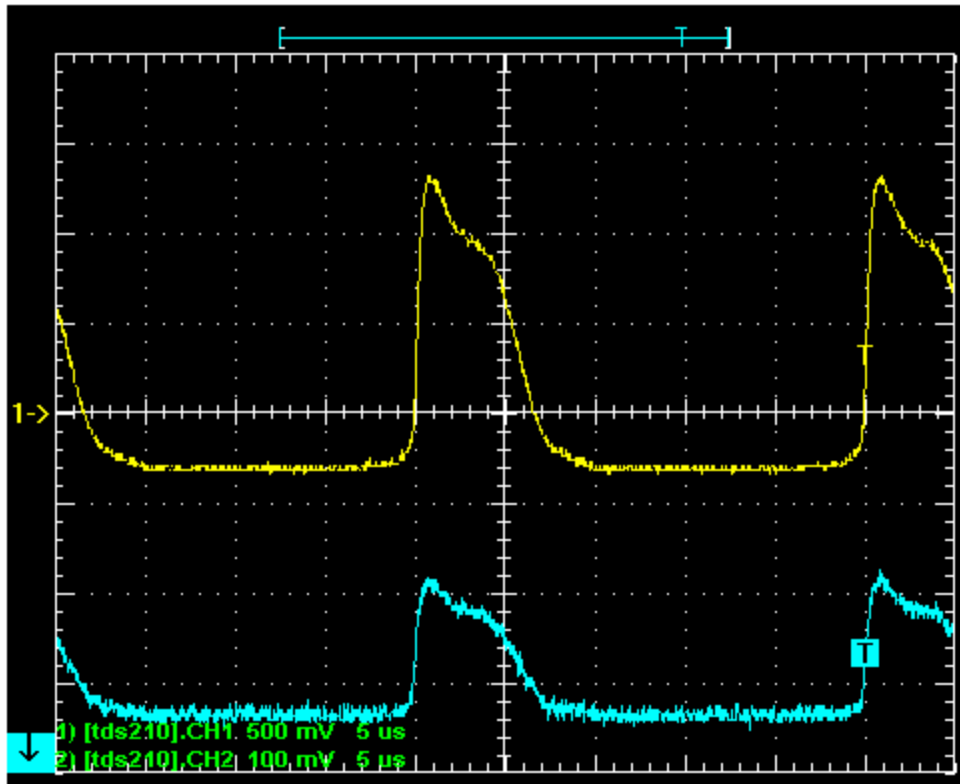
OPA 350 with **Detector SD100-12-22-021**

Note: This detector is virtually the same as the hybrid but amplifier is external.



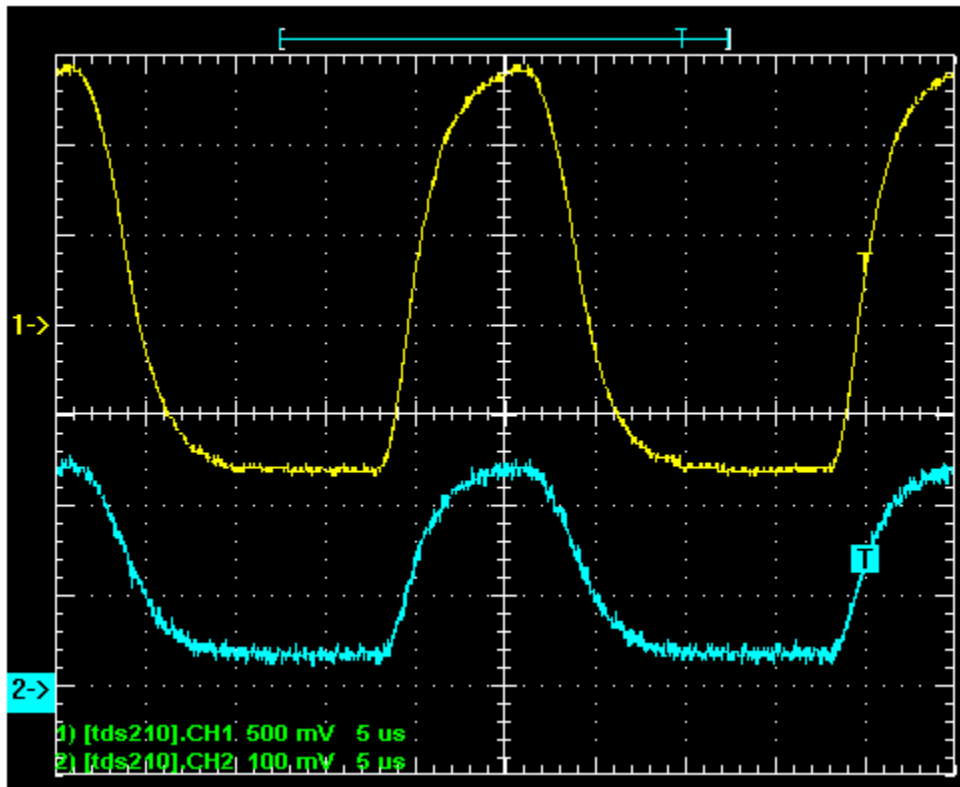
The gain peaking is a concern (that was not there in earlier experiments)

The next image is with the same diode and light source but with stage two amplifier installed (Ch1 is the output of the amp at x8 Ch 2 is x2)



This time the amp is on the output of the hybrid

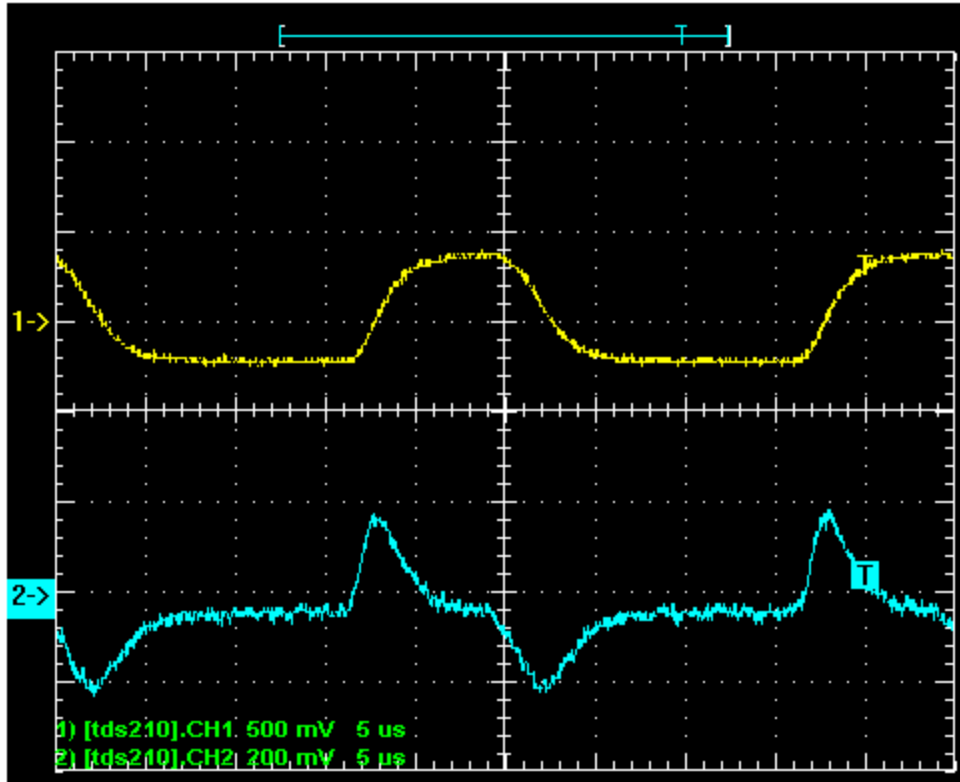
Ch 1 at X8 - amp output and Ch 2 at X7 Hybrid output



Notice the gain peaking has disappeared with the second stage loading

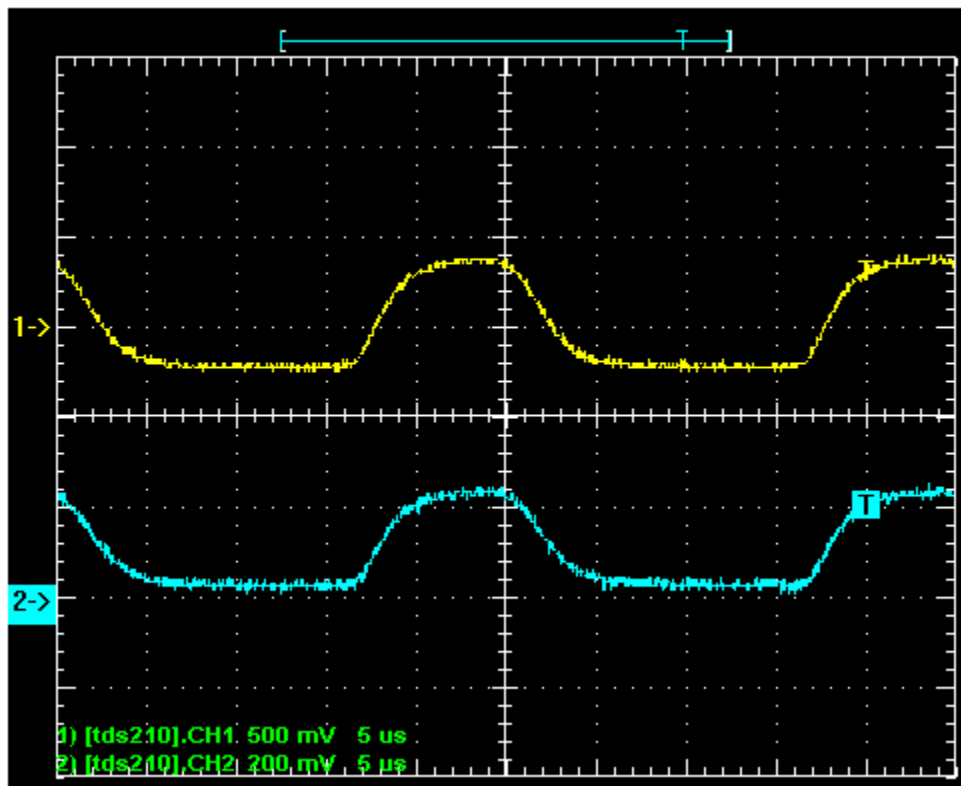
This image is with hybrid – to second stage amp to diff amp

Ch 1 is output of second stage amp (X8) and Ch 2 is output of diff amp (X9) (gain of stage 2 reduced)



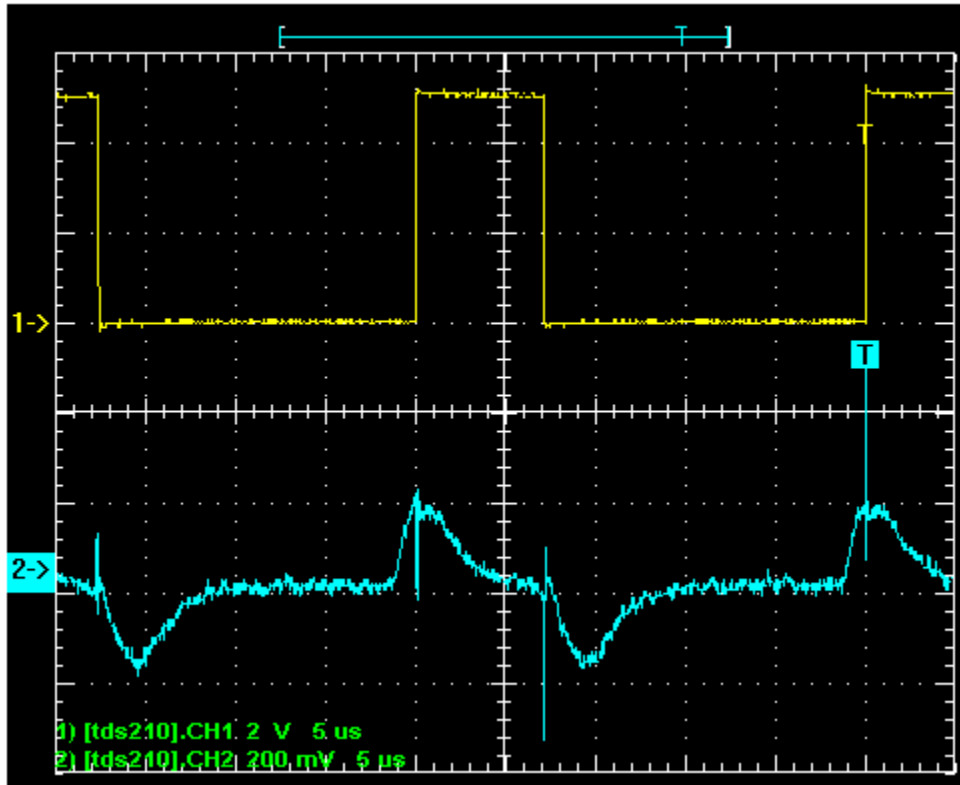
Notice the DC average level, but also the noise. The differentiator has resulted in loss of amplitude.

Output of hybrid Ch 2 – x7 compared with output of 2<sup>nd</sup> stage amp – ch1 at x8 Notice the scales



Comparison of Diff amp output Ch 2(x11) with schmit inverters ouput at Ch1 (x12) – R 18 adjusted for best result

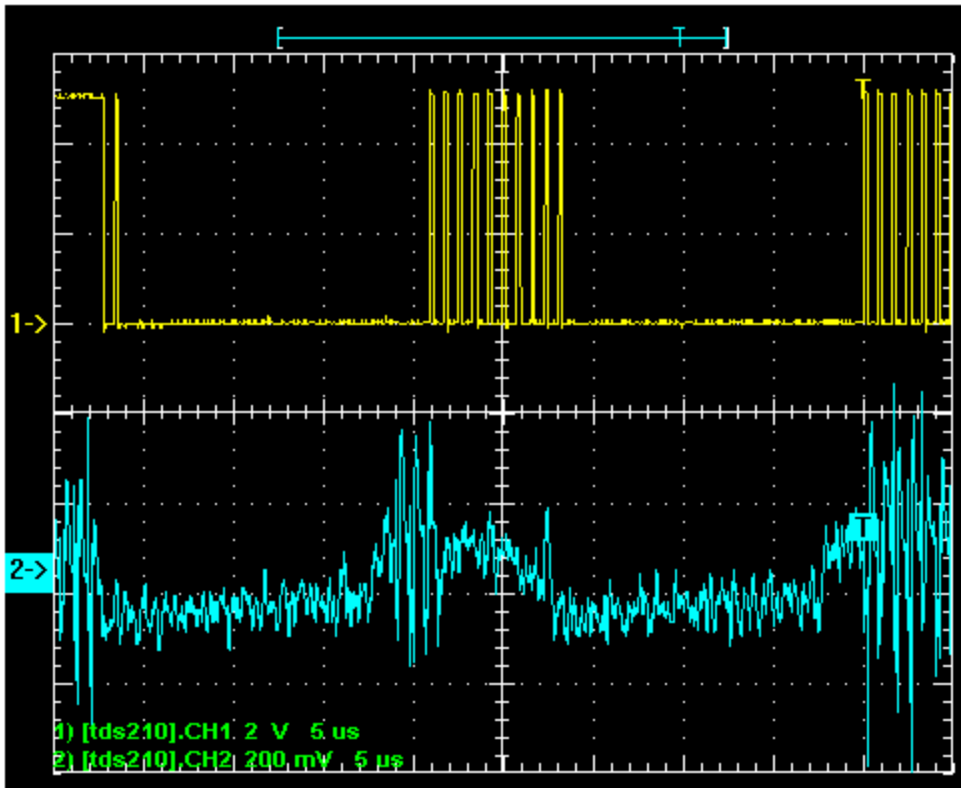
Note how the impulse noise feeds back – this is a problem that needs to be resolved (not sure how?)



At two meters from light source:

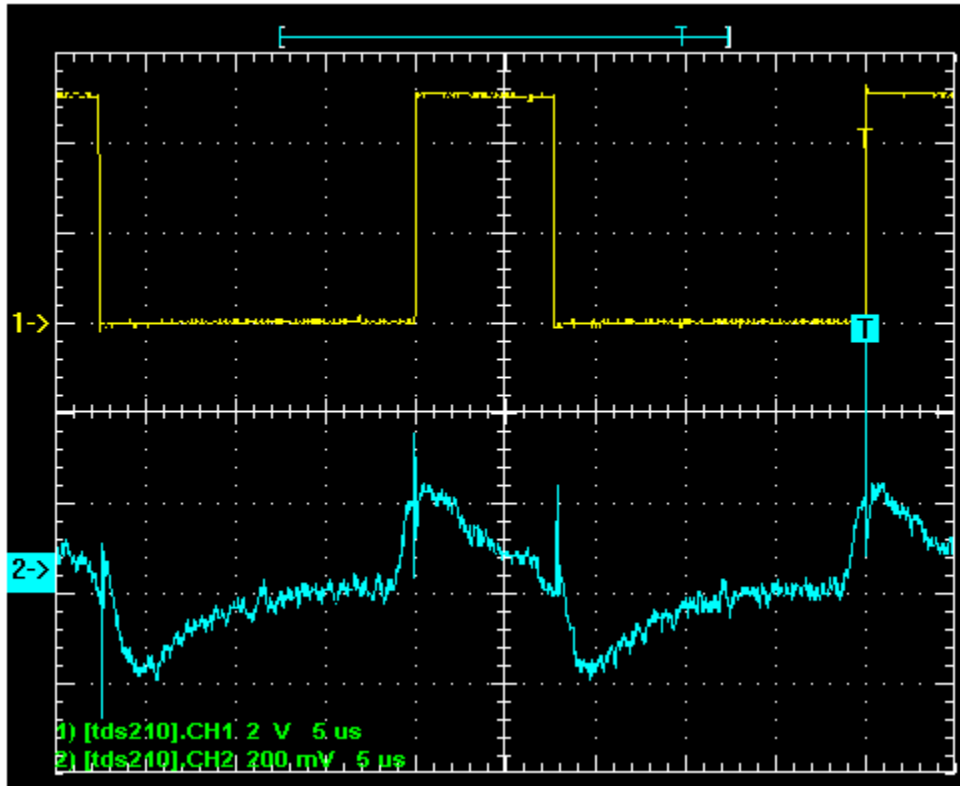
Amplifier gain 2<sup>nd</sup> stage increased – notice the problem – so to does noise get increased within the circuit – and the subsequent feedback of the pulses from the Schmitt



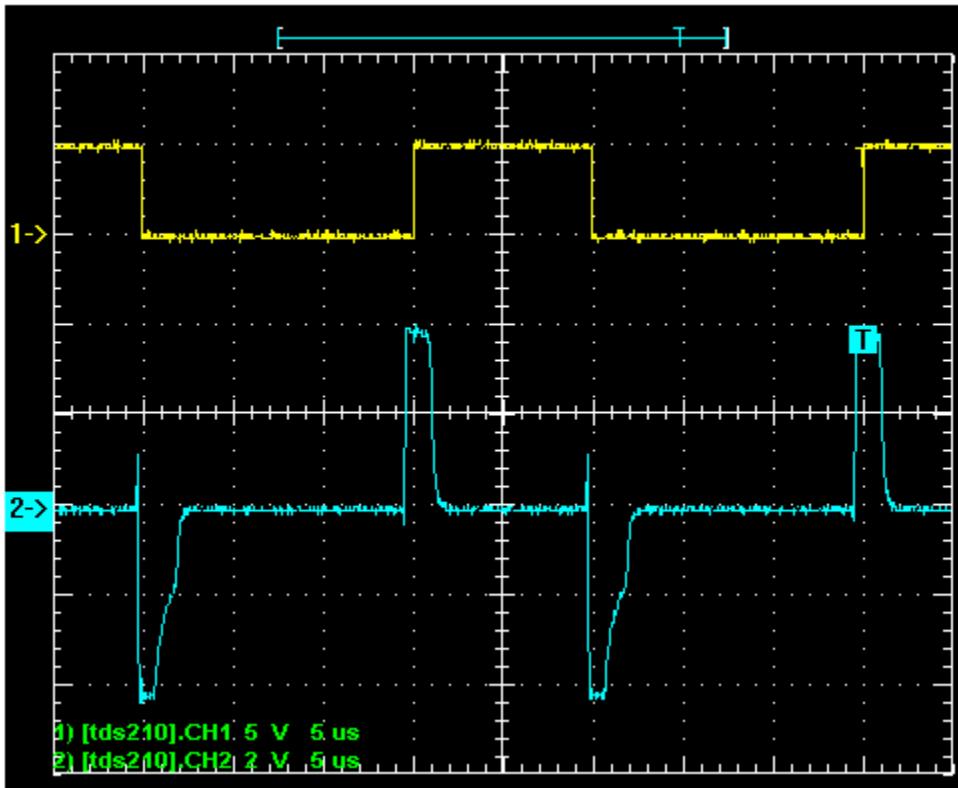


Same distance but with optical magnification instead of electrical  
- Note: I am not centered into the highest light beam level

Optical meter measurement at 2 meters – 9.62uW  
Highest reading is 156uW

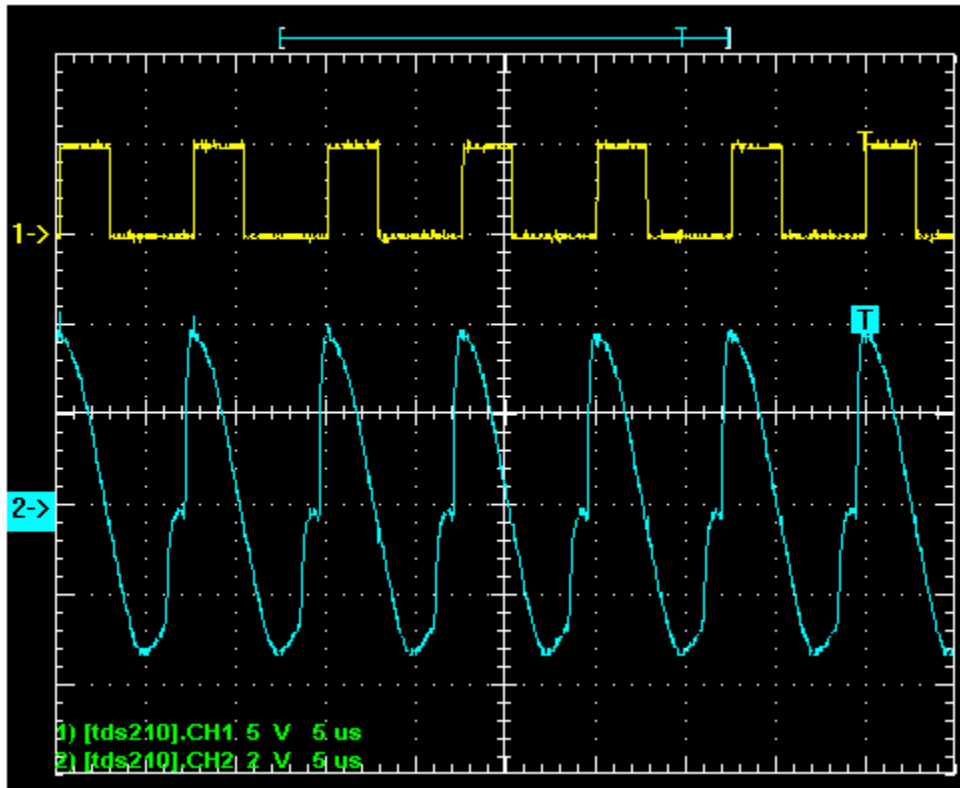


Below is with transmit lens giving 156uW reading

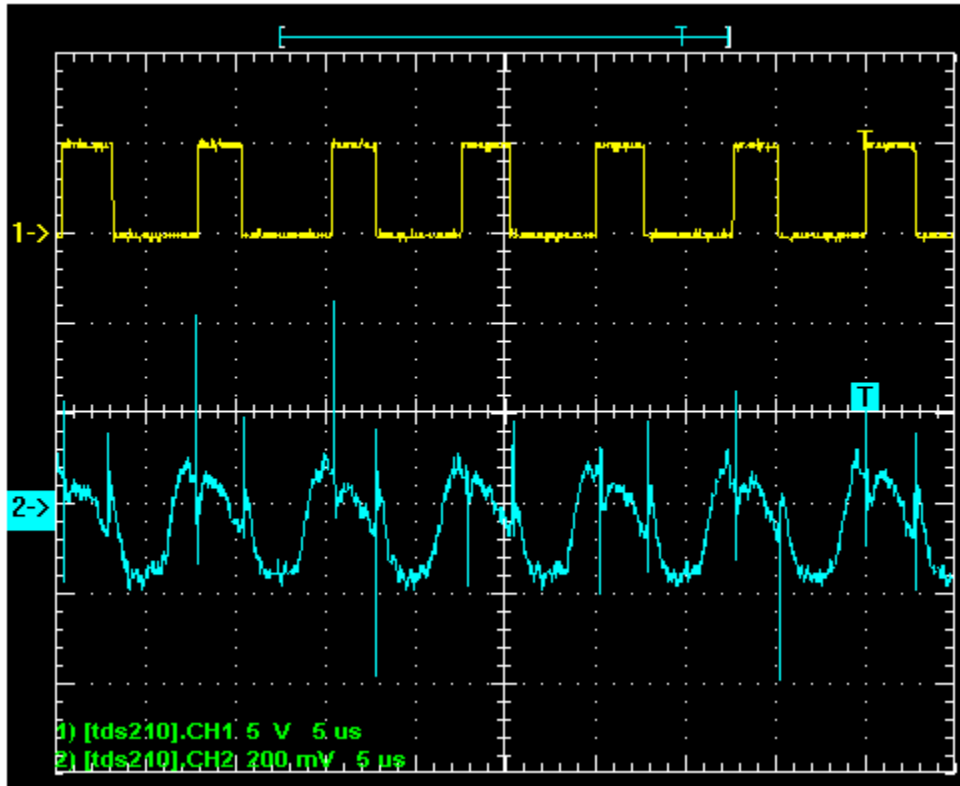


The above clearly shows that the diff-amp solution does provide a very wide dynamic range for light power, but that optical magnification is very critical to the success of this endeavor – also magnification at the second stage needs to be moderate – most of it should be done in the first stage. The problem is that the higher the magnification of the first stage, the lower the upper end frequency.

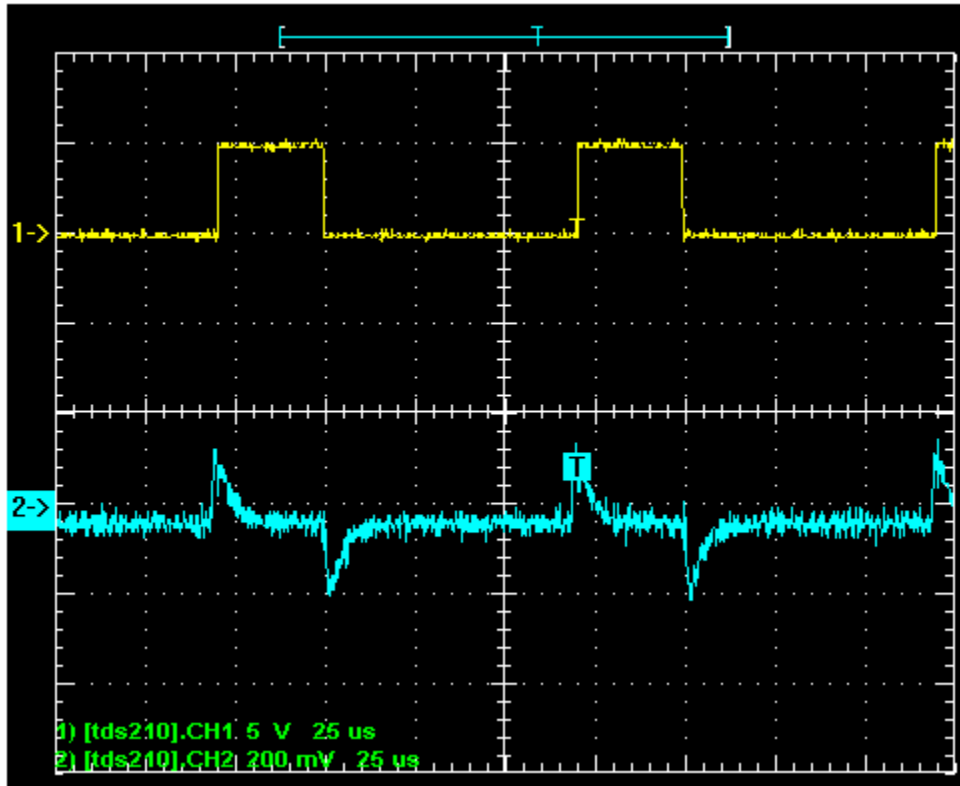
The next waveform is at high optical power – frequency = 135kHz



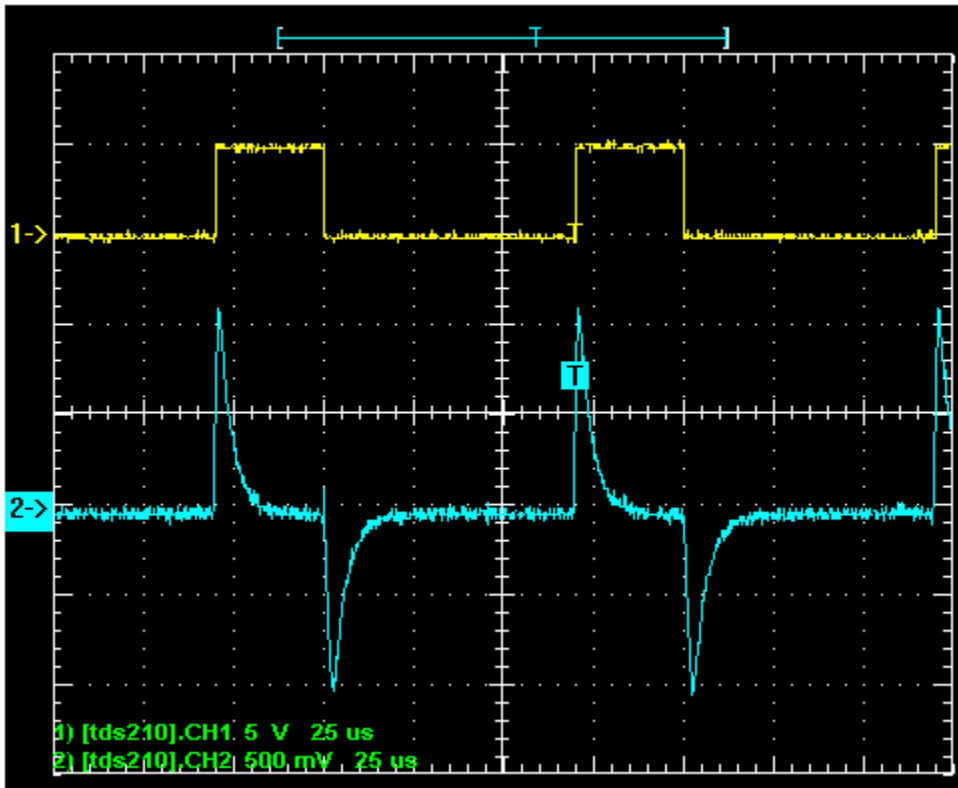
At lowest optical power (ambient and signal) = 10.3uW: Ambient = 1.5uW  
Frequency = 135kHz



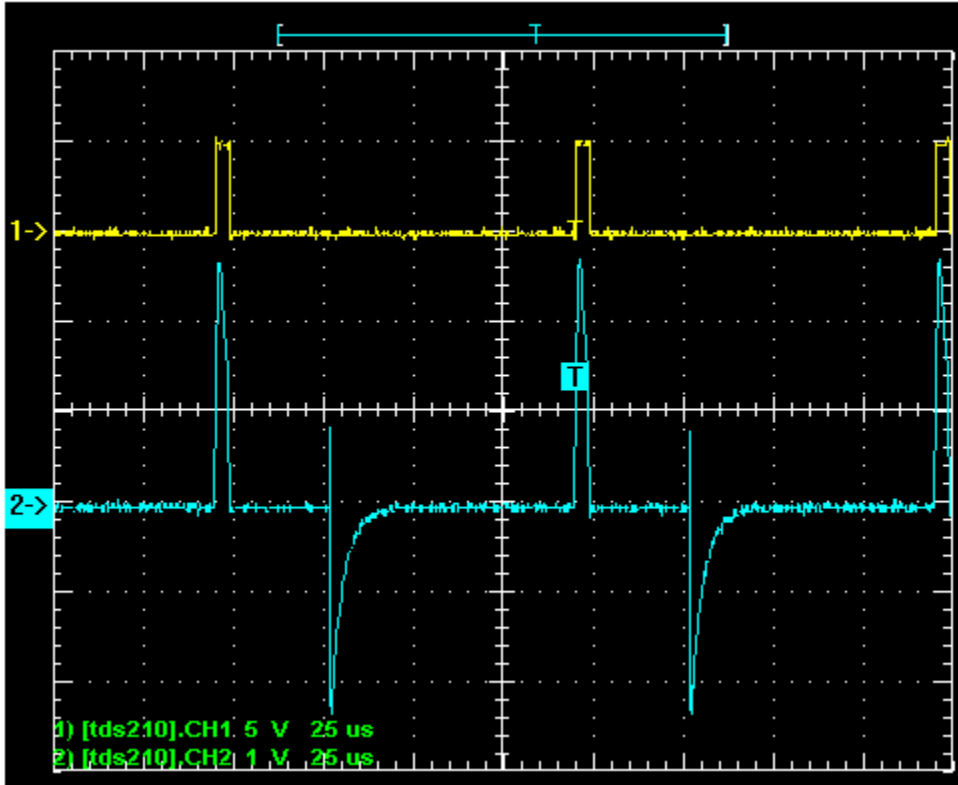
At low frequency of 10kHz - Optial power (ambient and signal) = 6.2uW



At High optical level 29.6uW  
F=10kHz



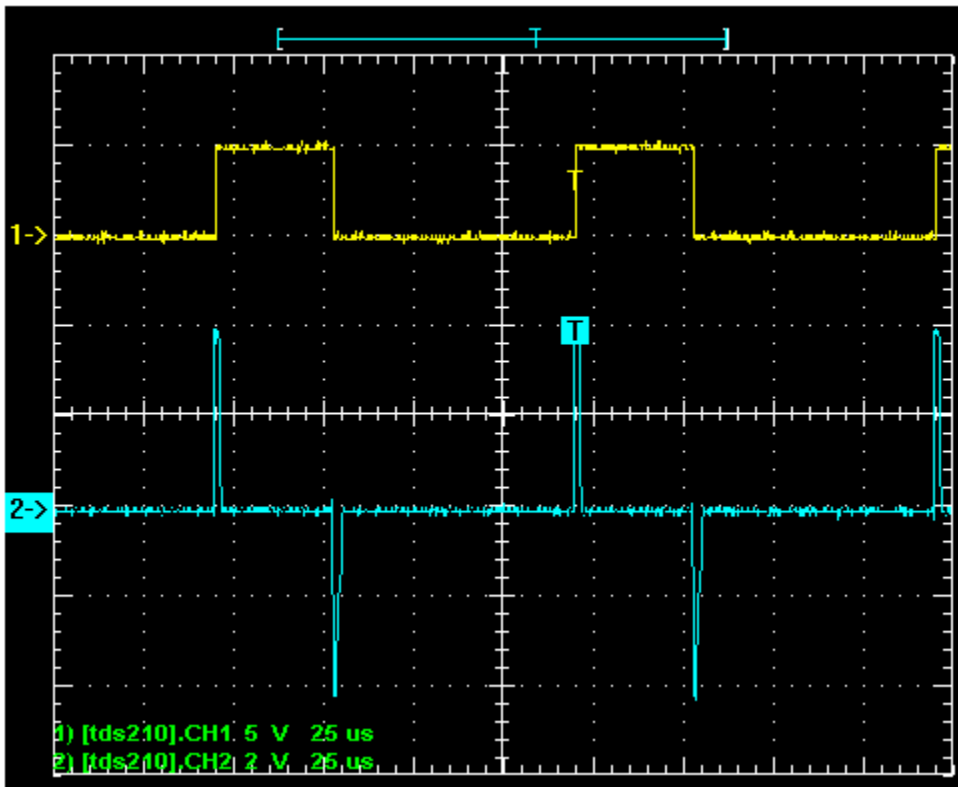
Caution: At higher power: range from 37.8uW - 67uW the schmit trigger falsely triggers



Slide above is at 67uW



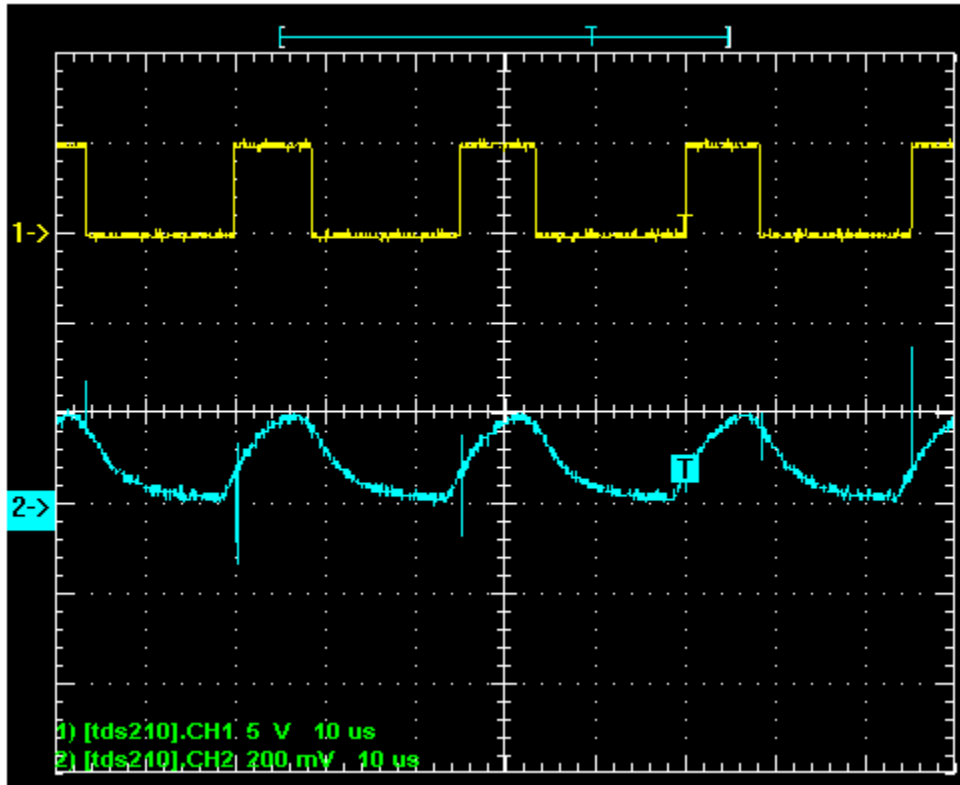
At higher power yet, it will work again:  
Power level at 68uW to 126uW



For the intermediate range where it falsely triggered, I went back and readjusted R18 for the trigger point and was able to maintain correct trigger through out the optical power range.

Input wave off of trans amp Ch2 at X7 to output pulses

Lowest power level for working: Apprx. 10uW (ambient and signal)  $f=40\text{kHz}$  ambient level 1.47uW

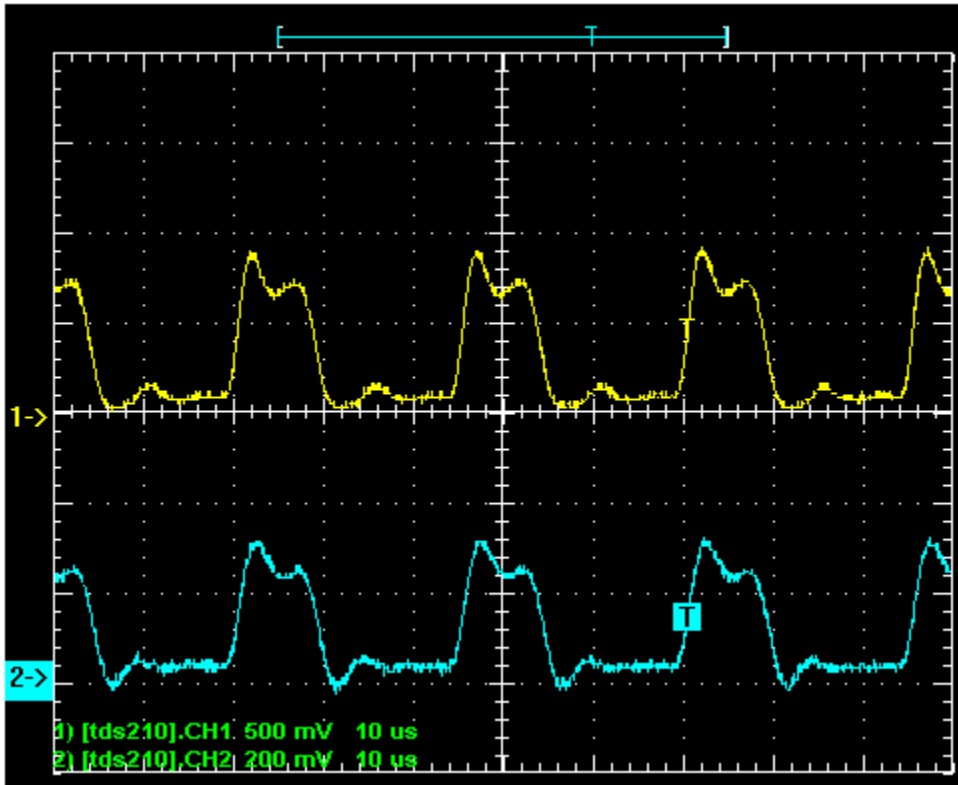


Notice how the output has been smoothed due to second stage loading

Detector: SD200-12-22-041 ND  
Distance = 1.2 meters

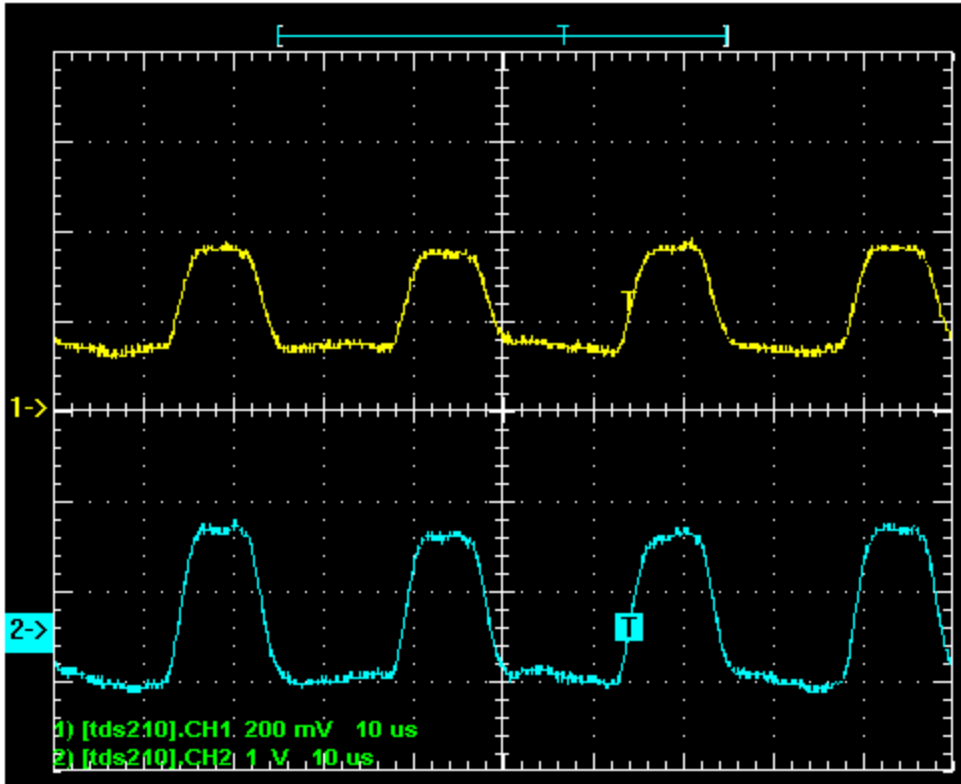
Final comparison  $f=40\text{kHz}$  30% duty cycle

Ambient level =  $2.24\mu\text{W}$  With blue pulse level =  $10.5\mu\text{W}$



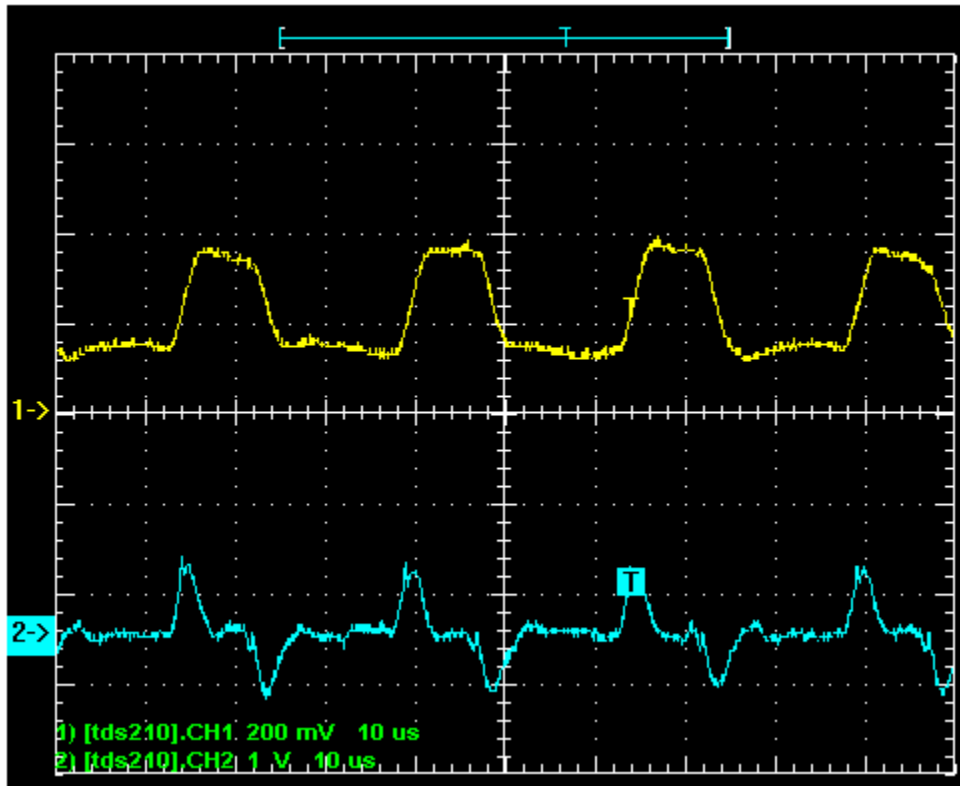
Notice the scales =Ch1 is at X2 (OPA350) Ch2 is at x7 (Hybrid)

Working with this detector SD200 – next image with 2<sup>nd</sup> stage amp installed and at 2 meters distance. Gain on second stage exactly the same for hybrid working scenario – again notice the gain peaking is gone.



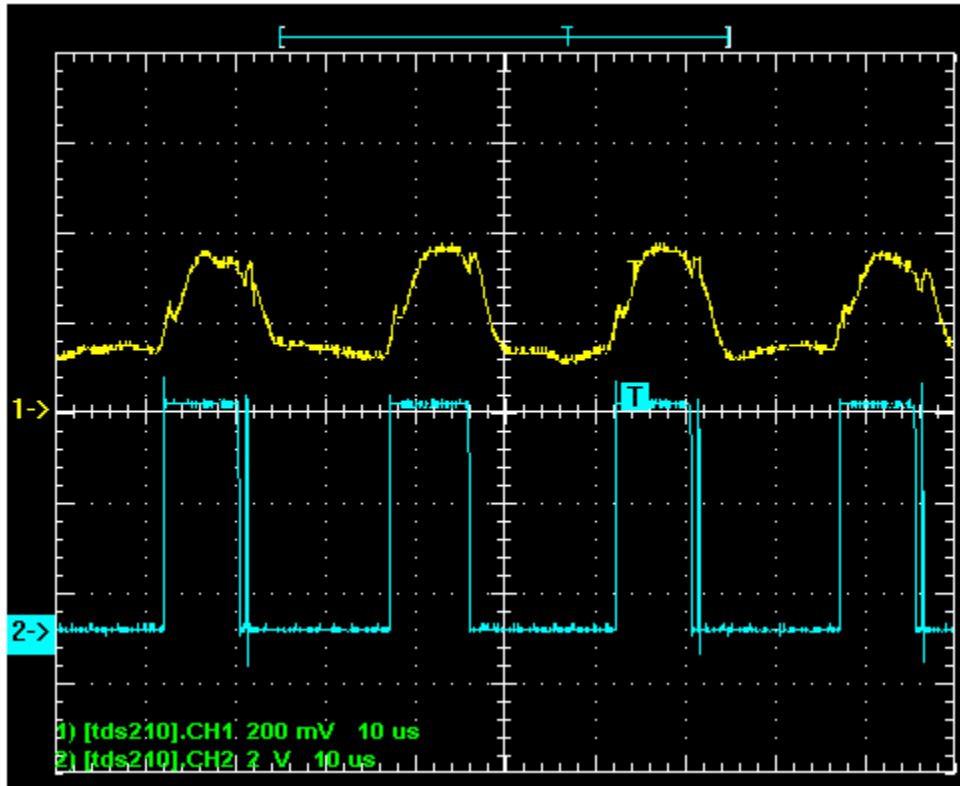
For above Ch1 is at X2 (output of transimpedance amp and ch2 is output of 2<sup>nd</sup> stage:

Next is the Diff amp output  
Ch2 at X11 and Ch1 at transimpedance output x2



This image is with ch1 at X2 and ch2 at x12 – output of Schmitt

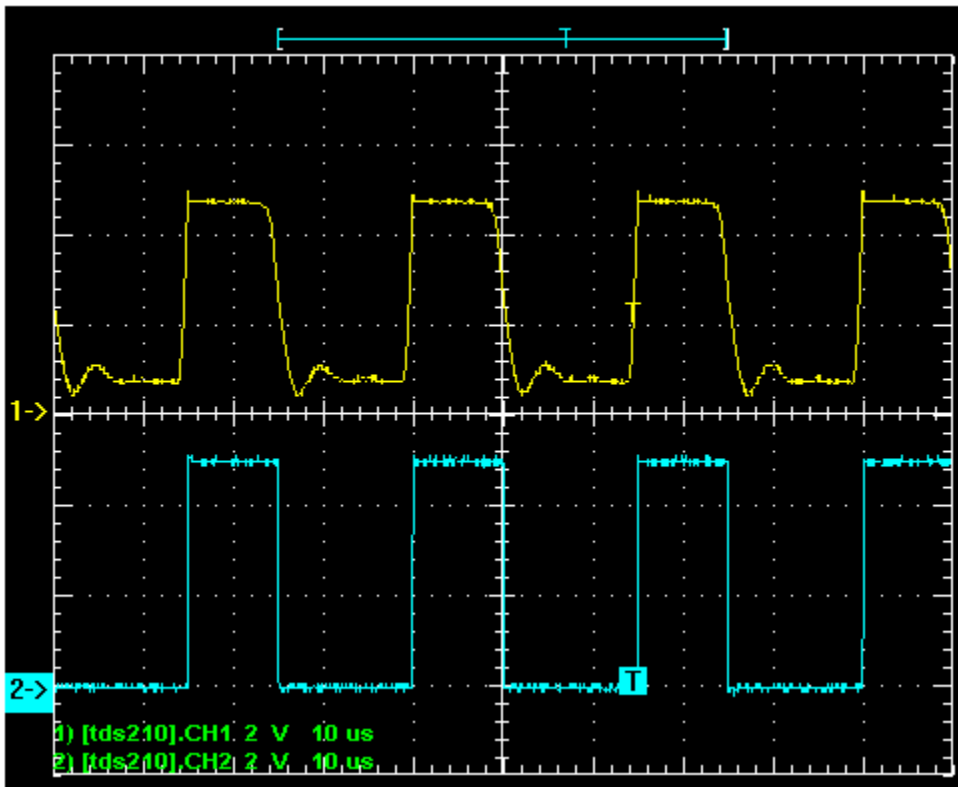
The Schmitt level has been adjusted slightly – there are some false spikes – caution



The light level for above is: 5.75uW (ambient and pulse) Ambient is at 2.5uW

The following is with lens power at transmit:

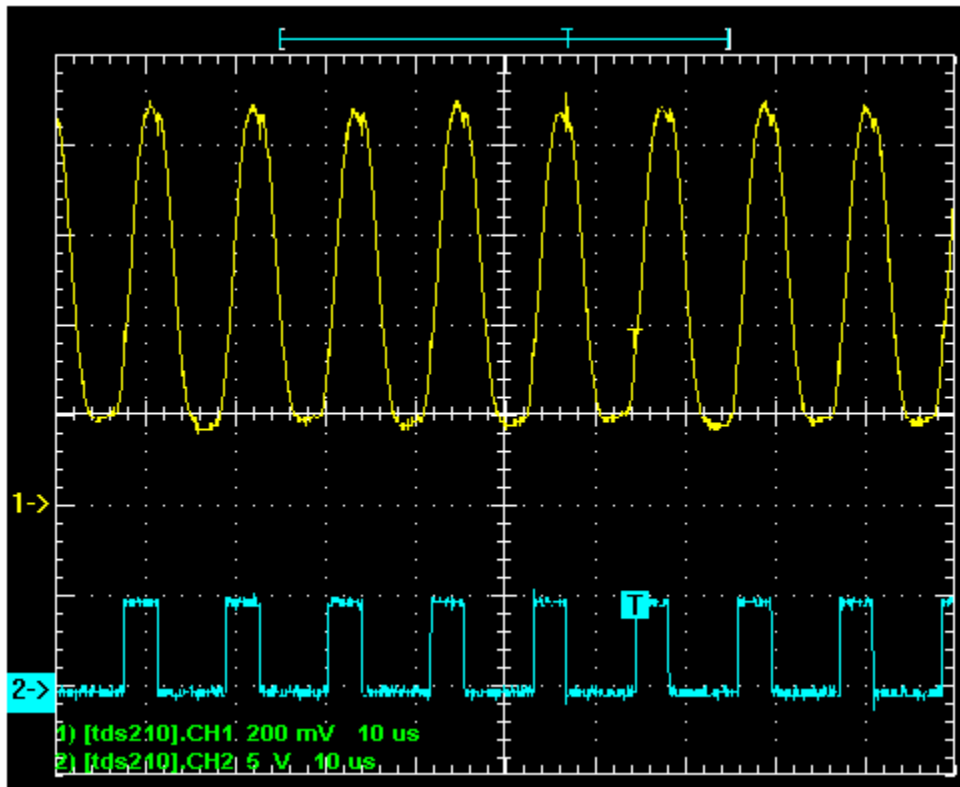
Light power is 150uW



At this level 2<sup>nd</sup> stage amp is full saturated at the two ends:

Frequency response for SD200

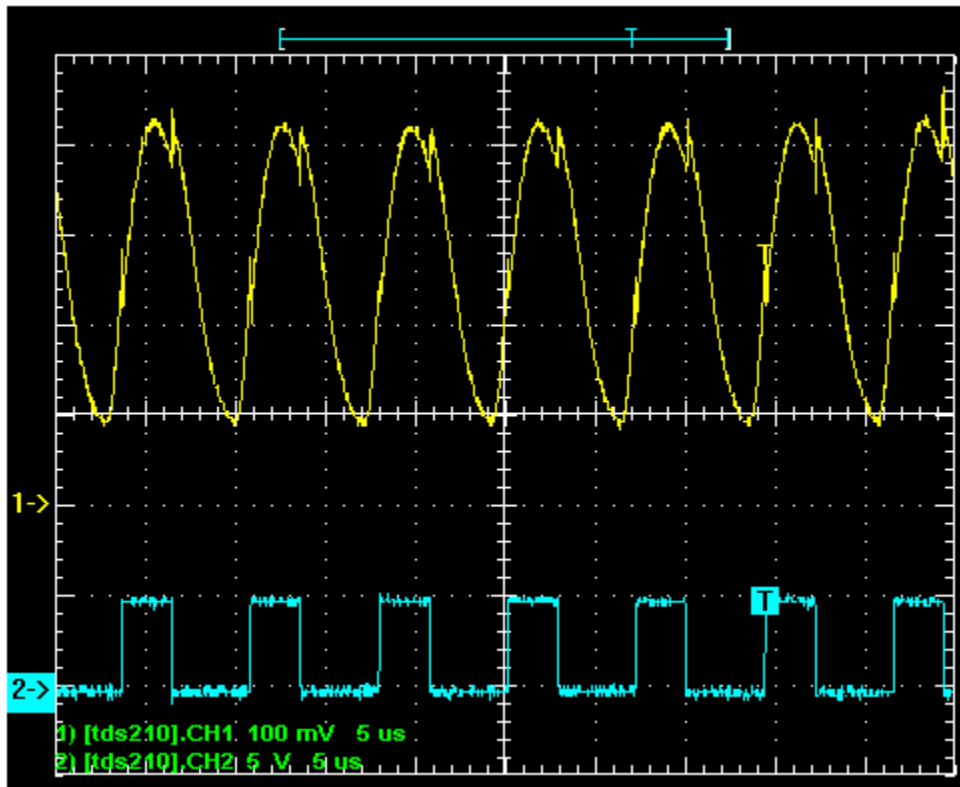
About 88kHz for image below:



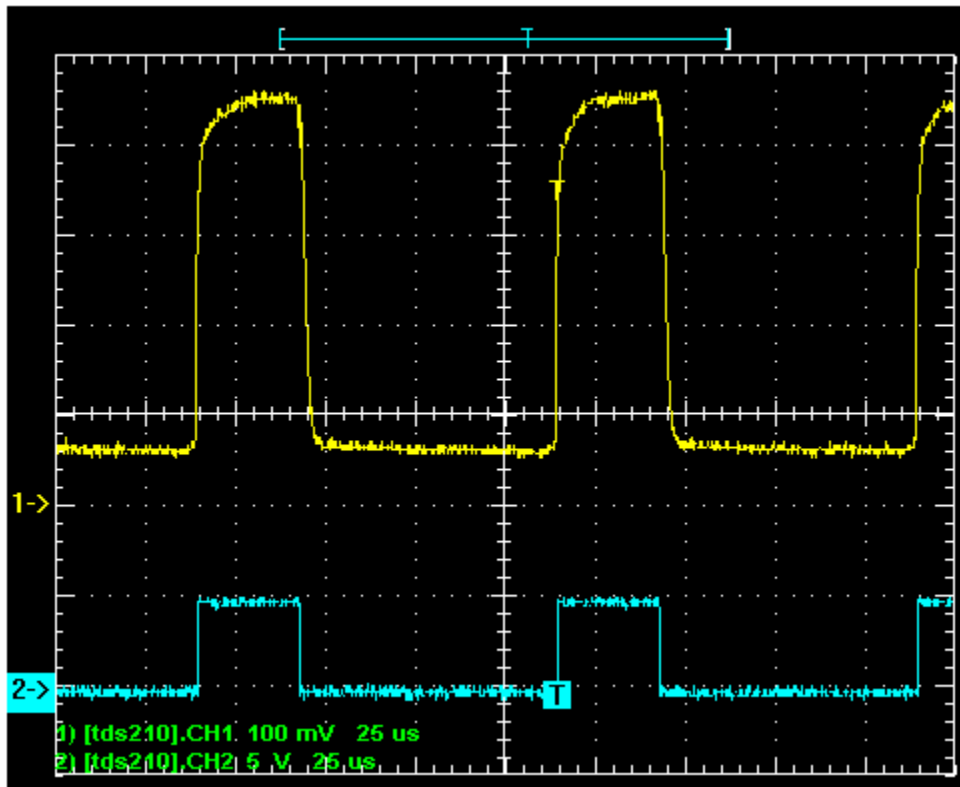


Frequency response for PDB-C142

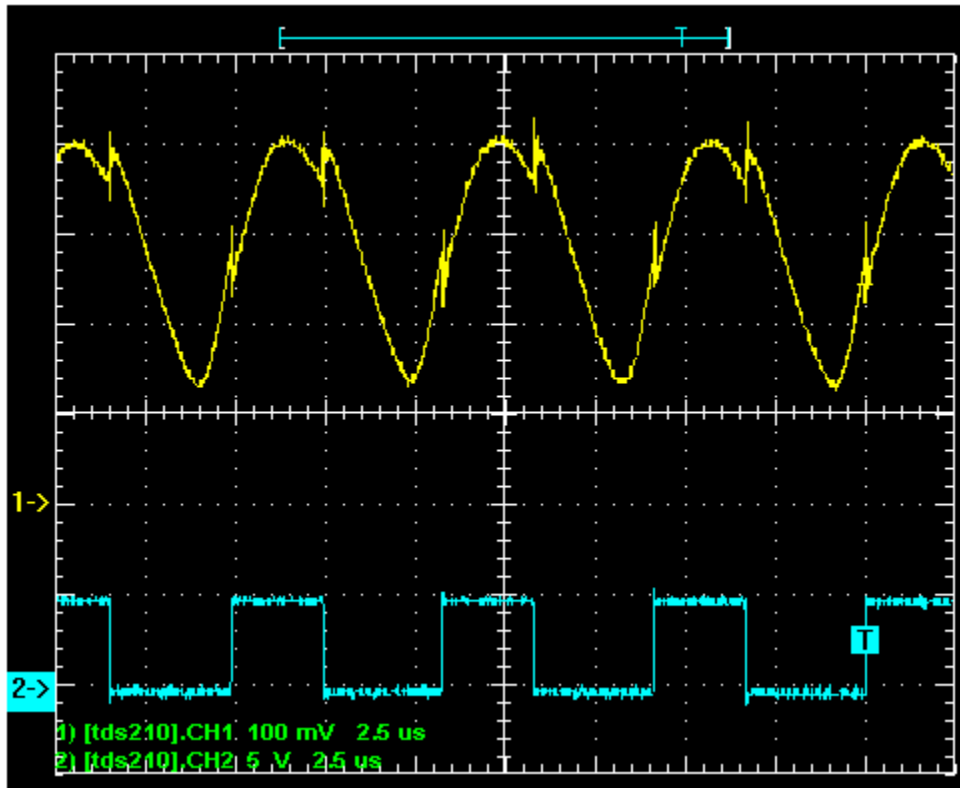
About 140kHz



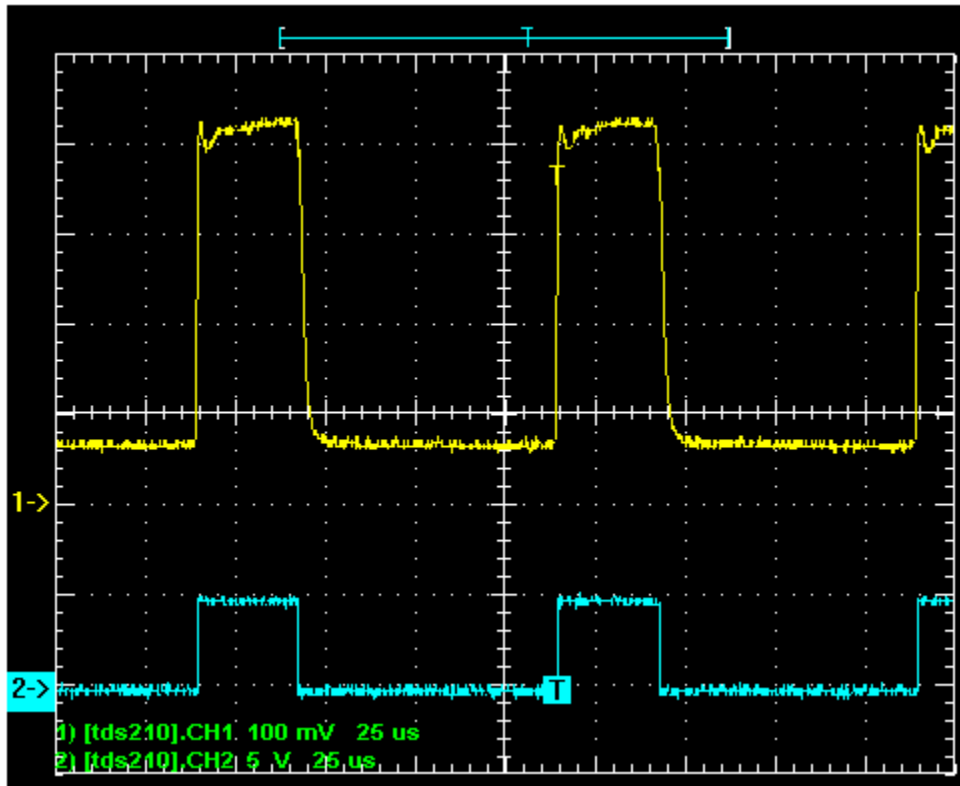
Doing this rigorously is difficult due to source concerns:  
At 10kHz output level of X2 = 412mV peak



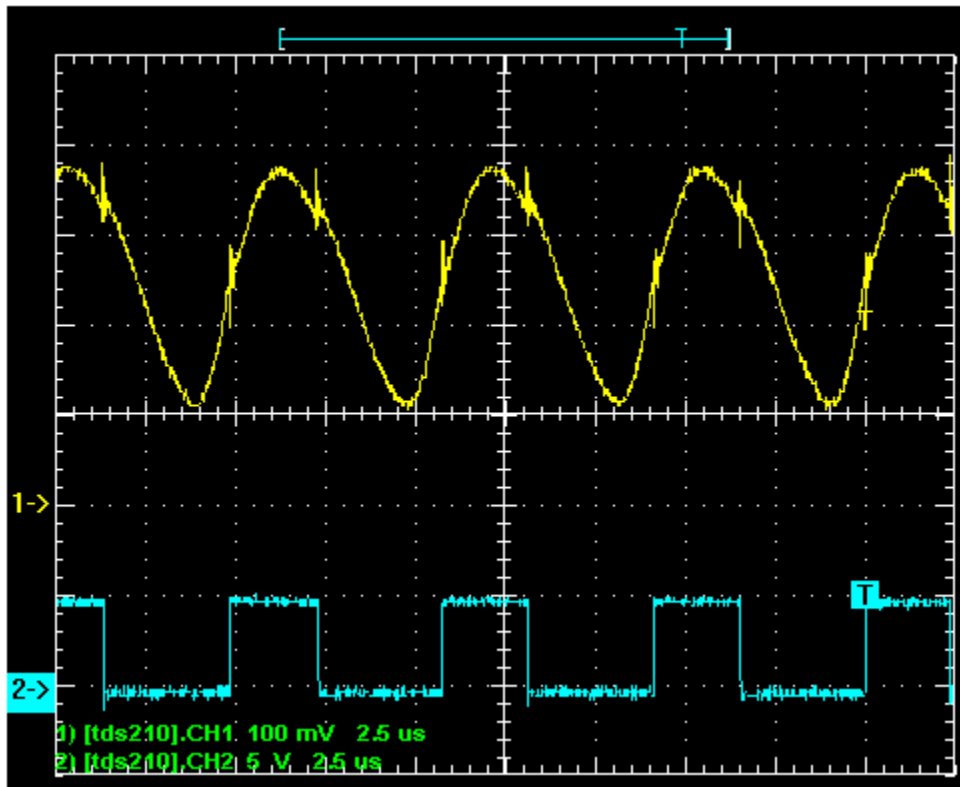
At 170kHz output level of X2 = 290mV peak (3dB down).



Frequency response for PDB C169 Side look  
At 10kHz pulse amplitude = 360mV

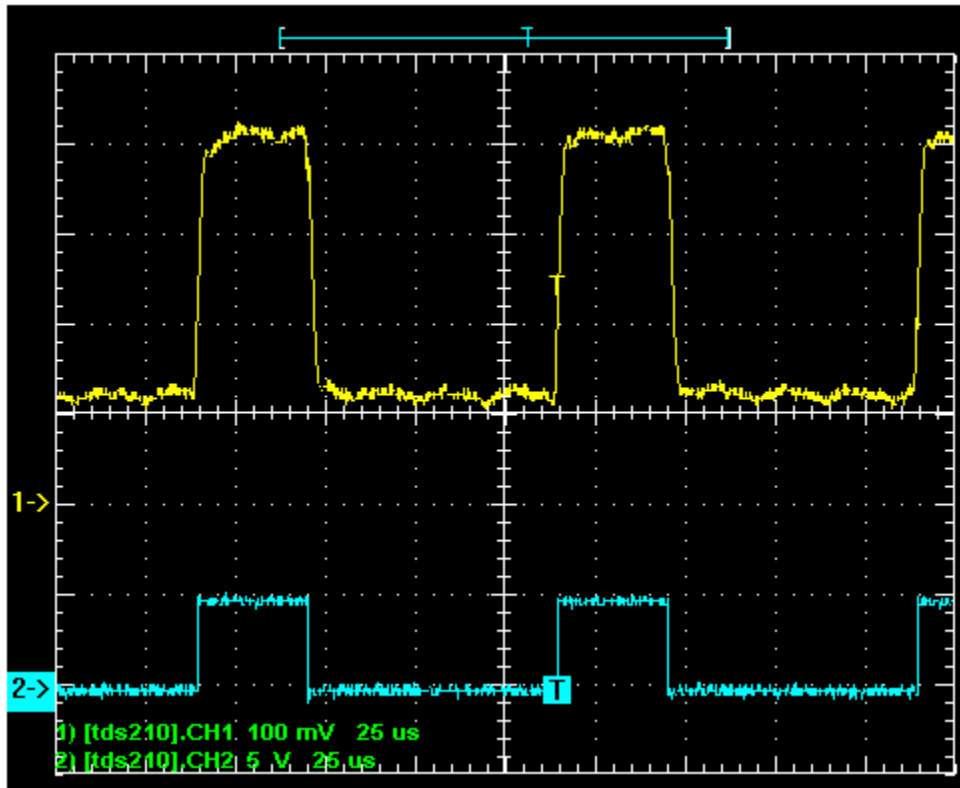


For sidelook 3dB down = 252mV  
F = 170kHz  
Replication of duty cycle is now not accurate

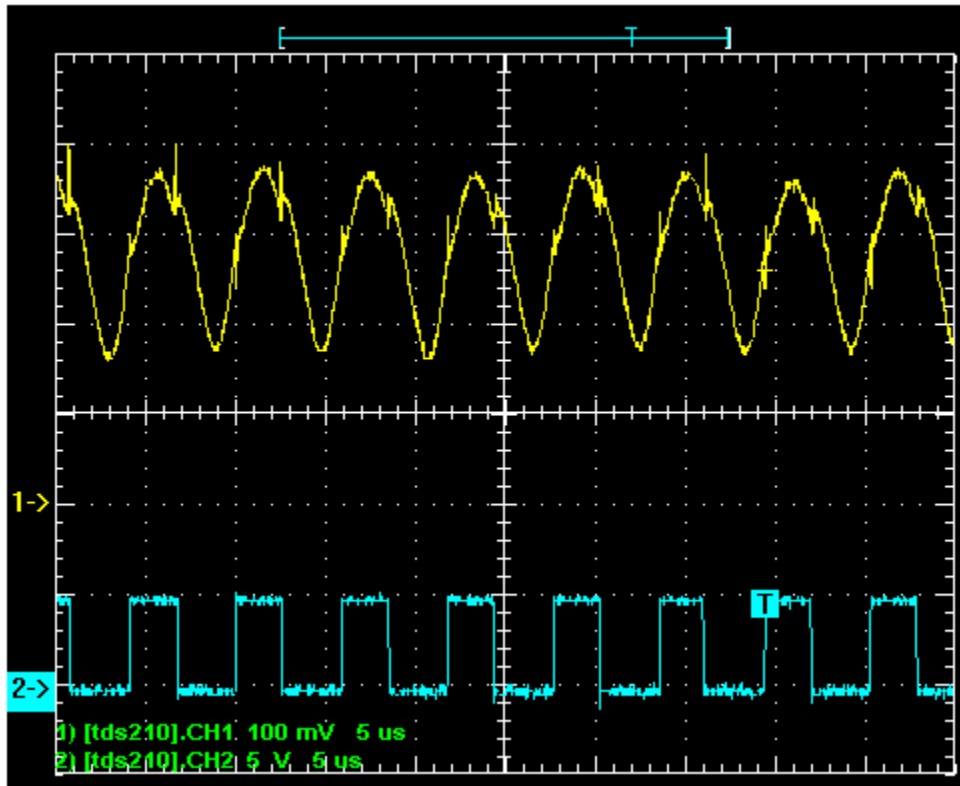


My estimate of limit:  
About 105kHz

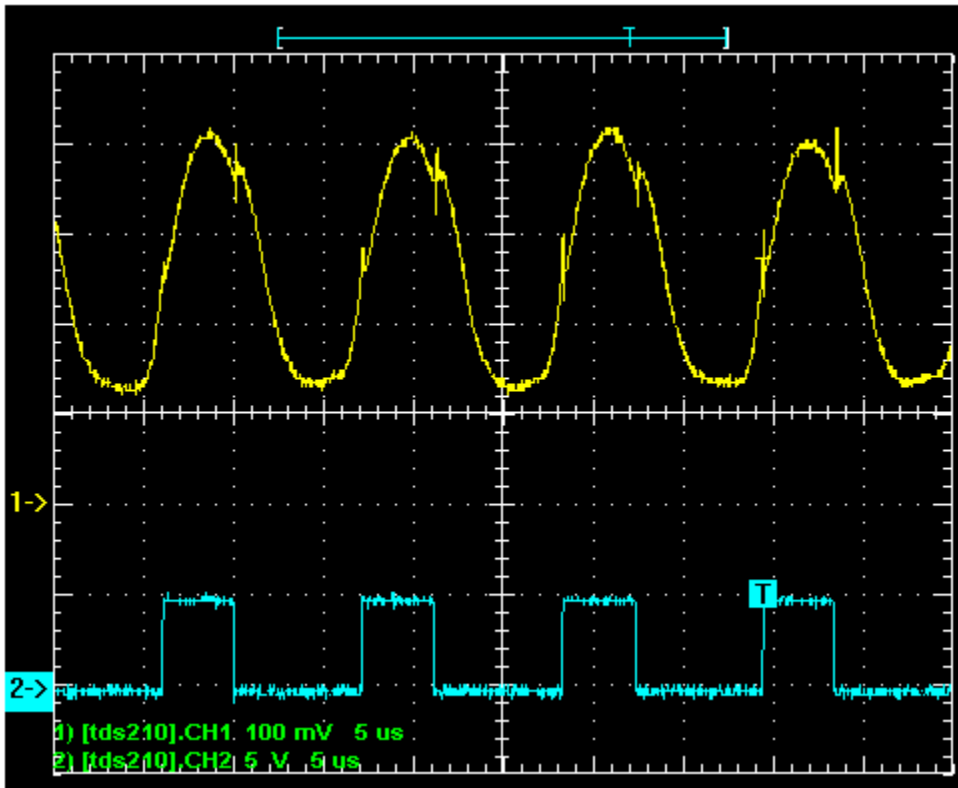
Frequency results for PDB C107  
At 10kHz output level = 284mV



The 3dB point is 201mV  
Again measures at 170kHz



But my interpretation of limit would be about 80 to 90 kHz

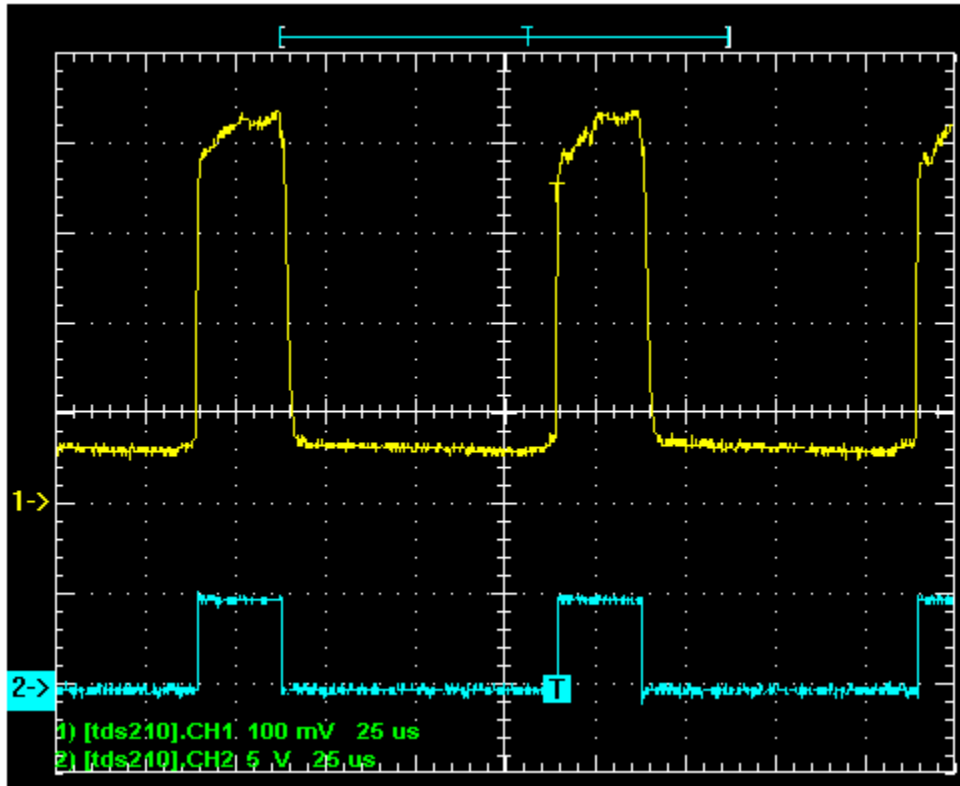


Reading above is 90kHz:

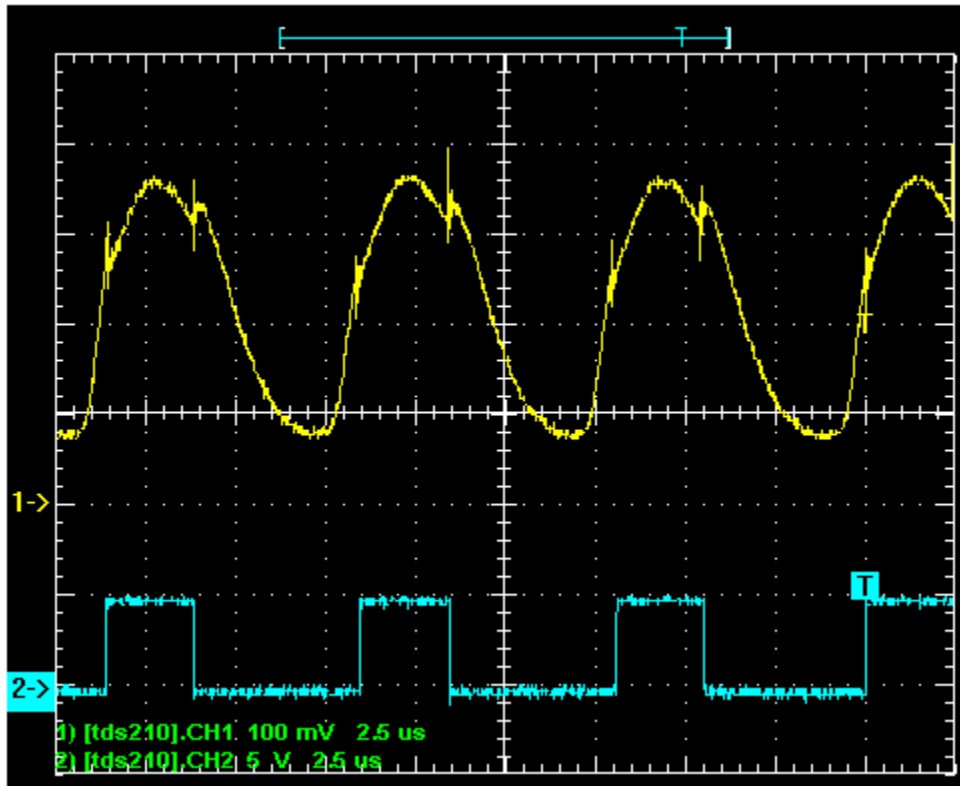


For SD100 – 12-22-021

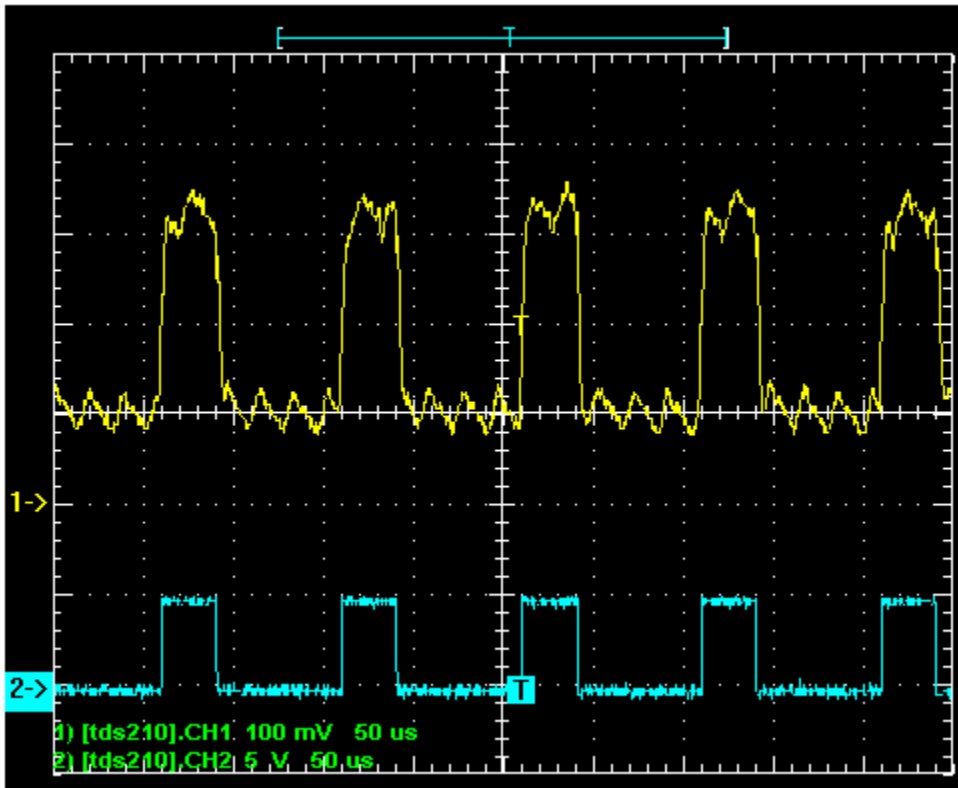
At 10kHz 340mV peak (note: I'm concerned that his unit is not functionally well – possible damage due to static discharge)



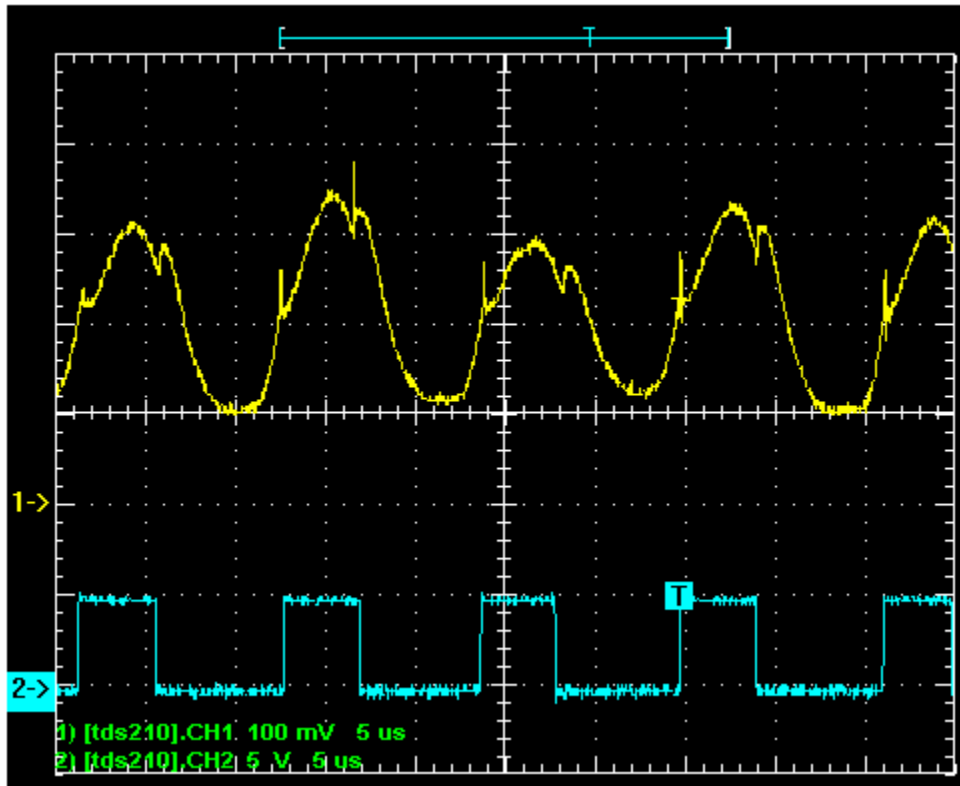
At -3dB level should be 255mV  
F = 150kHz



For SD200-12-22-041  
At 10 kHz (notice the noise) 252mV



3dB down at 178mV  
Frequency is about 90kHz



New Experiment:

Using second op-amp scenario – and bringing in GIC circuit

Using diode PBB-C142

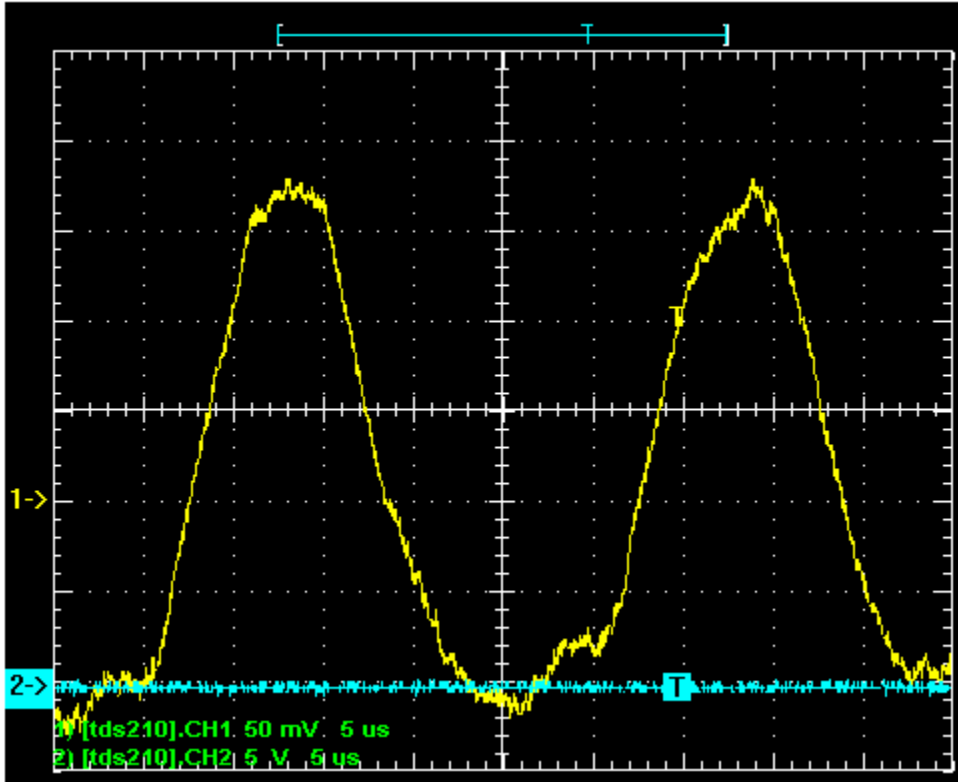
First scenario – results at 1.2 meter

Blue light – no lenses to help

Power level 11.9uW (ambient and pulse) – Ambient only 2.8uW

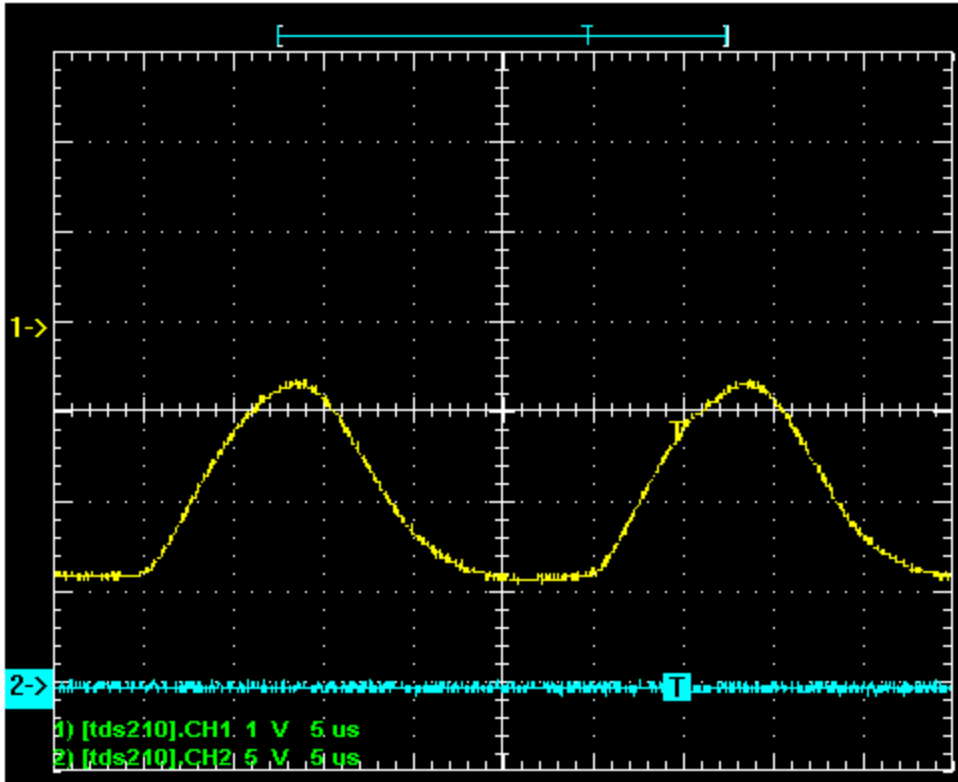
Negative DC offset of -2.6V

Scope setting is AC coupled for image

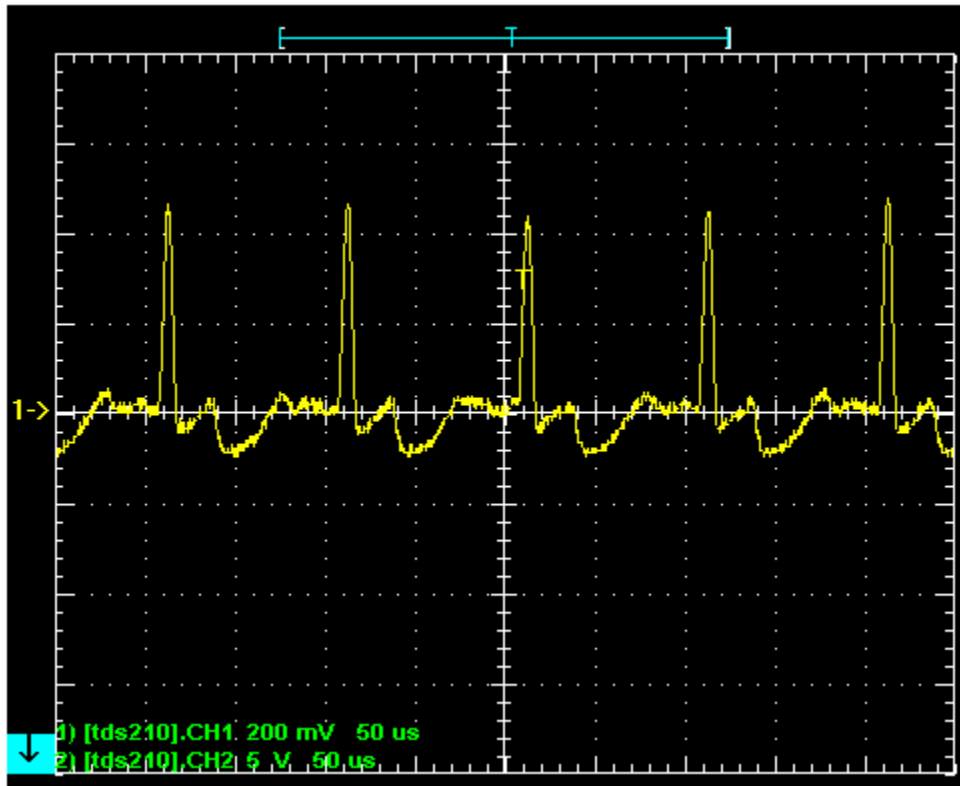


Now, at 2 Meters with transmit lens help  
Light power (ambient and pulse at 71uW) ambient – 2.1uW

Scope now DC coupled:



Now with GIC enabled and frequency at 10kHz 30% duty cycle.



Note for above, the scope is AC coupled  
The DC level that this wave is riding on is -4V  
The optical power is 44uW

Unfortunately this did not work as per the simulation.  
Reasons – stray capacitance and also choice of op-amp  
Note the negative spike reaches op-amp -V rail.

### Distance results

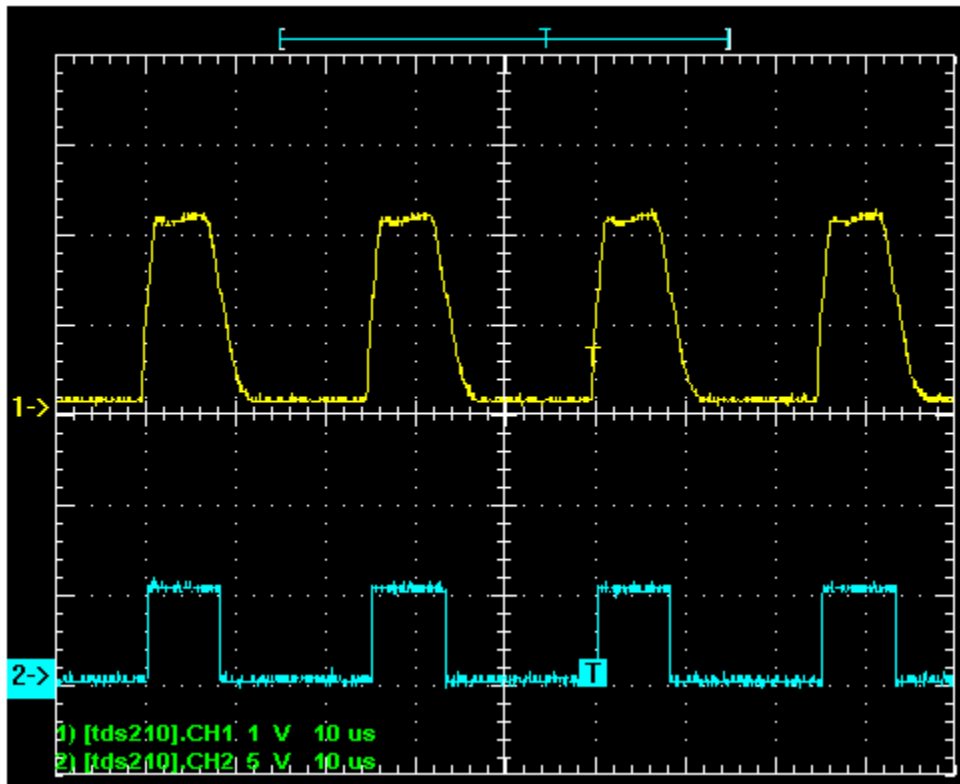
- transmit lens in place
- 2<sup>nd</sup> amp stage in place
- dif amp to schmit comparator to Schmitt buffers

Blue light conditions 16.8V, 1.5V f= 40kHz 30% duty cycle

At 30 meters (limit of hallway)

The following measured results

Ch1 at X2, Ch 2 at X12



As can be seen, at 30 meters we have over 2 Volts peak at the transimpedance stage – indicating we have a lot further to go before being out of range. This image was taken with hall way lights off

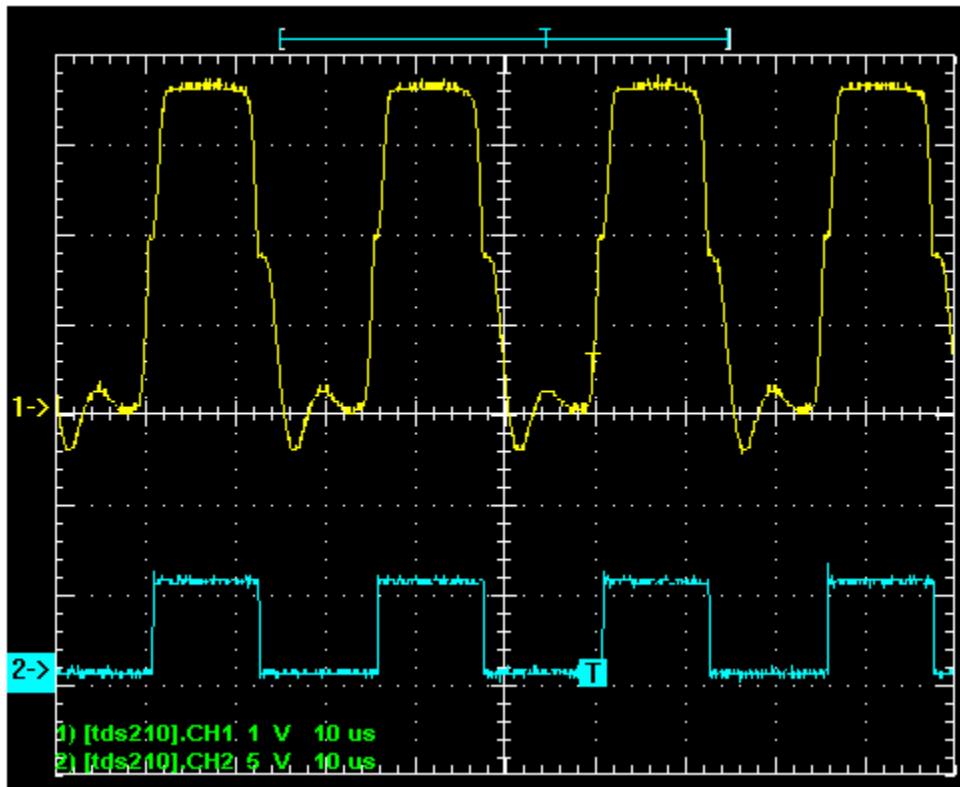
Ambient light to detector about  $238e-9W$

With lights on focused by lens at  $36.6\mu W$  – but the blue light focused gives a level of  $22.9e-6W$  - note that because the hall way lights are on the ceiling there focal point drops below the direct on focal point of the blue light – at the focal point of the blue light the ambient light level reads  $10.0e-6W$



Scope image hall way lights on – distance at 30meters

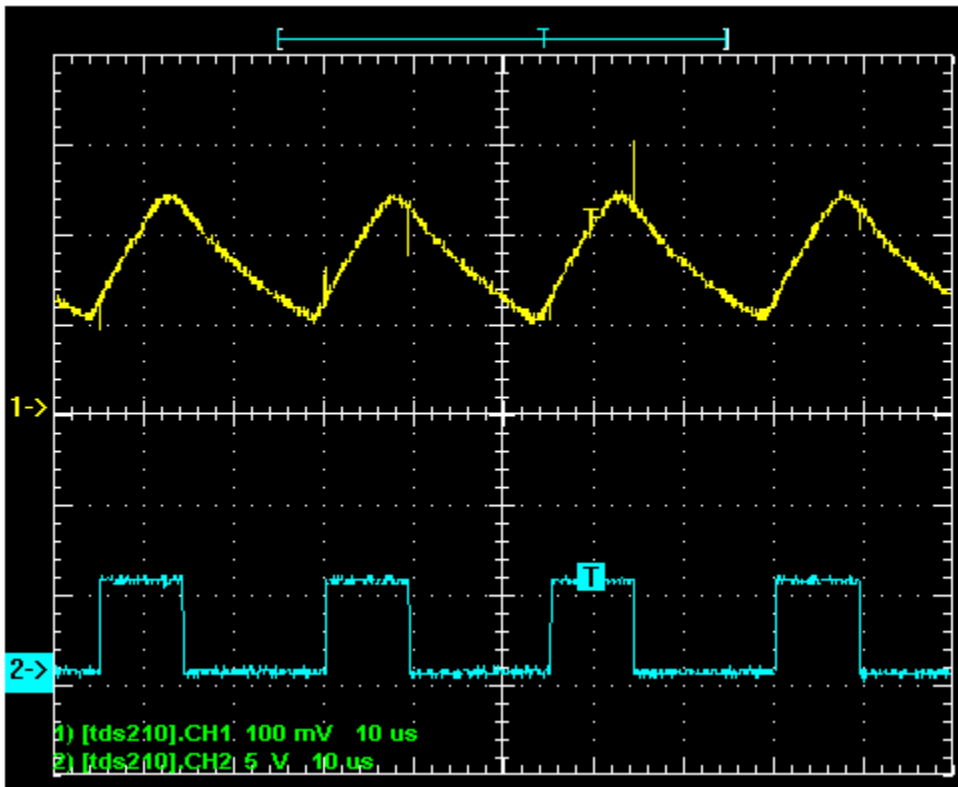
## Testing Hybrid amp at distance of 30 meters



As can be seen by above, with fully focused transmit and receiver, the hybrid amp is almost at peak voltage (the +5V) supply. Substantially greater distance can be achieved with this combination.

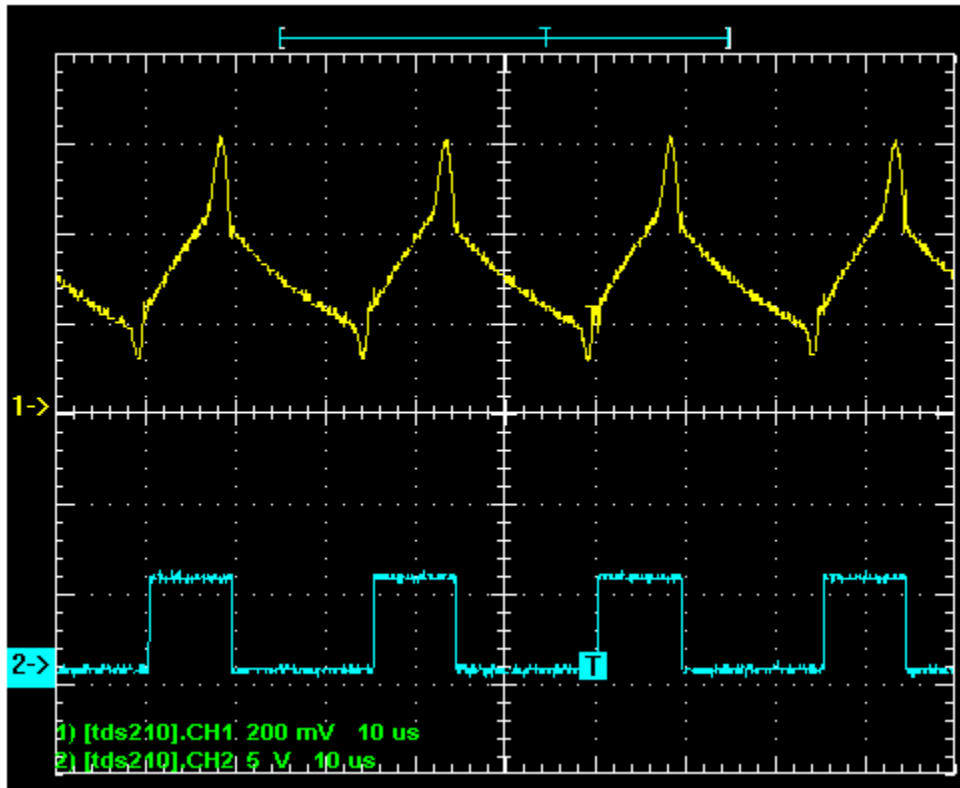
The bad part to this is how critical the focus is to reception.

The following is using the green LED source and Hybrid amp.



The received power level for green is quite a bit lower this may be due to transmitter not being aligned.

After readjusting I received the following:



I'm not clear on why the received waveform ch1 has a differentiated appearance. It could be that I increased the 2<sup>nd</sup> stage amp gain to high. However, what is important is that it's doable but only with good lensing.